Polymer Colloids

About the Cover

The surface of this 760 micrometer (0.76 mm) diameter hollow sphere consists of a monolayer of 7.9 micrometer monodisperse polystyrene particles. These particles had flocculated onto a nitrogen bubble that formed during a seeded emulsion polymerization experiment aboard the space shuttle orbiter *Challenger* (STS 7, June 1983). The principal investigator of these National Aeronautics and Space Administration sponsored experiments was the late Professor John W. Vanderhoff in whose memory this book is dedicated. Original scanning electron micrograph by Olga L. Shaffer, Emulsion Polymers Institute, Lehigh University.

ACS SYMPOSIUM SERIES **801**

Polymer Colloids

Science and Technology of Latex Systems

Eric S. Daniels, Editor
Lehigh University

E. David Sudol, Editor
Lehigh University

Mohamed S. El-Aasser, Editor
Lehigh University

American Chemical Society, Washington, DC

Polymer colloids : science and technology of latex

The paper used in this publication meets the minimum requirements of American National Standard for Information Sciences—Permanence of Paper for Printed Library Materials, ANSI Z39.48–1984.

Foreword

The ACS Symposium Series was first published in 1974 to provide a mechanism for publishing symposia quickly in book form. The purpose of the series is to publish timely, comprehensive books developed from ACS sponsored symposia based on current scientific research. Occasionally, books are developed from symposia sponsored by other organizations when the topic is of keen interest to the chemistry audience.

Before agreeing to publish a book, the proposed table of contents is reviewed for appropriate and comprehensive coverage and for interest to the audience. Some papers may be excluded to better focus the book; others may be added to provide comprehensiveness. When appropriate, overview or introductory chapters are added. Drafts of chapters are peer-reviewed prior to final acceptance or rejection, and manuscripts are prepared in camera-ready format.

As a rule, only original research papers and original review papers are included in the volumes. Verbatim reproductions of previously published papers are not accepted.

ACS Books Department

Preface

The diversity of research in polymer colloids continues to grow. Although the subject may seem narrow to those on the outside, it is witnessed by those of us inside as being rich in variety as can be seen by a glance at the chapter titles in this symposium book. It is an expanding field that can scarcely be contained in a single phrase or book.

This book is based on the Polymer Colloids Symposium held at Lehigh University, June 19–21, 2000, as part of the 74th Colloid and Surface Science Symposium. The former was organized to honor the memory of one of the leading figures in polymer colloids.

John William Vanderhoff was a man of diverse interests. He had two careers: the first at the Dow Chemical Company, where he spent 20 years; then moving in 1970 to his second at Lehigh University, where he spent the remainder of his career until retiring with emeritus status in 1998. He was cofounder of the Emulsion Polymers Institute at Lehigh and director of the National Printing Ink Research Institute. He coauthored more than 200 papers, and held 12 United States and 30 foreign patents. Among many notable accomplishments, he was principal investigator for a joint university–National Aeronautics and Space Administration (NASA) research program, which in 1982 produced the first commercial product to be made in space: 10 micrometer monodisperse polystyrene latex particles. As a result of this work, he was named a corecipient of the 1984 Inventor of the Year Award given by NASA. Besides his pioneering work of developing monodisperse latexes, other areas of notable accomplishment are in latex characterization, kinetics and mechanism of emulsion polymerization, competitive growth, inverse emulsion polymerization, and film formation and drying. His formidable memory and wide-ranging interests were exhibited in his discourse on many subjects in and out of the field of polymer colloids. John Vanderhoff touched the lives of many, particularly the professors, postdoctorates, students, and colleagues with whom he interacted. He will be remembered for his prolific research ideas, congeniality, and humor. He is missed by all of us.

This book contains a wide variety of chapters ranging from the academic to the practical. Although most chapters originate in academic labs, the majority are oriented toward industrial interests. The continuing move toward environmentally responsible products is largely responsible for this. Many types of latexes are represented: homopolymers, copolymers, and

natural polymers, those made with reactive surfactants and polymeric stabilizers, surface modified, hybrids, and blends. Processes vary from batch to semicontinuous, free radical, and controlled free radical, dispersion, and suspension. Kinetics, on-line monitoring, and control are represented as well.

During the past five years, more than the usual number of books have appeared with similar subject matter. This is evidence for the continuing growth in this field and the need to "keep-up" is part of the reason for this acceleration in published works. This book provides a snapshot of this field at this moment in time and should be valuable to those scientists and engineers engaged in polymer colloid research.

We would like to thank all those participating in this publication: the authors for their prompt response to the demands of publication deadlines and especially the unnamed reviewers whose constructive comments and criticism helped to better shape the presented work.

Eric S. Daniels
E. David Sudol
Mohamed S. El-Aasser

Emulsion Polymers Institute
Iacocca Hall
111 Research Drive
Lehigh University
Bethlehem, PA 18015–4732

Chapter 1

Overview of Polymer Colloids: Preparation, Characterization, and Applications

Eric S. Daniels, E. David Sudol, and Mohamed S. El-Aasser

Emulsion Polymers Institute and Department of Chemical Engineering, Lehigh University, Bethlehem, PA 18015-4732

Polymer colloids represent a complex heterogeneous system, and in many ways, the preparation of these materials is still very much an art. The application areas for polymer colloids are diverse, including their use as binders in non-woven fabrics and paper coatings, in synthetic rubbers, in interior and exterior paints, in adhesives, as impact modifiers in toughened plastics, as catalytic supports, in a number of medical diagnostic areas, as rheology modifiers, and many others. Interest in this area has been spurred by environmental considerations and governmental actions to switch from solvent-based to water-borne systems as well as the large number of scientific challenges that remain. This chapter presents an overview of the preparation, characterization, and applications of polymer colloids, as well as giving an idea of some of the future directions, advances, and challenges in this growing field.

A polymer colloid is usually defined as a dispersion of submicron polymer particles in a liquid (typically aqueous) medium. Research in this field has been very active for a number of years, but many scientific and practical challenges

1

remain to be addressed. The high degree of interest in polymer colloids is evidenced by a large number of publications, books, review articles, and symposia that have been held on this topic in the past several years (*1-9*). This chapter is divided into three sections which present a general overview of the field of polymer colloids. The first section details many of the diverse heterogeneous polymerization processes that are used to prepare latexes (in both aqueous and non-aqueous media) and describes the role of the various formulation components utilized in these systems. The second section summarizes some of the key characterization techniques which are employed to quantify the colloidal, molecular, and macroscopic properties of polymer colloids. The third section describes some of the interesting application areas for latexes.

Preparation of Polymer Colloids

A wide variety of processes are used to prepare polymer colloids. The most often utilized method is emulsion polymerization whereby a monomer(s) is polymerized via a free radical polymerization process in an aqueous medium in the presence of a stabilizer system. A dispersion of polymer particles in an aqueous environment (latex) results from this process. The latex can be used in this form in coatings applications (e.g., paints, paper coatings, carpet backing binders, etc.) or they can be separated from the medium and processed to form a bulk polymeric material for use in a number of applications (e.g., in high impact plastics).

Emulsion polymerization involves a complex heterogeneous chemical reaction. The formulation and process parameters strongly impact the characteristics of the resulting polymer particles. Formulation variables include: the types and amounts of the monomers used in the polymerization (principal monomers, functional monomers, crosslinkers), the type and concentration of the initiator (thermal or redox, water-soluble or oil-soluble), and the type and concentration of surfactant or stabilizer (anionic, nonionic, cationic, zwitterionic, polymeric, or protective colloid). In addition, small quantities of rheological modifiers, chain transfer agents, buffers, biocides and fungicides, antioxidants, and UV absorbers may be added (*10*).

Even though they are typically present in low concentrations in an emulsion polymerization, surfactants play a critical role in controlling the resulting particle morphology, particle size, and colloidal stability. However, surfactants may cause problems in films prepared from a latex in terms of increasing the water sensitivity of the film, migration to the surface of the film, which can cause unwanted alterations in the appearance of the coating (e.g., blushing) or migration to the polymer/substrate interface where adhesion of the latex coating

could be adversely affected by the presence of the surfactant. For these reasons, there has been a great deal of interest in the use of polymerizable surfactants in emulsion polymerization where the surfactant would be chemically bound to the latex particles to ensure colloidal stability, while not being able to migrate during film formation thereby alleviating the problems mentioned above (*11-14*).

Process variables may include the type and configuration of the reactor, the polymerization process (batch, semi-continuous, continuous, shot-growth, seeded), the feed strategy (of monomer(s), initiator, surfactant), the type of impeller (e.g., fluidfoil, Rushton turbine, paddle) and agitation rate, and temperature. The situation is even more complex since many of these variables interact with one another to influence the final product.

Mechanisms of particle nucleation in emulsion polymerization may include micellar, homogeneous, droplet, or combinations of these mechanisms. The type of mechanism is dependent on the water solubilities of the monomers used in the polymerization, the type of initiator, the type, concentration, and partitioning of the surfactant used in the formulation, and the state of the monomer dispersion (droplet size and stability) at the polymerization temperature. The rate of the polymerization is critical; these polymerizations are exothermic and a reactor must be able to safely remove the heat of reaction; the rate is controlled by the polymerization temperature, initiator and surfactant concentrations (influencing the number of particles that are generated), among other factors. The polymer particle size and size distribution will depend on these same variables; narrow distributions are achieved when all the particles are all nucleated in a relatively short time and then grow uniformly.

Thermodynamics plays many roles in an emulsion polymerization. The extent of phase compatibility between the different monomer and polymer components present during the polymerization, as well as the various interfacial tensions at the interphases present in the polymerizing system (e.g., polymer/polymer; polymer/aqueous phase) will all influence the final particle morphology. Many types of morphologies are possible, ranging from a "true" core/shell structure to asymmetric particles (raspberry-like, acorn-like, inverted core/shell) (*15-17*). Particle morphology also depends on polymer hydrophilicity/hydrophobicity, polarity, initiator type and concentration, the type and concentration of surfactant, and the core/shell ratio. In addition to carefully balancing these parameters to obtain a desired particle morphology, the formulator also may adjust the monomer/initiator/surfactant feed strategies as well as use compatibilizing agents (*18*) to achieve the morphology of interest

The modeling, monitoring and control of the emulsion polymerization process are of critical importance and are challenging. A number of mathematical models have been developed to describe the complex kinetics of the emulsion polymerization process (*19*); however, one stumbling block which still represents a great challenge in this field, is the determination and selection

of accurate kinetic rate constants; unfortunately, these values can vary widely in magnitude depending on the particular investigator and the experimental system. This makes the quantitative prediction of reaction kinetics difficult and is system dependent. Tools for characterizing the kinetics and mechanism of an emulsion polymerization reaction include the determination of the rate of polymerization by gravimetry, dilatometry, or reaction calorimetry. In particular, reaction calorimetry, which relates the heat of reaction to the polymerization rate, is a powerful and sensitive tool that may be used to obtain detailed kinetic data not obtainable by other means (20, 21). Samples may also be withdrawn from a reactor during the course of polymerization to determine the evolution in particle size, particle number, and particle morphology.

Once a model has been established, control of the process becomes important, and strategies to control a desired property of the latex (e.g., polymer composition, particle size and size evolution, or molecular weight) are important (22, 23). Related to this is the challenge of robust on-line monitoring and real-time control of the polymerization process and formulation variables and the development of precise on-line sensors that can feed back information into the process to control the desired property (24, 25). Many challenges still remain in this area such as the need to quickly and accurately measure and analyze an on-line dependent response (such as particle size or polymer composition) which can be fed back into the control strategy and adjust a formulation or process variable in time for the response to be controlled so as to achieve the desired outcome.

There are several other polymerization processes which are used to prepare submicron-size polymer colloids. Two important variations are the microemulsion and miniemulsion polymerization processes. These processes differ primarily in terms of the dispersed phase (i.e., monomer) droplet size and stabilization system. Microemulsions are translucent, with droplet sizes less than 0.1 μm, employ high emulsifier concentrations (15 to 30 %), typically utilize a short chain alcohol (≤ 5 carbons) as a costabilizer, and are thermodynamically stable. Miniemulsions are opaque (as are conventional emulsions), with droplet sizes between 0.05 to 0.5 μm (vs. > 1 μm for conventional emulsions), utilize emulsifier concentrations (0.5 to 5 %) similar to conventional emulsions (1-3%), and also employ a highly water-insoluble, low molecular weight costabilizer (unlike conventional emulsions) such as a long chain alkane (e.g., hexadecane) or long chain alcohol (e.g., cetyl alcohol) (≥ 12 carbons). Miniemulsions are stable over a period of time from hours to months compared to conventional (macroemulsions) emulsions which are only stable for short times (seconds or minutes). Polymerization of microemulsions results in the formation of small particles (ca. 50 nm), the disadvantage being the presence of a high concentration of surfactant in this system (26). The utilization and importance of the miniemulsion polymerization process has been growing since its discovery

around 1970, as evidenced by a large number of publications describing various aspects and applications of this technology (27-31). Another advantage of this process is that it allows one to prepare "artificial latexes" comprised of polymers, e.g., epoxies or polyurethanes, which cannot be prepared by a free radical process. This is accomplished via a direct miniemulsification procedure whereby the polymer is first dissolved in a solvent, and this mixture is added to an aqueous surfactant solution, subjected to high shear to create submicron droplets containing the polymer, and then the solvent is removed, thus creating a latex. A costabilizer is also used in this process to achieve the small droplet size.

Another area of intensive research interest over the past few years has been the controlled (living) free radical polymerization processes in which one can control the molecular weight, achieve a narrow molecular weight distribution, and obtain desired end groups (32). Three different approaches have been developed: stable free radical polymerization (SFRP), atom transfer radical polymerization (ATRP), and reversible addition-fragmentation chain transfer polymerization (RAFT). These processes differ in the type of initiation system which is utilized. One of the research challenges has been to utilize these controlled free radical approaches in water-borne systems rather than in bulk; a great deal of research effort has been (and still is being) devoted to determining the appropriate reaction conditions to achieve this goal (33-35). The promise of advanced materials has yet to be realized by this process.

Non-aqueous dispersions can be prepared by inverse emulsion, microemulsion and miniemulsion polymerization. Polyacrylamide is a well-known water-soluble polymer made by these processes. Non-aqueous media are also being used in preparing hydrophobic polymer particles via dispersion polymerization. These reactions start with a homogeneous system comprised of monomer, solvent, stabilizer, and initiator. With polymerization, the polymer particles precipitate out, forming particles stabilized by some form of steric stabilizer (e.g., block copolymer, homopolymer, graft copolymer). The medium can be polar or non-polar. Alcohol media have been used advantageously to prepare uniform particles in the 1 to 5 µm size range in a one-step process (36). An important recent variant of this process is the use of supercritical fluids (such as CO_2) as the dispersion medium instead of utilizing a conventional solvent in an attempt to develop a "green" environmentally-friendly polymerization process. Much research has been devoted to development of this type of dispersion polymerization system (37, 38); disadvantages of the process include the need to carry out the polymerization at high pressures requiring specialized polymerization equipment to carry out the reactions.

Characterization of Polymer Colloids

There are many techniques which are commonly used to characterize polymer colloids including those used to quantify the kinetics of the polymerization (e.g., conversion and polymerization rate), the colloidal properties (e.g., particle size, particle morphology), molecular properties related to the polymer itself (e.g., composition, molecular weight), and macroscopic properties of the final materials prepared from the polymer colloids themselves (e.g., mechanical behavior) (*39*).

Methods used to quantify and monitor the reaction kinetics were described in the previous section (e.g., following the conversion of monomer to polymer; the evolution in particle number with reaction time, etc.). Some key properties related to the colloidal nature of the dispersions include the solids content, the colloidal stability (e.g., coagulum level), and surface charge of the polymer colloid (*40*), the particle size and particle size distribution (measured using techniques such as dynamic light scattering (DLS), capillary hydrodynamic fractionation (CHDF), and electron microscopy (both transmission (TEM) and scanning (SEM)) (*41*). Other important properties include particle morphology (electron microscopy with a variety of staining agents, as well as via NMR (*42*)), and the rheology (related to particle-particle interactions) (*43*) of the dispersion (an interesting new optical tweezers technique to measure microviscosity in the environment surrounding a colloidal particle(s) is described by Ou-Yang) (*44*). Molecular properties of the (co)polymer include the polymer composition (e.g., sequence distributions) (quantified by FTIR, NMR, SANS, etc.), the thermal properties of the polymer, such as its glass transition temperature (T_g) or crystalline melting temperature (T_m) (measured by differential scanning calorimetry; DSC), or molecular weight and molecular weight distribution (measured by gel permeation chromatography (GPC), viscometry or osmometry). Macroscopic properties of materials derived from the polymer colloids would include their mechanical behavior (measured by tensile testing or dynamic mechanical spectroscopy), chemical (e.g., solvent resistance) and environmental resistance (e.g., to UV, water, humidity, block resistance, etc.), appearance, and toughness, among other factors. A great deal of information is available in the literature describing the transformation of a polymer colloid to a final cohesive material (e.g., film formation studies from latexes) (*45, 46*) which is beyond the scope of this chapter.

Applications of Polymer Colloids

There are many diverse areas where polymer colloids are utilized (*47*) ranging from coatings applications in paints (*48*), as a binder for paper coatings

(49), in tire manufacturing (50), as toughening agents in rubber-toughened plastics (51), in pressure sensitive adhesives (52), to their use in medical diagnostics (53). Many industrial coatings applications still utilize solvent-based formulations and there is considerable environmental pressure to reduce VOC levels while still maintaining the desirable properties that are often obtained with solvent-based coatings. The use of latex blends with two different polymer compositions (e.g., one with a film-forming composition and one with a high modulus polymer composition) is an attractive strategy to achieve this goal while obtaining synergies in the final coatings properties (54). There is also a continuous need for the development of new types of bulk materials with unique properties. These may be prepared by custom designing new types of polymer colloid composites and hybrids by controlling the polymer morphology and polymer compositions (55-57).

Another exciting and rapidly growing application area is the development of latexes with a wide variety of functional moieties present on the surface (58) which can be utilized to attach a wide number of biological ligands such as enzymes (59), antibodies (60), DNA fragments (61), etc., to the surface for a large number of medical diagnostic applications. The use of particles which may be radiolabeled (62) or tagged with fluorescent dyes (63) is also finding use in flow cytometry applications (64) and in the development of fluorescently-tagged micro-bioarrays where many diagnostic tests can be carried out simultaneously utilizing each polymer colloid particle as a unique reaction site for a specific bioreaction (e.g., antigen-antibody reaction) on individual color-encoded particles. In addition, the use of "smart" polymer colloids, where changes in structure can be triggered by environmental stimuli are increasingly being employed in this bioapplications area (65).

Finally, research in the self-assembly and ordering of monodisperse latexes into arrays and as templates is also growing rapidly for use in photonics, catalyst supports, and storage device applications. For example, monodisperse polymer particles can be laid down into an ordered array and the interstitial space filled with colloidal metal particles (66-68); the monodisperse polymer particles are then dissolved away, leaving a porous metallic substrate with well-defined pore sizes. Monodisperse polymer colloid templates have also been studied as a spacer layer in liquid crystal displays (69).

References

1. El-Aasser, M. S.; Smith, C. D., Eds. *Macromolecular Symposia* **2000**, *155(Emulsion Polymers)*; Wiley-VCH: Weinheim, Germany;.

2. Claverie, J.; Charreyre, M.-T.; Pichot, C., Eds. *Macromolecular Symposium* **2000**, *150 (Polymers in Dispersed Media. I.*); Wiley-VCH: Weinheim, Germany.

3. *Emulsion Polymerization and Emulsion Polymers;* Lovell, P. A.; El-Aasser, M. S., Eds.; John Wiley & Sons: Chichester, England, 1997.

4. *Polymeric Dispersions: Principles and Applications;* Asua, J. M., Ed.; Kluwer Academic Publishers: Dordrecht, 1997.

5. Blackley, D. C. *Polymer Latices Science and Technology. Volume 1: Fundamental Principles, Second Edition;* Kluwer Academic Publishers: Dordrecht, 1997.

6. Blackley, D. C. *Polymer Latices Science and Technology. Volume 2: Types of Latices, Second Edition;* Kluwer Academic Publishers: Dordrecht, 1997.

7. Blackley, D. C. *Polymer Latices Science and Technology. Volume 3: Applications of Latices, Second Edition;* Kluwer Academic Publishers: Dordrecht, 1997.

8. Fitch, R. M. *Polymer Colloids. A Comprehensive Introduction;* Academic Press: London, 1997.

9. Guyot, A. Recent Advances and Challenges in the Synthesis of Polymer Colloids, *Colloids Surf., A.* **1999**, *153(1-3)*, 11-21.

10. Klein, A.; Daniels, E. S. Formulation Components. In *Emulsion Polymerization and Emulsion Polymers;* Lovell, P. A., El-Aasser, M. S., Eds.; John Wiley & Sons: Chichester, U.K., 1997; pp. 207-237.

11. Asua, J. M.; Schoonbrood, H. A. S. Reactive Surfactants in Heterophase Polymerization, *Acta Polym.* **1998**, *49*, 671-686.

12. Guyot, A. Polymerizable Surfactants. *Surfactant Sci. Ser.* **1998**, *74 (Novel Surfactants)*, 301-332.

13. Hellgren, A.-C.; Weissenborn, P.; Holmberg, K. Surfactants in Water-Borne Paints. *Prog. Org. Coat.* **1999**, *35(1-4)*, 79-87.

14. Urquiola, M. B. The Role of Polymerizable Surfactants in Emulsion Polymerization, *Ph.D. Dissertation*, Lehigh University, 1992.

15. Okubo, M. Control of Particle Morphology in Emulsion Polymerization. *Makromol. Chem., Macromol. Symp. (Copolym. Copolym. Dispersed Media)* **1990**, *35-36*, 307-325.

16. Sundberg, D. C.; Durant, Y. G. Thermodynamic and Kinetic Aspects for Particle Morphology Control. In *Polymeric Dispersions: Principles and Applications;* Asua, J. M., Ed.; Kluwer Academic Publishers: Dordrecht, 1997, 177-188.

17. Dimonie, V. L.; Daniels, E. S.; Shaffer, O. L.; El-Aasser, M. S. Control of Particle Morphology. In *Emulsion Polymerization and Emulsion Polymers;* Lovell, P. A., El-Aasser, M. S., Eds.; John Wiley & Sons: Chichester, U.K., 1997; pp. 207-237.

18. Rajatapiti, P.; Dimonie, V. L.; El-Aasser, M. S. Latex Particle Morphology. The Role of Macromonomers as Compatibilizing Agents. In *Polymeric Dispersions: Principles and Applications*; Asua, J. M., Ed.; Kluwer Academic Publishers: Dordrecht, 1997, pp. 189-202.

19. Gilbert, R. G. *Emulsion Polymerization: A Mechanistic Approach*; Academic Press: London, U.K., 1995.

20. Varela de la Rosa, L.; Sudol, E. D.; El-Aasser, M. S.; Klein, A. Details of the Emulsion Polymerization of Styrene Using a Reaction Calorimeter. *J. Polym. Sci.: Part A: Polym.Chem.* **1996**, *34*, 461-473.

21. Varela de la Rosa, L.; Sudol, E. D.; El-Aasser, M. S.; Klein, A. Emulsion Polymerization of Styrene Using Reaction Calorimeter III. Effect of Initial Monomer/Water Ratio. *J. Polym. Sci.: Part A: Polym. Chem.* **1999**, *37*, 4073-4089.

22. Leiza, J. R.; Asua, J. M. Feedback Control of Emulsion Polymerization Reactors, In *Polymeric Dispersions: Principles and Applications*; Asua, J. M., Ed.; Kluwer Academic Publishers: Dordrecht, 1997, pp. 189-202.

23. Liotta, V.; Sudol, E. D.; El-Aasser, M. S.; Georgakis, C. Online Monitoring, Modeling, And Model Validation Of Semibatch Emulsion Polymerization In An Automated Reactor Control Facility. *J. Polym. Sci., Part A: Polym. Chem.* **1998**, *36(10)*, 1553-1571.

24. Schork, F. J. Process Modelling and Control. In *Emulsion Polymerization and Emulsion Polymers*; Lovell, P. A., El-Aasser, M. S., Eds.; John Wiley & Sons: Chichester, U.K., 1997; pp. 327-342.

25. Hergeth, W.-D. On-Line Characterization Methods, In *Polymeric Dispersions: Principles and Applications*; Asua, J. M., Ed.; Kluwer Academic Publishers: Dordrecht, 1997, pp. 267-288.

26. Candau, F. Microemulsion Polymerization. In *Polymeric Dispersions: Principles and Applications*; Asua, J. M., Ed.; Kluwer Academic Publishers: Dordrecht, 1997, pp. 127-140.

27. Sudol, E. D.; El-Aasser, M. S. Miniemulsion Polymerization. In *Emulsion Polymerization and Emulsion Polymers*; Lovell, P. A., El-Aasser, M. S., Eds.; John Wiley & Sons: Chichester, U.K., 1997; pp. 699-722.

28. Bechthold, N.; Tiarks, F.; Willert, M.; Landfester, K.; Antonietti, M. Miniemulsion Polymerization: Applications and New Materials. *Macromol. Sympos.* **2000**, *151 (Polymers in Dispersed Media)*, 549-555.

29. Aizpurua, I.; Barandiaran, M. J. Comparison Between Conventional Emulsion and Miniemulsion Polymerization of Vinyl Acetate in a Continuous Stirred Tank Reactor. *Polymer* **1999**, *40*, 4105-4115.

30. Chern, C.-S.; Liou, Y.-C. Styrene Miniemulsion Polymerization Initiated by 2,2'-Azobisisobutyronitrile. *J. Polym. Sci.: Part A: Polym. Chem.* **1999**, *37*, 2537-2550.

31. Schork, F. J.; Poehlein, G. W.; Wang, S.; Reimers, J.; Rodrigues, J.; Samer, C. Miniemulsion Polymerization. *Colloids Surf., A.* **1999**, *153(1-3)*, 39-45.

32. Matyjaszewski, K. Controlled Radical Polymerization, *ACS Symposium Series* 685, American Chemical Society: Washington, DC, 1998.

33. Matyjaszewski, K.; Qiu, J.; Shipp, D. A.; Gaynor, S. G. Controlled/ "Living" Radical Polymerization Applied to Water-Borne Systems. In *Macromolecular Symposia* **2000**, *155 (Emulsion Polymers)*; Wiley-VCH: Weinheim, Germany; pp. 15-30.

34. MacLeod, P. J.; Barber, R.; Odell, P. G.; Keoshkerian, B.; Georges, M. K., Stable Free Radical Miniemulsion Polymerization In *Macromolecular Symposia* **2000**, *155 (Emulsion Polymers)*; Wiley-VCH: Weinheim, Germany; pp. 31-38.

35. Pan, G.; Sudol, E. D.; Dimonie, V. L.; El-Aasser, M. S. Nitroxide-Mediated Living Free Radical Miniemulsion Polymerization of Styrene, *Macromolecules*, **2001**, *34*, 481-488.

36. Cawse, J. L. Dispersion Polymerization. In *Emulsion Polymerization and Emulsion Polymers*; Lovell, P. A.; El-Aasser, M. S., Eds.; John Wiley & Sons: Chichester, U.K., 1997; pp 743-761.

37. Young, J. L.; DeSimone, J. M. Frontiers in Green Chemistry Utilizing Carbon Dioxide for Polymer Synthesis and Applications. *Pure Appl. Chem.* **2000**, *72(7)*, 1357-1363.

38. Shiho, H.; DeSimone, J. M. Dispersion Polymerization of Glycidyl Methacrylate in Supercritical Carbon Dioxide. *Macromolecules* **2001**, *34(5)*, 1198-1203.

39. German, A. L.; van Herk, A. M.; Schoonbrood, H. A. S.; Aerdts, A. M. Latex Polymer Characterization. In *Emulsion Polymerization and Emulsion Polymers;* Lovell, P. A.; El-Aasser, M. S., Eds.; John Wiley & Sons: Chichester, U.K., 1997; pp 343-383.

40. Ottewill, R. H. Stabilization of Polymer Colloid Dispersions. In *Emulsion Polymerization and Emulsion Polymers;* Lovell, P. A.; El-Aasser, M. S., Eds.; John Wiley & Sons: Chichester, U.K., 1997; pp 59-121.

41. Collins, E. A. Measurement of Particle Size and Particle Size Distribution. In *Emulsion Polymerization and Emulsion Polymers;* Lovell, P. A.; El-Aasser, M. S., Eds.; John Wiley & Sons: Chichester, U.K., 1997; pp 385-436.

42. Landfester, K.; Spiess, H. W. Characterization of Particle Morphology by Solid-State NMR. In *Polymeric Dispersions: Principles and Applications*; Asua, J. M., Ed.; Kluwer Academic Publishers: Dordrecht, 1997, pp 203-216.

43. Schaller, E. J. Latex Rheology. In *Emulsion Polymerization and Emulsion Polymers;* Lovell, P. A.; El-Aasser, M. S., Eds.; John Wiley & Sons: Chichester, U.K., 1997; pp. 437-466.
44. Ou-Yang, H. D. Design and Applications of Oscillating Optical Tweezers for Direct Measurements of Colloidal Forces. In *Polymer-Colloid Interactions: From Fundamentals to Practice*; Durbin, P.; Farinato, R., Eds., John Wiley and Sons: New York, 1999, pp. 385-405.
45. Winnik, M. A. The Formation and Properties of Latex Films. In *Emulsion Polymerization and Emulsion Polymers*; Lovell, P. A.; El-Aasser, M. S., Eds.; John Wiley & Sons: Chichester, U.K., 1997; pp 467-518.
46. Richard, J. Film Formation, In *Polymeric Dispersions: Principles and Applications;* Asua, J. M., Ed.; Kluwer Academic Publishers: Dordrecht, 1997, pp 397-420.
47. Defusco, A. J.; Sehgal, K. C.; Bassett, D. R. Overview Of Uses Of Polymer Latexes. *NATO ASI Ser., Ser. E* **1997**, *335 (Polymeric Dispersions: Principles and Applications)*, 379-396.
48. Waters, J. A. Latex Paint Formulations. In *Polymeric Dispersions: Principles and Applications;* Asua, J. M., Ed.; Kluwer Academic Publishers: Dordrecht, 1997, pp 421-434.
49. Lee, D. I. Latex Applications in Paper Coatings. In *Polymeric Dispersions: Principles and Applications;* Asua, J. M., Ed.; Kluwer Academic Publishers: Dordrecht, 1997, pp 397-420.
50. Blackley, D. C. Diene-Based Synthetic Rubbers. In *Emulsion Polymerization and Emulsion Polymers;* Lovell, P. A.; El-Aasser, M. S., Eds.; John Wiley & Sons: Chichester, U.K., 1997; pp. 521-561.
51. Lovell, P. A.; Pierre, D. Rubber-Toughened Plastics. In *Emulsion Polymerization and Emulsion Polymers*; Lovell, P. A.; El-Aasser, M. S., Eds.; John Wiley & Sons: Chichester, U.K., 1997; pp 657-695.
52. Tobing, S. D.; Klein, A. Molecular Parameters and Their Relation to the Adhesive Perfomance of Acrylic Pressure-Sensitive Adhesives. *J. Appl. Polym. Sci.* **2001**, *79*, 2230-2244.
53. Pichot, C.; Delair, T.; Blaissari, A. Polymer Colloids for Biomedical and Pharmaceutical Applications. *NATO ASI Ser., Ser. E*, **1997**, *335 (Polymeric Dispersions: Principles and Applications)*, 515-539.
54. Robeson, L. M.; Vratsanos, M. S. Mechanical Characterization Of Vinyl Acetate Based Emulsion Polymer Blends. *Macromol. Symp.* **2000**, *155(Emulsion Polymers)*, 117-138.
55. Guyot, A. *Morphology Control of Polymer Colloids: A Route for Improving the Mechanical Properties of Materials.* Guyot, A., Ed. In *Polym. Adv. Technol.*, **1995**, *6(5)*.

56. Dong, H.; Gooch, J. W.; Poehlein, G. W.; Wang, S. T.; Wu, X.; Schork, F. J. Novel Waterborne Coatings Via Hybrid Miniemulsion Polymerization. *ACS Symp. Ser.* **2001**, *766 (Green Engineering)*, Anastas, P. T.; Heine, L. G.; Williamson, T. C., Eds., 8-17.

57. Satguru, R.; McMahon, J.; Padget, J. C.; Coogan, R. G. Aqeuous Polyurethanes- Polymer Colloids with Unusual Colloidal, Morphology, and Application Characteristics. *J. Coat. Technol.* **1994**, *66(830)*, 47-55.

58. Pichot, C.; Delair, T. *Microspheres, Microcapsules and Liposomes.* **1999**, *1 (Preparation & Chemical Applications)*, 125-163.

59. Yasui, M.; Shiroya, T.; Fujimoto, K; Kawaguchi, H. Activity of Enzymes Immobilized on Microspheres with Thermosensitive Hairs. *Colloids Surf., B.* **1997**, *8(6)*, 311-319.

60. Molina-Bolivar, J. A.; Galisteo-Gonzalez, F.; Quesada-Perez, M.; Hidalgo-Alvarez, R. Agglutination Kinetics of F(ab')2 Coated Polymer Colloids. *Colloid Polym. Sci.* **1998** *276(12)*, 1117-1124.

61. Hatakeyama, M.; Iwaro, S.; Fujimoto, K.; Handa, H.; Kawaguchi, H. DNA-Carrying Latex Particles for DNA Diagnosis. 1. Separation of Normal and Point Mutant DNAs According to the Difference in Hybridization Efficiency. *Colloids Surf., B.* **1998**, *10(3)*, 161-168.

62. Ercan, M. T.; Ugur, O. Radiolabeled Microparticles in Medical and Biological Research. *Microspheres, Microcapsules and Liposomes* **2001**, *3 (Radiolabeled and Magnetic Particulates in Medicine and Biology)*, 393-425.

63. Bhattacharyya, B.; Bhupati, R.; Halpern, B. D. Application of Monodisperse Functional and Fluorescent Latex Particles. *Polym. News* **1977**, *4(3)*, 107-114.

64. Vignali, D. A. A. Multiplexed Particle-Based Flow Cytometric Analysis. *J. Immunol. Methods* **2000**, *243(102)*, 243-255.

65. Kawaguchi, H.; Fujimoto, K. Smart Latexes for Bioseparation. *Bioseparation* **1998**, *7(4/5)*, 253-258.

66. Chen, Y.; Ford, W. T.; Materer, F.; Teeters, D. Facile Conversion of Colloidal Crystals to Ordered Porous Polymer Nets. *J. Am. Chem. Soc.* **2000**, *122 (42)*, 10472-10473.

67. Velev, O. D.; Tessier, P. M.; Lenhoff, A. M.; Kaler, E. W. Materials: A Class of Porous Metallic Nanostructures. *Nature (London)*, **1999**, *401*, 548.

68. Bartlett, P. N.; Birkin, P. R.; Ghanem, M. A. Electrochemical Deposition of Macroporous Platinum, Palladium, and Cobalt Films using Polystyrene Latex Sphere Templates. *Chem. Commun. (Cambridge)* **2000**, *17*, 1671-1672.

69. Kim, M.-H.; Kang, W.-S.; Kim, J.-D. Two Dimensional Template of Polystyrene as an Alignment Layer of Liquid Crystals. *Mol. Cryst. Sci. Technol., Sect. A* **2000**, *349*, 127-130.

Chapter 2

Colloidal Stability Analysis of a Core–Shell Emulsion Polymerization

E. C. Kostansek

Rohm and Haas Company, 727 Norristown Road, P.O. Box 904, Spring House, PA 19477

During the course of emulsion polymerization reactions many parameters which affect colloidal stability are varying significantly. This is especially true of core/shell systems such as the one discussed in this paper. In order to identify potential colloidal stability problem areas in the process, we took periodic samples from full-scale production emulsion polymerization reactions and measured/analyzed both latex and process parameters. Latex parameters included particle size, zeta potential, surface acid, surface hydrophobicity, and surfactant coverage. Process parameters included viscosity, agitation (shear rate), solids, and pH. Shear stability was measured and also calculated from DLVO theory with, and without, hydrophobic attraction energies. The results indicated a problem area in the process in terms of shear stability and possible gel formation and coagulation in the hydrophobic second stage of the process. Hydrophobic interactions appeared to be very important during that stage of the reaction based on the shear stability calculations and surfactant coverage data. This is the first time that such a detailed colloidal analysis of a commercial emulsion polymerization process has been reported in the literature.

13

Emulsion polymerizations are dynamic, colloidally complicated processes where colloidal parameters are changing continuously during the entire course of the reaction. This is especially true for core/shell latexes where the surface and bulk compositions change dramatically from stage to stage. Successive stages can have quite different hydrophobicities, glass transition temperatures, and morphologies. Because of these changes, colloidal stability of the latex particles can vary significantly from stage to stage. This can be manifested by poor mechanical stability, coagulation, and gel formation. Often it is difficult to solve stability problems because end-use performance limits the options for stabilizing the latex. For example, increased surfactant levels can sometimes improve colloidal stability, but might lead to increased foaming or decreased adhesion and water resistance in the final application. Often a combination of chemical and process changes is needed to solve the problem.

Because latex systems are colloidally complex, it can be difficult to ascertain the root causes of instability during the reaction. This makes it very challenging to do troubleshooting. Given this situation, we decided to thoroughly analyze all stages of a core/shell emulsion polymerization process which has demonstrated instability problems. The magnitude and practical importance of the problem is evident when one has to remove 10,000 gal. of coagulated latex from a kettle and start over! In order to accomplish our study, we took actual production samples of latex from all of the important points in the process and analyzed them for the most critical colloidal parameters. To our knowledge, this is first time in the literature that this has been attempted. The methods and results have been used to identify the causes of instability and should be applicable to other latex systems in general.

Experimental

Latex System

The latex system we studied was a seeded core/shell three-stage emulsion polymerization reaction containing the monomers methyl methacrylate (MMA), n-butyl acrylate (BA), and styrene (Sty). The seed, Stage I, and Stage III monomers were primarily MMA. Stage II was a crosslinked BA/Sty copolymer. The surfactant was sodium dodecylbenzenesulfonate (SDBS). Three 10,000 gal. batches were sampled at strategic points in the reaction and analyzed as described in the following sections. In this paper we will concentrate mainly on the results at the ends of each of the three stages. Results were very consistent from batch to batch and we report here the average values for the three batches.

Latex Variables

The latex variables studied were particle size, zeta potential, surfactant coverage, surfactant surface area at saturation, surface acid, and shear stability. Particle size was measured using a Brookhaven BI-90 instrument and electophoretic mobility was measured using a Malvern ZetaSizer III. Zeta potentials were calculated from the mobilities using the method of O'Brien and White (1). Surfactant coverage and surface area at saturation were determined by SDBS surfactant titration using a Wilhelmy plate tensiometer. Shear stability was measured using a Rheometrics DMA instrument with a cone and plate configuration.

Process Variables

Process variables studied were pH, temperature, polymer solids, viscosity, residual monomer, and shear rate of mixing. Polymer solids were determined gravimetrically and viscosity was measured using a Brookfield viscometer. Temperature and residual monomer were measured, but will not be discussed in this paper. The maximum shear rate the latex particles were subjected to was estimated based on agitator design and tip speed.

Results and Discussion

Particle Size, Solids, and Viscosity

The polymer solids, particle size, pH, and viscosity of the latex at various points in the polymerization reaction are listed in Table I. Solids ranged from 7.3% to 50%, particle size grew from the 105 nm seed to the 289 nm final product, and pH stayed in a narrow range between 5.7 and 6.8 during the reaction. Viscosity increased from the initial value of 3 cps to a maximum of 73 cps in Stage III to 42 cps for the final product. As mentioned previously, most of the remaining discussion will concentrate on the parameters associated with the three major stages of the polymerization.

Zeta Potential

Zeta potentials for the three reaction stages are shown in Figure 1. Measurement conditions were chosen to match actual reaction conditions as closely as possible. Zeta potential changed very little during the course of the

reaction. This would suggest that colloidal stability should be similar at all stages of the reaction. Unfortunately, our experience with this process tells us that this is not the case, so other parameters such as surface acid, surfactant coverage, and surface hydrophobicity needed to be explored to search for the causes of instability.

Table I. Selected Latex Parameters at Different Reaction Stages

Reaction Stage	% Solids	Particle Diameter	pH	Viscosity
Seed (MMA)	7.3	105	6.8	3
I (MMA)	33.3	206	6.5	6
II (BA/Sty)	45.6	294	5.7	39
III (MMA)	50.7	296	6.2	73
Final	50.0	289	6.0	42

Note: Solids in weight %, particle size in nm, and viscosity in cps.
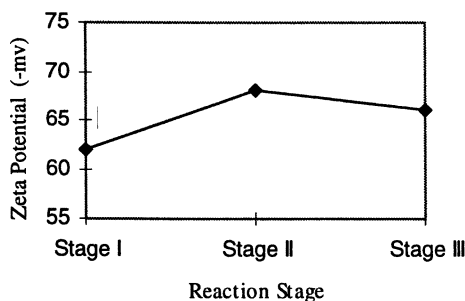
Figure 1. Latex zeta potential as a function of reaction stage.

Surface Acid

It is well known that surface acid can help stabilize latex particles (2-4). Even though we did not purposely add acidic monomer to this reaction, we measured surface acid in case some had formed through hydrolysis. Figure 2 shows the surface acid, expressed as %MAA based on polymer, as a function of reaction stage. There is indeed measurable surface acid which peaks at Stage II, but it is a small amount which probably contributes minimally to the stability.
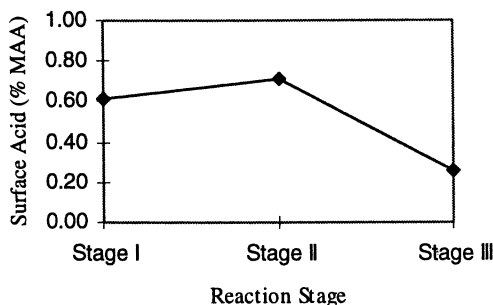
Figure 2. Latex surface acid (as MAA) as a function of reaction stage.

Surfactant Coverage and Surface Hydrophobicity

One of the critical parameters for latex stability is surfactant coverage. The useful thing about this measurement is that you derive both the % coverage of the surfactant and the surface area each surfactant molecule occupies at saturation. The first number gives an indication of the colloidal stability which has been designed into the process and the second number gives a quantitative measure of the surface hydrophobicity of the latex.

Latex particle surface hydrophobicity can be estimated using the surfactant titration results to calculate the surface area occupied by each surfactant molecule at saturation. The more hydrophobic a surface, the more surfactant will pack onto it, thus the smaller the surface area per molecule. We have found that 100% PMMA is hydrophilic and yields a value in the range of 130-140 $Å^2$/SDBS, whereas 100% PBA is relatively hydrophobic and yields values in the range of 25-35 $Å^2$/SDBS. For this process we found values, shown in Figure 3, demonstrating that Stage II is very hydrophobic and Stage III does not fully "cover" Stage II, so Stage III is more hydrophobic than Stage I.

Surfactant coverage in each stage is shown in Figure 4. From previous work (5) we know that hydrophilic surfaces such as PMMA require very low surfactant coverage to achieve mechanical stability. Even 20% coverage can be adequate. By this criterion Stage I is adequately stabilized and Stage III may be adequately stabilized. On the other hand, hydrophobic surfaces such as PBA or PSty often require surfactant coverage greater than 50% to achieve good stability. Clearly, the 14% surfactant coverage in Stage II is a potential problem.
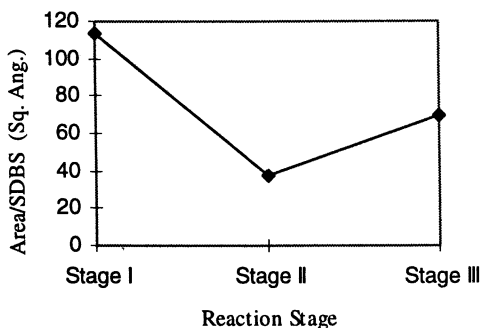
Figure 3. Area each SDBS surfactant molecule occupies on the latex surface saturated with SDBS. Area is expressed as Å² per molecule.
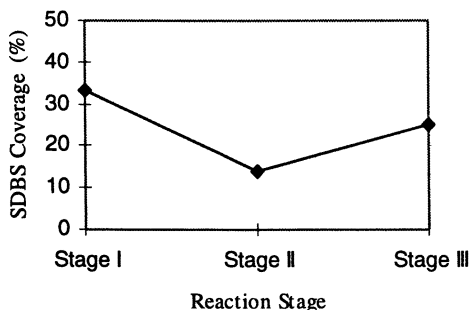
Figure 4. SDBS surfactant coverage of the latex as a function of reaction stage. Coverage is expressed as % of saturation as determined by surfactant titration.

Measured Shear Stability

One way of assessing the colloidal stability of latexes is to evaluate their mechanical stability using shear stability testing. For each stage of the reaction we measured the viscosity of the latex as a function of shear rate. Latexes generally demonstrate a reduced viscosity with increasing shear rate. If the latex becomes mechanically unstable and coagulates, then this is manifested by an

increase in viscosity at the critical shear rate. Figure 5 shows the shear stability curves for the samples from Stage I hold, Stage II monomer feed, and Stage II hold (in duplicate, for reproducibility). Stage I is shear stable up to 4000 s⁻¹, the limit of the measurement. By contrast, Stage II becomes shear unstable at the very low shear rate of 80 s⁻¹. Shear instability at 400 s⁻¹ is even evident during the monomer feed to Stage II. The maximum estimated shear rate in the reaction kettle in this stage is 260 s⁻¹, so there is a potential process problem as Stage II feed proceeds toward completion.

Figure 6 shows the shear stability for Stage III hold and the final latex. Clearly, these are shear stable up to 3000 sec⁻¹, the limit of the measurement.
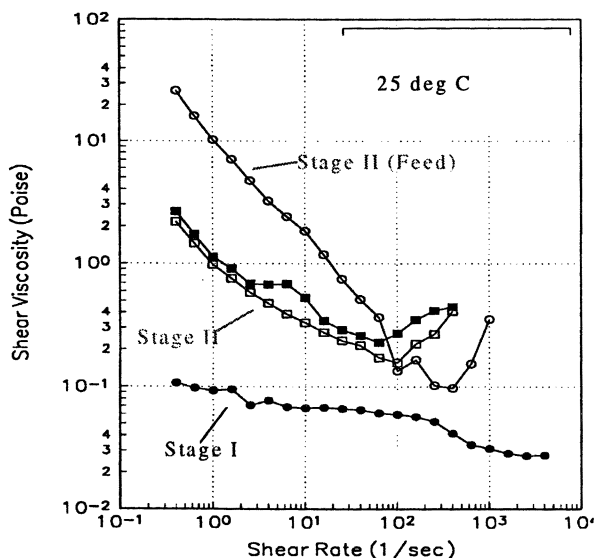
Figure 5. Latex viscosity as a function of shear rate for Stage I, Stage II monomer feed, and Stage II hold (in duplicate). Shear instability is evident for Stage II feed and hold.

Calculated Shear Stability

Particles are stable to mechanical shear if their interparticle potential energy, V_{tot}, exceeds the shear energy they are subjected to (6). This relationship can be expressed as $V_{tot} / kT > 4\eta\gamma a^3 / kT$, where k is the Boltzmann constant, T is temperature, η is the viscosity, a is the particle radius, and γ is the shear rate.

The right side of this expression is known as the Peclet number. Based on an estimated maximum shear rate in the reactor, the Peclet number was calculated to be between 30 kT and 40 kT during all of the reaction stages. Based on standard DLVO calculations (7) using the measured particle size, zeta potential, etc., the interparticle potential energy barrier during all of the stages was between 150 kT and 200 kT. According to these calculations, the particles should be extremely stable throughout the reaction, yet Stage II is obviously much less stable and prone to gel problems. This is shown in Figure 7, where the measured and classically calculated critical shear rates are compared.
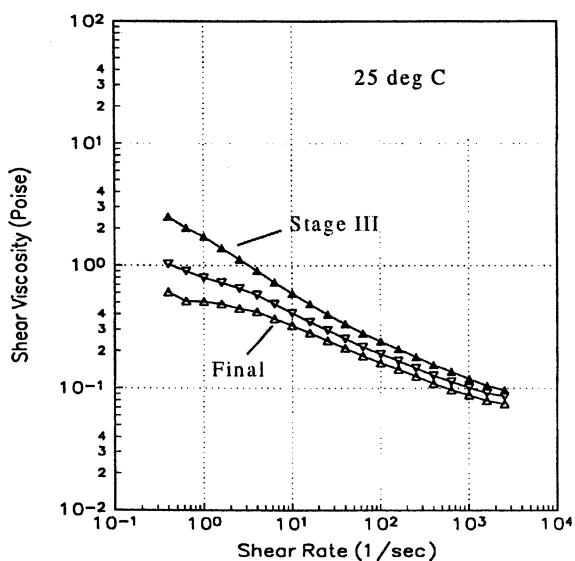
Figure 6. Latex viscosity as a function of shear rate for Stage III and final latex product. These are shear stable.

The major difference between Stage II and the other stages appears to be the increased hydrophobicity of the particle surface. In earlier work (5), we found that the hydrophobic attraction energy, V_s, can be estimated from the particle size and the % surfactant coverage on the particle. By adding V_s to the classical DLVO calculations, a new estimate of the shear stability can be calculated and it predicts poor shear stability for Stage II particles, as shown in Figure 8.
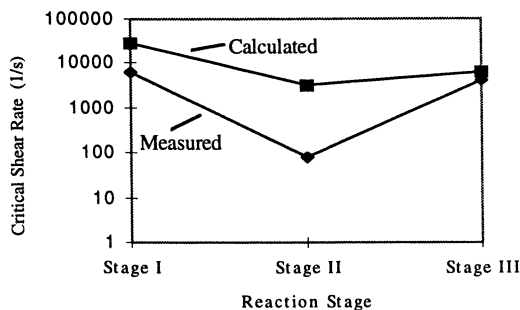
Figure 7. Calculated critical shear rate as a function of reaction stage using classical DLVO parameters. Stage I and Stage III actual measured critical shear rates are minimum limit values due to instrumental limitations.
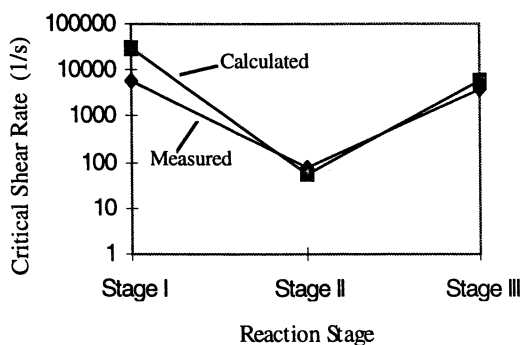
Figure 8. Calculated critical shear rate as a function of reaction stage using classical DLVO parameters plus hydrophobic attraction energy. Stage I and Stage III actual measured critical shear rates are minimum limit values due to instrumental limitations.

This good agreement with experimental results, in combination with our previous experience with such systems, suggests that hydrophobic interactions can play a significant role in process problems of coagulation and gel formation.

Conclusions

Emulsion polymerization reactions involve significant changes in colloidal properties during the course of the reaction. When both hydrophilic and hydrophobic stages are involved, classical DLVO colloid stability calculations may not necessarily identify unstable systems or their causes. A combination of

techniques is usually necessary to identify the root cause of colloidal instability during an emulsion polymerization reaction. Sampling and analyzing an emulsion polymerization reaction at several critical points can be very useful for troubleshooting and optimization. In the core/shell emulsion polymerization process analyzed in this paper, insufficient stabilization of the very hydrophobic Stage II was the cause of the process problems. An obvious approach to the problem is to increase the SDBS surfactant in Stage II to increase stability. Although this will work in principle, in practice the increased surfactant in the final product causes product performance problems. Fortunately, the colloidal analysis gave us some other options to pursue. These included adjustment of pH, agitation speed and agitator design, temperature, solids, and monomer feed conditions. Therefore, we have found detailed colloidal analysis of processes to be a useful approach to solving process problems which are often difficult to solve by more empirical methods.

Acknowledgments

References

1. O'Brien, R. W.; White, L. R. *J. Chem. Soc. Faraday Trans. II* **1978**, *74*, 1607.
2. Blackley, D. C. *Science and Technology of Polymer Colloids- Vol. I*; Poehlein, G.; Ottewill, R.; Goodwin, J., Eds.; Kluwer: Dordrecht, Holland 1983.
3. Aslamazova, T. R.; Bogdanova, S. V. *Colloid J.* **1995**, *57*, 135.
4. Aslamazova, T. R.; Bogdanova, S. V. *Colloid J.* **1995**, *57*, 143.
5. Kostansek, E. C. *Trends in Polymer Sci.* **1996**, *4*, 383.
6. Russel, W. B.; Saville, D. A.; Schowalter, W. R. *Colloidal Dispersions*; Cambridge Univ. Press: Cambridge, U.K., 1989.
7. Evans, D. F.; Wennerstrom, H. *The Colloidal Domain*; VCH: New York, NY, 1994.

Chapter 3

Particle Aggregation in Polymer Latexes

Marcel Verduyn, Jan Sefcik, Giuseppe Storti, and Massimo Morbidelli*

Laboratorium für Technische Chemie, ETH Zürich, Universitätstrasse 6, CH-8092 Zürich, Switzerland

Our aim is the fundamental effort to rationalize aggregation behavior of polymer latexes as a function of processing conditions and to formulate a unified approach to modeling particle size distribution in industrially relevant systems. This approach should result in quantitative and predictive engineering models indicating how one should manipulate operating conditions of polymerization reactors in order to achieve desired particle size distributions. We use population balance equations to model the time evolution of the particle size distribution in polymer latexes. The main challenge in using the population balance equations for quantitative description of aggregating systems is the determination of aggregation rate constants for a given composition, temperature, and flow conditions in the vessel. Colloidal interactions together with flow conditions and temperature determine the kinetics of particle aggregation. Although these factors are often coupled with each other in industrial conditions, we analyze them separately to achieve a proper physical description. We show examples of both experimental and modeling work on the characterization of polymer latex particles and their aggregation under a variety of conditions.

23

Modeling of the time evolution of particle size distributions in dispersions requires the use of population balance equations (*1*). For example, in the case of a batch emulsion polymerization reactor the appropriate population balance equation can be written as:

$$\frac{\partial f(v,t)}{\partial t}+\frac{\partial}{\partial v}\left(g(v,t)f(v,t)\right)=\frac{1}{2}\int_{v_0}^{v}K(v-v,v',t)f(v-v',t)f(v',t)\mathrm{d}v'-$$

$$\int_{v_0}^{\infty}K(v,v',t)f(v,t)f(v',t)\mathrm{d}v'+r_0(v_0)$$

(1)

where $f(v,t)$ is the density distribution of particles of volume v at time t. The first term on the left-hand side represents the accumulation and the second term represents growth due to polymerization, where $g(v,t)$ is the volume growth rate of a particle with volume v. The first two terms on the right-hand side account for particle aggregation and the last term accounts for nucleation (for details of this equation see (*1*)). The smallest - primary or nucleus - particle in the system has the volume v_0. Strategies for efficient solution of the population balance equation are available (*2*) once the matrix of aggregation rate constants, K (the collision kernel) is known.

Aggregation Rate Constants

The main challenge in using the population balance equations for quantitative description of aggregating systems is the determination of good aggregation rate constants K. They can generally be expressed as a product of collision frequency β and collision efficiency W^{-1}, $K=\beta/W$. Let us start from two well-known limiting cases for rapid aggregation without any repulsive barrier (*3*) introduced by Smoluchowski in 1917 that are especially relevant for polymer latexes:

1. Movement of an individual particle with collision radius a^c is due to Brownian motion with the corresponding diffusion coefficient D. This case is known as the perikinetic limit and the collision frequency is $\beta = 4\pi(a_1^c+a_2^c)(D_1+D_2)$.

2. Particles are carried by the fluid in a simple shear flow (a linear velocity profile with the uniform velocity gradient or shear rate G). This case is known as the orthokinetic limit with the collision frequency $\beta = 4G(a_1^c+a_2^c)^3/3$.

In the case of spherical particles one can use the Stokes-Einstein relationship, $D = kT/6\pi\mu a_h$, between the diffusion coefficient, D, and the hydrodynamic radius, a_h. Further, if the hydrodynamic radius is equal to the collision radius, we get for the perikinetic collision frequency $\beta_{peri} = (2kT/3\mu)(a_1+a_2)^2/(a_1 a_2)$. This is only weakly dependent on the particle size, while the orthokinetic collision frequency is strongly size dependent: $\beta_{ortho} = 4G(a_1+a_2)^3/3$. For a polymer latex swollen with monomer, as is the case during emulsion polymerization, it is reasonable to assume that two fluid colliding particles coalesce and their aggregate is again a sphere. For two equal size particles, the collision frequency in the perikinetic regime is $\beta = 8kT/3\mu = 1.23 \times 10^{-17}$ m^3/s in water at 25 °C, regardless of the particle size. In contrast, the orthokinetic collision frequency increases with the third power of particle size. Hence particles larger than a crossover size $a^* = (kT/4\mu G)^{1/3}$ corresponding to $\beta_{peri} = \beta_{ortho}$ undergo predominantly the flow driven aggregation. For a typical value of mean shear rate in a stirred vessel, $G = 100$ s^{-1}, we get this crossover at the particle diameter of $2a^* = 0.45$ μm.

The collision efficiency is the inverse of the stability ratio, W, related to the interparticle interaction energy, ψ (3). It was first introduced by Fuchs in 1934 and later corrected for the viscous resistance (4):

$$W = (a_1 + a_2) \int_{a_1+a_2}^{\infty} \frac{\exp(\psi(r)/kT)}{G(r,\lambda)r^2} dr \qquad (2)$$

Factor $G(r,\lambda)$ accounts for the viscous resistance caused by squeezing of fluid between two approaching solid surfaces and it is a function of the particle size ratio, $\lambda = a_1/a_2$. Appropriate expressions for solid and liquid interfaces are available (5).

While this is an appropriate approach for perikinetic conditions, in the case of particles carried by fluid flow, one has to account for the disturbance of fluid streamlines induced by the particles themselves. Resulting effects on aggregation rates have been previously modeled by numerous authors using trajectory analysis, but this was shown not to be a correct approach in the presence of Brownian diffusion (5). This simplified approach has not been satisfactory for proper understanding and predictive description of the kinetics of aggregation. We have previously suggested using a rigorous quantitative description of the relative particle motion in order to derive more realistic aggregation rate constants for emulsion polymerization systems (6), where both Brownian diffusion and fluid dynamics, always in the presence of interparticle interactions, determine these rate constants. We have shown that the additivity rule (i.e., a

simple linear combination of the two limiting expressions for K in the perikinetic and orthokinetic regimes, respectively) cannot be used for slowly aggregating systems (for more details see the last section).

Another important aspect of obtaining a realistic aggregation kernel in high shear turbulent flows is accounting for aggregate breakup. When an aggregate grows above the Kolmogorov scale of turbulent eddies (typically on the order of 50-100 μm), it is subject to turbulent stresses that can cause aggregate breakup and obviously affect the particle size distribution. We do not expand on this issue here; for further details see (3).

Interactions between Latex Particles

Our fundamental interest is to rationalize the aggregation behavior of latexes as a function of operating conditions. Let us now focus on relating the charging behavior of surfactant-stabilized polymer particles to the basic characteristics of a starting latex, such as: particle size and volume fraction, bulk solution concentrations of surfactant, initiator and salt. Surface charge density in turn determines the strength of electrostatic colloidal interaction between particles. Colloidal interactions together with flow conditions and temperature determine the kinetics of particle aggregation. All these factors are often coupled with each other in industrial conditions, but we would like to analyze them separately to achieve a proper physical description, which would then allow describing their dependencies correctly.

Colloidal particles are subject to forces due to interparticle interaction energy ψ. The interaction energy can be attributed to various sources. The most important interparticle forces and their origins are:

1. Born forces are repulsive forces always operating at atomic length scale. They occur when two atoms or molecules are in close contact so that their electron clouds overlap.
2. Forces arising from the electromagnetic fluctuations of matter; called van der Waals forces, are always operating and attractive when two particles of the same material are considered.
3. Electrostatic forces arising from the interaction between ionic diffuse layer surrounding the colloidal particles. The ionic diffuse layer is balancing the particle surface charge, which is due to ions adsorbed or bound to the surface. When two particles are equally charged, this force is always repulsive.
4. Other forces: steric, hydration, hydrophobic, etc. We do not expand on this topic here; see (7) for further discussion.

The total energy of interparticle interaction, ψ, is expressed as the sum of the respective contributions listed above. In the case of spherical symmetry for the interaction force, as expected for spherical latex particles, ψ varies in the radial direction only. Then it can be expressed as a function of dimensionless center-to-center distance, $\xi = r/a$, where a is the arithmetic mean of radii of interacting particles, a_1 and a_2, and r is their center-to-center distance. At close contact between two particles, the interparticle forces are balancing each other at the point of the primary minimum of interaction energy. Born repulsion increases very steeply for smaller separations and decays rapidly for larger ones. If the aggregation of particles in the primary minimum can be considered to be irreversible for practical purposes at $\xi = 2$, the Born repulsion is appropriately described by the hard core approximation ($\psi_{Born} = 0$ at $\xi > 2$, $\psi_{Born} = +\infty$ at $\xi \leq 2$) to ensure that solid particles do not penetrate each other. Combining the Born hard core repulsion with the attractive van der Waals and repulsive electrostatic interactions, $\psi(\xi) = \psi_{att}(\xi) + \psi_{rep}(\xi)$, results in the framework of the classical DLVO theory introduced by Landau, Derjaguin, Verwey and Overbeek in the 1940's (7).

van der Waals Attractive Interaction

The attractive potential energy of interaction, ψ_{att}, can be calculated assuming that intermolecular van der Waals forces are pairwise additive and integrating over the interior volume of two interacting particles. The result for two spheres was obtained by Hamaker in 1937 and in a dimensionless form (scaled by kT) it can be expressed as (3):

$$\psi_{att}(\xi) = -\frac{Ha}{6}\left[\frac{8\lambda}{(1+\lambda)^2}\left(\frac{1}{\xi^2-4}+\frac{1}{\xi^2-4\Lambda^2}\right)+\ln\left(\frac{\xi^2-4}{\xi^2-4\Lambda^2}\right)\right] \qquad (3)$$

where Ha is the dimensionless Hamaker constant (scaled by kT) and $\Lambda = (1-\lambda)/(1+\lambda)$. We do not consider retardation effects (8) which are important over larger distances than those usually relevant to calculation of a stability ratio, W, for aggregation kinetics.

Electrostatic Repulsive Interaction

Electrical diffuse layer interactions can be thought of in terms of two limiting regimes, where either the surface potential, Φ, or the surface charge

density, σ, remains constant. If particles approach each other sufficiently slowly, electrostatic equilibrium can be maintained by redistribution of the surface charge, and hence the surface potential remains constant. However, in the other limiting case, during the time scale of a Brownian encounter, the diffusion of ions necessary to maintain electrostatic equilibrium is not fast enough so that particles approach each other with constant surface charge rather than constant surface potential. Situations intermediate between these two limiting cases can be modeled using the charge regulation regime taking into account shifting ionic equilibria during the particle approach (9). Note that the surfaces of the polymer particles are assumed to be smooth and the surface charge is assumed to be homogeneously distributed. It is useful to consider two limiting cases of constant surface potential and constant surface charge.

Linear theory suitable for small surface potentials ($\Phi < kT/e$) is based on the Debye-Hückel approximation (linearization of Poisson-Boltzmann equation) to calculate the exact repulsive interaction energy for two flat plates. Then one can use the Derjaguin formula (8) to calculate the corresponding interaction between spheres at separations small compared to their radius ($h \ll 1$) by expanding the potential as a series in powers of $1/\kappa a$ (so that it is required that κa is large, cf. (8)). For the case of constant surface potential this approach was used by Hogg, Healy and Fürstenau (10):

$$\psi_{rep}(\xi) = 2\pi N_R Ha \frac{\lambda}{(1+\lambda)^2}\left(1+\Phi^2\right)\times$$

$$\left[\frac{2\Phi}{1+\Phi^2}\ln\left(\frac{1+\exp\{-\kappa a(\xi-2)\}}{1-\exp\{-\kappa a(\xi-2)\}}\right) + \ln\left(1-\exp\{-2\kappa a(\xi-2)\}\right)\right] \quad (4)$$

where $\Phi = \Phi_2/\Phi_1$ is the ratio of particle surface potentials, $Ha = A/kT$ is the dimensionless Hamaker constant and $N_R = \varepsilon a\Phi_1^2/A$ expresses the importance of the repulsive forces relative to the attractive ones (11). As surface potentials become larger, the linear theory becomes progressively less accurate compared to the full solution of the non-linear Poisson-Boltzmann equation. For example, Oshima and Kondo (12) developed a more accurate approximation of the non-linear potential energy of interaction for the case of equal spheres (again, it is required that $h \ll 1$ and $\kappa a \gg 1$). In the limit of $\Phi \ll kT/e$ we recover the linear formula (eqn. 4).

For the case of constant surface charge, an expression similar to that for the constant potential case (eqn. 6) was derived. However, while the constant potential expression is accurate as the gap $h = \xi-2$ diminishes, the constant charge expression leads to infinite surface potentials for h approaching zero and thus the Debye-Hückel approximation becomes inaccurate. Therefore for the

case of the constant surface charge such an expression is not suitable for calculation of a stability ratio for aggregation kinetics. Instead, one can use a method recently introduced by Oshima (*13*) based on analytical approximations for the potential energy of interaction between two flat plates accurate at short distances ($\kappa a h$ <2). The potential energy of interaction between two equal spheres is then computed by numerical integration of the Derjaguin formula, avoiding expansions in powers of $1/\kappa a$ and thus resulting divergence of the interaction energy at zero surface-to-surface separation. For further details see (*13*).

Example: Modeling Emulsion Polymerization of Vinyl Chloride

The population balance equation model for the emulsion polymerization of vinyl chloride was presented (*14*), accounting for a detailed kinetic scheme of polymerization and interparticle interactions including the van der Waals attractive term (eqn. 3) and the electrostatic repulsion term (eqn. 4). Effects of particle aggregation in the perikinetic regime during emulsion polymerization were analyzed. It was shown that aggregation plays an important role in the emulsion polymerization process, since it not only modifies the particle size distribution, but also affects the conversion history. In Figure 1 we show the time evolution of conversion during the emulsion polymerization of vinyl chloride calculated with: (a) no aggregation; (b) $\Phi_1 = 40$ mV, $I = 20$ mM; and (c) $\Phi_1 = 40$ mV, $I = 50$ mM, where Φ_1 is the particle surface potential and I is the ionic strength (eqn. 8). In Figure 2 we show the corresponding final particle size distributions.

Parametric analysis also showed that only a large addition of salt may cause a significant variation in aggregation behavior, while the effect of surface potential even by a few percent causes variation over many orders of magnitude in colloidal stability. This result helps to explain the poor agreement between experimentally-measured doublet formation rates and classical perikinetic regime theory in the presence of the electrostatic repulsion (*18*).

Characterization of Surfactant Stabilized Latex Particles

Surfactant Adsorption Isotherm

Sodium dodecyl sulfate (SDS) in a latex is partitioned between the surface of the polymer particles and the aqueous phase. The overall mass balance for SDS in the latex dispersion can therefore be written as $C_{s,tot} = C_{s,w} + S_p\gamma$, where $C_{s,tot}$ is the total concentration of SDS in the latex dispersion, expressed in moles
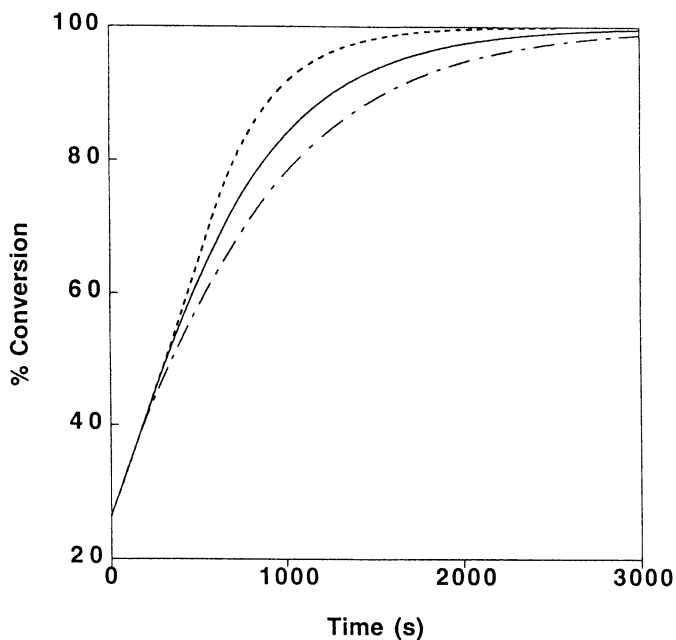
Figure 1. Conversion during emulsion polymerization of vinyl chloride.
Calculations with: no aggregation (dashed line); $\Phi_1=40$ mV, $I=20$ mM (solid
line); $\Phi_1=40$ mV, $I=50$ mM (dot-dashed line).
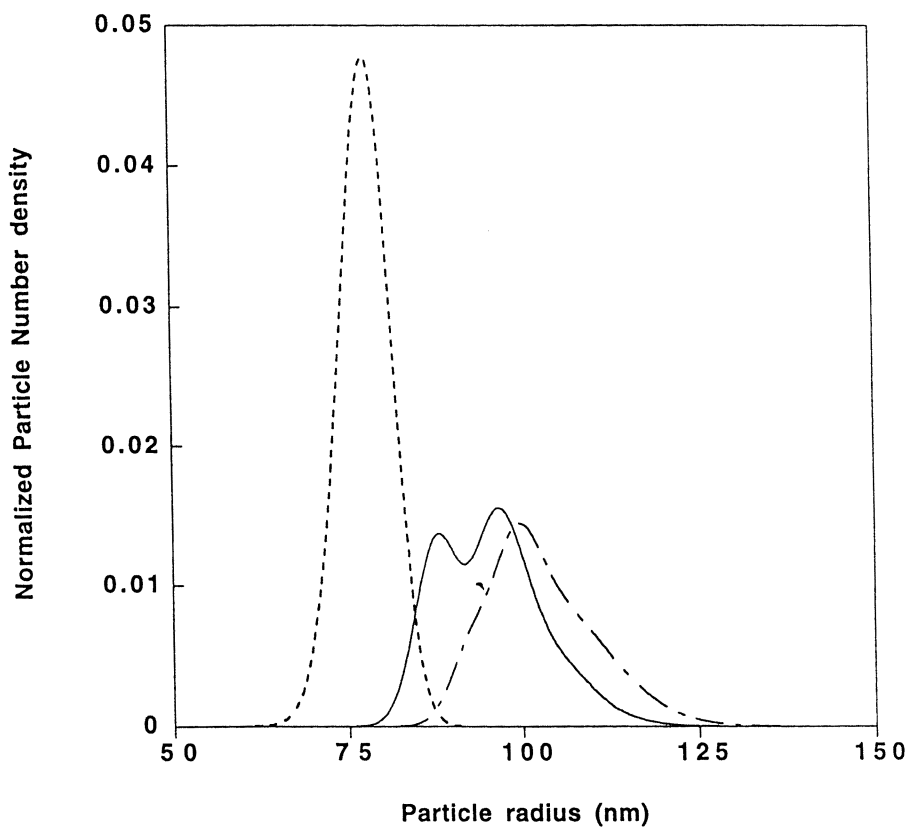
Figure 2. Final particle size distribution for emulsion polymerization of vinyl chloride. Calculations with: no aggregation (dashed line); Φ_1=40 mV, I=20 mM (solid line); Φ_1=40 mV, I=50 mM (dot-dashed line).

per unit volume of aqueous phase. $C_{s,w}$ is the SDS concentration in the aqueous phase, S_p is the particle surface area per unit volume of the aqueous phase, and γ is the concentration of SDS on the surface of the polymer particles (mol/m^2).

To determine the surfactant adsorption isotherm, the aqueous phase SDS concentration was measured (15) using ion chromatography at different values of the total SDS concentration in the system. The experimental adsorption isotherm was very well described with a Langmuir expression:

$$\gamma = \frac{6.4 \times 10^{-3} \, C_{s,w}}{1 + 1.5 \times 10^3 \, C_{s,w}} \quad (5)$$

Our data also agree well with recently published data for the adsorption of SDS from water on polystyrene layers (16). In a typical polystyrene latex with a solid weight fraction of about 15% and the average particle diameter of 0.1 μm, only about 2% of the SDS remains in the aqueous phase.

Surface Charge and Ionic Diffuse Layer

Electrostatic charges on the surface of colloidal polymer particles are partly due to ionic end groups of the polymer chains (because of the initiator used during emulsion polymerization) but the main contribution is due the dissociated groups of surfactant molecules adsorbed on the particle surface. The surfactant molecules have a nonpolar tail that is in close contact with the polymer particle surface and an ionic head, which prefers the aqueous side. The adsorption of surfactant molecules results in a dissociable surface group density, σ_0, calculated as $\sigma_0 = \gamma N_A$, where γ is the surfactant surface concentration (mol/m^2) on the polymer particle. The calculation of γ will be discussed later. A certain amount of surfactant counterions does not dissociate and their surface density is σ_i. Consequently, the net surface charge density σ equals $\sigma_0 - \sigma_i$. The distribution of charge immobilized near the surface can be also modeled in more detail using Stern layer models of varying complexity in conjunction with appropriate counterion adsorption isotherms (17).

The interplay between energy and entropy of counterions free to move in the aqueous phase together with the requirement of macroscopic electrical neutrality implies the presence of a diffuse layer around each particle. The potential energy of repulsion, ψ_{rep}, for a pair of particles is due to electrostatic repulsion when these diffuse layers overlap. The surface electrostatic potential, Φ, is needed to calculate the potential energy of repulsion for the pair of particles. The surface charge density can be related to surface electrostatic potential using an appropriate model describing the diffuse layer.

For the case of 1-1 electrolytes we can use the Gouy-Chapman model where the (non-linear) Poisson-Boltzmann equation is solved for the potential in the diffuse layer around a spherical particle:

$$\sigma = \frac{\varepsilon kT\kappa}{e}\left[2\sinh\left(\frac{e\Phi}{2kT}\right)+\frac{4}{\kappa a}\tanh\left(\frac{e\Phi}{4kT}\right)\right] \tag{6}$$

This equation gives the surface charge density within 5% of an accurate numerical solution of the Poisson-Boltzmann equation for any value of surface potential Φ and $\kappa a > 0.5$ (8). Here a is the radius of the particle and κ (inverse of the Debye decay length) is given by:

$$\kappa = \sqrt{\frac{2e^2 N_A I}{\varepsilon kT}} \tag{7}$$

where the ionic strength, I, is calculated as:

$$I = \frac{1}{2}\sum_i z_i^2 c_{i,\infty} \tag{8}$$

$c_{i,\infty}$ being the bulk concentration of ions of type i. N_A is the Avogadro number, e is the charge of an electron, and ε is the electric permittivity of the aqueous phase.

Example: Coalescence in Surfactant-Stabilized Latexes

Brownian aggregation kernel was developed for latexes stabilized by adsorbed emulsifier with detailed physico-chemical description of the diffuse layer, including the Stern layer and dissociation equilibrium of emulsifier ionic groups at the particle. The Stern layer model accounts for the adsorption of counterions on the ionic groups of the emulsifier. The counterion adsorption equilibrium was described using a Langmuir expression (15).

Aggregation behavior of poly(vinyl acetate) seed latexes swollen with the monomer was studied at various operating conditions (particle size, ionic strength, stirring rate, and geometry) (18). For typical operating conditions used in this study (reactor volume 1-2 L, stirring rates 400-1400 rpm, various impellers) it was observed that fluid dynamics did not significantly affect particle aggregation (Figure 3). This indicates that local shear rates were not high enough to reach the orthokinetic regime, so that perikinetic aggregation was dominant.
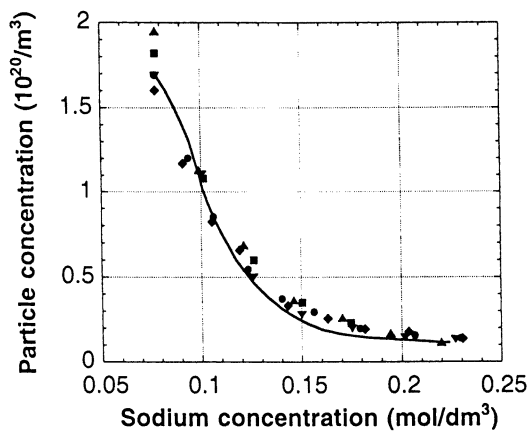
Figure 3. Particle number concentration in swollen poly(vinyl acetate) latex 30 minutes after salt addition. Symbols show experimental data for various stirring conditions. Line shows model prediction for perikinetic regime.

This is in agreement with theoretical calculations (*6*) for thin diffuse layers, which was the case under the operating conditions examined.

The equilibrium constant of the Langmuir isotherm for the counterion adsorption on the ionic groups of the emulsifier was estimated by fitting the experimental data for the particle size evolution of a particular latex at a particular salt concentration. Using this kernel, the aggregation of poly(vinyl acetate) particles was modeled with the population balance equation in good agreement with the experimental data covering a range of operating conditions in terms of particle size, salt concentration, and fluid stirring. In Figure 3 we show the particle number concentration in swollen poly(vinyl acetate) latex at 30 minutes after the salt addition, when the particle size and number reaches a plateau, i.e. changes very slowly at the timescale considered. It can be seen that there is little impact from different stirring conditions represented by various symbols in Figure 3, where the solid line shows the model prediction for perikinetic regime.

Effect of Fluid Motion: Two Particle Aggregation Model

As mentioned above, the evolution of the particle size distribution in an aggregating dispersion can be described using population balance equations with an appropriate aggregation kernel, whose reliability is determined by the adopted particle aggregation model. In the classical approach by Smoluchowski, later modified to account for interparticle interactions, the aggregation rate constants for spherical particles are given for two limiting regimes: diffusion driven (perikinetic) and simple shear flow driven (orthokinetic). Effects of fluid flow on particle aggregation below the turbulent eddy scale were previously modeled using trajectory analysis. However, these simplified approaches have not been satisfactory for proper understanding and description of aggregation phenomena (*5*).

We used the convection-diffusion equation describing the relative motion of a pair of particles embedded in a turbulent eddy inside a well mixed vessel to derive more realistic particle aggregation rate constants (*6*). This equation, also called the pair probability equation, constitutes a rigorous and comprehensive mathematical model of particle aggregation. It accounts for the three main mechanisms underlying particle aggregation:

1. Brownian diffusion,
2. particle-particle interactions,
3. convection by fluid flow.

The evaluation of local flux contributions from the first two mechanisms was the same as discussed earlier. The pair probability equation accounting for all these mechanisms of particle transport was solved numerically and the aggregation rate coefficient for each pair of colliding particles was obtained as a function of particle sizes, turbulence intensity, emulsifier coverage and ionic strength.

Through the model, a series of parametric calculations was performed to investigate the effect of various operating parameters of interest in applications such as particle size, ionic strength, and mixing intensity on the aggregation rate constant. In all cases it was found that the results of the rigorous model approach the limits of perikinetic and orthokinetic aggregation, as described by simpler models previously developed in the literature, for very small and very large values of the Peclet number, respectively. For fast aggregating systems, we have shown that the diffusive and convective contributions to the aggregation rate are independent, so that the additivity assumption for the fluxes can be used to calculate the overall aggregation rate for intermediate values of the extension rate. However, in general, only the rigorous model results are appropriate for intermediate values. Systems undergoing slow aggregation in the presence of repulsive barrier exhibit a strong non-linear coupling between convection and diffusion, which causes both the flux additivity assumption and the trajectory analysis to fail. In Figure 4 we show the aggregation rate constant vs. shear rate E for slow aggregation ($a = 100$ nm, $\lambda = 1$, $N_R = 2.39$, $\Phi = 1$, $\kappa a = 10.4$) calculated from the rigorous model compared to the sum of perikinetic and orthokinetic contributions (underprediction in intermediate regime) and to the flux from trajectory analysis plus diffusive contribution (overprediction in intermediate regime). An extent of coupling between convection and diffusion is determined by the thickness of electrical double layer. As can be seen in Figure 5, a dependence of the aggregation rate constant on the Peclet number $Pe=Ea^2/D_0$, where D_0 is the particle mutual diffusion coefficient, is sensitively dependent on the thickness of the electrical double layer.

To apply this model to simulate aggregation under experimental conditions, population balance equations are employed, along with an effective approach to its numerical solution. A code implementing the aggregation model discussed above in the population balance was developed. Its numerical solution was achieved by the discretization method proposed by Ramkrishna (2). The resulting model was used to simulate the behavior under reaction conditions. The population balance model was modified by adding nucleation and growth terms. A comprehensive kinetic scheme was considered to describe the polymerization reaction both in aqueous and particle phase. Along with standard reactions such as initiation, propagation and terminations, different branching mechanisms have been included to allow the simulation of systems with nonlinear polymer chains. The calculated conversion and molecular weight distribution compared well with
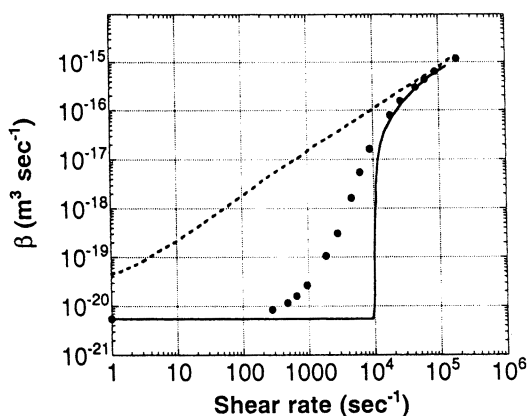
Figure 4. Aggregation rate constant for slow aggregation of spherical particles in extensional flow. Sum of perikinetic and orthokinetic contributions: solid line; Trajectory analysis plus diffusive contribution: dashed line; Rigorous model: symbols.
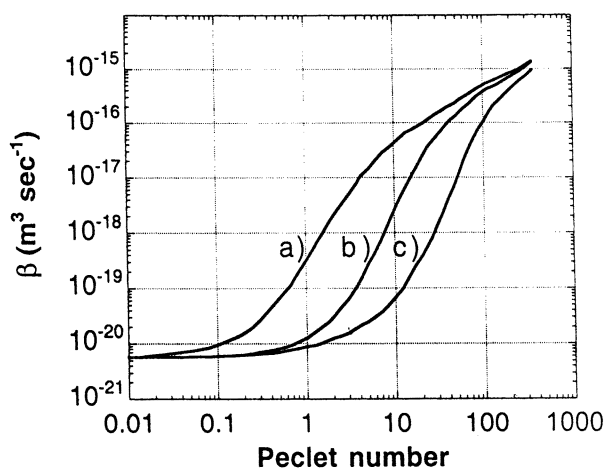
Figure 5. Aggregation rate constant for particles with the same stability ratio but different thickness of the electrical double layer. (a) κ =83 nm, (b) κ =9.6 nm, (c) κ =2.3 nm.

the experimental one for the emulsion polymerization of vinyl chloride in semibatch (*19*).

Conclusions

We used population balance equations to model the time evolution of the particle size distribution in polymer latexes. The main challenge in using the population balance equations for quantitative description of aggregating systems is the determination of aggregation rate constants for a given composition, temperature, and flow conditions in the vessel. Colloidal interactions together with flow conditions and temperature determine the kinetics of particle aggregation. Although these factors are often coupled with each other in industrial conditions, we analyzed them separately to achieve a proper physical description. This allowed us to rationalize the aggregation behavior of polymer latexes as a function of processing conditions and to suggest an approach to modeling particle size distribution in industrially relevant systems. This approach should lead to quantitative and predictive engineering models indicating how one should manipulate operating conditions of polymerization reactors in order to achieve desired particle size distributions.

Acknowledgments

References

1. Min, K. W.; Ray, W. H. On the Mathematical Modeling of Emulsion Polymerization Reactors. *Journal of Macromolecular Science - Reviews in Macromolecular Chemistry* **1974**, *C11*, 177-255.
2. Ramkrishna, D. *Population Balances*; Academic Press: London, 2000.
3. Elimelech, M.; Gregory, J.; Jia, X.; Williams, R. A. *Particle Deposition and Aggregation*; Butterworth-Heinemann: Woburn, MA, 1995.
4. Spielman, L. A. Viscous Interactions in Brownian Coagulation. *Journal of Colloid and Interface Science* **1970**, *33*, 562-571.
5. van de Ven, T. G. M. *Colloidal Hydrodynamics*; Academic Press: London, 1989.

6. Melis, S.; Verduyn, M.; Storti, G.; Morbidelli, M.; Baldyga, J. Effect of Fluid Motion on the Aggregation of Small Particles Subject to Interaction Forces. *AIChE Journal* **1999**, *45*, 1383-1393.

7. Israelachvili, J. N. *Intermolecular and Surface Forces* (2nd Edition); Academic Press: London, 1992.

8. Russel, W. B.; Saville, D. A.; Schowalter, W. R. *Colloidal Dispersions*; Cambridge University Press: Cambridge, 1989.

9. Behrens, S. H.; Borkovec, M. Electrostatic interaction of colloidal surfaces with variable charge. *Journal of Physical Chemistry B* **1999**, *103*, 2918-2928.

10. Hogg, R.; Healy, T. W.; Fürstenau, D. W. Mutual Coagulation of Colloidal Dispersions. *Transactions of Faraday Society* **1966**, *62*, 1638-1651.

11. Zeichner, G. R.; Schowalter, W. R. Use of Trajectory Analysis to Study Stability of Colloidal Dispersions in Flow Fields. *AIChE Journal* **1977**, *23*, 243-253.

12. Oshima, H.; Kondo, J. Approximate Analytic Expression for Double-Layer Interaction at Moderate Potentials. *Journal of Colloid and Interface Science* **1988**, *122*, 591-592.

13. Oshima, H. Diffuse Double-Layer Interaction between Two Identical Spherical Colloidal Particles. *Journal of Colloid and Interface Science* **2000**, *225*, 204-208.

14. Melis, S.; Ghielmi, A.; Storti, G.; Morbidelli, M. Aggregation phenomena in emulsion polymerization of vinyl chloride. *Entropie* **1998**, *212/213*, 65-72.

15. Verduyn, M. Ph.D. thesis, Swiss Federal Institute ot Technology (ETH), Zürich, **1999**.

16. Turner, S. F.; Clarke, S. M.; Rennie, A. R.; Thirtle, P. N.; Cooke, D. J.; Li, Z. X.; Thomas, R.K. Adsorption of Sodium Dodecyl Sulfate to a Polystyrene/Water Interface Studied by Neutron Reflection and Attenuated Total Reflection Infrared Spectroscopy. *Langmuir* **1999**, *15*, 1017-1023.

17. Lyklema, J. *Fundamentals of Interface and Colloid Science* (Volume II); Academic Press: London, 1995.

18. Melis, S.; Kemmere, M.; Meuldijk, J.; Storti, G.; Morbidelli, M. A Model for the Coagulation of Polyvinyl Acetate Particles in Emulsion. *Chemical Engineering Science* **2000**, *55*, 3101-3111.

19. Forcolin, S.; Marconi, A. M.; Ghielmi, A.; Butte, A.; Storti, G.; Morbidelli, M. Coagulation Phenomena in Emulsion Polymerisation of Vinyl Chloride. *Plastics, Rubber and Composites* **1999**, 28, 109-115.

Chapter 4

Probing the Effects of Polymer–Particle Interactions in Solution by Microrheology

L. A. Hough and H. D. Ou-Yang

Department of Physics, Lehigh University, 16 Memorial Drive East, Bethlehem, PA 18015

In this study, the technique of oscillating optical tweezers is used to determine the storage and loss moduli of a transient polymer network in the vicinity of a silica particle. The motivation for this study arises from the recent interests in the differences between the microrheology and macrorheology of polymer and biopolymer systems. One difference comes from interactions between the probe particle surface and the polymer media. To study the effects of surface interactions, we use a polymer with hydrophobic end groups and a hydrophilic backbone, probed by silica particles. Although the qualitative behavior is similar between microrheology and bulk rheology measurements, the differences are significant. Specifically, the plateau modulus of the polymer solution measured by the optical tweezers is significantly smaller than that measured by conventional bulk rheology techniques. The relaxation time, however, is measured to be significantly longer than that measured by conventional techniques. To our knowledge, there is not a theory that predicts the rheological behavior of polymer media including surface interactions.

40   © 2002 American Chemical Society

Most polymer solutions exhibit interesting flow properties that are quite different from the flow of simple liquids. Much of these unusual flow behaviors originate from the viscoelastic nature of these polymer materials. Viscoelastic materials store and dissipate energy in relative amounts in response to mechanical stress applied at different rates. When oscillatory shear stress is applied to viscoelastic materials, the resulting strain is composed of an in-phase and an out-of-phase part. The in-phase elastic response is determined by the storage modulus, $G'(\omega)$, and the out-of-phase viscous response is determined by the loss modulus, $G''(\omega)$.

Many of the recent advances in rheology are based on the understanding of the relationship between material structural and dynamic properties and the mechanical response function, or the viscoelasticity, of the material. Rheology makes it possible to gain useful information about the polymer structure and the dynamic change of the structural changes under imposed stress by measuring the storage and loss moduli, even though it is not always possible to visualize the polymer structures directly.

Traditionally, the storage and loss moduli are determined with a macroscopic mechanical rheometer. In this case, measured quantities reflect a spatial average over the length scale of the sample, usually on the order of a few millimeters. Recently, new microrheology methods have been developed which determine the storage and loss moduli from the thermal, or forced motion of individual colloidal probe particles (1-4). Microrheology differs from conventional macroscopic rheology in that it probes the local viscoelastic properties in the vicinity of a colloidal probe particle with length scales comparable to the length scale of homogeneity and a large dynamic frequency range. Determining the local viscoelastic properties near colloidal probe particles may prove useful in testing theories of surface-polymer interactions, as well as theories of polymer dynamics on a microscopic scale. In this paper, the effect due to surface interactions between a polymer solution and a colloidal particle on the storage and loss moduli is determined by utilizing oscillating optical tweezers.

The Forces on a Particle in an Oscillating Optical Tweezer

Optical tweezers, also known as laser traps, were first developed by Ashkin (5). A laser trap is produced by a large electric field gradient from a strongly focused laser beam. There are many ways to calculate the force a laser exerts on a trapped particle. For particles comparable to, or smaller than, the wavelength of the light of the trapping laser, the electrostatic potential approximation works well. From the consideration of the electrostatic potential produced by a

polarizable particle in an electrostatic field, the force on the particle from a laser with a Gaussian intensity profile can be approximated as (6,7):

$$\vec{F} = -\alpha \frac{n_1 V}{cR^2}\left(\frac{n_2^2 - n_1^2}{n_2^2 + 2n_1^2}\right) I_0 e^{-r^2/R^2} r\hat{r} \equiv k_{ot} r e^{-r^2/R^2}\hat{r} \tag{1}$$

where α is a geometrical factor of the order one, n_1 and n_2 are the indices of refraction of the solvent, and the particle respectively, V is the volume of the particle, c is the speed of light, R is the radius of the laser beam at $1/e^2$ of the intensity at the axis, I_0 is the laser intensity, and r is the distance between the centers of the particle and the laser trap. For small displacements $r \ll R$, the force follows Hooke's law with a spring constant k_{ot}. Since the wavelength of the laser is on the order of a micron, this is a good approximation for the micron-sized particles used in this study.

Equation of Motion of a Particle Trapped in an Oscillating Tweezer in a Neat Liquid

If a particle in an optical tweezer is allowed to oscillate by oscillating the tweezers via a piezo mirror, the equation of motion of the particle takes on the following form (4,7,8):

$$m\ddot{x} + 6\pi\eta a\dot{x} + k_{ot}x = k_{ot}Ae^{i\omega t} + f(t) \tag{2}$$

where m is the mass of the particle, η is the dynamic viscosity, a is the radius of the particle, A is the amplitude of the oscillating tweezer, ω is the angular frequency of the oscillating tweezer, and $f(t)$ is the fluctuating Brownian thermal force. In the absence of a driving force, equation 2 can be solved in frequency space to obtain the power spectrum of a thermally fluctuating particle in a harmonic potential (9). In our case, because of the way that the data are acquired, only time-average position of the center of mass is relevant, such that equation 2 has a steady-state solution:

$$\bar{x}(t) = D(\omega)e^{i(\omega t - \delta)} \tag{3}$$

where $\bar{x}(t)$ is measured over a time period, $\tau \gg 1/\omega$, and the amplitude and phase shift of the response are:

$$d(\omega) = \frac{D}{A} = \frac{k_{ot}}{\sqrt{(6\pi\eta a\omega)^2 + (k_{ot} - m\omega^2)^2}} \qquad (4a)$$

$$\delta(\omega) = \tan^{-1}\frac{6\pi\eta a\omega}{k_{ot} - m\omega^2} \qquad (4b)$$

To detect the position of the center of mass of the particle, the forward scattering of the particle from the trapping laser itself is collected (10). In this case, the time average position of the center of mass is given by a transformation from the moving reference frame relative to the oscillating laser, to the stationary lab frame. The transformation is given by:

$$\bar{x}(t) = \bar{x}'(t) - Ae^{i\omega t} \qquad (5a)$$

where, $\bar{x}'(t)$ indicates the position relative to the oscillating laser. The position can be decomposed into a measured phase, $\delta'(\omega)$, and displacement, $d'(\omega)$. The relations between the phase and displacement relative to the oscillating reference frame and phase and the displacement relative to the stationary lab frame are given by:

$$d(\omega) = \sqrt{d'^2 - 2d'\cos(\delta') + 1} \qquad (5b)$$

$$\delta(\omega) = \tan^{-1}\frac{d'\sin\delta'}{d'\cos\delta' - 1} \qquad (5c)$$

Equation of Motion of a Particle Trapped in an Oscillating Tweezer in a Viscoelastic Material

If the particle is placed in a viscoelastic material, rather than a purely viscous liquid, the equation of motion of the center of mass of the particle reduces to the form:

$$(-m\omega^2 + 6\pi a G^*(\omega) + k_{ot})d(\omega)e^{-i\delta(\omega)} = k_{ot} \qquad (6)$$

where $G^*(\omega)$ is the complex shear modulus, such that $G^*(\omega)=G'(\omega)+iG''(\omega)$, and where the in-phase component, $G'(\omega)$ is the storage modulus, and the out-of-

phase component, $G''(\omega)$ is the loss modulus. If k_{ot} is determined by fitting the measured phase and displacement to equation 4, in a neat liquid of well-defined frequency-independent viscosity, then $G'(\omega)$ and $G''(\omega)$ can be determined from the following relations (4):

$$G'(\omega) = \frac{k_{ot}}{6\pi a}\left[\frac{\cos\delta}{d} - 1 + \frac{m\omega^2}{k_{ot}}\right] \qquad (7a)$$

$$G''(\omega) = \frac{k_{ot}\sin\delta}{6\pi ad} - \omega\eta_{solvent} \qquad (7b)$$

Experimental

Experimental Setup

The experimental apparatus shown in Figure 1, consists of an optical tweezer formed by focusing an independently-steered laser beam (Spectra Physics Millenia, $\lambda = 532$ nm), using a microscope objective (Olympus UplanApo 100x NA 1.35) in an inverted microscope (Olympus IX-70). The trap is oscillated with a high-frequency piezo-driven mirror S224 (Physik Instrumente). To detect the center of mass of the particle's position, forward scattered light is collected by the microscope condenser, CDSR, and projected to a split photodiode, PS. The photodiode is located at the optical conjugate point of the trap such that there is not a signal when the particle is in the center of the laser. The signal from the photodiode is then sent to a lock-in amplifier, where the phase shift and displacement of the center of mass of the particle's oscillation relative to that of the laser beam is measured.

Experimental Procedure and Results

In this study, individual 1.6 micron diameter SiO_2 particles (Duke Scientific) are placed into forced harmonic motion using the method described above. The oscillation amplitude of the laser is A=40 nm. Figures 2 and 3 show the phase and normalized displacement of a 1.6 micron particle in water averaged over 10 frequency sweeps. The data set so obtained is converted from the oscillating frame to the stationary lab frame by the use of equations 5b and 5c. Because the dynamic viscosity of water is known, $\eta = 0.0092$ Poise, the only fitting parameter in equations 4a and 4b is the spring constant, k_{ot}. The solid lines are generated from equations 4a and 4b with the single fitting parameter, k_{ot}=0.0175 dynes/cm.
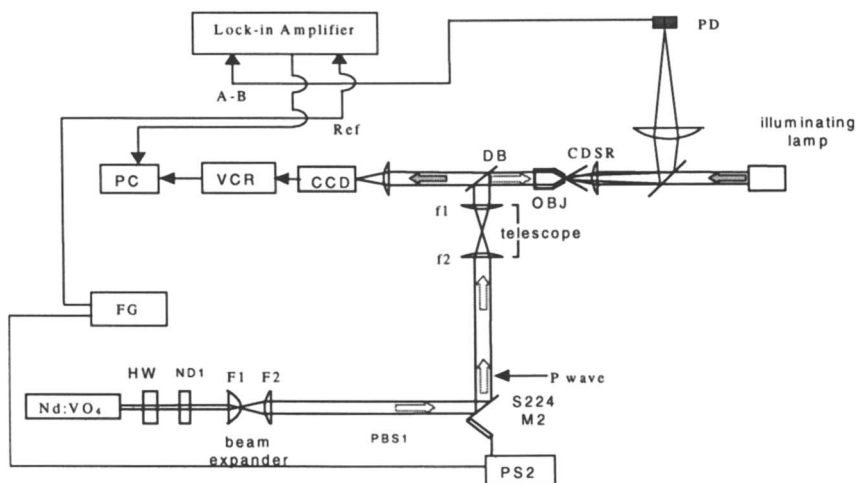
Figure 1. A schematic of dual-tweezer setup. HW is a half-wave plate, ND, neutral density filter, PBS, polarizing beam splitter, S224 is the piezo-controlled mirror, PS, piezo power supply, DB, dichroic mirror to allow laser beam to reflect and long wavelength illuminating light to pass. The sample is located immediately to the right of the objective lens OBJ. (Reproduced from reference 4. Copyright 1999 Kluwer Academic Publishers.)
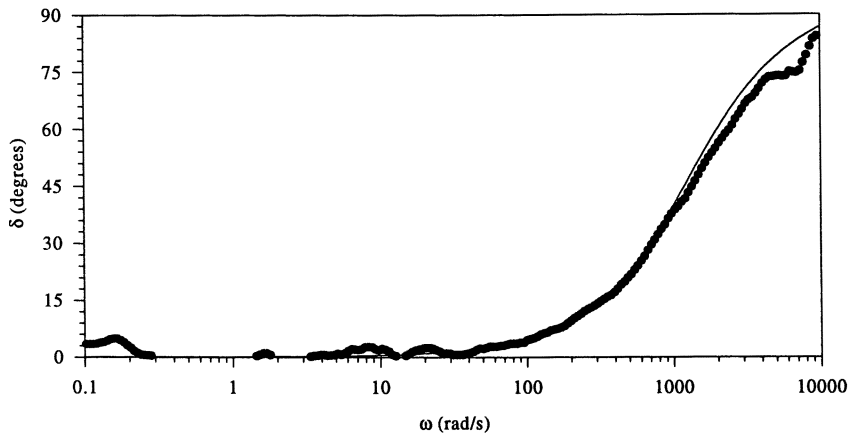
Figure 2. Phase vs. frequency data for a 1.6 micron SiO_2 particle in water. The solid line is generated from equation 4b with $k_{ot}=0.0175$ dynes/cm.
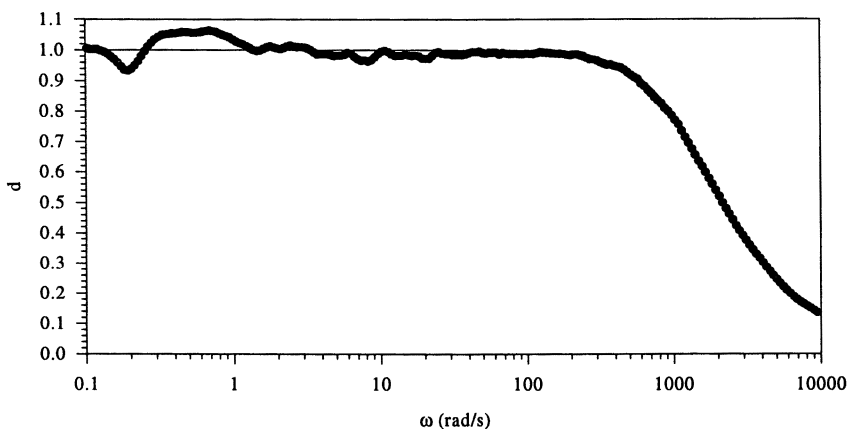
Figure 3. Normalized displacement vs. frequency data for a 1.6 micron SiO_2 particle in water. The solid line is generated from equation 4a with $k_{ot}=0.0175$ dynes/cm.

If the approximate form for the force of the trap on the particle given in equation 1 is valid, the spring constant should scale linearly with laser power.

As a test, the spring constant is determined at several different laser intensities as shown in Figure 4. As predicted, the spring constant varies linearly with the laser power.
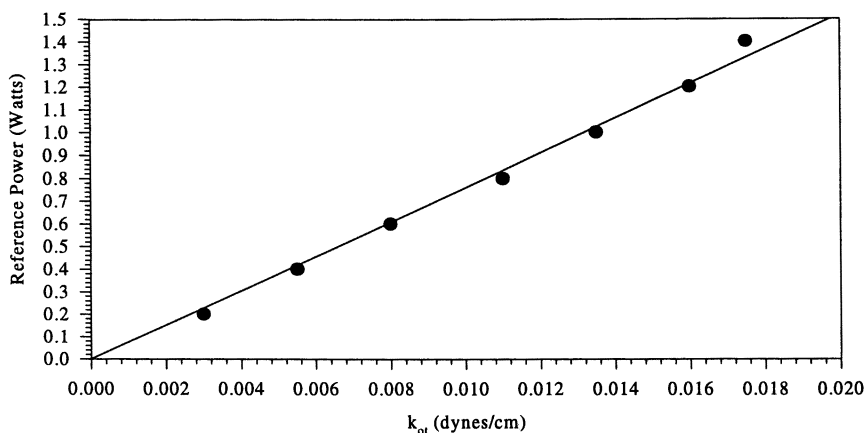
Figure 4. Laser power vs. spring constant as determined by measuring the phase and displacement of a 1.6 micron SiO_2 particle in water.

After the calibration of the spring constant, the method is applied to a solution containing a transient polymer network. A 1.5% solution of hexadecyl-terminated polyethylene oxide (MW=31000 g/mol, Union Carbide) in water, is used as the viscoelastic material *(11-15)*. This polymer forms a network of bridged micelles in solution, and the viscoelastic moduli are known to obey the Maxwell model *(11,15,14)*. The single relaxation time is known to be the lifetime of the hydrophobes in the micelle *(12)*. With the presence of colloidal particles in the solution, the hydrophobic end-groups of the polymer absorb strongly onto hydrophobic surfaces, and weakly charged backbones of the polymer absorb weakly onto hydrophilic surfaces. Because silica has a hydrophilic surface, the storage and loss moduli measured near the silica particle should be affected by adsorption.

Figures 5 and 6 are the normalized displacement and phase shift of a 1.6 micron SiO_2 particle in the polymer solution when the reference trap power is 1.4 W, averaged over 10 runs. There is little variation of the phase shift and the displacement from particle to particle.

From the data shown in Figures 6 and 7, the storage and loss moduli are determined by equations 7a and 7b, and shown in Figure 7. The white data points correspond to the loss modulus, $G''(\omega)$, whereas the dark data points correspond to the storage modulus $G'(\omega)$. The circles indicate data obtained by
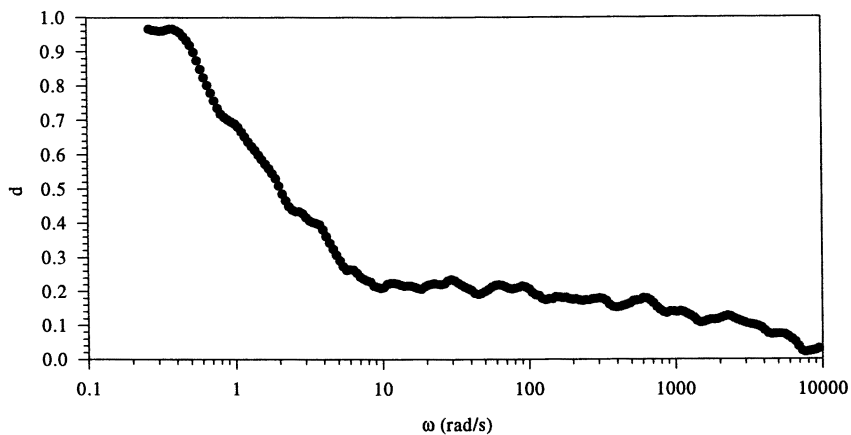
Figure 5. Normalized displacement vs. frequency of 1.6 micron SiO$_2$ particle in a 1.5% polymer solution.
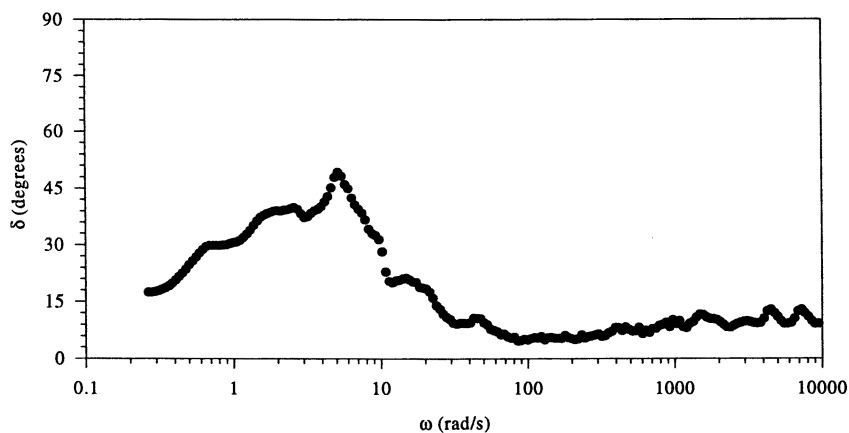
Figure 6. Phase vs. frequency of a 1.6 micron SiO$_2$ particle in a 1.5% polymer solution.

the optical tweezers, the boxes are data obtained by a conventional rheometer. After averaging the data over several particles, the plateau modulus is determined to be $G_\infty = 83 \pm 14$ dynes/cm^2 and the relaxation time is determined to be $\tau = 0.164 \pm .04$ s. The data obtained from the conventional rheometer indicate a plateau modulus of $G_\infty = 600$ dynes/cm^2 and a relaxation time of $\tau = 0.06$ s.
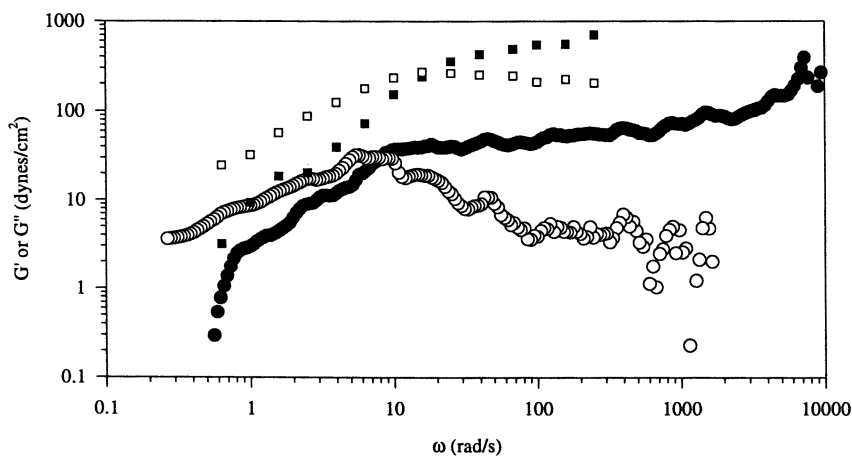
Figure 7. G' or G" vs. frequency for a 1.5% polymer solution. The white data points correspond to the loss modulus, G"(ω), whereas the dark data points correspond to the storage modulus G'(ω). The circles indicate data obtained by the optical tweezers, the boxes are data obtained by a conventional rheometer.

Recently, theorists have predicted that the rheological properties near a colloidal particle differ from bulk rheological properties (*16*). However, there is not a specific theory that relates the microscopic structure of the polymer network, in the vicinity of a probe particle, in the presence of absorption, to the dynamic response of the network. In absence of a complete theory, some qualitative observations can be made. Specifically, a smaller plateau modulus indicates a smaller number of polymer junctions per volume in the probed area, while the longer relaxation time is due to the longer lifetime of hydrophobes in a micelle (*12*). While these results may indicate a concentration gradient in the vicinity of the particle as indicated by the smaller plateau modulus, further tests in which the concentration and molecular weight are varied are needed to confirm this hypothesis. The results from the optical tweezers have been

confirmed qualitatively by another microrheology technique, Diffusing Wave Spectroscopy (data not show) (*1*).

Conclusions

Using a micron-size particle as a probe, we find that the dynamic moduli are quite different than those measured by a conventional macroscopic rheometer. The differences in both the plateau modulus and the relaxation time are most likely due to the interactions between the probe particle surface and the polymer network. The weak adsorption of the polymer onto the probing particle appears to produce a lower polymer bridging density as indicated by the lower plateau modulus. However, the resident lifetime of the hydrophobes in each junction appears to increase as indicated by the longer relaxation time.

In order to detect the effect of local polymer structures and dynamics, we have developed a method to probe the rheology in the microscopic environment in the vicinity of a silica probe particle. Since this technique does not depend on thermal motion, a range of non-thermal and high shear experiments are possible. This technique has the potential to probe localized structures at various length scales in homogeneity in a variety of polymer and colloid systems.

References

1. Mason, T. G.; Weitz, D. A. *Phys. Rev. Lett.* **1995**, *74*, 1250-1253.
2. Crocker, J. C.; Valentine, M. T.; Weeks, E. R.; Gisler, T.; Kaplan, P. D.; Yodh, A. G.; Weitz, D. A. *Phys. Rev. Lett.* **2000**, *85*, 888-891.
3. Bausch, A. R.; Ziemann, F.; Boulbitch, A. A.; Jacobson, K.; Sackmann, E. *Biophys. J.* **1998**, *75*, 2038-2049.
4. Hough, L. A.; Ou-Yang, H. D. *J. Nanoparticle Res.* **1999**, *1*, 495-499.
5. Ashkin A., *Phys. Rev. Lett.* **1970**, *24*, 156-159.
6. Simmons, R. M.; Finer, J. T.; Chu, S.; Spudich, J. A. *Biophys. J.* **1996**, *70*, 1813-1822.
7. Ou-Yang, H. D., "Design and Applications of Oscillating Optical Tweezers for Direct Measurements of Colloidal Forces" *in Polymer-Colloid Interactions: From Fundamentals To Practice*; Dubin, P.; Fainato, R.; Eds,; John Wiley and Sons: New York, NY,1999, Chapter 15, 385-405.
8. Valentine, M. T.; Dewalt, L. E.; Ou-Yang, H. D. *J. Physics: Condens. Matter (UK)* **1996**, *8*, 9477-9482.
9. Schnurr, B.; Gittes, F.; MacKintosh, F. C.; Schmidt C. F. *Macromolecules*, **1997**, *30*, 7780-7792.

10. Visscher, K.; Gross, S. P.; Block, S. M. *IEEE J. Selected Topics Quan. Elect.* **1996**, *2*, 1066-1076.
11. Jenkins, R. D. *Ph.D. Dissertation*, Lehigh University, Bethlehem, PA, 1990.
12. Semenov, A. N.; Joanny, J. F.; Khoklov, A. R. *Macromolecules* **1995**, *28* 1066.
13. Tanaka, F.; Edwards, S. F. *J. Non-Newtonian Fluid Mec.* **1992**, *43,* 247.
14. Pham, Q. T.; Russel, W. B.; Lau, W. *J. Rheol.* **1997**, *42*, 159.
15. Annable T.; Buscall, R.; Ettelaie, R.; Whittlestone, D. *J. Rheol.* **1993**, *37*, 695-726.
16. Levine, A. J.; Lubensky, T. C. *Phys. Rev. Lett.* **2000**, *85,* 1774-1777.

Chapter 5

The Role of "Free Charge" in the Deposition of Latex Particles onto Pulp Fibers

B. Alince[1], J. Kinkal[1,2], F. Bednar[1,3], and T. G. M. van de Ven[1]

[1]Pulp and Paper Research Centre, McGill University, 3420 University Street, Montreal, QC H3A 2A7, Canada
[2]Visiting student from the Institute of Chemical Technology, Prague, Czech Republic
[3]Visiting student from the Slovak Technical University, Bratislava, Slovakia

Electrostatic interactions between latex particles and oppositely charged surfaces can be affected by the "free charge" of a latex which represents the ionic compounds formed during polymerization or present as emulsifiers and which do not become an integral part of the latex particles. It is demonstrated that a cationic latex does not deposit on anionic fibers suspended in water until an excess of "free charge" is eliminated. This can be achieved by introducing an oppositely-charged polyelectrolyte capable of forming a neutral complex with the "free charge". Another possibility is to remove the "free charge" from the latex before its application using fibers as a scavenger.

The properties of a quasi-random assembly of fibers, such as paper, are modified by introducing a polymer. Often the purpose is to improve mechanical behavior and resistance to water by replacing the natural interfiber bonds with

polymer bonds and changing the characteristic nature of the fiber surface. In this role the polymer will be most effective when covering the fibers uniformly which can be achieved by treating the fibers before being formed into a sheet.

A most convenient way of incorporating hydrophobic polymer into a sheet of paper appears to be an addition of latex to fibers suspended in water. Provided that the latex and the fibers are oppositely charged, the latex particles will deposit on the fibers due to electrostatic attraction. Since fibers in water are negatively charged, the latex particles must be positively charged. Alternatively the fibers can be treated with cationic polyelectrolyte to provide them with positive charge in order to attract the negatively-charged anionic latex. Upon forming a sheet from such latex-covered fibers, dewatering and drying, the latex particles will coalesce into a film on the fiber surface.

To achieve a uniform coverage of fiber it is important that the repulsion between latex particles, which are driven to the fibers by electrostatic attraction, is strong enough to prevent their homocoagulation. The result is then a monolayer of discrete particles covering the fiber surface. Although it is possible to introduce anionic latex into anionic fibers by using cationic retention aids, the uniformity will suffer. The cationic polyelectrolyte flocculates the latex which then deposits in the form of aggregates. Thus the efficiency will decrease and for full fiber coverage considerably more latex will be required.

The first attempts using cationic latexes failed because the latex did not deposit on the anionic fibers. The reason appears to be that a wrong type of latex was used with the charge orginating from cationic emulsifiers. Because these are physically adsorbed on the latex particles they may, in the presence of fibers, desorb and transfer to the fiber without taking the particle along. It was therefore concluded that the charge must be an integral part of the latex particles. This can be achieved by using cationic comonomer and/or cationic initiator. Such latexes, prepared in the absence of emulsifiers and cleaned by flash evaporation, behaved as expected. They deposit on clean fibers forming a monolayer of discrete particles. Moreover, the laboratory handsheets formed from such fibers had much improved mechanical properties and were water repellent (*1-4*).

However, when commercial and experimental cationic latexes, obtained from a variety of sources, were investigated, their behavior was rather erratic. Some would deposit up to a limited amount, some would deposit in tap or contaminated water, but not in deionized water. Such experience could lead to a premature dismissal of the whole idea and could cast doubts concerning the applicability of the basic rules of colloidal interactions. The intention here is to point out several factors that are responsible for the observed behavior and which have to be taken into account when dealing with realistic systems rather than a well-defined model system in the laboratory.

Experimental

Materials

Softwood bleached kraft fibers were washed several time to remove fines. The latexes were either commercial or experimental supplied by several producers. The model latex was prepared in our laboratory in the absence of emulsifier.

Methods

Latex Deposition on Fibers

In general, a suspension of one gram of fibers in 500 mL water was kept under slow (80 rpm) paddle stirring, and an appropriate amount of latex was added. A sample of supernatant was withdrawn by a syringe equipped with a filter tip to exclude fibers. Light transmittance of the sample was converted to concentration using the established linear relationship between log transmittance and concentration. The difference between the amounts of latex added and that found in the supernatant is taken as the amount deposited on fibers. The kinetics of deposition was determined by taking samples in timed intervals starting 15 seconds after the latex addition.

Colloidal Stability

The rate of destabilization was measured using a Photometric Dispersion Analyser PDA 2000 (Rank Brothers, Cambridge, UK). The principle of PDA is based on detecting the change in size that takes place when particles aggregate due to loss of stability. The stability is expressed as a stability ratio $W = k_f / k_i$ where k_i is a given rate, and k_f is the fast rate.

Charge

The electrophoretic mobility of particles was determined using a Mark II microelectrophoretic apparatus (Rank Brothers, Cambridge, UK) equipped with a flat cell.

Results and Discussion

Deposition of Model Cationic Latex on Pulp Fibers

Poly(styrene-co-butadiene) latexes, prepared in the absence of emulsifiers, using cationic comonomer diethylaminoethyl methacrylate (DEAEMA), and subjected to flash evaporation, deposit on clean fibers suspended in distilled water. The deposition is driven by electrostatic attraction between positively-charged latex and negatively-charged fibers. The charge of both (expressed as electrophoretic mobility) as a function of pH is shown in Figure 1. In Figure 2 an example of deposition at neutral pH is shown as a function of time for different latex additions. The rate of deposition increases with increased latex addition which is expected because of the increased frequency of collisions between latex particles and fibers. The maximum deposition of 140 mg latex per gram of fiber indicates a monolayer coverage of the fiber surface by closely-packed latex particles, considering that the size of this latex is 255 nm in diameter and the available surface of one gram of fibers is around 1 m^2. A micrograph in Figure 3 shows that this is indeed so.
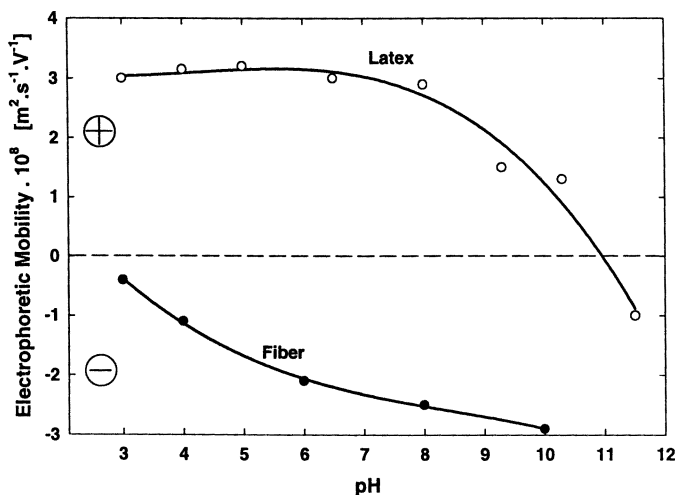
Figure 1. Electrophoretic mobility as a function of pH for anionic fibers and a particular cationic latex.
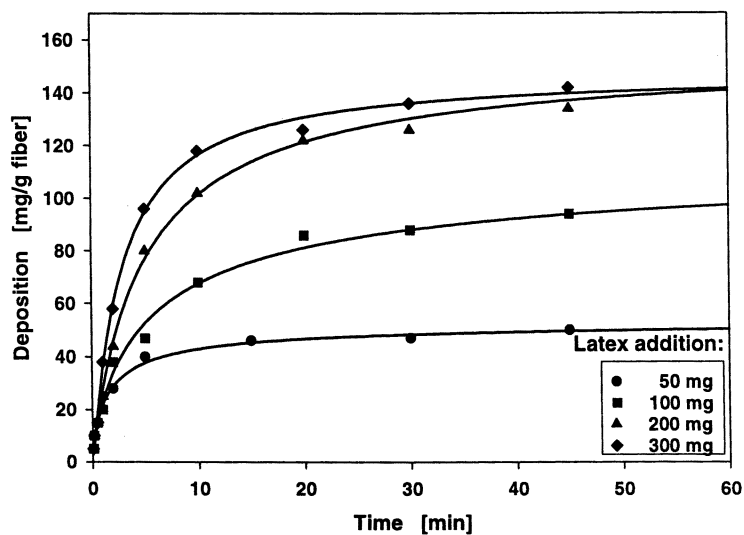
Figure 2. Deposition of clean cationic latex on fibers suspended in water measured for different latex addition as a function of time. One gram fiber + latex/500 mL.
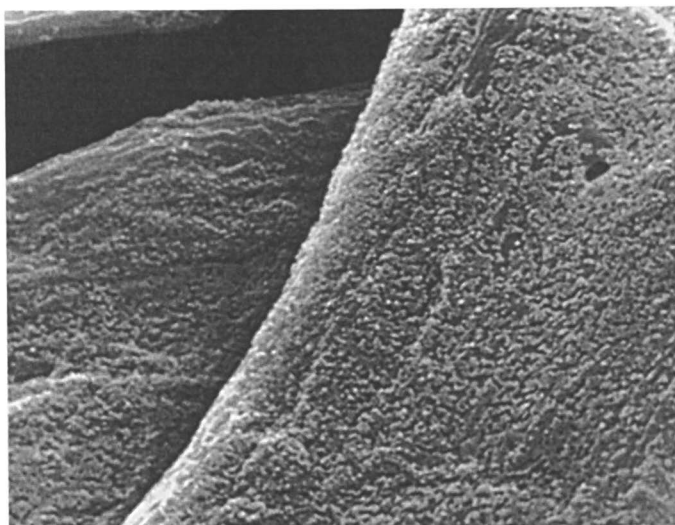
Figure 3. Deposition of latex particles on pulp fibers as observed by SEM.

Effect of Cationic "Free Charge"

"Free charge" represents the ionic compounds formed during polymerization or present as emulsifiers and which do not become an integral part of the latex particles. By adsorbing on fiber they make it less attractive to latex and depending on their concentration, they may prevent deposition completely. A typical example is in Figure 4 where the deposition of a commercial type of acrylic cationic latex, measured as a function of time, is shown for different latex additions. At low latex addition and consequently also low "free charge" content, all the latex deposits (up to ~ 30 mg/g). However, with increased latex addition, the extent of latex deposition decreases and finally at 100 mg latex addition there is enough "free charge" available to adsorb on the fibers to prevent practically any deposition.
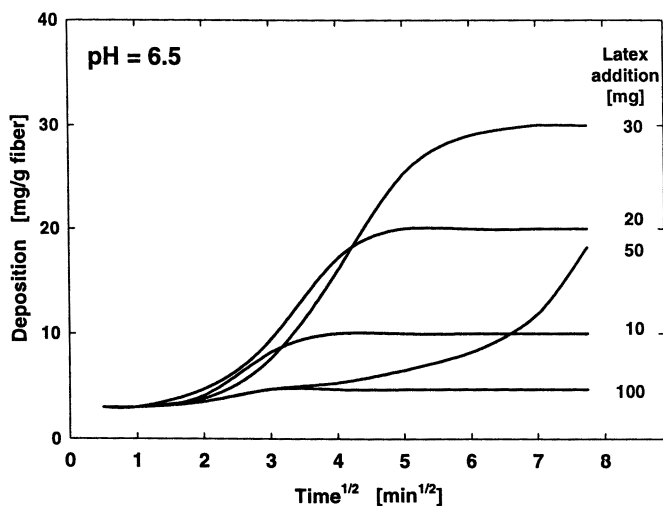
Figure 4. Deposition of commercial cationic latexes on fibers suspended in water measured for different latex additions as a function of time. The experimental points are omitted for the sake of clarity. Square root of time is used to emphasize the initial deposition. One gram fiber + latex/500 mL.

Another aspect, the delayed onset of deposition, seen in Figure 4, is also of interest. The process of "free charge" adsorption is apparently faster than the deposition on latex particles. The free charge initially adsorbs on the external surface of the fibers but with time it moves inside the fiber wall, and thus the original surface charge of fiber is restored. Obviously, with increasing content of free charge this process will take longer and consequently the onset of deposition will be more delayed.

Elimination of Cationic "Free Charge"

For the purpose of eliminating the detrimental effects of "free charge" on latex deposition several possibilities can be envisaged. One of them is to consume the "free charge" by introducing an oppositely-charged polyelectrolyte thus forming a neutral complex. An example is shown in Figure 5. Cationic latex does not deposit because of an excess of "free charge". Addition of anionic sulfonated kraft lignin (SKL) before the latex is added results in increased deposition. However, overcharging the system with anionic compounds (100 mg SKL/g latex) also causes a reversal of the latex charge and consequently no deposition.

In order to evaluate the content of "free charge" and thus to determine the appropriate addition of oppositely-charged polyelectrolyte, the knowledge of latex stability and charge as a function of the polyelectrolyte addition is useful. In Figure 6 the stability and charge of cationic latex is shown as a function of SKL addition. The stability ratio W is the ratio of the rate of fast destabilization and the given rate. This means that for $W=1$ (log $W=0$) the system is unstable and for $W=\infty$ it is stable (within a given period of time). $W>1$ means the system destabilizes, but at a slower rate. As can be seen, the latex behaves as expected in a system that is electrostatically stabilized; i.e., fast coagulation takes place at charge neutralization. What is important for our purpose is the amount of SKL required to reach this point. If more of the SKL is needed, that indicates that more cationic charge (both free and that associated with the latex) is present. The determined amount of SKL then provides guidance for the required SKL addition to eliminate the "free charge".
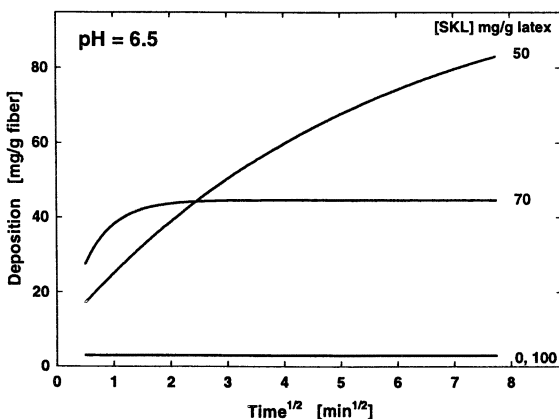
Figure 5. Deposition of commercial latex in the presence of sulfonated kraft lignin. One gram fiber + 100 mg latex/500 mL.
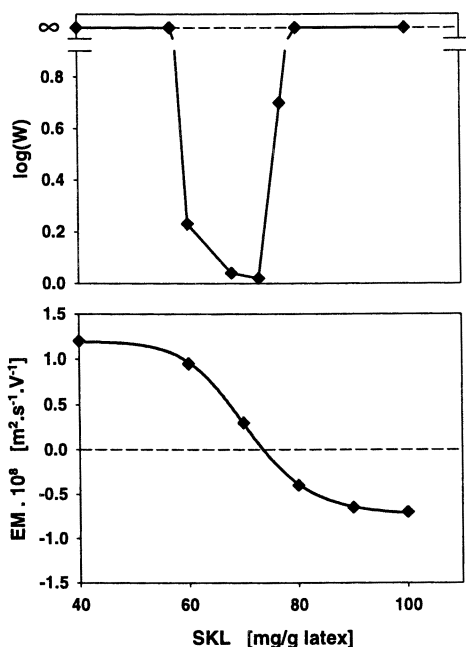
Figure 6. Stability and electrophoretic mobility of commercial latex at pH 6.5 as a function of sulfonated kraft lignin addition. Log W=∞ — colloidaly stable. Log W=0 — fast coagulation.

A comparison of Figure 5 and Figure 6 shows that in the absence of SKL the latex is stable and positively charged, but does not deposit likely due to an excess of "free charge". Addition of 50 mg SKL per gram latex into a system composed of one gram fiber and 100 mg latex results in deposition. The latex is still stable and positively charged as seen in Figure 6. At a SKL addition of 70 mg per gram the latex coagulates because the SKL eliminates both the "free charge" and the latex charge (Figure 6). The coagulated latex still deposits (Figure 5) but to a lesser extent and at a faster rate. This is in accordance with the theoretical prediction that the rate increases with increasing size. However, due to coagulation, the latex deposits in the form of aggregates as seen in Figure 7 instead of discrete particles as shown in Figure 3. Because of their large size, the aggregates in the mixed system are susceptible to hydrodynamic forces which interfere with their tendency to deposit, and thus, the extent of deposition decreases. Increasing SKL addition to 100 mg per gram latex results in stable,

but negatively-charged latex (Figure 6) which does not deposit as seen in Figure 5.
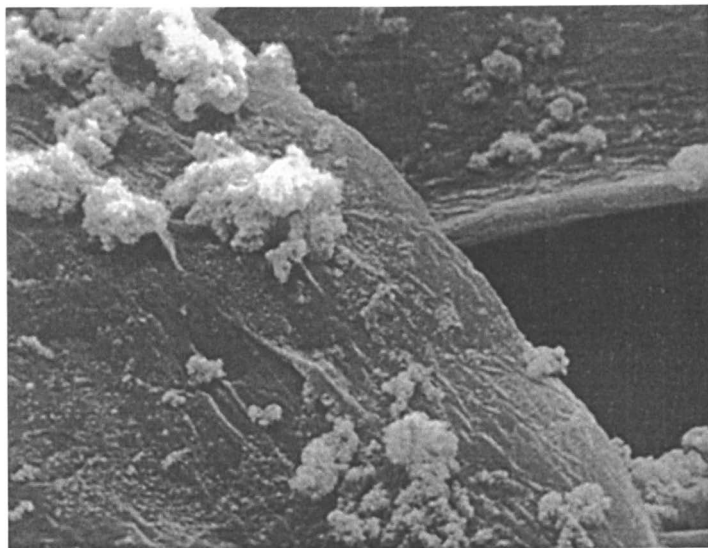
Figure 7. Deposition of latex aggregates on fibers as observed by SEM.

It must be realized that the optimum SKL addition would differ depending on pH. The degree of dissociation of both the cationic groups and the anionic groups is pH dependent, and as a result, with increasing pH, the cationic charge decreases, while the anionic charge increases. Since the formation of a neutral complex between oppositely-charged polyelectrolytes is essentially a stoichiometric interaction between ionic groups, less anionic material will be required to neutralize the cationic "free charge" at higher pH. This also means that the amount of SKL needed to destabilize the cationic latex will decrease with increasing pH as shown in Figure 8. At pH 2 one gram of latex is destabilized by 120 mg SKL while at pH 10 only 40 mg is necessary. Consequently to induce deposition of a given latex at low pH more SKL is required, while at high pH less SKL is needed.

The fact that the cationic charge decreases with increasing pH also means that the detrimental effect of "free charge" becomes less pronounced. It also helps that the anionic charge of fibers increases as shown in Figure 1. Consequently, at higher pH, more "free charge" can be tolerated and the latex deposition at pH 10 might proceed as shown in Figure 9. The pattern is different from that shown in Figure 4 at pH 6.5. One problem, however, has to be

realized. The charge of this latex at pH 10 (cf. Figure 1) might not be strong enough to ensure latex stability, and consequently, the latex might deposit in the form of aggregates as shown in Figure 7.
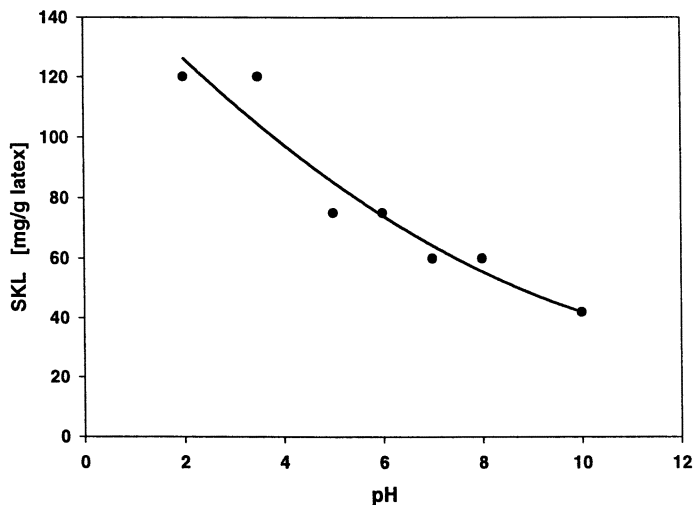
Figure 8. Amount of sulfonated kraft lignin for inducing fast coagulation of latex as a function of pH.
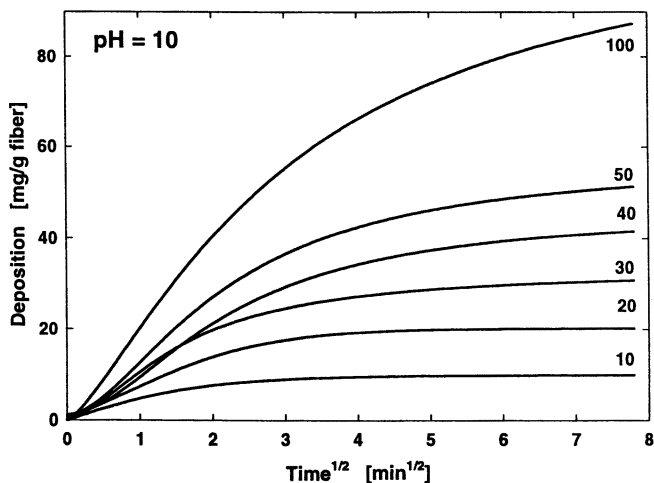
Figure 9. Deposition of commercial cationic latex at pH 10 measured for different latex additions as a function of time. One gram fiber + latex/500 mL.

When the latex coagulates and thus is deposited as aggregates, its efficiency could be seriously affected because at a given amount of introduced latex less fiber surface is covered. This would mean that the intended purpose, i.e., protecting the fibers against water and replacing interfiber bonding to improve mechanical properties, would be more difficult to achieve or else more of the latex will be needed to match the performance of fibers covered by a monolayer of discrete particles.

So far the need to eliminate the excess of cationic "free charge" has been demonstrated using a particular acrylic latex with average size 200-300 nm and $T_g \sim 20$ °C. Other experimental samples from various sources behave similarly. Two examples of poly(styrene-co-butadiene) latexes are shown in Figure 10 (120 and 230 nm and $T_g \sim 20$ °C). Their content of "free charge" is different as documented by the amount of SKL required to cause destabilization and to reach the isoelectric point shown in the upper part in Figure 10. In the absence of SKL they deposit to a limited extent, as seen in the bottom part of Figure 10, because of an excess of "free charge" (represented by double plus sign). The latex with smaller particle size coagulates at SKL addition around 100 mg/g at which point it is also deposits. At 150 mg SKL/g it becomes negatively charged and consequently does not deposit. The larger latex particles already coagulate around 50 mg SKL/g. Addition of 100 mg SKL/g results in reversing the charge, thus preventing deposition.

Removal of Cationic "Free Charge" by Fibers

The problems resulting from the presence of "free charge" could be alleviated by removing it from the latex before its application. The common methods used for latex cleaning, like dialysis and ion-exchange resins, were not very effective. However, the use of fiber as a scavenger for the "free charge" is quite successful. An example of what happens is shown in Figure 11. Latex added to fibers suspended in either tap water or deionized water does not deposit. After 15 min of mixing, the fibers are separated by filtration and a fresh charge of fibers is introduced. Now the latex deposits in tap water. In deionized water the procedure must be repeated four times before the onset of considerable deposition. The experiment indicates that the "free charge" is adsorbed by fiber and thus is effectively removed from the latex. If so, then the stability and charge of latex determined as a function of SKL must also change. This is shown in Figure 12. The original latex requires about 200 mg/g to lose its charge and coagulate in both deionized and tap water. After one step cleaning in tap water the required amount of SKL drops to about 30 mg/g. This means that the content of "free charge" decreased sufficiently and the latex deposits. The content of "free charge" decreases after one step in deionized water, but still remains high

enough to prevent deposition. Only after the fourth step does the content of "free charge" become sufficiently low for deposition to take place. From Figure 12 it follows that the amount of charge removed from latex by fibers (one step in tap water and in 4 steps in distilled water) is equivalent to a charge of about 170 mg SKL/g latex.
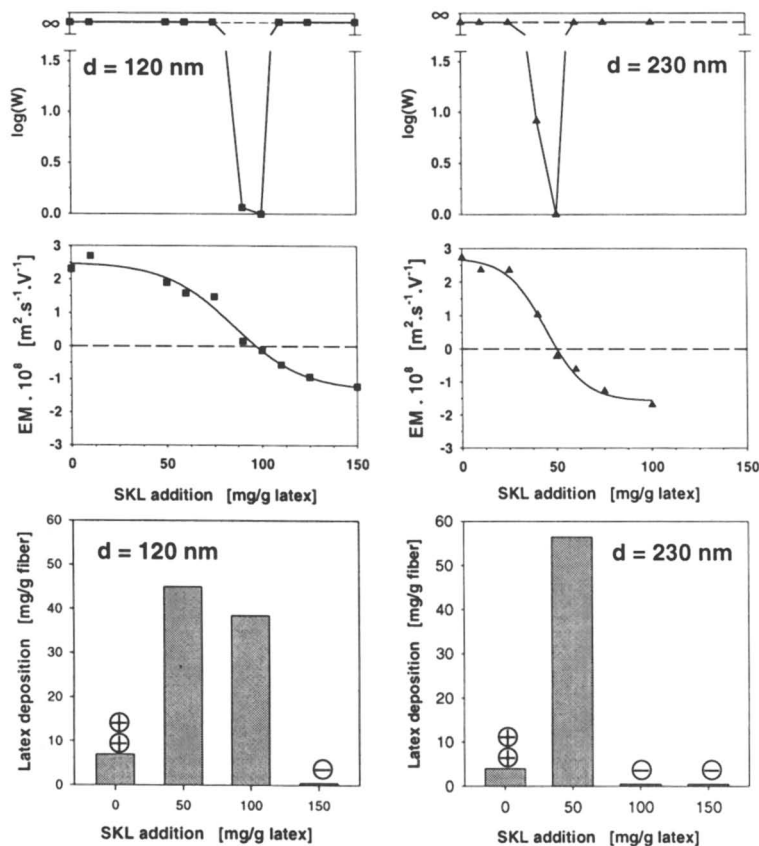
Figure 10. Stability and electrophoretic mobility of cationic experimental latexes as a function of sulfonated kraft lignin addition (upper). Deposition of experimental cationic latexes in the presence of anionic sulfonated kraft lignin. One gram latex + 100 mg latex/500 mL (lower).
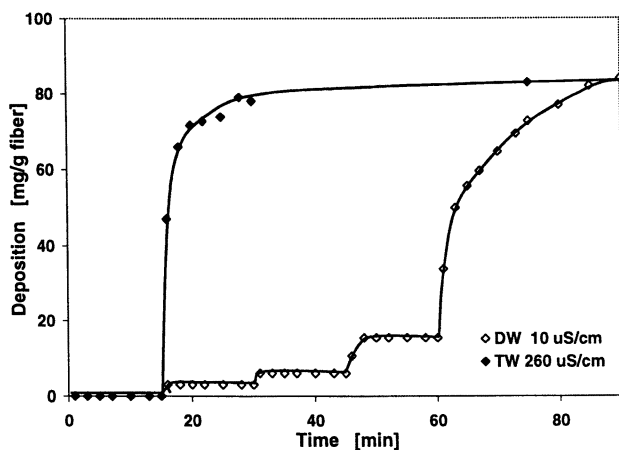
Figure 11. Deposition of experimental cationic latex in deionized and tap water after stepwise (15 min) cleaning with pulp fibers. One gram fiber per step/500 mL. Latex addition 100 mg.
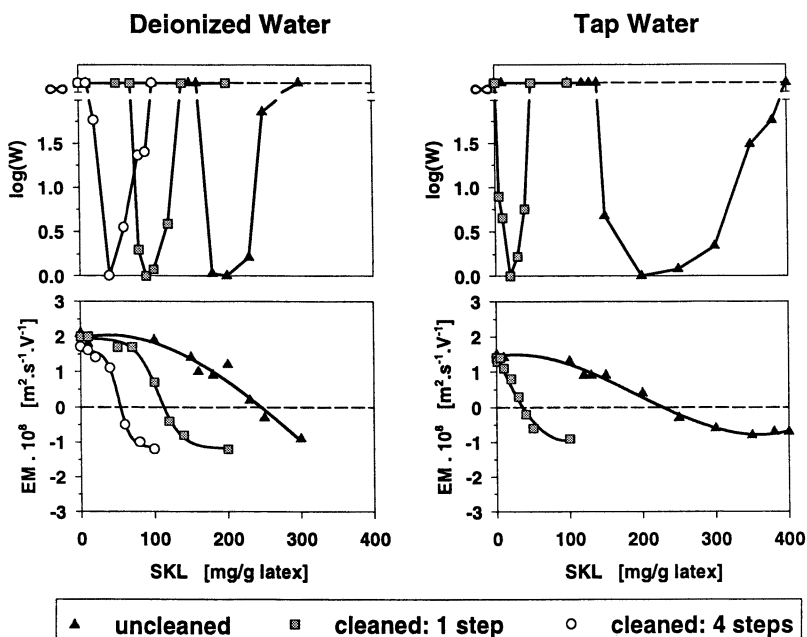
Figure 12. Stability and electrophoretic mobility of experimental cationic latex as a function of sulfonated kraft lignin addition of original and cleaned latex in deionized and tap water.

Why the cleaning process is more effective in tap water is not quite clear but it is often observed that a given latex deposits in tap water but not in deionized water. It can be argued that in the presence of salt the adsorption of "free charge" by fibers is enhanced which is a phenomenon known in polyelectrolyte adsorption on cellulosic fibers (for low salt concentrations). However, the results shown in Figure 13 indicate that other factors might be involved. When deionized water was adjusted by the addition of calcium bicarbonate to the same conductivity as tap water (260 μS/cm) the latex deposition in the second step increased, but an additional step was needed for full deposition. The performance of tap water was matched only at higher conductivity (500 μS/cm).
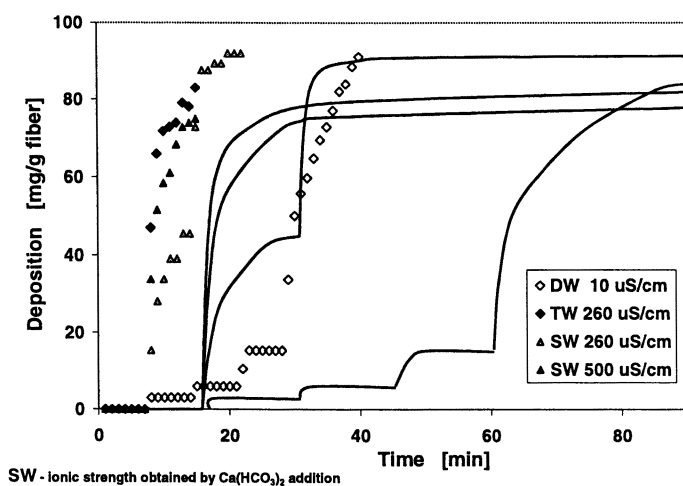
Figure 13. Deposition of experimental cationic latex in deionized water, tap water, and standard water after stepwise (15 min) cleaning with pulp fibers. One gram fiber per step/500 mL. Latex addition 100 mg.

Effect of Anionic Contaminants in Process Water

In industrial processes the suspension of fibers in water is not a clean system. For chemical fibers, no matter how well the fibers are washed after pulping, a variety of solubles leach out. These are generally negatively charged. In the case of fibers obtained by mechanical pulping the situation is worse because they may not be washed at all. Recycled fibers contain additives used in papermaking. It is therefore not surprising that the behavior of latex introduced into such a system is affected. Since the contaminants are mostly anionic in

nature it is the cationic latex which is particularly vulnerable. It may coagulate and even its charge may be reversed as shown in Figs. 6, 10 and 12 where the stability and charge of cationic latex is determined as a function of anionic sulfonated kraft lignin. It is of interest to note, however, that the presence of "free charge", which is detrimental to latex deposition in a clean system becomes actually an advantage in a contaminated one.

In a clean system anionics are added to eliminate the excess of cationic charge and thus promote deposition. In a contaminated system the anionics are already present. The ideal case would be if the cationic "free charge" and the anionic contaminants will be eliminated by mutual interaction.

From the above it is apparent that in order to predict the probability of latex deposition or to explain the absence of deposition, an investigation of the stability and the charge of latex in a given supernatant is essential.

Effect of Anionic "Free Charge"

Deposition of anionic latex takes place on fibers, the charge of which is reversed by adsorbing cationic polyelectrolyte. An example is provided by using four commercial polystyrene latexes of different size. In Figure 14 is shown their stability and charge as a function of polyethylenimine (PEI) addition. The amount of PEI required for eliminating the charge and thus causing destabilization is equivalent to the anionic charge that is present, both the "free charge" and the latex charge. The 60 nm latex contains the most charge, an amount about equivalent to 50 mg PEI/g, whereas, for the 200 nm latex the equivalent amount is 10 mg PEI/g and for the 400 and 750 nm latexes the amount is 5 mg PEI/g. Their deposition on fibers pretreated with PEI and washed free of unadsorbed PEI is shown in Figure 15 as a function of latex addition. All the latexes deposit quantitatively up to a given maximum. The deposition decreases with increased additions apparently due to an excess of "free charge" delivered by the latex.

It is of interest to note that, with the exception of the 750 nm latex, the maximum deposition is close to the calculated coverage of one gram fiber (1 m^2) by a monolayer of closely-packed discrete particles – 30, 100 and 200 mg/g for the 60, 200 and 400 nm particles. (For the 750 nm particles it will be 375 mg/g).

From the maximum deposition and the charge delivered by the latex it is possible to evaluate the amount of anionic charge which can be present before becoming detrimental. The data in Table 1 show that the system can tolerate the presence of anionics up to 0.9 mg PEI equivalent per gram of fiber.

The detrimental effect of "free charge" is obvious in the case of 750 nm latex because its maximum deposition is below the calculated full coverage of fibers (375 mg/g). The effect of removing the anionic "free charge" by PEI-treated fiber on latex deposition is shown in Figure 16. At the latex addition of

500 mg per gram fiber in deionized water, about 40 mg of latex deposits in deionized water and about 100 mg in tap water. By removing the fibers and introducing a new charge of PEI treated fibers the deposition in tap water is about 350 mg/g (close to full coverage of fibers). In deionized water the same deposition is achieved after an additional step of cleaning.
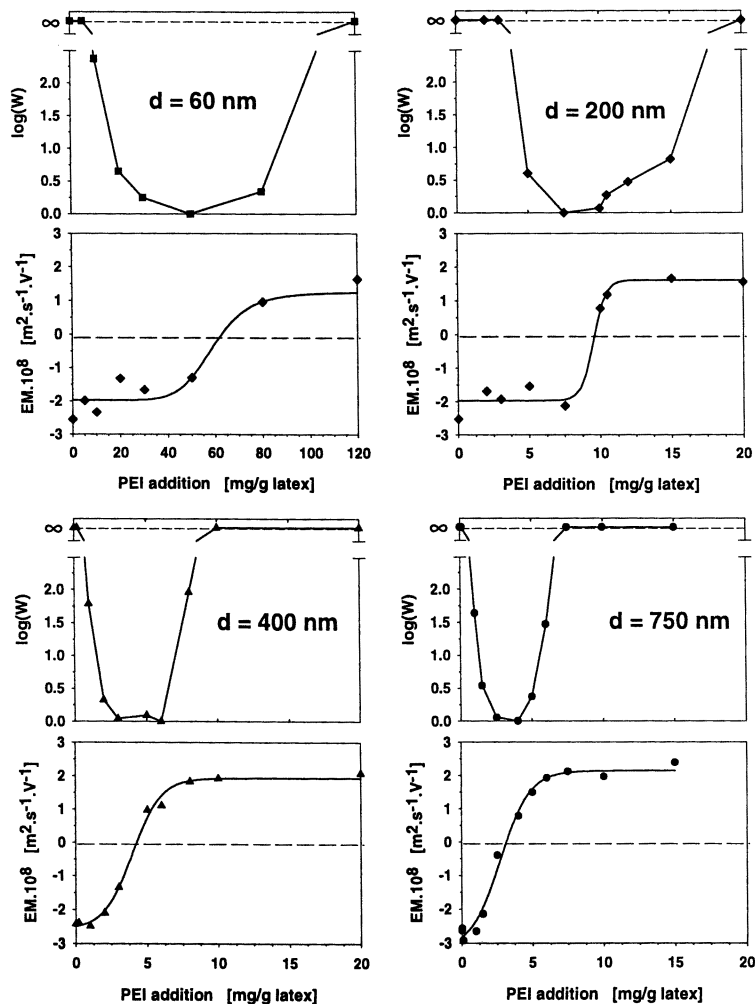
Figure 14. Stability and electrophoretic mobility of commercial anionic latexes as a function of poly(ethylenimine) (PEI) addition.
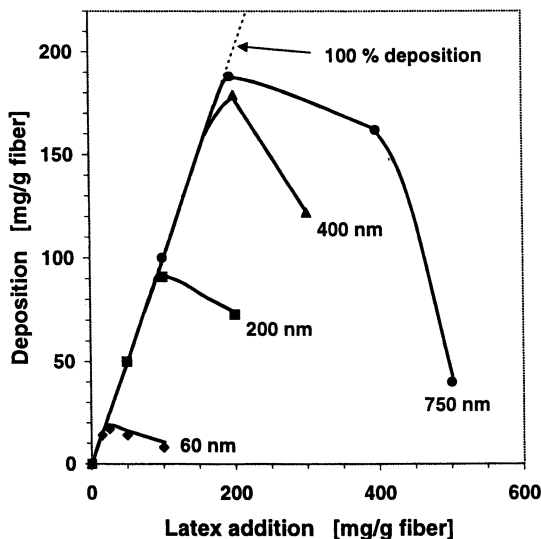
Figure 15. Deposition of commercial anionic latexes on poly(ethylenimine)-treated fibers as a function of latex addition. One gram fiber + latex/500 mL.

Table I. Evaluation of Tolerated Anionic Charge

Latex sample	nm	60	200	400	750
Charge in PEI equiv.	mg PEI/g latex	50	10	5	5
Maximum deposition	mg latex/g fiber	18	90	180	190
Charge delivered by latex at maximum deposition (in PEI equiv.)	mg PEI/g fiber	0.9	0.9	0.9	0.9
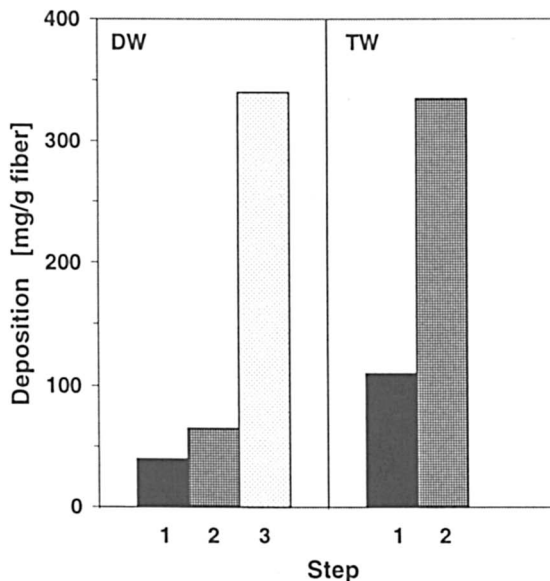
Figure 16. Deposition of commercial anionic latex 750 nm on poly(ethylenimine)-treated fiber in deionized and tap water after stepwise (15 min) cleaning with PEI treated fibers. One gram fiber per step/500 mL. Latex addition 500 mg.

Conclusions

When dealing with a realistic system, the presence of "free charge" and particularly its effect on latex-fiber electrostatic interactions must be considered. Excess of cationic "free charge" delivered by addition of latex is detrimental to latex deposition on fibers dispersed in water because it adsorbs on fibers and makes them nonattractive. An excess of anionic contaminants in water also prevents cationic latex deposition because they adsorb on latex and reverse its charge. It is therefore necessary to determine the content of both contaminants and "free charge" and decrease them to a level that can be tolerated.

Elimination of "free charge" can be realized by introducing an oppositely-charged polyelectrolyte to form a neutral complex. Anionic contaminants can be eliminated by the addition of cationic polyelectrolyte. In the ideal case the cationic "free charge" will be neutralized by the anionics present in the process water. This also means that the presence of "free charge" is actually beneficial in contaminated water. The other possibility is to remove the "free charge" by using fibers as a scavenger. However, in this case, the presence of anionics will be detrimental and will have to be eliminated.

Acknowledgment

References

1. Alince, B; Inoue, M; Robertson, A.A., *J. Appl. Polym. Sci.* **1979**, *23*, 539-548.
2. Alince, B. *J. Appl. Polym. Sci.* **1979,** *23*, 549-560.
3. Alince, B. *Tappi J.* **1999,** *82(3)*, 175-187.
4. Alince, B. *J. Appl. Polym. Sci.* **2000,** *76*, 1677-1682.

Chapter 6

The Effect of Hydrophilic Nonionogenic Comonomers on Flow Properties of Carboxylated Latexes

Jaromír Šňupárek[1], Otakar Quadrat[2], Jiří Horský[2], and Martin Kaška[1]

[1]Department of Polymeric Materials, University of Pardubice,
532 10 Pardubice, Czech Republic
[2]Institute of Macromolecular Chemistry, Academy of Science of the Czech Republic,
162 06 Prague, Czech Republic

Different copolymer latexes containing hydrophilic nonionic functional groups were thickened with a model alkali-swellable latex based on ethyl acrylate / methacrylic acid / N,N´-methylenebisacrylamide copolymer and the thickening efficiency was investigated. The thickening process was closely related mainly to the volume fractions of both the nonionic and the alkali-swellable latex particles.

Copolymer latexes containing hydroxyl or amide groups are frequently utilized in water-borne coatings. The reactive functional groups are loci for polymer chain crosslinking with melamine resins or with polyisocyanates. Highly carboxylated latex copolymers that are alkali-soluble or alkali-swellable increase the viscosity of water-borne vehicles. Copolymers comprising both nonionogenic comonomers as they are, e.g., hydroxyethyl methacrylate or

71

methacrylamide, and ionogenic acrylic or methacrylic acid are frequently used in shell layers in core-shell particles. Steep increases in viscosity during neutralization of such copolymer latexes is important for the vehicle rheology; however, it also may cause difficulties in their practical application. Thus, a good knowledge of the flow behavior of such vehicles is very important. At present, the mechanism of such thickening processes is not fully understood. It is assumed (*1-3*) that, after neutralization of the originally acidic material, electrostatic repulsions between ionized carboxylic groups attached to polymer chains of the latex and thickener leads to particle swelling, which increases steric and electrostatic particle interactions. Also bridging flocculation or volume restricting flocculation may appear (*1,2*). These structural changes result in high resistance to deformation in the flow field and, consequently, in an increase in non-Newtonian viscosity, yield stress, and dynamic moduli of the thickened system. Flow properties of three model latexes of copolymers containing a small amount of acrylic acid, as well as a reactive hydrophilic monomer, either methacrylamide (MAAm) or 2-hydroxyethyl methacrylate (HEMA) in two of the latexes, and thickened with a model alkali-swellable thickener (AST) have been investigated using capillary viscometry and dynamic and steady shear measurements.

Experimental

Latex Preparation

The basic copolymer latex comprising butyl acrylate, styrene, and acrylic acid (L-0) and the other two also with MAAm (L-M) or HEMA (L-H) comonomers have been prepared by a non-seeded semi-continuous emulsion copolymerization with a monomer emulsion feed. The solids content of the prepared latexes was 50 wt%. The AST has been prepared similarly by emulsion copolymerization of ethyl acrylate, methacrylic acid and N,N'-methylenebisacrylamide. In the case of the carboxyl-containing dispersion, the polymerization was carried out only to a low (7 wt%) solids content to reduce unpredictable crosslinking of particles by chain transfer. The pH of the resulting latexes was 2-3. The emulsion polymerization procedure that was used guaranteed a homogeneous statistical copolymer composition of latex particles (*4-6*). The hydrodynamic diameter of the latex particles as measured by dynamic light scattering (Auto-Sizer LoC, Malvern Instruments, UK) ranged between 150 and 170 nm. The copolymer compositions are given in Table I.

Table I. Composition of Latexes (wt%)

Monomer	L-0	L-M	L-H	AST
Butyl acrylate	56.5	51.5	60	
Styrene	41.5	36.5	28	
Methacrylamide		10		
2-hydroxyethyl methacrylate			10	
Acrylic acid	2	2	2	
Ethyl acrylate				82.5
Methacrylic acid			15	
N,N'-methylenebisacrylamide				2.5

Materials

Technical grade monomers, ethyl acrylate, *n*-butyl acrylate, and acrylic acid (Chemical Works, Sokolov, Czech Republic), styrene (Kaučuk Kralupy, Czech Republic), 2-hydroxyethyl methacrylate, methacrylic acid and *N,N'*-methylenebisacrylamide (Röhm, Darmstadt, Germany) were used. Polymerizations were carried out in a 2.5 L stirred glass reactor under a nitrogen atmosphere using a redox ammonium peroxodisulfate–sodium bisulfite initiating system (for hydroxy containing samples) or ammonium peroxodisulfate alone (for carboxylated low-solids dispersion of the thickener). Disponil AES 60 (sodium poly(ethylene glycol) alkylaryl ether sulfate, Henkel, Germany) in an amount of 2 wt% of the active component (relative to the monomers) was used as an emulsifier.

Sample Preparation and Viscometry

In this study we aimed at the thickening of medium-concentrated latexes (25 wt%). Thickened samples were prepared by addition of dilute aqueous ammonia to mixtures of originally acidic latexes with the alkali-swellable dispersion to reach the required pH, 9.2-9.3. pH measurements were carried out with a digital pH meter (Radiometer, Copenhagen) with a combined electrode, GK 2321 C. Viscosity measurements were performed at 25 °C with samples stabilized for one day after adjustment of the pH.

The relative viscosity $\eta_r = \eta/\eta_o$, where η is the viscosity of latices and η_o is that of the dispersion medium, was measured using an Ostwald capillary viscometer. Rheological experiments were performed using a Weissenberg

rheogoniometer (model R–16, UK) with a cone-and-plate system with a cone diameter of 5 cm and a complementary angle of 2°.

Results and Discussion

Capillary viscometry indicated that the dependencies of viscosity of different neutralized latexes on their particle concentration considerably differ as is shown in Figure 1. It could be assumed that during neutralization of the originally acid latexes the effective hydrodynamic volume of latex particles (intrinsic viscosity $[\eta]$) increased due to electrostatic interactions of ionized carboxylic groups, which was manifested in an increase of the latex viscosity. The $[\eta]$ values were obtained as an intercept of the $\Phi_L/\ln\eta_r$ vs. Φ_L plot (Figure 2) according to the Mooney equation (7)

$$\eta_r = \exp\{[\eta]\ \Phi_L/(1- (\Phi_L/\Phi_c))\} \tag{1}$$

where Φ_L is a volume fraction of unneutralized latex particles and Φ_c is a critical particle volume fraction corresponding to a fully occupied space.
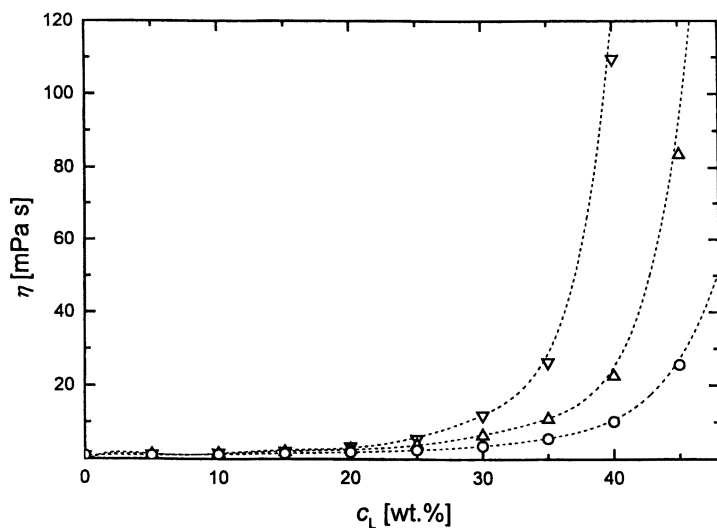
Figure 1. Dependence of latex viscosity, η, on the particle concentration, c_L.
$\bigcirc = L-0$, $\triangle = L-M$, $\nabla = L-H$.
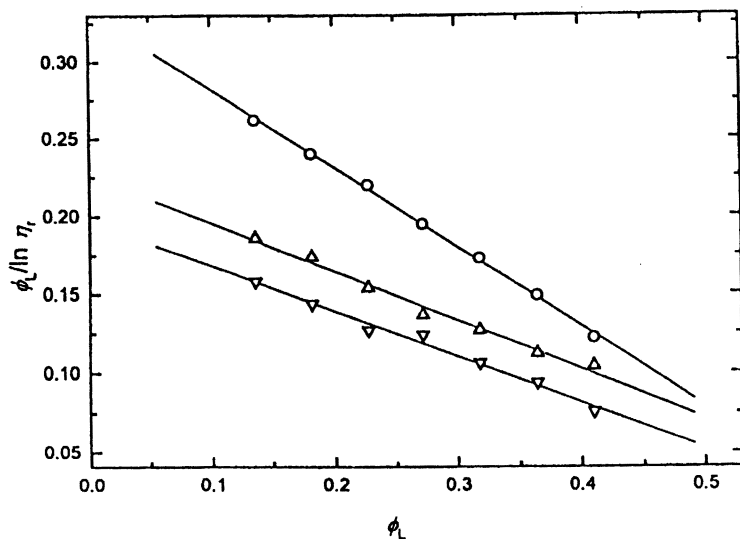
Figure 2. The Mooney plot. Points denoted as in Figure 1.

Similar differences in viscosity found in the original model latexes appeared also in thickened latexes. Here, the strongest thickening effect manifested both in the highest viscosity-latex particle concentration dependence (Figure 3) and in the strongest pseudoplasticity of thickened latex (Figure 4) seen in the HEMA-containing copolymer latex. The thickening efficiency of the latex with MAAm comonomer and especially of the latex without hydrophilic groups was lower. It is obvious that the hydrodynamic volume of the latex particles, and consequently the latex viscosity, is considerably influenced by the presence of a hydrophilic comonomer used (Table II).

A relation between the effective hydrodynamic volume of neutralized particles and that of original acid particles before the neutralization can be characterized by a volume swelling ratio, q:

$$q = [\eta]/[\eta_o] \qquad (2)$$

where $[\eta_o]$ corresponds to the Einstein theoretical value of 2.5 for rigid undeformable spheres (*8*).
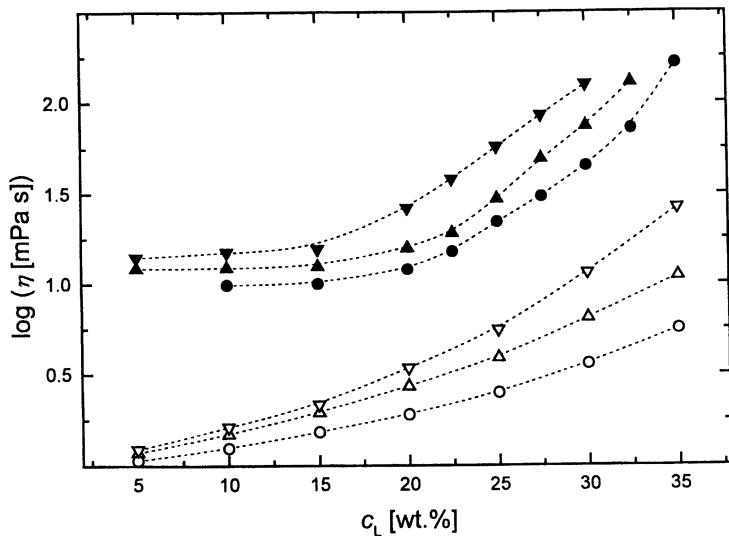
Figure 3. Dependence of viscosity, η, of original latexes (open points) and latices thickened with 1 wt% of the thickener (filled points) on particle concentration, c_L. Points denoted as in Figure 1.
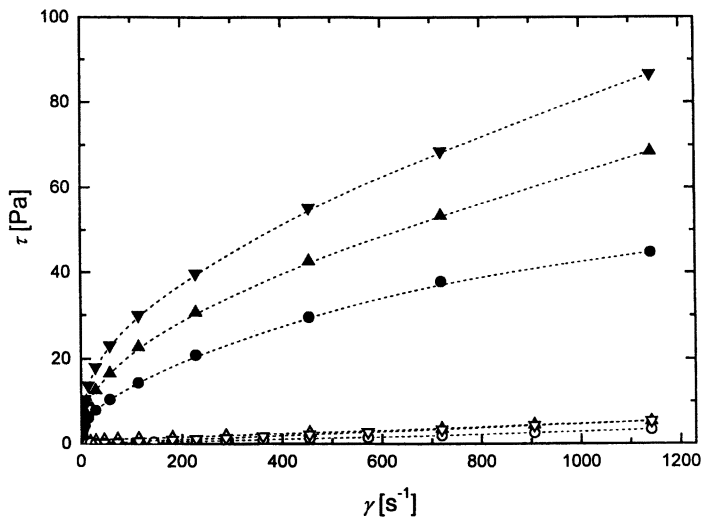
Figure 4. Dependence of shear stress, τ, on shear rate, γ, of 25 wt.% latexes thickened with 2 wt% of the thickener. Points denoted as in Figures 1 and 3.

Table II. The Effective Hydrodynamic Volume (Intrinsic Viscosity [η]) of Neutralized Particles

Latex	[η]	q	Φ_L^*	c_T	Φ_T^*	$\Phi_L^* + \Phi_T^*$
L-0	3.01	1.20	0.26	1.0	0.39	0.65
L-M	4.21	1.68	0.36	0.81	0.32	0.68
L-H	5.07	2.02	0.44	0.65	0.25	0.69
AST	44	17.6				

where q is the volume swelling ratio, Φ_L^* is the volume fraction of swollen latex particles of 25 wt% of latexes, c_T and Φ_T^* are the concentrations and volume fractions of the AST in the thickened system of viscosity $\eta = 21.4$ mPa.s (corresponding to 25 wt% of L-0 with 1 wt% of AST)

The dependence of viscosity of the thickened 25 wt% latexes on the thickener concentration, presented in Figure 5 shows that the viscosity (21.4 mPa.s) corresponding to latex L-0 with 1 wt% of the thickener present can be reached for latex L-M with 0.81 wt% of the thickener present and for the latex L-H with only 0.65 wt% of the thickener (c_T). These results suggest that the intensity of the thickening process is closely related to the volume fraction of both the latex and the thickener particles. Figure 6 shows that for the thickened 25 wt% latexes of viscosity 21.4 mPa.s, the sum of the volume fractions of the swollen latexes (Φ_L^*) and the thickener (Φ_T^*) (Figure 6b) with the volume swelling ratio is nearly constant (Table II) or increases only slightly (Figure 6c).

Conclusions

In general, the thickening process depends on two main factors: (a) the structure and number of particles present in the thickened systems, and (b) their steric and electrostatic interactions. It is obvious that the hydrodynamic volume of the latex particles is an important factor controlling both viscosity of the original neutralized latexes and their thickening process and that the hydrodynamic properties of latexes thickened with an alkali-swellable thickener depend predominantly on the total hydrodynamic volume of the latex and the thickener particles and not on any specific interactions of comonomers located on the particle surface. Consequently, latexes of high hydrodynamic particle volume require a smaller amount of the thickener to adjust the required rheological properties of the thickened system.
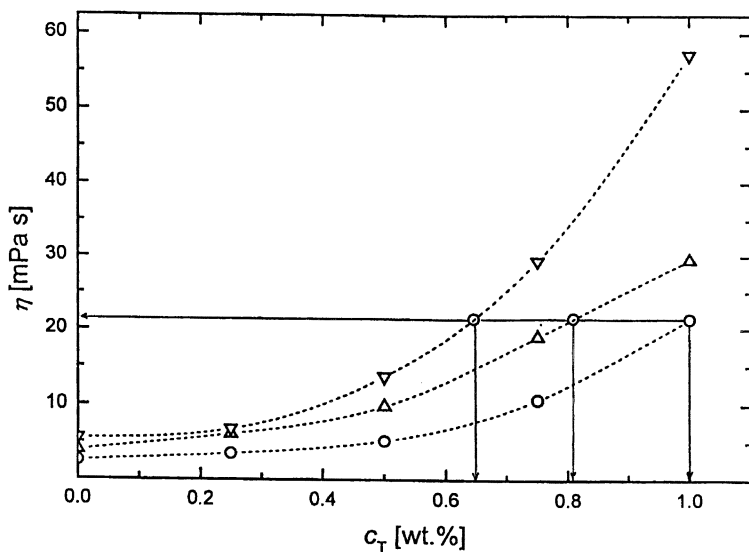
*Figure 5. Dependence of viscosity of 25 wt.% thickened latexes on the
thickener concentration, c_T. Points denoted as in Figure 1.*
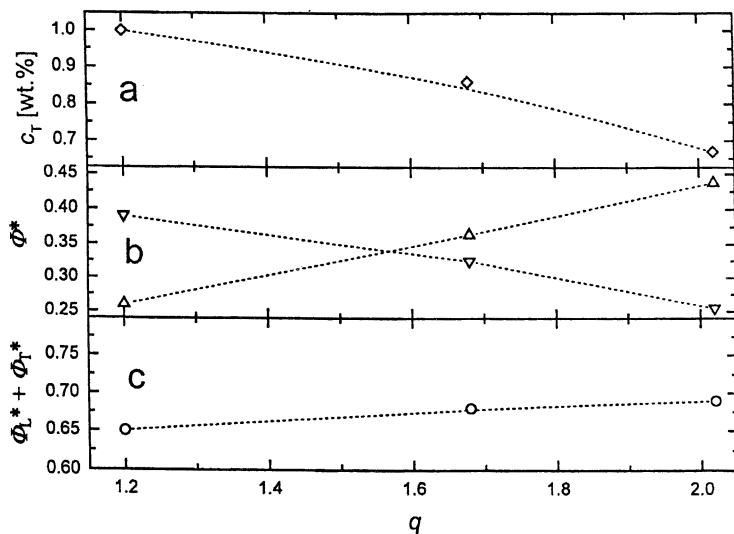
*Figure 6.   Relationship between the thickener concentration c_T, $\Phi*$ the sum
of Φ_L* + Φ_T* and the volume swelling ratio q.
$\triangledown$ ($\Phi* = \Phi_T*$), $\triangle$ ($\Phi* = \Phi_L*$)*

Acknowledgment

References

1. Fordyce, D. B.; Dupre, J.; Toy, W. *Official Digest* **1959,** *2,* 284.
2. Štern, P.; Bradna P.; Quadrat, O. *Rheol. Acta* **1992,** *31,* 361.
3. Bradna, P.; Štern, P.; Quadrat, O.; Šňupárek, J. *Colloid Polym. Sci.* **1995,** *273,* 324.
4. Šňupárek, J.; Krška, F. *J. Appl. Polym. Sci.* **1976,** *20,* 1753.
5. Šňupárek, J. *Makromol. Chem. Suppl.* **1985,** *10/11,* 129.
6. Morgan, J. W.; Jensen, D. P. *Makromol. Chem. Suppl.* **1985,** *10/11,* 59.
7. Mooney, M. J. Colloid Sci. **1951,** *6,* 162
8. Einstein, A. *Ann. Phys., (Leipzig),* **1905,** *17,* 459; **1906,** *19,* 271; **1911,** *34,* 511.

Chapter 7

Seeded Growth: Avoidance of Secondary Particle Formation

D. S. Jayasuriya[1] and R. H. Ottewill[2]

[1]Johnson Polymer, 8310 16th Street, Sturtevant, WI 53177
[2]School of Chemistry, University of Bristol, Bristol BS8 1TS, United Kingdom

In a seeded emulsifier-free polymerization formation of a new batch of particles (secondary nucleation) can occur in addition to growth of the seed particles. In an earlier work an explanation was proposed in terms of the poor colloid stability of the nucleated particles and the probability of their heterocoagulation with the seed particles. Hence, this mechanism implied a dependence on the number of seed particles present. A detailed investigation of the critical number concentration of seeds is now reported.

Aqueous phase polymerization of styrene in the absence of emulsifier was shown to provide a means of preparing monodisperse spherical particles in the diameter range 0.1 to 1.0 μm (*1*). Moreover, variation of electrolyte concentration in emulsifier-free systems also provided a useful means of controlling particle size.

This paper is dedicated to the Memory of John Vanderhoff, friend and colleague for many years.

80　　　　　　　　　© 2002 American Chemical Society

In earlier work a number of authors suggested that coagulation processes played an important part in the process of particle formation in emulsion polymerization (*2,3,4,5*). Basically the concept was that once nucleation occurred to form the first nuclear particles the probability was that these would have insufficient charged groups for the small particle sizes to be colloidally stable (*6,7,8,9*). In view of the high number concentration, coagulation could occur over a short period of time until the coagulae became large enough to attain stability as individual colloidal particles.

Since the size of the initial stable particles controls the number concentration of the system during the diffusional growth period then for the same initial monomer concentration it could be anticipated that the final diameter in the media of higher ionic strength would be larger.

Subsequently, it was shown (*10*) that by adding seed particles to an emulsifier-free polymerization, larger particles, ca 1.0 to 4.0 μm, could be prepared. This concept was based on the idea that colloidal nuclear particles heterocoagulate with the seed particles and hence provide a means of growing the seed particles. However, it was also found necessary to maintain the number concentration of seed particles above a certain value, i.e. a critical number concentration, N_C. This contribution gives a more detailed evaluation of the concept.

Experimental

Equipment for Emulsifier-free Polymerizations

All the polymerizations were carried out in a three-necked round-bottomed Pyrex flask with a capacity of 150 cm^3. A PTFE paddle stirrer (type Q-ST 7/2) was used via the central neck; as recommended previously (*1*), it was placed 1 cm from the base of the flask. The second inlet of the flask was used for a nitrogen input which passed the gas over the surface of the aqueous mixture. The third inlet was used for a water-cooled condenser. The flask was maintained at constant temperature, by immersion up to the neck, in a thermostatted-water bath.

Seeded Emulsifier-free Polymerization

The seed latex dispersed in 50 cm^3 of water was added to the flask and washed in with a further 50 cm^3 of water. This was followed by the addition of a sodium chloride solution, 35 cm^3, which was washed in with 13 cm^3 of water. The stirrer and nitrogen flow were then started. After 10 minutes the stirrer was

stopped momentarily for addition of the requisite amount of styrene. A further 20 minutes was allowed to flush oxygen from the system and to allow temperature equilibrium at 60 °C to be attained. A known concentration of potassium persulfate solution was added and washed in with 20 cm^3 of water.

After a period of 24 hours the flask was removed from the bath and then after leaving to stand for a few minutes unreacted monomer was decanted through a filter funnel packed with glass wool.

Preparation of Seed Latexes

All the polystyrene particles prepared for use as seed latexes were prepared by the method previously described (*1*); the conditions for the preparation of a particular seed-particle size were read from the nomograph given in that paper. The procedure as described for seeded-growth polymerization was used with the following modifications. The stirrer speed was changed to 350 r.p.m.. Water (1340 cm^3) was added in place of the seed dispersion followed by sodium chloride dissolved in water (60 cm^3) and a further quantity of water (30 cm^3) was used in the transfer. These latexes were listed as RB53, RB85, DSJ 2 and DSJ 3. All latexes were cleaned by mixed-bed ion-exchange treatment and their monomer content, surface charge density and particle size distribution determined.

Results

Seeded Growth Polymerization

An example of polystyrene latex particles formed by an emulsifier-free seeded-growth polymerization using the seed latex RB85 is illustrated by the transmission electron micrograph shown in Figure 1. The latex was also characterized by time-average angular-light-scattering with the results analyzed using Mie theory (*11*) computations incorporating a zeroth order log-normal distribution function (*12*). The histogram resulting from electron microscopy is shown in Figure 2 and compared with that from light-scattering. Electron microscopy gave a number-average diameter of 2.19 μm and light scattering a diameter of 2.145 μm.

It is clear from these results that very monodisperse polystyrene particles with a diameter greater than 1 μm can be formed by using a seeded-growth polymerization.
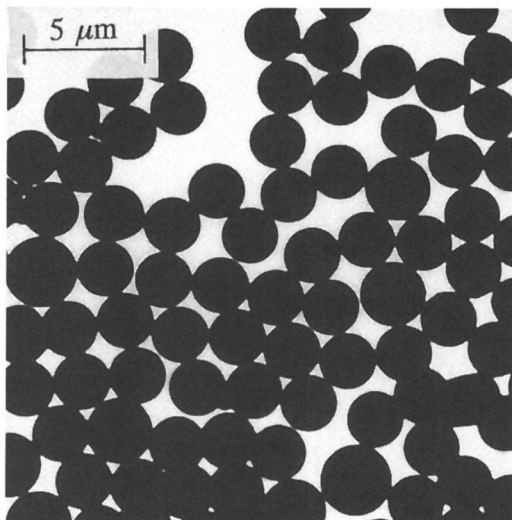
Figure 1: Electron micrograph of polystyrene latex, A(10), from an emulsifier free preparation using seed latex RB85.
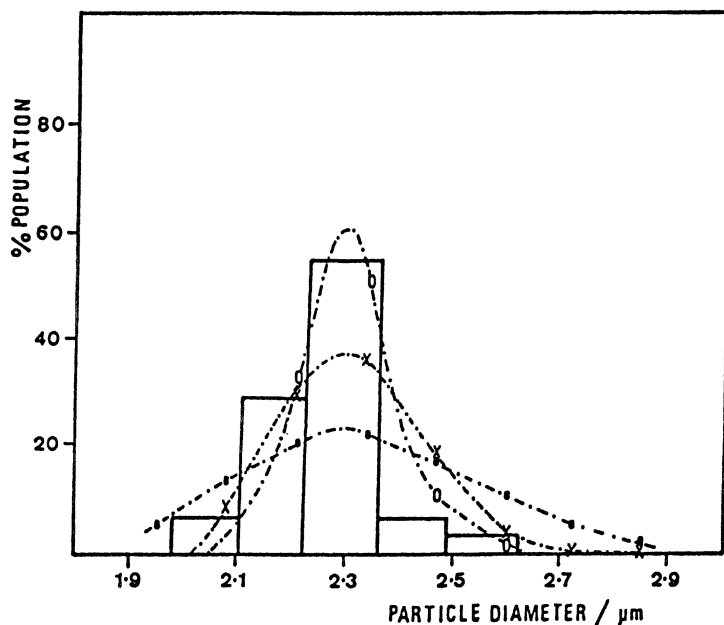
Figure 2: Particle size distributions for latex A(10) from electron microscopy (block) and light scattering (lines) coefficients of variation on the mean radius of 4%, 6% and 10%.

Dependence of Initial Growth Rate on Seed Particle Concentration

Light scattering measurements were used to monitor the radius of particles of latex RB85, which were used as seed particles, in an emulsifier-free system as a function of time at different number concentrations. The conditions used were, initiator concentration 1.58×10^{-3} mol dm^{-3}, sodium chloride concentration 0.025 mol dm^{-3}, styrene 0.72 mol dm^{-3} at a temperature of 60 °C. Results are presented in Figure 3 in the form of particle radius as a function of time for four different number concentrations. These data clearly indicate that the rate of increase in particle radius, R, has a strong dependence on the seed number concentration N_S and that as the number of seed particles increased so the initial rate of increase in particle radius decreased.

The initial gradients obtained from Figure 3 as $(dR/dt)_{t \to 0}$, provide a suitable means of making a comparison between reactions originating from the same latex particles, since all variables were the same except N_S. Thus some results are plotted in logarithmic form in Figure 4 as log $(dR/dt)_{t \to 0}$ against $\log(N_S)$. The results gave a linear plot which fitted the equation:

$$\text{Log } (dR/dt)_{t \to 0} = -1.036 \log(N_S) - \log C \qquad (1)$$

with log C a constant equal to 1.33. Alternatively, this equation can be expressed in the form:

$$(dR/dt)_{t \to 0} = 1.0/ C[N_S] \qquad (2)$$

indicating, that within experimental error, the initial rate of particle growth was inversely proportional to the number of seed particles initially present in the preparation.

Another factor noticed in previous work (10) was that below a certain number concentration of seeds, denoted the *critical number concentration*, N_C, new particles were formed and hence secondary growth occurred in addition to the growth of the seed particles.

Determination of the Critical Number Concentration, N_C

The objective of the investigation was to investigate the value of N_S at which secondary particles were formed, i.e., N_C, under similar conditions of polymerization. Consequently, an estimate was made of the number of new particles formed as a function of the number of seed particles, N_S, in the preparation. For example, as a function of reaction variables such as seed number concentration, initiator concentration and ionic strength.
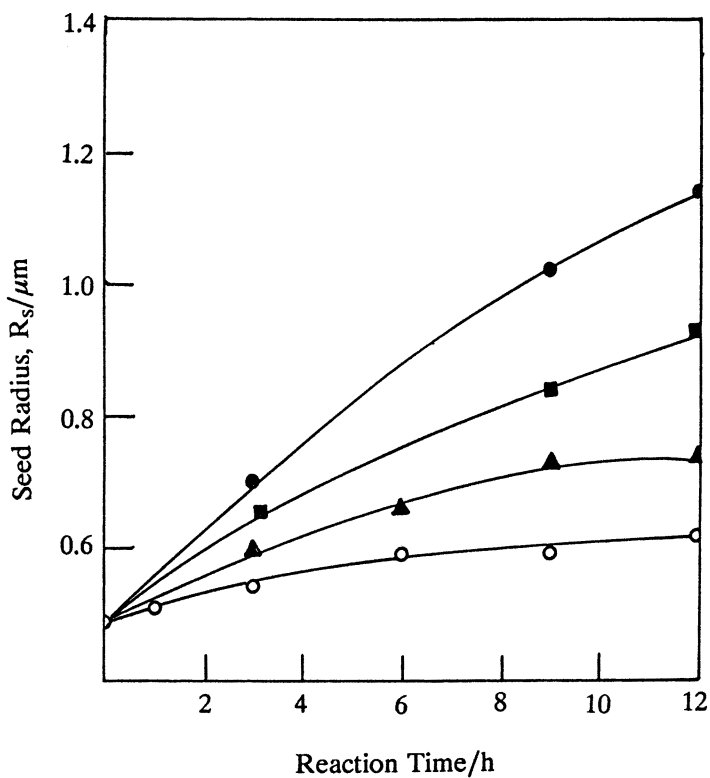
Figure 3: Kinetics of growth of seed particles of RB85 at various values of
$N_s/10^{13} \ dm^{-3}$: ●, 0.75; ■, 1.35; Δ, 1.5; ○, 4.5.
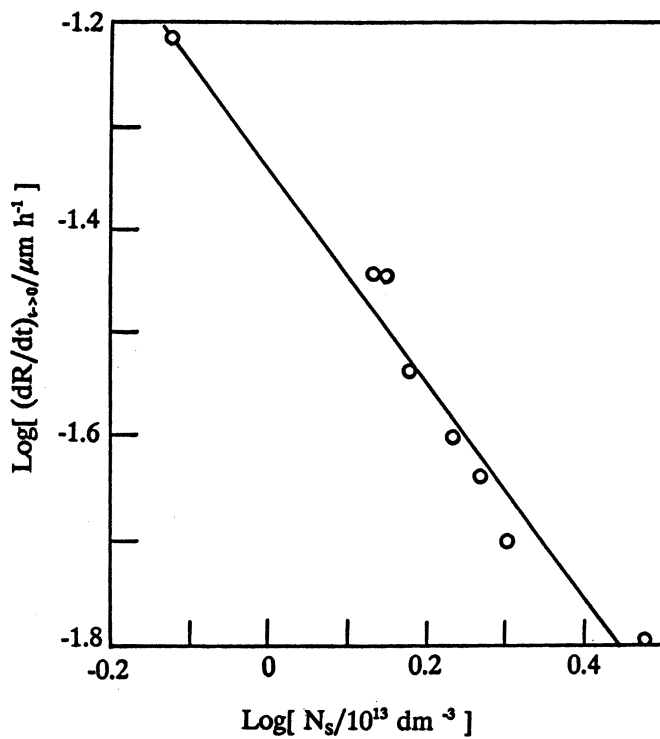
Figure 4: Log of growth rate against log of seed number concentration.

In general, experiments were carried out over a range of N_S values and an estimate made of the number of new particles generated, ΔN, at each seed concentration. Transmission electron microscopy as used in previous work (*10*) formed a convenient method of estimating this number.

Dependence of N_C on the Radius of Seed Particles

Figure 5 shows a plot of ΔN as a function of N_S for experiments carried out using latex DSJ 3 as the seed particles. The value obtained for N_C was $2.8 \pm 0.2 \times 10^{13}$ dm^{-3}.

Values of N_C for different seed particles are given in Table I and plotted in the form of Log(N_C) against Log(R_S) in Figure 6 with R_S the radius of the seed particle in μm. This plot shows clearly that N_C depends on R_S^2 and this is confirmed by the data given in Table I for several seed particles.

Table I. N_C for Various Seed Particles

Seed Latex	R_S/μm	N_C/dm^{-3}	$N_C R_S^2$/μm^2
DSJ 3	0.345	2.8×10^{13}	3.33×10^{12}
DSJ 2	0.445	1.7×10^{13}	3.36×10^{12}
RB 53	0.457	1.7×10^{13}	3.33×10^{12}
RB 85	0.485	1.5×10^{13}	3.53×10^{12}
Y-1[*]	1.040	3.5×10^{12}	3.79×10^{12}
			Average = 3.50×10^{12}

[*] SOURCE: Reproduced with permission from reference 10. Copyright 1976.

Effect of Ionic Strength and Initiator Concentration

Some results were obtained, within a limited range, of the effect of changing ionic strength and initiator concentrations. At low initiator concentrations reactions were very slow and at higher sodium chloride concentrations coagulation occurred. The seed latex used was RB 85, with a styrene concentration of 0.72 mol dm^{-3} at a temperature of 60 °C. The results are presented in Table II.
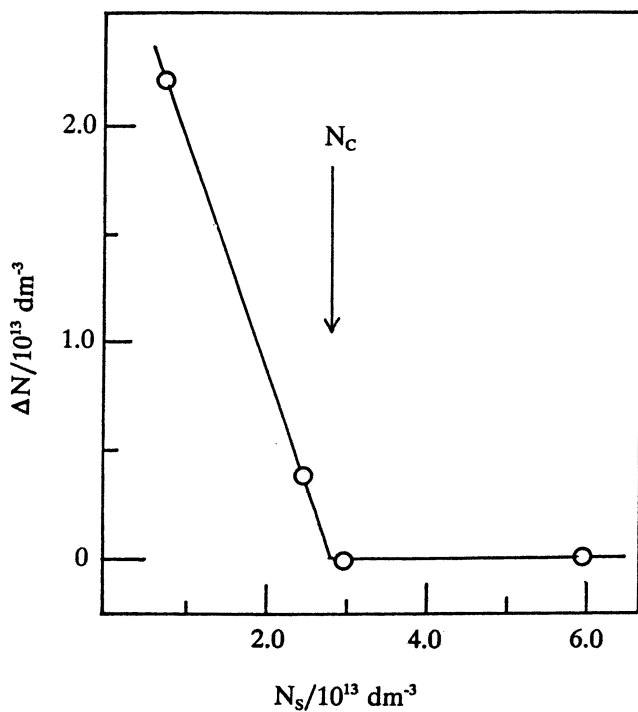
Figure 5: Secondary growth, ΔN, against number concentration of added seeds of latex DSJ 3.
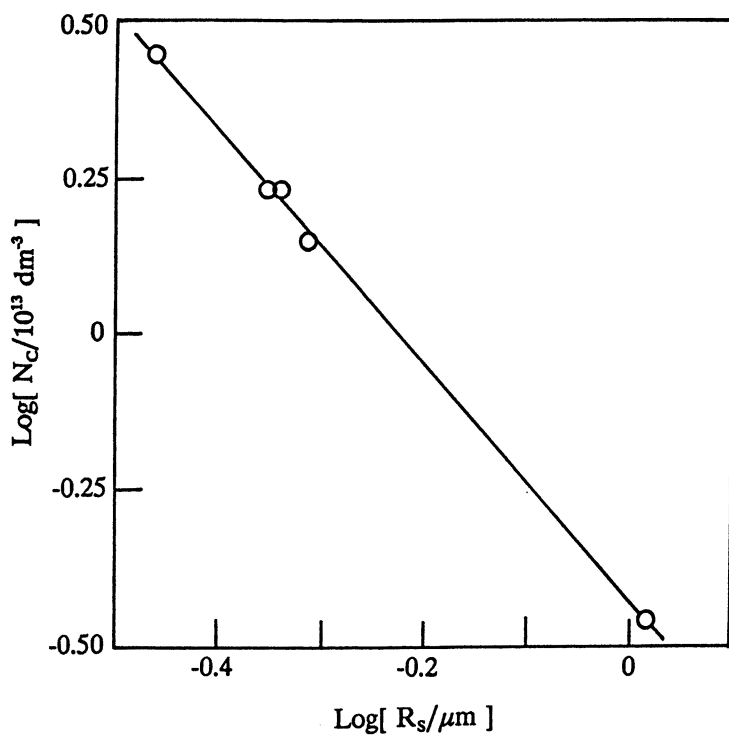
Figure 6: Log (N$_C$) against log (seed radius); (see Table I)

Table II. Variation of N_C with Ionic Strength and Initiator Concentration

Initiator (10^{-3} mol dm^{-3})	0.395	1.58	3.95	8.20
Ionic Strength (10^{-2})	N_C (10^{13} dm^{-3})			
0.119	1.85-2.0	–	–	–
0.474	–	1.5-1.85	–	–
1.185	–	–	1.85-2.0	–
2.460	< 1.85	–	1.35-1.5	2.0-2.5

Within the practical limits of initiator and ionic strength the results appear to indicate, that within experimental error, the effect on N_C was rather small.

Discussion

The experimental studies reported confirm that it is possible to prepare monodisperse polymer colloid particles of polystyrene using a seeded-growth emulsifier-free polymerization. The concept of a critical number concentration, N_C, suggested by the work of Chung-Li et al (10) is also substantiated. Moreover, experiments with seed particles over a range of seed radii, R_S, indicated that for given conditions of initiator, ionic strength, styrene concentration and temperature the parameter, $N_C R_S^2$, had a constant value, i.e., the process depended on the surface area of the seed particles. Hence, from this value the value of N_C could be estimated from a particular series of preparations.

In earlier work (10) it was clearly demonstrated that the rate of uptake of styrene monomer in an aqueous phase by preformed particles was slow. Although the Morton equation (14) is applicable to a system in thermodynamic equilibrium the rate of reaching equilibrium was shown to be slow (10).

The alternative mechanism suggested (10) was that of heterocoagulation between the preformed seed particles, with a number concentration, N_S, and kinetically forming monomer-rich nuclear particles with a number concentration of N_N. Hence on the basis of heterocoagulation three kinetic equations can be considered giving for that rate of disappearance of particles,

Seed-Seed

$$-dN_S/dt = k_O N_S^2 / W_{SS} \tag{3}$$

Nuclear-Nuclear

$$-dN_N/dt = k_O N_N^2 / W_{NN} \qquad (4)$$

Seed-Nuclear

$$-dN_N/dt = k_O N_N N_S / W_{NS} \qquad (5)$$

where W is the stability ratio which is directly related to the pairwise interaction parameter, V_{int}, by the integral equation (15):

$$W = 2 \int_0^\infty \exp(V_{int}/kT) du /(u+2)^2 \qquad (6)$$

with $u = h/R$, where h = the surface-to-surface separation of the particles and R = the radius of the particles.

Under the conditions used, the seed particles were quite stable under the pH and electrolyte concentrations used. Hence, the rate of coagulation of these particles can be taken as zero.

The newly formed nuclear particles, however, were small and dependent on the number of growing chains, their molecular mass and the number of end-groups in the unit. Previous work has shown (8) that these will initially be colloidally unstable and are likely to homocoagulate with themselves or heterocoagulate with the seed particles. For conditions that $N_S \gg N_N$ then the latter is likely to be the dominant process.

The conditions thus place emphasis on equation (5) the seed-nuclei heterocoagulation process. Hence, unless N_S is large enough to scavenge the nuclei as formed the nuclei will grow and form particles large enough to be colloidally stable but of different size to the seed particles thus giving a second crop of particles.

The term k_O in equations (3) to (5) is the rate constant for a diffusion-controlled reaction. Hence, the flux of nuclear particles towards the seed particles will depend on the area of the seed particle available at a given moment, i.e., in the early stages, $4\pi R_S^2 N_C$, thus emphasizing N_C as a critical variable.

These factors appear to confirm the suggestion that monomer is conveyed to the seed particles by monomer swollen small unstable colloidal particles which consequently form growth sites on the seed particle surface.

It has also proved possible to model the process in terms of the experimental variables (16) and this will be reported in a later publication.

References

1. Goodwin, J. W.; Hearn, J.; Ho, C. C.; Ottewill, R. H. *Colloid Polym. Sci.* **1970,** *252,* 464.
2. Goodwin, J. W.; Hearn, J.; Ho, C. C.; Ottewill, R. H. *Br. Polymer J.* **1970**, *5,* 347.
3. Dunn, A. S; Chong, L. C. *Br. Polymer J.* **1970**, *2*, 49.
4. Kotera, A.; Furusawa, K.; Takeda, Y. *Kolloid Z. u Z. Polymere*, **1970**, *239, 677.*
5. Kotera, A.; Furusawa, K.; Kudo, K. *Kolloid Z. u Z. Polymere*, **1970**, *240, 857.*
6. Fitch, R. M.; Tsai, S. H. *Polymer Colloids* (Ed. R.M. Fitch); Plenum Press: New York, **1971**, p.73 & 103.
7. Fitch, R M. *Brit. Polymer J.* **1973**, *5*, 467.
8. Goodwin, J. W.; Ottewill, R. H.; Pelton, R.; Vianello, G.; Yates, D. E. *Br. Polymer J.* **1978**, *10*, 173.
9. Fitch, R. M. *Polymer Colloids*, Academic Press: London, **1997**, 28 & 147.
10. Chung-Li, Y.; Goodwin, J. W.; Ottewill, R. H. *Prog. Colloid Polym. Sci.* **1976**, *60*, 163.
11. Mie, G. *Annalen der Physik*, **1908**, *25*, 377.
12. Espenscheid, W. F.; Kerker, M.; Matijevic, E. *J. Phys. Chem.* **1964**, *68*, 3093.
13. Ottewill, R. H. *Polymeric Dispersions: Principles and Applications*, J.M. Asua, Ed., NATO ASI **1997**, *E337*, 42.
14. Morton, M.; Kaizerman, M. W.; Altier, J. *J. Colloid Sci.* **1954**, *9*, 3.
15. Fuchs, N. *Z. Physik*, **1934**, *28*, 147.
16. Jayasuriya, D. S.; Ottewill, R. H. to be published.

Chapter 8

On-Line Monitoring of Emulsion Polymerization

Klaus Tauer[1], Klaus Padtberg[1], and Carlo Dessy[2]

**[1]Max Planck Institute of Colloids and Interfaces, Am Mühlenberg,
D-14476 Golm, Germany**
[2]WGE Dr. Bures GmbH & Co KG, Hauptstrasse 20, D-14624 Dallgow, Germany

On-line monitoring of changes of characteristic parameters during emulsion polymerizations offers advantages with respect to verifying mechanisms, controlling the process, and tailoring product properties. Only methods are considered which allow an in-line monitoring, i.e., methods without sampling or by-passing. Examples are presented concerning the application of conductivity measurements in combination with turbidity measurements, surface tension measurements, and FT-IR spectroscopy. Each method leads to specific results and conclusions with respect to the mechanism, thus underlying the importance of the combination of methods.

To be able to follow the course of a reaction is a challenge since chemical transformations of matter have been consciously utilized. The ultimate goals of on-line monitoring are to see in situ what is going on, to avoid sampling and off-line analysis, to have a perfect documentation of the processes, and finally to save time as well as money. For laboratory scale investigations, an important additional reason is that real on-line monitoring does not disturb the reacting system with a reaction volume ranging from a few milliliters up to a maximum of

© 2002 American Chemical Society 93

two liters. On-line monitoring means no off-line samples and no by-pass; in other words, the reaction mass is unchanged and remains during the entire reaction inside the reactor. In this sense in-line and on-line monitoring are used interchangeably.

Besides the human senses, temperature is one of the oldest probes to follow a chemical reaction. Consequently, reaction calorimetry has been for more than 35 years a useful tool to measure the rate of heat evolution during a reaction (*1*). There have been several papers appearing over the last six years describing the application of reaction calorimetry to investigate emulsion polymerizations (*2 - 7*). It is a very universal tool, but additional information or model assumptions are needed to find a correlation to the particular reaction, as for instance a combined hardware and software approach as described for methyl methacrylate (MMA) and vinyl acetate (VAc) emulsion copolymerization in (*8*). Besides calorimetric data such procedures require the knowledge of process models and, where appropriate, additional data from off-line sampling (e.g., gas chromatography) (*9 - 16*).

Besides reaction calorimetry, other different analytical techniques have been used (*17, 18*): density measurements of the reaction mixture (*19*), the propagation velocity of ultrasound (*20, 21*), conductance measurements (*22*), near-infrared spectroscopy (*23, 24*), near-infrared Raman spectroscopy (*25, 26*), NMR spectroscopy (*27*), fluorescence spectroscopy (*28*), surface tension measurements (*29*), and a combination of conductivity and turbidity (*30 - 32*). Most of these techniques, including reaction calorimetry, are used to detect the monomer conversion (density measurements, ultrasound, infrared and Raman spectroscopy, NMR spectroscopy) and thus to acquire conversion time curves. The advantage of reaction calorimetry is that the heat flow, which is a measure of the polymerization rate, is directly obtained and faulty numerical differentiation can be avoided. Furthermore, the heat flow signal is a result of processes taking place in the entire reaction volume. It reflects all events in the reactor, presupposing that the heat transfer through the reactor jacket is quick and does not change during the reaction. Whereas, spectroscopic probes average only over a limited volume. Thus, in both cases, it is not automatically clear, whether the signal represents in each case the entire reaction volume. Consequently, reactor fouling and spatial inhomogeneities have to be avoided to get trustworthy results from on-line monitoring.

Equation (1) can be considered as the basic relation in the case of in-line monitoring of compartmentalized polymerizations. H_F is the heat flow, r_p is the rate of polymerization, M is the overall monomer concentration, t is the time, V_P is the total polymer volume, D is the average particle diameter, and N is the particle concentration. It is assumed that the major part of the detected heat is produced during the propagation reaction but not during the other reactions like

initiator decomposition and physical changes (nucleation or swelling) during the polymerization. This is experimentally confirmed for most polymerizations.

$$H_{\mathrm{F}} \equiv r_{\mathrm{P}} = -\frac{\mathrm{d}M}{\mathrm{d}t} = \frac{\mathrm{d}V_P}{\mathrm{d}t} \propto \left(D^3 \cdot \frac{\mathrm{d}N}{\mathrm{d}t} + N \cdot D^2 \cdot \frac{\mathrm{d}D}{\mathrm{d}t} \right) \qquad (1)$$

Equation (1) leads immediately to two important conclusions. Firstly, the r_{P}-curve practically contains all information about the polymerization process. Secondly, for a compartmentalized polymerization, this information can be only extracted if an additional on-line method is applied. The second method should preferably be a method to analyze the particle size or better, the particle size distribution (PSD). Such a combination has been described in (12, 14) where the latex from the reactor is passed through a sampling loop via a density meter (to determine the monomer conversion) into a capillary hydrodynamic fractionation apparatus (to measure the PSD).

The aim of this contribution is to describe the application of in-line methods to investigate emulsion polymerizations. Particularly, results are presented for the application of the combination of conductance and turbidity measurements, to surface tension measurements, and to Fourier transform infrared (FT-IR) spectroscopy. Special emphasis is placed on a comparison of monomers with very different water solubilities, i.e., styrene (STY), MMA, and VAc.

Experimental

Materials

Styrene, methyl methacrylate, vinyl acetate, sodium hydroxide, ferrous chloride, cetyl trimethyl ammonium bromide (CTAB), and potassium peroxodisulfate (KPS) all from Sigma-Aldrich were used as received except the monomers. E30 (from Leuna Werke) is an alkylsulfonate surfactant with an average carbon chain length of 15. SE1030 (a gift from Th. Goldschmidt AG, Germany) is a diblock copolymer consisting of poly(ethylene glycol) with a molecular weight of $3000 \mathrm{\,g\,mol}^{-1}$ and polystyrene with a molecular weight of $1000 \mathrm{\,g\,mol}^{-1}$. The monomers were distilled under reduced pressure to remove inhibitors and stored in a refrigerator. Prior to use, the monomers were checked regarding oligomer formation during storage by adding a drop to an excess of methanol. Only oligomer-free monomers were used. The water was taken from a Seral purification system (PURELAB Plus™) with a conductivity of $0.06 \mathrm{\,\mu Scm}^{-1}$ and degassed prior to use.

Polymerizations

The reactor for simultaneous on-line conductivity and turbidity measurement is an all Teflon™ reactor with a reaction volume of 400 mL. Details of this equipment have been described elsewhere (*30*). For the polymerization, 390 g of water and 5 g of monomer were allowed to equilibrate in the reactor at 70 °C. The polymerization was started by injecting 10 mL of a 4.15 mM (MMA, VAc) or 20.75 mM (STY) potassium peroxodisulfate (KPS) solution. Conductivity and turbidity values were recorded every ten seconds before the injection of the initiator solution and every second afterwards.

On-line surface tension measurements have been carried out as described in detail elsewhere (*29*) with a γ-1001 apparatus (WGE Dr. Bures, Germany). For the continuous polymerizations the reactor was equipped with an overflow lip to adjust the reaction volume to ca. 70 mL. A monomer emulsion (2 L of water, 30 g of monomer, and variable amounts of emulsifier) and an initiator solution (4 g of KPS in 2 L of water) were fed into the reactor with two LsmaTec® pumps (Fluid Metering Inc., USA) with a flow rate of 1.2 mL/min. The polymerization temperature was 70 °C. During the polymerizations approximately 1 mL of latex was withdrawn from the reactor at certain times for particle size measurements utilizing dynamic light scattering (NICOMP model 370, Particle Sizing Systems, USA).

The FT-IR investigations were carried out with a Bio-Rad FTS 6000 spectrometer on an ATR ZnSe crystal with a thickness and a length of 4 mm and 80 mm, respectively. The angle of incidence is 45 ° and there are 19 reflections in the crystal with 10 reflections on the top face. The penetration depth under these conditions is in the mid-IR region between 250 and 400 nm. The temperature on the ATR crystal was 30 °C for the polymerization experiments and varied between room temperature and 60 °C for the investigation of phase transitions. To carry out the polymerizations, a few milliliters of a saturated aqueous MMA solution were placed on the crystal and after thermal equilibration the reaction was started at 30 °C by adding a few drops of both a KPS and a ferrous sulfate solution.

Results

Turbidity and Conductivity Measurements

In previous publications (*30 - 32*), we have shown that a combination of turbidity and conductivity measurements is a very useful tool to investigate the on-line emulsion polymerization of styrene initiated with KPS, either surfactant-free or in the presence of nonionic surfactants.

The time-dependent (t – polymerization time) ratio between the transmission curve ($\vartheta(t)$) and the difference between the theoretical and the practical conductivity curves ($\Delta\kappa(t) = \kappa_{th}(t)-\kappa_{ex}(t)$) corresponds to the fourth power of the change in the average particle size ($D(t)$). Knowing $D(t)$ it is now possible to calculate the polymer concentration (C) from the specific turbidity ($\tau(t)/C$) by using tables of scattering functions backwards. Figure 1 clarifies this principle of measurements schematically. Note, between the transmission and the turbidity (τ), the relation $\tau = \ln(\vartheta/100)$ exists. It is obvious that the procedure depicted in Figure 1 is a general possibility to describe the emulsion polymerization process completely. If conductivity measurements cannot be applied, either because the conductivity difference ($\Delta\kappa$) is too low or $\kappa_{th}(t)$ is not known, the procedure is nevertheless applicable if an independent on-line particle size determination is possible. However, reliable in-line particle size measurements in stirred vessels seem to be impossible at the moment. In the sense of on-line characterization of emulsion polymerizations, this is a necessary field for future developments. Examples, which allow the application of the procedure according to Figure 1 are surfactant-free emulsion polymerizations of STY, MMA, and VAc with KPS as initiator. These monomers are considerably different regarding their water solubilities (STY < MMA < VAc) and hence differences in the nucleation behavior are expected (*33, 34*).

the principle
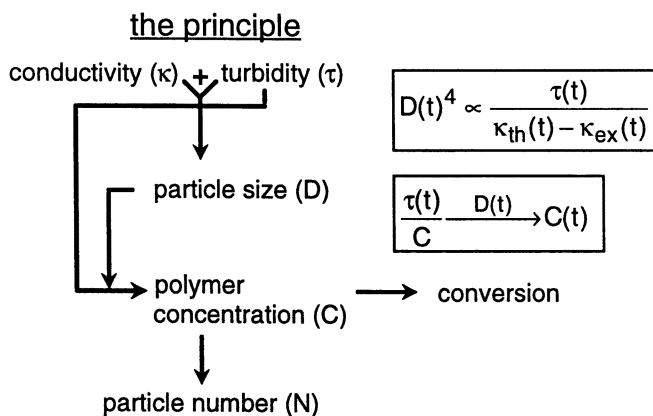
Figure 1. On-line monitoring of emulsion polymerization by in-line measurements of average particle size and turbidity.

With a model based on the classical nucleation theory, the radical polymerization kinetics in the aqueous phase, and the Flory-Huggins theory of

polymer solutions, the nucleation behavior of these three monomers was simulated (*35*). A result of these examinations is that with increasing water solubility of the monomer the pre-nucleation period increases and the nucleation occurs later after the initiator injection. An extensive experimental examination of the emulsifier-free emulsion polymerization of STY has shown that a bend in the conductivity-time curve indicates the onset of nucleation, i.e., the time when the first crop of particles is formed (*30, 31*).

A comparative examination of the three monomers has now shown that the time when the bend in the conductivity-curve occurs correlates strongly with the water solubility of the monomers (cf. Figure 2). Thus, the experimental findings confirm the results of the model calculations.

Note, all results concerning particle nucleation shown here represent the typical behavior from at least 10 repetitions of each experiment. This high number of repetitions is necessary as the rate of nucleation is an exponential function of the energy of activation and hence extremely influenced by small fluctuations in the experimental conditions (temperature, composition of the liquid phase, character and purity of interfaces, etc.).
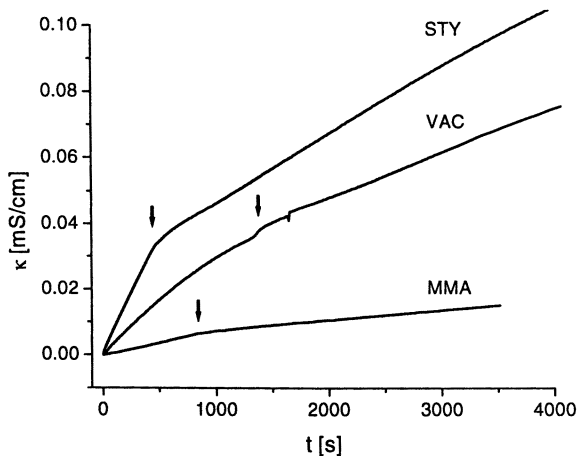
Figure 2. Change of the conductivity during the initial state of surfactant-free emulsion polymerizations; KPS injection at t = 0. The arrows indicate the onset of nucleation. Note, that the KPS concentration in the case of STY is five times higher than for VAc and MMA. In all cases, the κ values are set to zero just after the initiator injection.

Besides the bend as a common feature of the conductivity-time-curves, characteristic differences between the three monomers are obvious. Especially in the case of VAc and STY the difference in the conductivity does not correspond to the initiator concentrations employed. The reason for this behavior becomes clear with a closer look at the conductivity during the thermal equilibration period. The data depicted in Figure 3 clearly shows changes in the conductivity during the thermal equilibration period. Not only for VAc but also for MMA, a steady increase in the conductivity is observed, whereas the conductivity is unchanged over the entire equilibration period for STY.
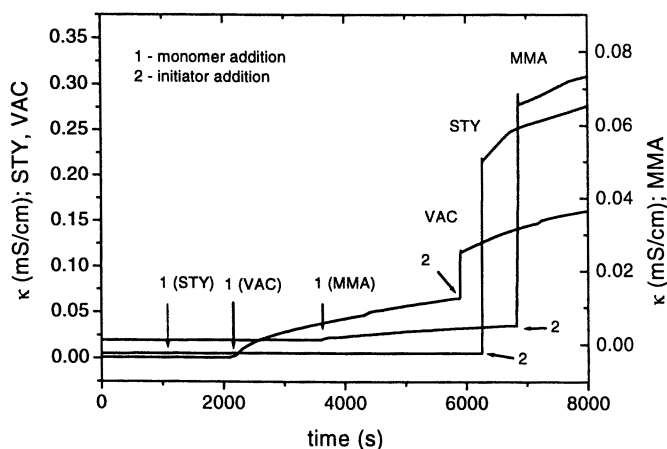
Figure 3. Conductivity change during the entire experiments for STY, MMA and VAc as monomers, respectively. The time between marks 1 and 2 is the thermal equilibration period after monomer addition.

The observed increase in the conductivity clearly is the result of hydrolysis which leads for MMA and VAc to the formation of methacrylic acid and acetic acid, respectively. Note, that the hydrolysis for VAC is much stronger than for MMA. The experimental verification that hydrolysis of MMA and VAc occurs during the thermal equilibration period in pure distilled water is of considerable importance for the particle nucleation process of monomers with hydrolyzable bonds. The important conclusion is, that compared to monomers which are resistant against hydrolysis, the conditions during the pre-nucleation period for monomers with ester bonds are not predetermined alone by the recipe. The formation of methanol/methacrylic acid and acetaldehyde/acetic acid during the

pre-nucleation period of MMA and VAc, respectively, has a distinct influence on the nucleation behavior. In both cases the solubility of the nucleating oligomers as well as the interfacial tension of the nucleus to the surrounding liquid phase are changed compared to the neat system. Note, solubility of the nucleating species and interfacial tension of the nucleus to the surrounding liquid are two important variables influencing the nucleation process (*31, 35*). These results prove both the usefulness and the high sensitivity of conductivity measurements for on-line investigations of emulsion polymerizations. The reactor for these investigations has two optical windows and acts simultaneously as a cell for transmission measurements. Note, $\vartheta(t)$ does not react on the hydrolysis of the ester bonds although the optical path-length in this reactor-cell is almost 10 cm. However, the transmission-time curves show characteristic differences between the three monomers (cf. Figure 4). These differences are due to a different development of particle number and particle size after the first particle nucleation event. It is interesting to note that the transmission at a given time decreases not only with increasing water solubility, but also with increasing rate of hydrolysis of the monomers. The much stronger decrease in the case of STY is additionally of course due to the higher KPS concentration leading to both higher radical production and higher ionic strength. A closer look at the change in the transmission in the time domain where the bend in the conductivity-time curve occurs reveals another interesting effect. This behavior is called "jumbo"-effect and although the transmission changes only about 1%, it is a very typical behavior for all three monomers. The "jumbo"-effect is obviously caused by alterations in the optical properties of the reaction system during the nucleation period. Seemingly, the optical density of the reaction system decreases, which could be possibly due to density fluctuations during the homogeneous nucleation and which reflects the fact that the properties of critical nuclei can be considerably different from those of mature latex particles. This approach is in agreement with modern theoretical reflections on homogeneous nucleation (*36, 37*). Note, density fluctuations indicates both spatial regions of higher as well as of lower density. A completely satisfying explanation of the observed effect is not yet possible.

In summary, the above presented experimental results show that conductivity and turbidity measurements are very useful for on-line investigations of emulsion polymerizations. The on-line combination of both methods is especially suited to throwing light upon the nucleation period during the initial stage of ab initio polymerizations.
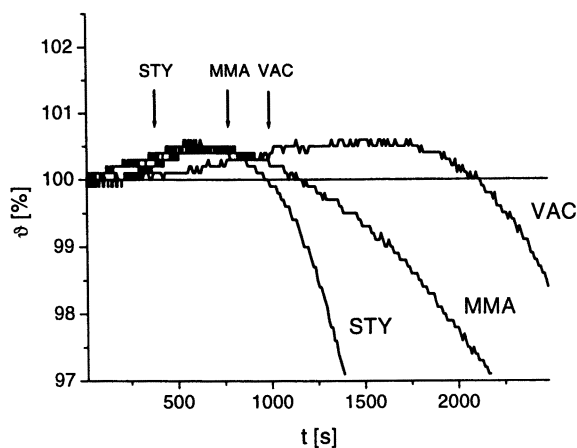
Figure 4. Transmission change in the time domain of the bend in the conductivity-time curve. The arrows indicate the occurrence of the bends in the conductivity curves.

Surface Tension Measurements

Due to the use of emulsifiers in almost all technical emulsion polymerizations, on-line surface tension measurements *per se* are of particular interest. Such a technique promises both important insights regarding the mechanism of the polymerization and possibilities to minimize the emulsifier level, which is of special interest to improve application properties. Recently, a modified bubble pressure technique, the so-called bubble pressure difference (BPD) technique, has been reported which allows one to measure on-line surface tensions even if the reactor contents are stirred (*29*). This technique is based on the experimental finding that the difference between the maximum and the minimum pressure during bubble formation correlates strongly with the surface tension of the surrounding solution. For instance, the applicability of this technique has been shown during surfactant synthesis and surfactant-free emulsions polymerizations (*29*). Note, the method is suited to follow changes in the surface tension rather than to measure absolute values of the surface tension. In this sense, the values of the surface tension are considered to be apparent values at given particular conditions (γ_{app}). Note, that the method works optimally with of the bubble frequency of about 0.5 s^{-1}. This indicates that the method is in a transition state between dynamic and static measurements although it is very likely that under the particular conditions γ_{app} is closer to the static than the dynamic surface tension (*38, 39*) especially for pure liquids and

low molecular weight surfactant solutions. If the reactor is equipped with the surface tension probe, which is nothing else than two capillaries with equal immersion depth, and a temperature probe, the measurement of the temperature dependence of the surface tension is quite easy. The result of such a measurement for pure water is shown in Figure 5. The almost linear decrease with increasing temperature is clear to see.
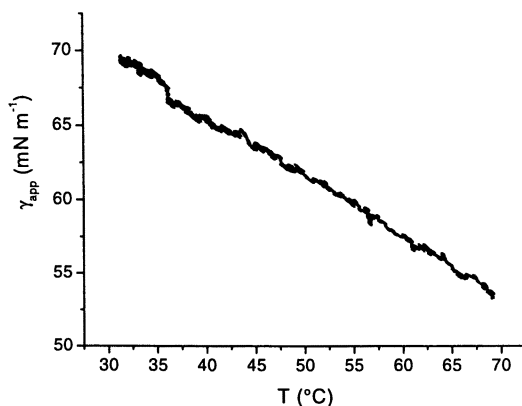
Figure 5. Dependence of the surface tension of pure water on temperature as measured with the BPD method.

Of course, the temperature dependence of γ_{app} is influenced by the composition of the aqueous phase and hence different values of $d\gamma_{app}/dT$ are determined for instance for different surfactant solutions. The data depicted in Table I show that the BPD method is suited to distinguish clearly between solutions of different surfactants.

Table I. Temperature Coefficient of γ_{app} for Different Aqueous Solutions

Surfactant	$d\gamma/dT \, (mNm^{-1}grd^{-1})$
E30 (alkylsulfonate)	$- 0.2073 \pm 0.016$
SE1030 (block copolymer)	$- 0.3975 \pm 0.035$
CTAB (cationic surfactant)	$- 0.2430 \pm 0.035$
None	$- 0.4135 \pm 0.016$

Note: The concentration was in all cases 1 g of surfactant in 200 mL of water.

The temperature dependence of the interfacial tension is a point which is absolutely of some meaning at least for theoretical considerations of emulsion polymerizations where interfacial energies are used to explain experimental results. In previous investigations of surfactant-free emulsion polymerizations, it was shown that the BPD method is sensitive to the monomer dissolved in the aqueous phase.

Just after the start of the polymerization with KPS, an increase in γ_{app} is observed which is caused by the consumption of the monomer in the aqueous phase (29). The situation is different if the BPD method is used to follow emulsion polymerizations in the presence of surfactants (cf. Figure 6).

The curves depicted in Figure 6 represent the very typical behavior as even the two maximums in the case of VAc are reproducible. Compared to the surfactant-free polymerizations, the increase in γ_{app} takes place at much later times and leads to much higher γ_{app} values. In order to clarify the reason for the increase, the surface tension of the final latexes was checked by the Du Nouy ring method. The values for all three systems at room temperature were about 33 mN m^{-1}. Obviously, the increase is not caused by a decrease in the free surfactant concentration due to adsorption. Possibly, changes in the composition of the aqueous phase are responsible for the increase. As mentioned above, the method works in a transition state between static and dynamic surface tension and, thus a change in the viscosity of the aqueous phase changes γ_{app}. The dynamic surface tension correlates directly to the viscosity of the solution (40). Note, the viscosity of a dispersion is also higher than that of water. Whether it is the viscosity of the dispersion or of the continuous phase which influences the course of the surface tension, independent viscosity measurements must be applied additionally (for instance the power input by the stirrer).

To complete the experimental data of the experiments depicted in Figure 6, it is should be mentioned that the average particle size of the final latexes clearly depends on the monomer. These are for STY, MMA, and VAc 9.4 nm, 15.6 nm, and 37.5 nm, respectively.

The use of on-line surface tension measurements to investigate continuous emulsion polymerizations is of special interest as sustained oscillations of the surface tension in the steady state are frequently reported (41, 42). The data plotted in Figure 7 are a proof that with the BPD method, continuous polymerizations can be investigated. This particular experiment lasted almost a week and the BPD equipment worked without any problems. During the run, the surfactant concentration in the feed was decreased from 1.285 g of E30 per liter water to 0.76 g L$_W^{-1}$ up to zero. To determine the average particle size, samples were withdrawn from the reactor and investigated by dynamic light scattering. The polymerization was started with a batch polymerization and after 30 minutes the feed streams were switched on. The changes of both quantities correlate over

the entire polymerization. A stepwise decrease in the emulsifier concentration leads to a stepwise increase of both γ_{app} and D. Figure 8 shows a magnification of the transition range between where the emulsifier concentration was changed (transition between A and B in Fig. 7).
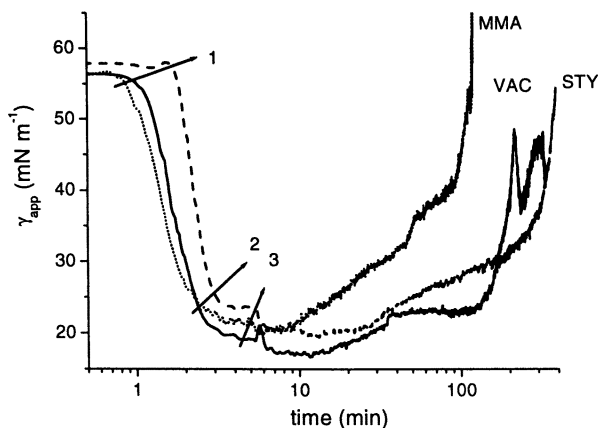
Figure 6. On-line surface tension measurements during batch emulsion polymerizations of STY (dashed line), MMA (dotted line), and VAc (solid line). Recipe: 70 g of water, 1.05 g of monomers, 0.175 g of E30, 0.14 g of KPS, and 70 °C. 1 – E30 addition; 2 – monomer addition; 3 – KPS addition.

The sensitivity of the BPD apparatus is high enough to follow the changes caused by an alteration of the emulsifier concentration. In that particular case, both the on-line and the off-line data set change in an expected manner. However, an interesting feature, which is only detectable with an on-line technique, is the overshoot of γ_{app} before the new steady state is reached. Both records depicted in Figure 8 admit the supposition that there are correlations between D and γ_{app} also on smaller time-scales. However a qualified analysis is not possible at the moment due to the differences in the quality of both data sets. The BPD method creates huge data files as the pressure difference during the formation and detachment of each bubble is used to calculate γ_{app}. At the moment, it is not yet clear how it is possible to separate the inherent scatter of the BPD method and the changes which are caused by the continuous polymerization. Note, during investigations of continuous emulsion polymerizations with off-line sampling, changes in the latex surface tension have been observed also on the time-scale of minutes (*42*). Anyway, a decision needs further experiments preferably in combination with another on-line method.
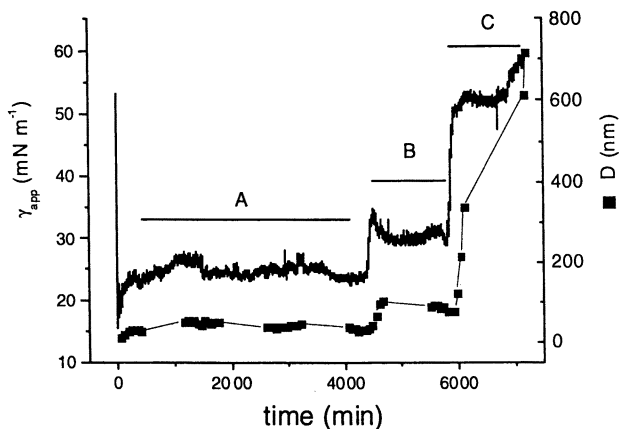
Figure 7. Change of γ$_{app}$ and average particle size (D) during a continuous emulsion polymerization of MMA. Recipe:70 g of water, 0.14 g of KPS, 0.16 g of E30, 1.05 g of MMA for the batch period; (cf. experimental part for conditions during feed period). A – 2.285 g E30 /L$_W$, B – 0.76 g E30 / L$_W$, C – no E30.
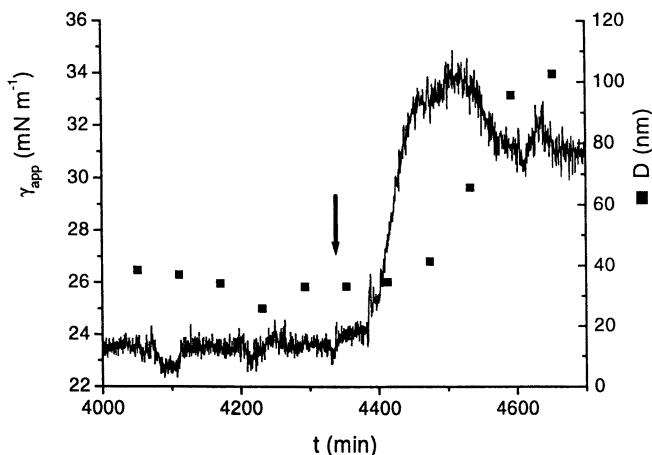
Figure 8. Change of γ$_{app}$ and D during a continuous emulsion polymerization of MMA in the transition range when the emulsifier concentration in the feed is reduced (from A to B, cf. Fig. 7). The arrow marks the set point where the emulsifier concentration was lowered.

In conclusion of this part, besides all problems the BPD method is generally suited to measure on-line changes of the surface tension inside stirred reactors. As the bubble pressure depends mainly on the surface tension and the viscosity of the surrounding liquid, the combination with on-line viscosity measurements will improve the reliability of surface tension measurements based on the Laplace equation.

FT-IR Spectroscopy

Vibrational spectroscopy is *per se* sensitive to both inter- and intramolecular interactions. It is a powerful tool in colloid sciences not only for structure elucidation but also for the investigations of aggregation processes and molecular transformations. FT-IR spectrometers nowadays possess high speed data collection, great flexibility and versatility (*43*). Furthermore, the energy throughput is high and the detection sensitive enough that measurements are possible even in aqueous systems. Raman spectroscopy can be considered almost as a common spectroscopic technique to follow closely the intensity of double bonds during the course of a radical polymerization also in aqueous systems (*17, 18, 25, 26, 44*). Much fewer examples are known where FT-IR spectroscopy is used to monitor polymerizations in an aqueous medium (*23, 24*). As FT-IR spectroscopy is sensitive to molecular interactions more information should be accessible than "only" conversion data. Figure 9 shows a FT-IR spectrum of an aqueous MMA solution at 30 °C before the polymerization was started with a redox initiator system KPS / ferrous sulfate.

Note, at the start of the polymerization the solution was completely transparent but it became turbid in the course of the polymerization. During the polymerization of this solution on the ZnSe-ATR crystal the FT-IR spectrum changes in a very specific way as the intensity of certain bands decreases and that of other bands increases (cf. Figure 10).

During the reaction the C-O-C – stretching vibration (1159 cm^{-1}) and the characteristic backbone vibration (1300 cm^{-1}) strongly decreases. Only slight decreases are observed in the regions of the CH_2 – wagging (941 cm^{-1}) and the C=C– stretching (1636 cm^{-1}) vibrations. The intensities of the CH_3 – deformation (1438 cm^{-1}) and of the second band in the doublet of the C-O-C – stretching vibrations remain almost constant. Possibly the most interesting feature is the increase in the intensity of the C=O– stretching vibration (1720 cm^{-1}), which can possibly be explained by an aggregation of PMMA-oligomers during the nucleation period. This increase starts approximately in the middle of
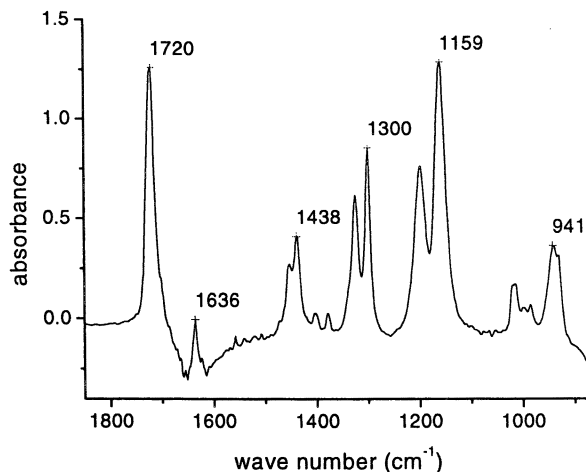
Figure 9. FT-IR spectrum of an aqueous solution saturated with MMA at 30 °C (ZnSe-ATR crystal). A peak assignment to single vibrations is possible in the following way: 941 cm^{-1}: CH$_2$ wagging; 1159 cm^{-1}: C-O-C stretching (doublet with 1200 cm^{-1}); 1300 cm^{-1}: backbone; 1438 cm^{-1}: CH$_3$ deformation; 1636 cm^{-1}: C=C stretching;1720 cm^{-1}: C=O stretching

the reaction (cf. Figure 10). Also the data depicted in Figure 11 confirm that the transition from a solution to a dispersion causes characteristic changes in the FT-IR spectrum.

The spectra shown in Figure 11 were recorded in such a way that an aqueous solution of the oligomers was placed on a ZnSe-ATR crystal at 25 °C (spectrum A).

Then the solution on the ATR-crystal was heated. As the oligomers possess a lower critical solution temperature in the range between 40 °C and 60 °C, the solution turns into a dispersion (spectrum B). Finally, the dispersion was kept at 60 °C until the water was evaporated and the spectrum of the solid was recorded after cooling to 25 °C (spectrum C).

For the nucleation period during an emulsion polymerization, the transition from a solution to a dispersion is of special interest. The data summarized in Figure 12 reveal that it is possible to closely follow the transition from a solution to a dispersion by means of FT-IR spectroscopy.
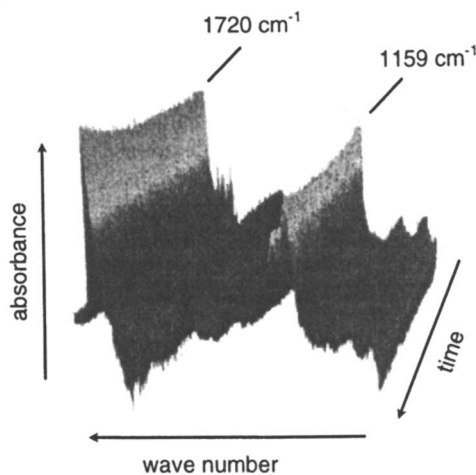
Figure 10. Change in the FT-IR spectra during the polymerization of an aqueous MMA solution started with a persulfate – ferrous sulfate redox system at 30 °C. The polymerization was carried out on a ZnSe-ATR crystal. The reaction volume of about 2 ml was protected against air by a cover which allowed purging of the space over the reaction mixture with nitrogen. 10 spectra per second were recorded over a duration of 10 minutes. During this time the completely transparent MMA solution was converted into a latex.
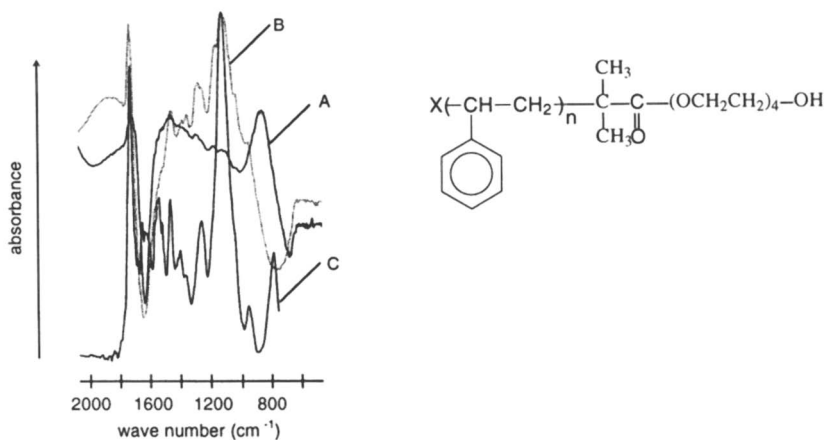
Figure 11. FT-IR spectra of polystyrene oligomers with poly(ethylene glycol) end groups (cf. Inserted formula where X depends on the termination mode) in different physical states. A – solution at 25 °C; B – dispersion at 60 °C; C – solid at 25 °C; The spectra are dominated by the poly(ethylene glycol) block.

The time-dependent data in Figure 12 clearly show the onset of the phase transition. It is supposed that this is the point where the intensities of the bands at 1100 cm^{-1} and 1720 cm^{-1} start to increase. As the increase lasted over almost one minute information about the kinetics of phase separations are principally accessible.
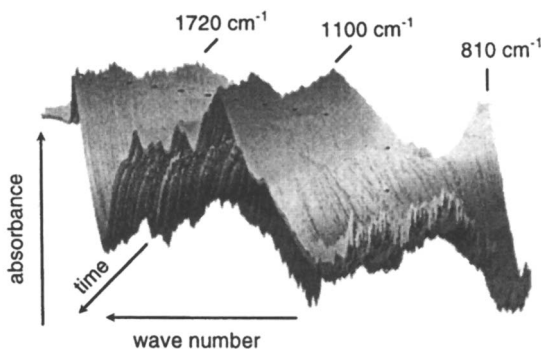
Figure 12. Change in the FT-IR spectra of polystyrene oligomers with poly(ethylene glycol) end groups (cf. caption of Figure 11) during the transition from a solution into a dispersion; during the duration of the experiment (4 minutes) the temperature was raised from 30 °C to 60 °C and 5 spectra were recorded per second.

In summary, FT-IR spectroscopy is a powerful tool to investigate emulsion polymerization not only with respect to the monomer consumption but also regarding particle nucleation. Fast FT-IR techniques allows the acquisition of kinetic information about phase transitions on the time scale of milliseconds.

Conclusions

Nowadays several techniques are available which allow an on-line or in-line monitoring of emulsions polymerizations with high accuracy and high speed. Fast techniques offer possibilities to investigate processes with characteristic times in the sub-second range. So it is in principle possible to closely follow the polymerization regarding very different time scales from minutes typical for the monomer conversion up to milliseconds for phase transitions during the nucleation process.

An important task for future developments is the search for combinations of methods as there is no single universal method that allows the on-line characterization of the whole process in the sense as depicted in Figure 1.

From the technical point of view, the future challenges are even harder as the high solids contents of commercial emulsion polymerizations brings about problems which can be avoided in labscale investigations at low solids. The most important problem is obviously a fouling of the probes due to polymer deposition at higher solids contents. It will be a matter of future investigations whether or not radical scavengers at the walls of the probe can be applied to avoid fouling.

But despite all difficulties and problems, compared to the present-day situation, on-line investigations of emulsion polymerizations will enable several benefits especially regarding production control, product quality, and scientific understanding of the process.

Acknowledgments

References

1. Landau, R. N. *Thermochimica Acta* , **1996**, 289, 101-126.
2. de la Rosa, L. V.; Sudol, E. D.; El-Aasser, M. S.; Klein, A. *J. Polym. Sci. Polym. Chem.* **1996**, 34, 461-473.
3. Gloor, P. E.; Warner, R. *J. Thermochimica Acta* **1996**, 289, 243-265
4. de Arbina, L. L.; Gugliotta, L. M.; Barandiaran, M. J.; Asua, J. M. *Polymer* **1998**, 39, 4047-4055.
5. Tauer, K.; Müller, H.; Schellenberg, C.; Rosengarten, L. *Colloid Surf. A-Physicochem. Eng. Asp.* **1999**, 153, 143-151.
6. de la Rosa, L. V.; Sudol, E. D.; El-Aasser, M. S.; Klein, A. *J. Polym. Sci. Polym. Chem.* **1999**, 37, 4054-4065.
7. Gugliotta, L. M.; Vega, J. R.; Antnione, C. E.; Meira, G. R. *Polym. React. Eng.* **1999**, 7, 531-552.
8. Santos, A. M.; Févotte, G.; Othman, N.; McKenna, T. F. *J. Appl. Polym. Sci.* **2000**, 75, 1667-1683.
9. de Buruaga, I. S.; Arotcarena, M.; Armitage, P. D. ; Gugliotta, L. M.; Leiza, J. R.; Asua, J. M. *Chem. Eng. Sci.* **1996**, 51, 2781-2786.

10. de Buruaga, I. S.; Echevarria, A.; Armitage, P. D.; de la Cal, J. C.; Asua, J.M. *AIChE J.* **1997**, 43, 1069-1081.
11. Yabuki, Y.; McGregor, J.F. *Ind. Eng. Chem. Res.* **1997**, 36, 1268-1275.
12. Liotta, V.; Georgakis, C.; Sudol, E. D.; El-Aasser, M. S. *Ind. Eng. Chem. Res.* 1997, 36, 3252-3263.
13. Saldivar, E.; Ray, W. H. *AIChE J.* **1997**, 43, 2021-2033.
14. Liotta, V.; Sudol, E. D.; El-Aasser, M. S., Georgakis, C. *J. Polym. Sci. Polym. Chem.* **1998**, 36, 1553-1571.
15. Echevarria, A.; Leiza, J. R.; de la Cal, J. C.; Asua, J. M. *AIChE J.* **1998**, 44, 1667-1679.
16. Arzamendi, G.; Sayer, C.; Zoco, N.; Asua, J. M. *Polym. React. Eng.* **1998**, 6, 193-223.
17. Hergeth, W.-D. in *Polymeric Dispersions: Principles and Applications* (ed. J. M. Asua), Kluwer, Dordrecht, **1997**, 243-256.
18. Hergeth, W.-D. in *Polymeric Dispersions: Principles and Applications* (ed. J. M. Asua), Kluwer, Dordrecht, **1997**, 267-288.
19. Schork, F. J.; Ray, W. H. *J. Appl. Polym. Sci.* **1983**, 28, 407-430.
20. Apostolo, M.; Canegallo, S.; Siani, A.; Morbidelli, M. *Macromol. Symp.* **1995**, 92, 205-221.
21. Canegallo, S.; Apostolo, M.; Storti, G.; Morbidelli, M. *J. Appl. Polym. Sci.*, **1995**, 57, 1333-1346.
22. Reimers, J. L.; Schork, F. J. *J. Appl. Polym. Sci.* **1996**, 60, 251-262.
23. Wu, C. C.; Danielsen, J. D. S.; Callis, J. B.; Eaton, M.; Ricker, N. L. *Process Contr. Qual.* **1996**, 8, 1-23.
24. Wu, C. C.; Danielsen, J. D. S.; Callis, J. B.; Eaton, M.; Ricker, N. L. *Process Contr. Qual.* **1996**, 8, 25-40.
25. Ozpozan, T.; Schrader, B.; Keller, S. *Spectrochimica Acta A - Molec. Spectr.* **1997**, 53, 1-7.
26. Alkhanbashi, A.; Dhamdhere, M.; Hansen, M. *Appl. Spectr. Rev.* **1998**, 33, 115-131.
27. Landfester, K.; Spiegel, S.; Born, R.; Spiess, H. W. *Coll. Polym. Sci.* **1998**, 276, 356-361.
28. Rudschuck, S.; Adams, J.; Fuhrmann, *J. Macromol. Chem. Phys.* **1998**, 199, 771-776.
29. Tauer, K.; Dessy; C.; Corkery, S.; Bures, K.-D. *Coll. Polym. Sci.* **1999**, 277, 805-811.
30. Kühn, I.; Tauer, K. *Macromolecules* **1995**, 28, 8122-8128.
31. Tauer, K.; Kühn, I. in *Polymeric Dispersions: Principles and Applications* (ed. J. M. Asua), Kluwer, Dordrecht, **1997**, 49-65.
32. Tauer, K.; Deckwer, R.; Kühn, I.; Schellenberg, C. *Coll. Polym. Sci.* **1999**, 277, 607-626.

33. Fitch, R. M. *Polymer Colloids: A Comprehensive Introduction*; Academic Press: San Diego, London, Boston, New York, Sydney, Tokyo, Toronto:, **1997**.
34. Gilbert, R. G. *Emulsion Polymerization A Mechanistic Approach*; Academic Press: London, San Diego, New York, Boston, Sydney, Tokyo, Toronto: **1995**.
35. Tauer, K.; Kühn, I. *Macromolecules* **1995**, 28, 2236-2239.
36. Gunton, J. D. *J. Statist. Physics* **1999**, 95, 903-921.
37. Duan, R.-G.; Liang, K.-M.; Gu, S.-R. *Physics Letters A* **2000**, 266 370-376.
38. Fainerman, V. B. *Colloids Surf.* **1992**, 62, 333-347.
39. Khim., K. D.; Deignan, P. *Fuel* **1995**, 74, 295-300.
40. Fainerman, V. B.; Makievski, A. V.; Miller, R. *Coll. Surf A: Physicichem. Eng. Asp.* **1993**, 75, 229-235.
41. Ley, G.; Gerrens, H. *Makromol. Chem.* **1974**, 175, 563-.
42. Tauer, K.; Müller, I. *Acta Polymerica* **1993**, 44, 285-293.
43. Rintoul, L; Panayiotou, H.; Kokot, S.; George, G.; Cash, G.; Frost, R.; Bui, T.; Fredericks, P. *Analyst* **1998**, 123, 571-577.
44. Yu, J.; Liu, H.-Z.; Chen, J.-Y. Chin. *J. Polym. Sci.* **1999**, 17, 603-606.

Chapter 9

Challenges in On-Line Control of Composition and Molecular Weight Distribution of Nonlinear Emulsion Copolymers

M. Vicente, J. R. Leiza, and J. M. Asua*

Institute for Polymer Materials (POLYMAT) and Grupo de Ingeniería Química, Departamento de Química Aplicada, Facultad de Ciencias Químicas, The University of the Basque Country, Apdo. 1072, 20080, Donostia-San Sebastián, Spain

The applicability of the control strategies developed for the simultaneous control of copolymer composition and MWD of linear polymers to nonlinear polymers is investigated. It was shown that a reasonable control of both properties could be achieved for the emulsion copolymerization of methyl methacrylate and butyl acrylate when the process was carried out under semi-flooded conditions. The industrial implications of this process are discussed.

Acrylic latexes account for an important part of commercial emulsion polymers. Many applications of these latexes require the formation of a continuous film with high mechanical strength. Both the film formation process and the mechanical properties of the film strongly depend on the chemical composition and molecular weight distribution (MWD) of the polymer. Chemical composition mainly determines the glass transition temperature (T_g) of a copolymer (*1*). On the other hand, MWD affects important end-use properties of the film such as elasticity, strength, toughness, and solvent resistance.

© 2002 American Chemical Society 113

Copolymer composition is the molecular property of a polymer more often controlled using both open-loop and closed-loop control strategies (2-9). To achieve this goal, an a priori simple, but not always easily attainable, condition must be fulfilled: the ratio of the comonomers in the polymerization loci should be controlled.

The control of the MWD of emulsion polymers by means of closed-loop control strategies is a challenging subject because the feasibility of the on-line measurement of the MWD for emulsion systems remains to be demonstrated. In addition, the compartmentalized nature of the emulsion polymerization, generally speaking, makes the MWD non-observable from typically available on-line measurements (monomer conversion and temperatures). Nevertheless, under some conditions of practical significance, the MWD of emulsion polymers is not affected by the compartmentalization of the system. A typical example is when chain transfer agent is used and the kinetic chain length is controlled by the chain transfer reaction to CTA in linear polymer systems (10). For these systems, the desired MWD may be decomposed into a series of instantaneous MWDs to be produced at different stages of the process (11). Each of the instantaneous MWDs can be obtained by adjusting the monomer/CTA ratio. This feature has been used to produce narrow, broad, and even bimodal distributions of styrene homopolymers (10-12) and styrene/butyl acrylate copolymers (13).

This work explores the applicability of the mentioned approach to control on-line the MWD of nonlinear emulsion polymers. Nonlinear polymers are formed through several reactions including chain transfer to polymer and propagation to terminal double bonds. A key aspect of these processes is that they involve inactive polymer chains, namely, "dead" polymer chains that are converted into active radicals modifying their molecular weight. This may jeopardize the strategy of building the desired MWD from a series of well-defined instantaneous MWDs. The simultaneous on-line control of the copolymer composition and molecular weight distribution in the emulsion copolymerization of methyl methacrylate and butyl acrylate was considered. This system undergoes extensive chain transfer to polymer that yields a branched copolymer and eventually gel (14-15).

Control Strategy

Figure 1 summarizes the control strategy used in this work. For linear polymer systems in which the chain transfer to CTA is the main termination event, the desired MWD can be tailored by producing a series of well-defined MWDs at different stages of the process, as qualitatively illustrated in Figure 2 (11). For a copolymerization system, the instantaneous number-average chain length and the chain length distribution are given by:
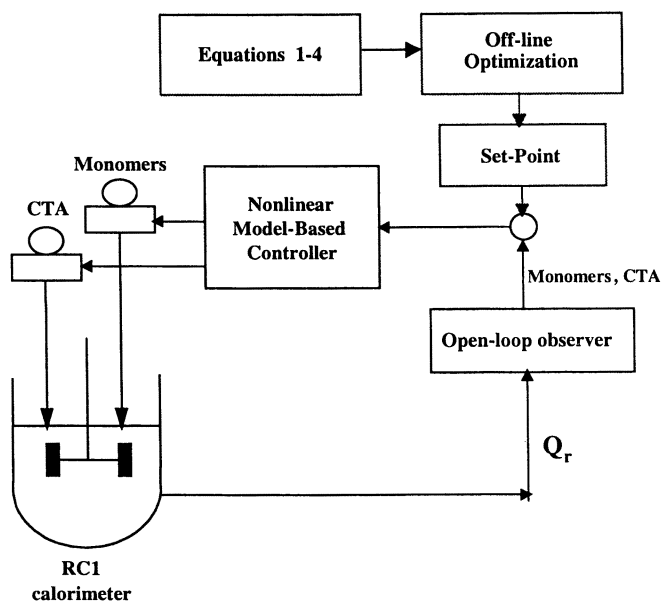
Figure 1. Control strategy.
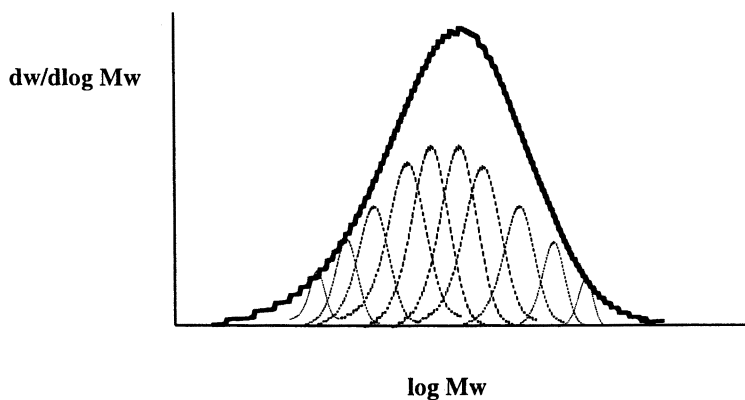
Figure 2. Decomposition of the desired MWD (———) into a series of instantaneous MWDs (- - -).

$$\overline{X}_{ni} = \frac{\left(k_{p}[M]_{p}\right)_{av}}{k_{tr,CTA}[CTA]_{p}} \tag{1}$$

$$W(n) = \frac{n}{\overline{X}_{n_i}^2} \exp\left[-\frac{n}{\overline{X}_{n_i}}\right] \tag{2}$$

where
$$\left(k_{p}[M]_{p}\right)_{av} = \overline{k}_{PA}[A]_{p} + \overline{k}_{PB}[B]_{p} \tag{3}$$

and $[A]_p$, $[B]_p$, and $[CTA]_p$ are the concentrations of monomers A and B, and CTA in the polymer particles, $\overline{k}_{pA}$ and $\overline{k}_{pB}$ are the average propagation rate constants of monomers A and B, $k_{tr,CTA}$ is the chain transfer rate coefficient, n is the chain length and $W(n)$ is the instantaneous fraction of polymer of length n. Note that equation (2) is known as the most probable distribution and it is calculated from the Schultz-Flory distribution (*16*) when the polydispersity index (PI) is equal to two.

Copolymer composition can be simultaneously controlled by keeping the comonomer ratio at the following value:

$$\frac{[B]_p}{[A]_p} = \frac{-(C_{inst}-1) + \sqrt{(C_{inst}-1)^2 + 4r_A r_B C_{inst}}}{2C_{inst} r_B} \tag{4}$$

where C_{inst} is the desired instantaneous copolymer composition and r_A and r_B are the monomer reactivity ratios.

Equations (1-4) allow the production of a linear polymer of given composition and MWD. However, these equations have an infinite number of solutions for $[A]_p$, $[B]_p$, and $[CTA]_p$, each one yielding a different polymerization rate, and hence a different process time (in general, the higher the monomer concentration the higher the polymerization rate and the shorter the process time). On the other hand, the safety of the operation may impose some limits on the amount of monomer in the reactor. An optimization algorithm is used to calculate the concentration profiles of monomers and CTA (set-points in Figure 1) that allow the maximum production of an emulsion copolymer of the desired quality under safe conditions (*13*).

Experimental

The control strategy described above was used in an attempt to produce a MMA/BA copolymer having a MMA/BA copolymer composition of 50/50 with a weight-average molecular weight of 400,000 g/mol and minimum polydispersity index (PI=2). The recipe used is shown in Table I.

Table I. Recipe used for the Production of the MMA/BA Copolymers

Ingredient	Run 1			Run 2		
	Total (g)	Initial Charge (g)	Feed (g)	Total (g)	Initial Charge (g)	Feed (g)
MMA	175	0	175	175	0	175
BA	225	0	225	225	0	225
H_2O	800	760	40	800	760	40
TDM	0.4	-	0.4	0.4	-	0.4
$K_2S_2O_8$	1.5	1.5	-	1.0	1.0	-
$NaHCO_3$	1.5	1.5	-	1.0	1.0	-
SLS	2	1.8	0.2	2	1.8	0.2

Three feed streams were used; the first two were neat monomers and the third one was a preemulsion of the CTA (tert-dodecyl mercaptan) prepared by sonication (Branson Sonifier). Technical grade monomers were used and all chemicals were used as received. Deionized water was used throughout the work. A reaction calorimeter (RC1, Mettler-Toledo) was used to calculate on-line the heat of polymerization and this value was used as the input of an open-loop observer that allows for the calculation of the unreacted concentration of monomers and CTA in the reactor. These concentrations were compared with optimal trajectories (set-points) of these variables calculated by means of the off-line optimization and a nonlinear controller determined the flow rates of monomers and CTA required to track these trajectories. A detailed description of this system can be found elsewhere (*12, 13*).

Samples were withdrawn during the reaction and the monomer conversion, copolymer composition, and MWD were determined off-line by using gravimetry, gas chromatography (GC), and size exclusion chromatography (SEC). The GC apparatus was a Shimadzu GC-14A fitted with a polar column (BP20, SGE; 25 m long and 0.53 mm wide; stationary phase: polyethylene glycol) and Flame Ionization Detector. The SEC apparatus was equipped with a

pump (Waters 510 Milford USA), a refractometer detector (Waters 2410) and 2 columns in series (Styragel HR4, HR6; 10^4 and 10^6 Å). It was operated at 30 °C, with a flow rate of THF of 1 mL/min. Latex samples were dissolved in THF prior to injection. The molecular weight of the samples was calculated by means of the universal calibration technique using polystyrene standards (Polymer Laboratories). The Mark-Houwink constants used in this work were: $K_{pBA} = 12.2 \times 10^{-5}$ (dL/g), $a_{PBA} = 0.7$ (*17*) and $K_{PMMA} = 7 \times 10^{-5}$ (dL/g), $a_{PMMA} = 0.71$ (*18*).

Results and Discussion

The off-line optimization was solved (assuming that chain transfer to polymer was not significant) and the trajectories required to produce the desired copolymer were calculated (Figure 3) and used in run 1. Figures 4a and 4b show the cumulative copolymer composition and the number- and weight-average molecular weights produced in run 1, respectively. It can be seen that the desired copolymer composition was obtained, but the weight-average molecular weight, $\bar{M}_w$, deviated from the target value, namely $\bar{M}_w$ increased as the process evolved to complete conversion. The number-average molecular weight, $\bar{M}_n$, approximately followed the target value.
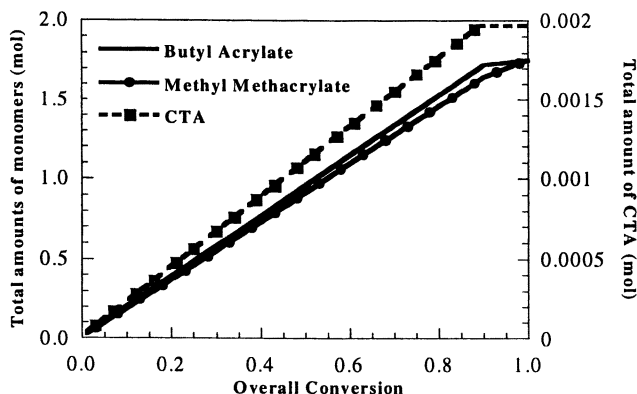
Figure 3. Optimal trajectories for the total amounts of monomers and CTA used in run 1 to produce a copolymer of MMA/BA of 50/50 composition, =400,000 $\bar{M}_w$ and PI=2.
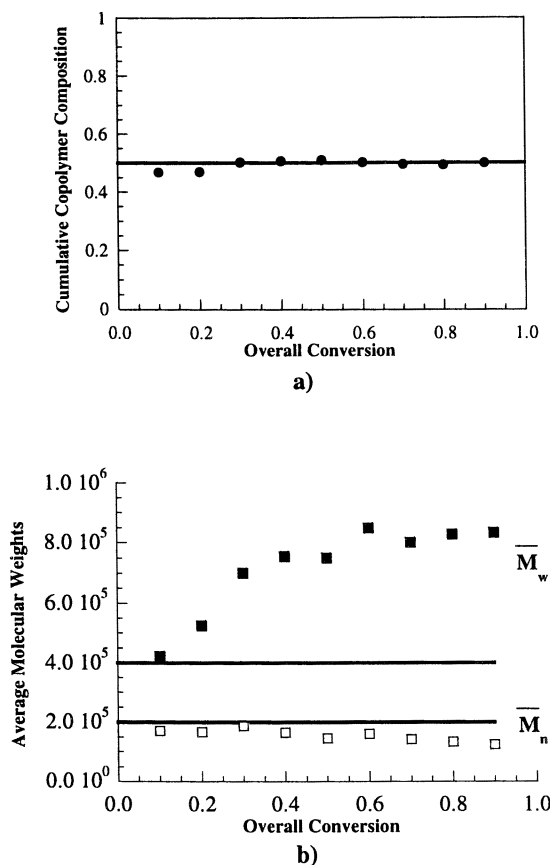
Figure 4. Evolution of the cumulative copolymer composition (referred to MMA, Figure 4a) and cumulative average molecular weights(Figure 4b) produced in run 1. Legend: desired values (——) and experimental results (●, ■, □).

Run 1 proceeded under rather starved conditions (Figure 5). Under these circumstances, this polymerization system is prone to suffer intermolecular chain transfer to polymer (*14,15*). This process made the inactive polymer chains become active, reentering into the polymerization and increasing their molecular weight. The number-average molecular weight was not affected by the process

because the total number of polymer chains was not affected by intermolecular chain transfer to polymer.
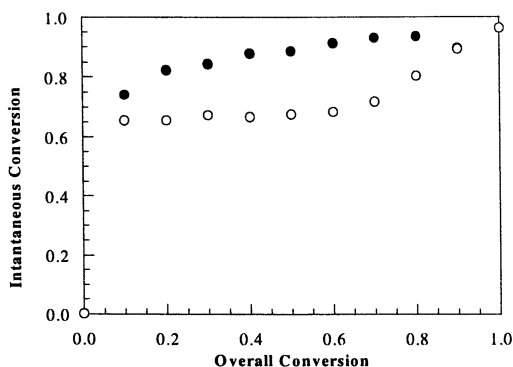
Figure 5. Evolution of the instantaneous conversions for runs 1 (●) and 2. (○).
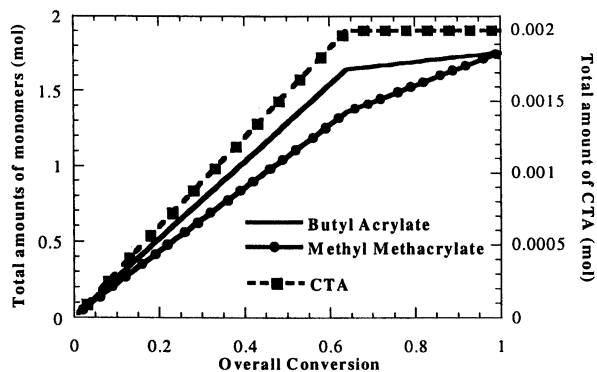
Figure 6. Optimal trajectories for the total amounts of monomers and CTA used in run 2.

Intermolecular chain transfer to polymer increases as monomer conversion increases. Therefore, a way to reduce the importance of this process is to work under semi-flooded conditions, namely at lower instantaneous monomer conversions. New optimal trajectories for both monomers and CTA were

calculated relaxing the constraint on the maximum amount of monomer in the reactor, namely, the reactor was allowed to work under semi-flooded conditions. The new trajectories are shown in Figure 6. This process was more rapid than run 1 and the most reactive monomer (MMA) and the CTA were almost completely added into the reactor for an overall conversion close to 65% in comparison to the 90 % conversion required in run 1 (Figure 3).
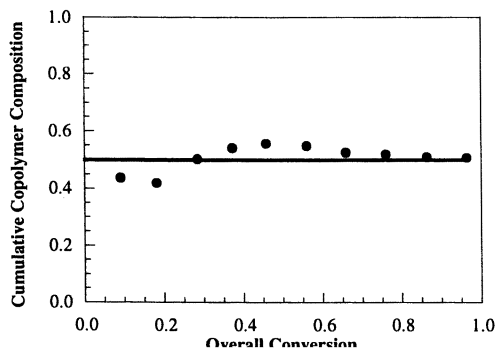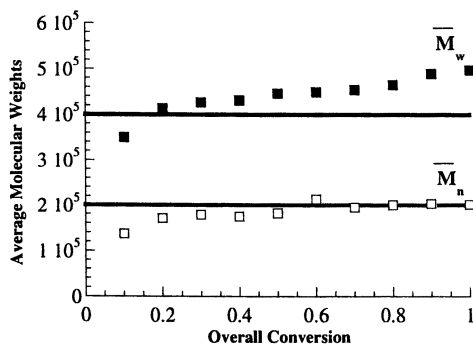
b)

Figure 7. Evolution of the cumulative copolymer composition (referred to MMA, Figure 7a) and cumulative average molecular weights (Figure 7b) produced in run 2. Legend: desired value (———) and experimental results (●, ■, □).

Figure 5 presents the evolution of the instantaneous conversion in run 2. It can be seen that the process proceeded under semi-flooded conditions (65% instantaneous monomer conversion) during most of the process. This ensured a lower concentration of polymer in the polymer particles, and hence less probability for chain transfer to polymer and a greater chance for the control approach to succeed. Actually, this is observed in the results presented in Figure 7. Copolymer composition was again well controlled (Figure 7a) and the weight-average molecular weight only deviated significantly at overall conversions higher than 70% (Figure 7b). This corresponds to the increase in instantaneous monomer conversion during the final stages of the polymerization (Figure 5). This is an additional proof that the extensive intermolecular chain transfer to polymer was responsible for the deviation of the weight-average molecular weight.

It is worth pointing out that, from an industrial point of view, the polymerization rates achieved in run 2 may lead to situations that may exceed the heat removal capability of the reactor, and therefore to thermal runaway scenarios. Figure 8 shows the comparison between the heat released by the polymerization in runs 1 and 2. It can be seen that run 2 was carried out three times as fast as run 1.
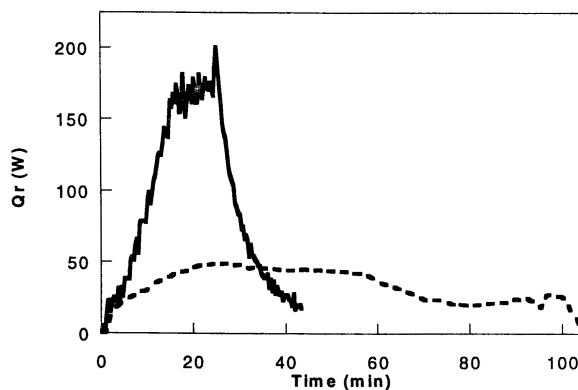
Figure 8. Evolution of the heat released by polymerization in run 1 (‐ ‐ ‐) and in run 2 (——).

Therefore, care should be taken when dealing with comonomer systems that may undergo extensive intermolecular chain transfer to polymer. Although the approach proposed for linear polymers (*13*) might work under some specific circumstances, as those shown in run 2, a more reliable and robust strategy should be used. Such a strategy must take into account the distinctive features that the intermolecular chain transfer to polymer (or more generally any kinetic mechanism leading to long chain branched polymers) introduces in the development of the MWD. Thus, it can be easily proved that in the presence of intermolecular chain transfer to polymer, the instantaneous number and weight-average molecular weights are given by the following equations (*1, 19*):

$$\overline{X}_{ni} = \frac{\left(k_p [M]_p\right)_{av}}{k_{tr,CTA}[CTA]_p} \tag{5}$$

$$\overline{X}_{wi} = 2\frac{\left\{\left(k_p [M]_p\right)_{av} + k_{tr,pol}[v_2]\right\}}{k_{tr,CTA}[CTA]_p + k_{tr,pol}[v_1]} \tag{6}$$

where v_1 and v_2 are the first and second moments of the cumulative polymer chain length distribution. From these equations it is clear that the polydispersity index is different from two and depends on the molecular weights of the inactive polymer. Therefore, the concept of building a given MWD by producing well-defined instantaneous MWDs at different stages of the process (as shown in Figure 2) does not hold. The trajectories for monomer and CTA concentrations calculated by the approach described above (*11,13*) are not sufficient to ensure the production of the desired copolymer.

A successful approach requires accounting for all the kinetic events affecting the MWD in a significant way. Work is in progress to develop a robust general control strategy for nonlinear emulsion polymers.

Conclusions

This paper explores the possibility of extending the control strategies developed for simultaneous on-line control of copolymer composition and MWD of linear polymers to nonlinear polymers. Nonlinear polymers are formed through processes such as chain transfer to polymer and propagation involving terminal double bonds. Using the emulsion copolymerization of methyl methacrylate and butyl acrylate as a case study, it was shown that the present control strategy allows a reasonable simultaneous control of both properties

when working under semi-flooded conditions. However, the polymerization rates reached under these conditions may lead to situations in which the heat released by polymerization in industrial reactors cannot be removed, leading to thermal runaways. A more generally applicable control strategy is needed to circumvent these drawbacks.

Acknowledgments

References

1. Odian, G. *Principles of Polymerization*; Wiley: New York, 1991.
2. Guyot, A.; Guillot, J.; Pichot, C.; Ríos-Guerrero, L. In *Emulsion Polymers and Emulsion Polymerization*; Bassett, D. R.; Hamielec, A. E., Eds. ACS Symposium Series, 165, American Chemical Society: Washington (DC) 1981, pp. 415.
3. Dimitratos, J.; Georgakis, C.; El-Aasser, M. S.; Klein, A. *Control of Product Composition in Emulsion Copolymerization*; Polymer Reaction Engineering 33; Eds. Reichert, K. H. and Geiseler, W., V. C. H.: New York, 1989.
4. Leiza, J. R.; de la Cal, J. C.; Meira. G. R.; Asua J. M. *Polym. Reac. Eng.* **1993**, *1(4)*, 461-498.
5. Canegallo, S.; Canu, P.; Morbidelli, M. J.; Storti G. *Appl. Polym. Sci.* **1994**, *54*, 1919-1935.
6. Urretabizkaia, A.; Leiza, J. R.; Asua, J. M. *AIChE J.* **1994**, *40*, 1850-1864.
7. Sáenz de Buruaga, I.; Echevarría, A.; Armitage, P. D.; de la Cal, J. C.; Leiza J. R.; Asua, J. M. *AIChE J.* **1997**, *43*, 1069-1081.
8. Févotte, G.; McKenna, T. F.; Othman, S.; Hammouri, H. *Chem. Eng. Sci.* **1998**, *53*, 773-786.
9. Sáenz de Buruaga, I.; Leiza, J. R.; Asua, J. M. *Polym. React. Eng.* **2000**, *8(1)*, 39-75.
10. Storti G.; Morbidelli, M. *Open-loop Control of Polymerization Reactors.* Asua J.M. (ed), Polymer Dispersions. Principles and Applications. Kluwer Academic Publishers, Dordretch, 1997.
11. Echevarría, A.; Leiza, J. R.; de la Cal, J. C.; Asua, J. M. *AIChE J.* **1998**, *44*, 1667-1679.

12. Vicente, M.; BenAmor, S.; Gugliotta, L. M.; Leiza, J. R.; Asua, J. M. *Ind. Eng. Chem. Res.* **2001**, 40, 218-227.
13. Vicente, M.; Leiza, J. R.; Asua, J. M. Accepted for publication in *AIChE J.* **2000**.
14. Sayer, C.; Lima, E. L.; Pinto, J. C.; Arzamendi, G.; Asua, J. M. *J. Polym. Sci. Part A: Polym. Chem.* **2000**, *38*, 367-375.
15. Sayer, C.; Lima, E. L.; Pinto, J. C.; Arzamendi, G.; Asua, J. M. *J. Polym. Sci. Part A: Polym. Chem.* **2000**, *38*, 1100-1109.
16. Billmeyer, F. W., *Textbook of Polymer Science*, Wiley-Interscience, New York. 1962.
17. Beuerman, S.; Paquet, D. A.; McMinn, J. H.; Hutchinson, R. A. *Macromolecules.* **1996**, *29*, 4206-4215.
18. Brandup, J. and E. H. Immergut, eds., *Polymer Handbook,* 2nd ed., Wiley Interscience, New York. 1989.
19. Butté, A.; Ghielmi, A.; Storti, G.; Morbidelli, M. *Macromol. Theory Simul.* **1999**, *8*, 498-512.

Chapter 10

Kinetics of Emulsion Polymerization of Styrene in the Presence of Polyurethane Resins

I. W. Cheong[1], M. Nomura[2], and J. H. Kim[1,*]

[1]Nanosphere Process and Technology Laboratory, Department of Chemical Engineering, Yonsei University, Seoul 120-749, Korea
[2]Department of Material Science and Engineering, Faculty of Engineering, Fukui University, Fukui 910-8507, Japan

The role of reactive and non-reactive polyurethane resins in the emulsion polymerization of styrene was investigated. They exhibited low cmc values, high internal viscosities, and high solubilization ability for hydrophobic materials, i.e., pyrene. Continuous nucleation and broad particle size distribution were remarkable in the resin system, especially near and above the cmc. The average number of radicals per particle was below 0.5 and the parameter m in the resin system showed higher values than the estimated values from classical micellar nucleation theory.

In our recent work, non-reactive polyurethane resins were synthesized by polyaddition reactions of isophorone diisocyanate (IPDI), polypropylene glycol (1,2-PPG, MW: 750 and 2000 g/mol), and dimethylol propionic acid (DMPA). The polyurethane resins contained carboxylic groups, DMPA, in their backbones.

Therefore, they were water-soluble or water-dispersible according to the degree of neutralization of the carboxylic groups. The polyurethane resins exhibited surface-active properties, such as micelle or aggregate formation, change of surface tension, and the ability to solubilize hydrophobic materials.

126

Aggregate numbers of the resins were 7.2 and 6.6 for PUR-2000 and PUR-750, respectively. The solubilization ability of the resin for pyrene increased as the resin concentration increased, as is the case with electrolyte concentration. The solubilization ability was much higher than that of SDS (sodium dodecyl sulfate) at the same concentration (1). Several batch emulsion polymerizations of styrene were conducted in the presence of the polyurethane resin. The average particle sizes of the polystyrene latexes were very small (10 ~ 100 nm) and the size distributions were very broad. The emulsion polymerizations of styrene using the resins as emulsifiers showed somewhat different kinetic dependencies on the stabilizer and initiator concentrations compared to conventional anionic surfactants. It was found that the kinetic exponents describing the effect of the resin and initiator concentrations on the number of particles were 0.63-0.66 and 0.38-0.39, respectively (2). For the rate of polymerization, the exponents were lower than the values from Smith-Ewart theory. Moreover, there was no variation between the initial and final particle size especially in the small particle size range (5 ~ 15 nm). Broad particle size distributions and continuous nucleation were notable in comparison with a conventional surfactant system. This difference was mainly attributed to the hydrophobicity, relatively high molecular weight, and high internal viscosity of the resin molecules, which builds up a rather thick surface layer on the colloidal particle like protective colloids.

In this work, a reactive polyurethane resin was synthesized by introducing 2-hydroxyethyl methacrylate (HEMA) for a comparative study between the previous non-reactive and the reactive resins. The HEMA was reacted with NCO-terminated polyurethane prepolymer at room temperature by using dibutyltin dilaurate as a catalyst. The reactive polyurethane resin has vinyl groups at each end of the main chain. Thus, the resin can take part in the polymerization reaction with styrene monomer during the emulsion polymerization. The existence of HEMA monomer units in the resin was confirmed by ^{13}C NMR. The chemical structures of PUR-750 and PUR-750HEMA are illustrated in Figure 1.

Experimental

Materials

Styrene monomer was obtained from Wako Pure Chemical Ind. (Japan) and purified by distillation under a nitrogen atmosphere. Commercial sodium dodecyl sulfate (SDS), potassium persulfate (KPS), and potassium bicarbonate (KHCO$_3$) were extra pure grade and were used without further purification. Distilled and deionized (DI) water was used in all experiments. Two kinds of

polyurethane resins were synthesized and used in emulsion polymerizations of styrene. Properties of the resins are given in Table I.

(a)

(b)
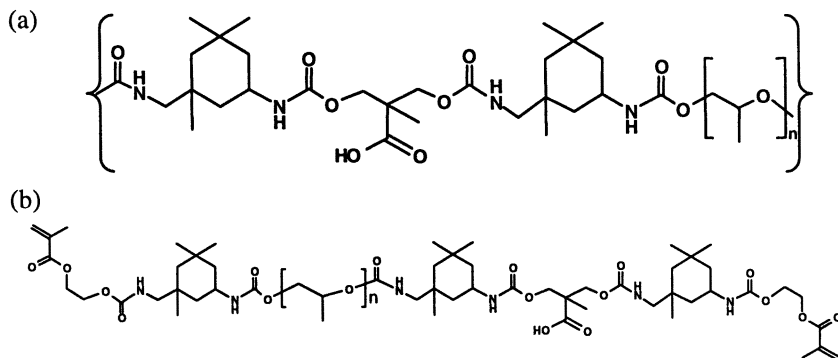
Figure 1. Simplified chemical structures of the polyurethane resins; (a) repeating unit of PUR-750; (b) PUR-750HEMA.

Table I. Physical Properties of the Polyurethane Resins

Property	Type of Resin	
	PUR-750	*PUR-750HEMA*
$\bar{M}_n$ (g/mol)	5600	5700
$\bar{M}_w$ (g/mol)	11000	7000
PDI ($\bar{M}_w / \bar{M}_n$)	2.05	1.23
AV[1] (mg KOH/g PUR)	47.4	48.7
cmc[2] (mM in water)	0.36	0.28
N_{agg}[3] (-)	7.2	Not analyzed

1. Acid value (AV) was measured by titration method.
2. Critical micelle concentration (cmc) was measured by surface tension.
3. Aggregation number was measured by pyrene fluorescence method (excitation and emission wavelengths were 345 and 380 nm).

Emulsion Polymerization

Emulsion polymerizations were carried out in a double-jacketed 1L glass reactor, equipped with a mechanical stirrer, a thermometer, a reflux condenser, a temperature controller, an initiator funnel, and a nitrogen inlet. The basic recipe

for emulsion polymerization in the presence of the resin is given in Table II. The reactor was charged first with the desired amount of PUR solution (5 wt% solids content), styrene, KHCO$_3$, and DI water. The calculated amount of KPS solution was added into the initiator funnel. A highly pure nitrogen gas was used to purge the reactor for 20 min to remove dissolved oxygen in the reaction mixture. The polymerization was initiated by dripping in the initiator solution, which had been deoxygenated with the nitrogen gas. The reaction temperature was adjusted at 60 ± 1 °C in a thermostated water bath. The stirring rate was kept at 400 rpm.

Table II. Basic Recipe for Emulsion Polymerization of Styrene Using the Polyurethane Resins

Components	Amount (g)	wt% (base material)
Styrene	20.000	5.7 (total wt.)
Polyurethane Resin[1]	0.100 ~ 5.000	0.5 ~ 25.0 (monomer wt.)
KPS	0.020 ~ 0.200	0.1 ~ 1.0 (monomer wt.)
KHCO$_3$[2]	0.007 ~ 0.070	
DI water	328.000	

1. The resins were dissolved in water using appropriate sodium hydroxide before the polymerization and degree of neutralization was fixed at 100%.
2. Same molar concentration of buffer as KPS.

Latex Characterization

The monomer conversion was determined by gravimetry using a 100 ppm hydroquinone in methanol solution as a short-stop agent. 6-8 g latex samples obtained from the reaction vessel were immediately quenched with 4-5 drops of the short-stop solution and cooled after a predetermined time of polymerization. Particle size and distribution of the latexes were analyzed by electron microscopy (H-600A, Hitachi, Japan) and dynamic light scattering (Photal DLS-7000, Otsuka Electronics, Japan) at 25 °C. Diluted samples were measured in the dynamic scattering mode. Average particle sizes were calculated by counting over 500 particles in the TEM photos. The number of particles was calculated from the monomer conversion and the average particle size obtained from the electron micrographs as follows:

$$N_p = \frac{6m_o X_p}{\pi \bar{D}_v^3 \rho_p} \tag{1}$$

where N_p is the number of particles in the system, $\overline{D}_v$, the volume-average diameter, X_p, fractional conversion, m_o, amount of monomer with respect to the aqueous phase, and ρ_p, the density of polymer. The rate of polymerization can be expressed by the following equation:

$$R_p = \frac{k_p \bar{n} [\mathrm{M}]_p N_p}{N_A} \qquad (2)$$

where, $\bar{n}$ is the average number of radicals per particle, $[\mathrm{M}]_p$, concentration of styrene monomer in the polymer particles, and N_A, Avogadro's constant. The propagation rate coefficient was obtained using the following equation (3):

$$k_p = 1 \times 10^{7.63} \ \mathrm{L \ mol^{-1} s^{-1}} \exp(-32{,}510 \ \mathrm{J \ mol^{-1}} / RT) \qquad (3)$$

The maximum rate of polymerization ($R_{p,max}$) was calculated from the slopes of conversion as a function of time from 0.2 to 0.4 fractional monomer conversion. Subsequently, the number of particles was calculated in the period of constant polymerization rate. The monomer concentration in the polymer, $[\mathrm{M}]_p$, is a function of monomer conversion, X_p. In Interval II, it was assumed that $[\mathrm{M}]_p$ was constant at 5.5 mol/L polymer. The $\bar{n}$ was obtained using eq. (2). Parameters related to $\bar{n}$ were calculated by the semi-empirical equation introduced by Nomura (4). In the calculation, aqueous phase termination of free radicals was assumed to be negligible. Thus, the following equation can be used:

$$\bar{n} = 0.5 \left[\left\{ \left(\alpha' + \frac{\alpha'}{m} \right)^2 + 2 \left(\alpha' + \frac{\alpha'}{m} \right) \right\}^{0.5} - \left(\alpha' + \frac{\alpha'}{m} \right) \right] + \left(0.25 + \frac{\alpha'}{2} \right)^{0.5} - \frac{1}{2} \qquad (4)$$

where, $\alpha' = \rho_w v_p / k_{tp} N_p$ and $m = k_f v_p / k_{tp}$. ρ_w is the rate of radical production per unit volume of water and was approximately given by $\rho_w = 2 f k_d [I_0]_w$. v_p is the volume of a particle, k_{tp}, the rate constant of mutual termination of radicals in the particles, and k_f, the rate constant of desorption of radicals from a particle (5). The decomposition rate coefficient (6) was expressed as follows:

$$f k_d = 96 \times 10^{15} \mathrm{s^{-1}} \exp(-143{,}250 / RT) \qquad (5)$$

Results and Discussion

In all experiments, the two polyurethane resins given in Table I, PUR-750 and PUR-750HEMA, were used. The existence of -COOH groups from DMPA and unsaturated carbon bonds from HEMA were confirmed by ^{13}C NMR spectra. No peaks indicating a side reaction between carboxyl and isocyanate groups (amide bond peak) were detected in the spectra. As seen in Table II, the appropriate amount of DI water was used for maintaining a constant initiator concentration, and total solid content. Subsequently, the total solid contents of all the emulsion latexes were about 5.7 wt%.

Particle Size and Particle Size Distribution

Figure 2 shows TEM photos of polystyrene latexes prepared in the presence of the reactive polyurethane resins (PUR-750HEMA) after the completion of polymerization. Variation in the resin concentration ranged from below to above the cmc. The cmcs of PUR-750 and PUR-750HEMA were measured as 0.36 and 0.28 mM in water, respectively. Figures 2 (e) and (f) represent latexes prepared at the resin concentrations below the cmc, 0.133 and 0.053 mM in water. The volume-average particle sizes ranged from 30 to 120 nm depending on the concentration of the resin.

Above the cmc, the particle size distribution was very broad; however, the distribution became narrower as the resin concentration decreased. In addition, a large number of small particles were freshly nucleated up to high fractional conversions (< 0.8) as were observed in the TEM photos. Below the cmc, the particle size distribution was narrow and the PDI was smaller than 1.1. In this case, few freshly-nucleated small particles were detected. In this paper the particle size distributions of the polystyrene latexes prepared using PUR-750 (non-reactive type resin) are not illustrated, however, the distributions showed similar trends.

In both cases, the particle size distributions were very broad and continuous nucleation was observed especially near and above the cmc. Continuous nucleation was explained by the characteristics of the polyurethane resins. The polyurethane resin demonstrated a superior solubilization ability for hydrophobic materials and they have relatively high molecular weight and high internal viscosity in comparison with conventional short chain surfactants. Therefore, a few high molecular weight polyurethane resins can form an aggregate in the aqueous phase both above and below the cmc since the resins have relatively broad molecular weight distribution as well. The aggregate can be a locus of polymerization, as well as act as a polyelectrolyte. The molecular weight and acid number can significantly affect the formation of aggregates and the surface
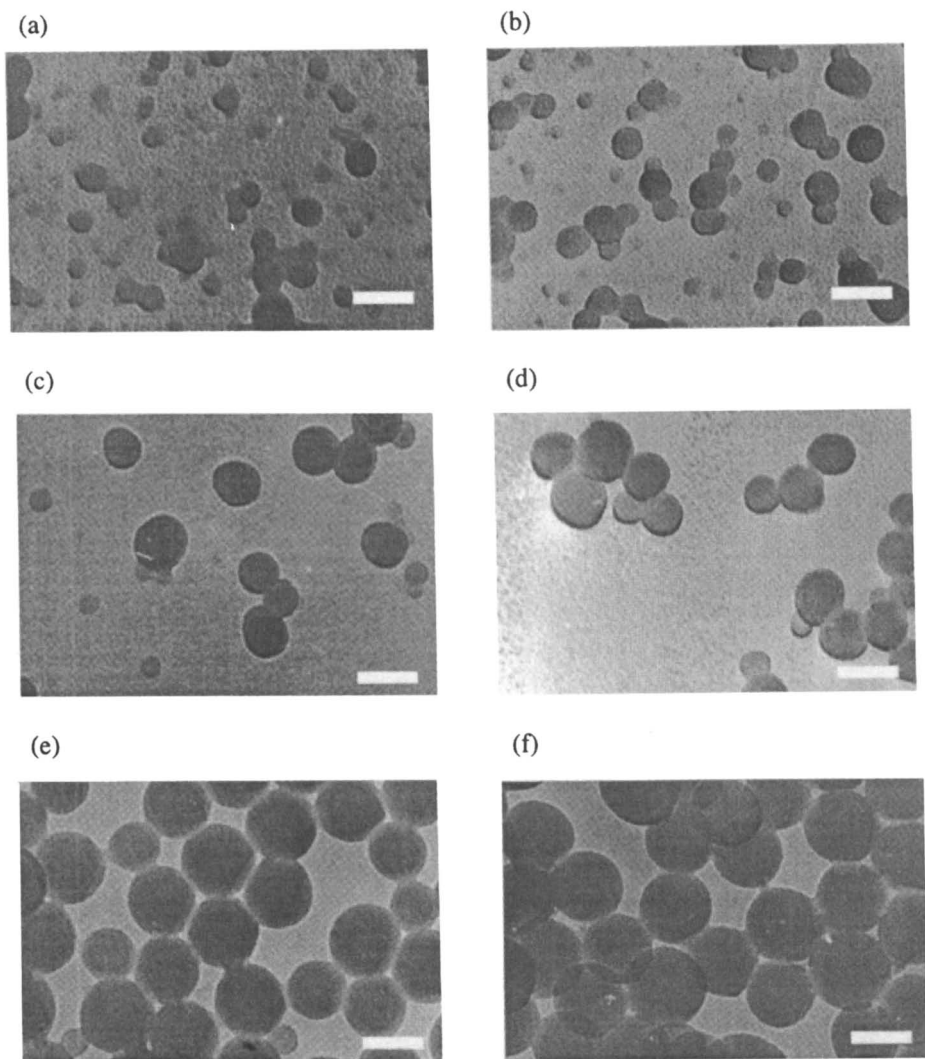
Figure 2. TEM photos of final polystyrene latexes prepared using the PUR-750HEMA with different concentrations; (a) 25 wt%; (b) 15 wt%; (c) 10 wt%; (d) 5 wt% ; (e) 1.25 wt% ; (f) 0.5 wt% based on monomer; bar = 100 nm, magnification =30K.

active properties. It was difficult to make aggregates or micelles to produce new particles for the resins having high acid numbers and relatively low molecular weights and they showed somewhat different kinetic behavior (7, 8).

Rate of Polymerization and Final Number of Particle

Figure 3 (a) shows the relationship between the rate of polymerization, $R_{p,max}$, and resin concentration. The dependencies, estimated from the slope of 1st-order regressions, were 0.48 and 0.34 for PUR-750HEMA and PUR-750, respectively. According to the micellar nucleation theory, the exponent should be 0.6. In the case of the reactive resin, PUR-750HEMA, the exponent was higher than that of PUR-750. These results can be explained by the high polymerization rate of HEMA monomer and the irreversible adsorption behavior of the PUR-750HEMA resin. It was found that all the polymerization data was located on the same linear line regardless of the existence of the cmc. This result suggested that the nucleation mechanisms below and above the cmc should be the same. From the slopes, it can be suggested that the aggregates formed by a few high molecular weight resins could be a polymerization locus in emulsion polymerization due to its high solubilization ability and high internal viscosity. However, it cannot be concluded that the particle nucleation follows a specific nucleation theory due to insufficiency of influential evidence concerning the particle nucleation. In the case of the effect of initiator concentration on $R_{p,max}$ in Figure 3 (b), the exponents showed a similar trend considering the classical micellar nucleation theory.

Figure 4 shows the final number of particles with the variation of resin and initiator concentrations. The exponents from the slopes were 0.78 and 0.69 for PUR-750HEMA and PUR-750, respectively. The final number of particles in PUR-750HEMA was relatively higher than that of PUR-750. These high exponent values have been observed often in homogeneous nucleation systems. In this work, however, these high values were due to the characteristics of the resin molecules as mentioned above. Moreover, from the slopes in Figure 4 (b), it was found that the exponent for the dependence of particle number on initiator concentration was higher in the case of PUR-750HEMA than that of PUR-750. This tendency can be explained by the role of unsaturated carbon bond in PUR-750HEMA. All through the reaction, secondary particles were nucleated continuously; however, PUR-750HEMA reacted with styrene monomer and it could be chemically anchored onto a freshly nucleated particle. In comparison with PUR-750HEMA, PUR-750 resin molecules could adsorb to stabilize preexisting growing particles rather than adsorbing to the freshly nucleated precursor particle.

(a)
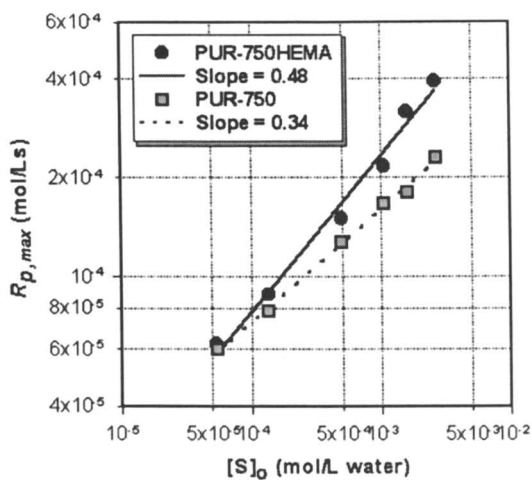
(b)
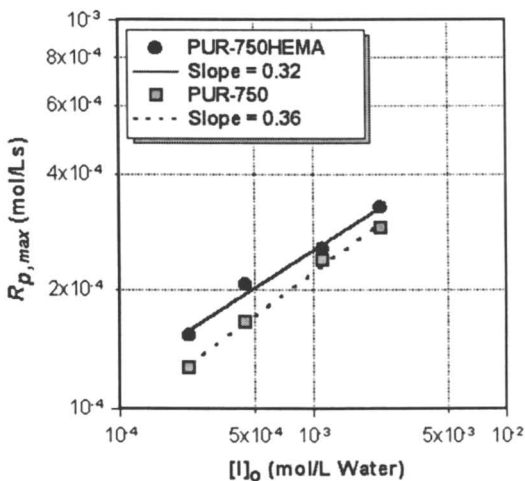
Figure 3. (a) Rate of polymerization ($R_{p,max}$) versus initial resin concentration; round symbols: PUR750-HEMA; square symbols: PUR-750; (b) rate of polymerization versus initial initiator concentration; round symbols: PUR750-HEMA; square symbols: PUR-750.

(a)
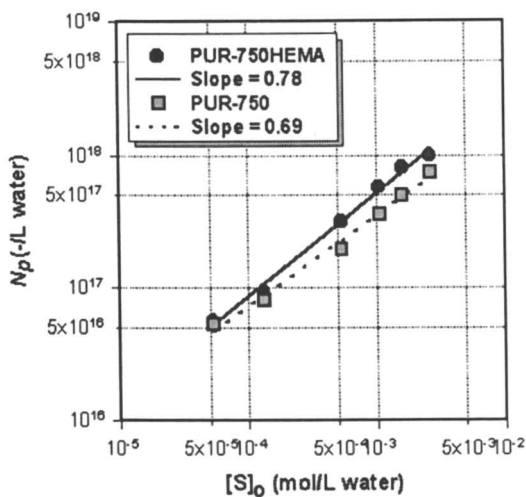
(b)
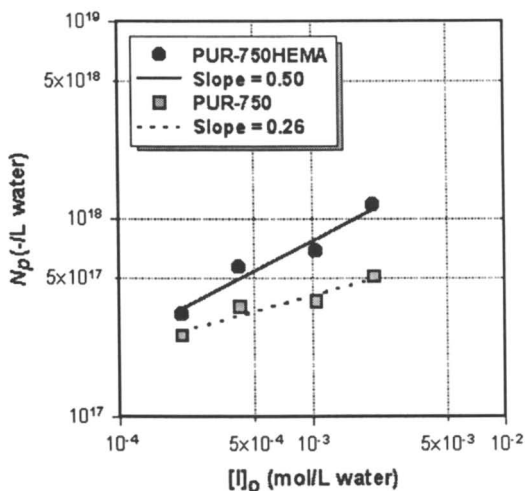
Figure 4. (a) Final number of particles versus initial resin concentration; round symbosl: PUR750-HEMA; square symbols: PUR-750; (b) final number of particles versus initial initiator concentration; round symbols: PUR750-HEMA; square symbols: PUR-750.

Average Number of Radicals per Particle

Figure 5 shows average number of radicals per particle, $\bar{n}$, as a function of the parameter, α'. The $\bar{n}$ values for both resins were below 0.5. The parameter m showed higher values than estimated from conventional styrene/SDS emulsion systems. m has been reported as 1×10^{-4} in a polystyrene/SDS latex system with 62 nm volume-average particle size. For some water-soluble monomers, such as vinyl chloride and vinyl acetate, m has been reported as 2×10^{-3} from the results of Ugelstad and Nomura (9). In this work, the high value of m was because of the unique properties of polyurethane resins. High m values implied that the radical loss process was dominant during the emulsion polymerization. The radical loss could occur by radical desorption due to the chain transfer reaction to resin molecules as well as styrene monomer. Especially, the transfer reaction to the resin leads to grafting reaction with the monomer or to termination by another radical entering from water phase. In fact, a grafting portion of the monomer was observed at 40% based on the total monomer according to our unpublished results. As mentioned above, chain-transferred resin molecules desorb from the growing particles and might be terminated in the aqueous phase. Radical desorption was significant especially in PUR-750, non-reactive resin system. According to the micellar nucleation theory, $R_{p,max}$ should be directly proportional to N_p. In this resin system, $R_{p,max}$ was proportional to $N_p^{0.62}$ and $N_p^{0.49}$ for PUR-750HEMA and PUR-750, respectively.

Surface Tension Analysis

Figure 6 shows the surface tensions for resin solutions only and the polystyrene latexes prepared using these resins. PUR-750HEMA showed better surface activity than that of PUR-750. In the case of the polystyrene latexes, the surface tension of PUR-750HEMA was much higher in comparison with that of PUR-750. From these results, it was concluded that PUR-750 (non-reactive resin) desorbed from the growing polymer particles during the polymerization; therefore, the surface tension value was low. At a higher concentration of the resin, a large number of the resin molecules existed in the aqueous phase. Consequently, the rate of continuous nucleation increased due to the free resin molecules or aggregates of the molecules.
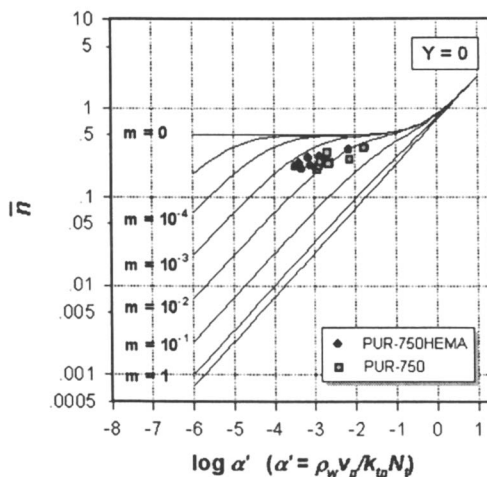
Figure 5. The average number of radicals per particle as a function of the parameter α' (aqueous phase termination is negligible, Y = 0); round symbols: PUR750-HEMA; square symbols: PUR-750.
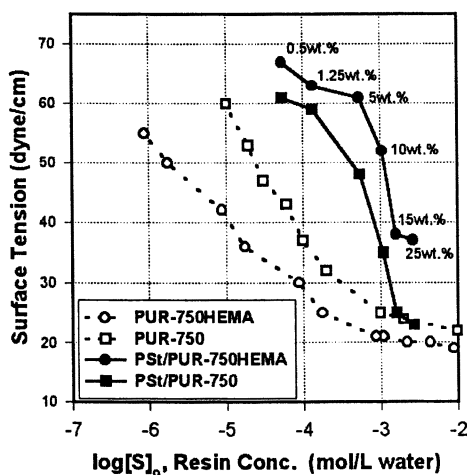
Figure 6. Surface tensions of the polyurethane resins and final polystyrene latexes prepared using the resins; round symbols: PUR750-HEMA; square symbols: PUR-750.

Conclusions

Polymeric or polymerizable surfactants are usually tailor-made and subsequently they exhibit unique properties as seen in many recent publications. In this work, the polyurethane resins showed a different behavior in comparison with those of conventional styrene/short-chain surfactant systems. Discrepancies in the power dependency of the polymerization rate and the final number of particles on the resin or initiator concentration was illustrated and explained by the typical properties of the resins, such as relatively high molecular weight and broad molecular weight distribution, high internal viscosity, and superior solubilization ability for hydrophobic materials. It was concluded that the low $\bar{n}$ and high value of m were due to radical loss process which was dominant all through the reaction.

Acknowledgments

References

1. Cheong, I. W.; Nomura, M.; Kim, J. H. *Macromol. Chem. Phys., in press.*
2. Cheong, I. W.; Nomura, M.; Kim, J. H. *Macromol. Chem. Phys., in press.*
3. Buback, M.; Gilbert R. G.; Huchinson, R. A.; Klumperman, B.; Kutcha, F. D.; Manders, B. G.; O'Driscoll, K. F.; Russell, G. T.; Schweer, J. *Macromol. Chem. Phys.*, **1995**, *196*, 3267.
4. Nomura, M.; Fujita, K. *Makromol. Chem. Suppl.*, **1985**, *10/11*, 25.
5. Ugelstad, J.; Mørk, P. C.; Aassen, J. *J. Polym Sci.*, **1967**, *A-1*, *5*, 2281.
6. Behrman, E. J.; Edward, J. O. *Rev. Inorg. Chem.*, **1980**, 2, 179.
7. Lee, D. Y.; Kim, J. H. *J. Appl. Polym. Sci.* **1998**, *69*, 543.
8. Kato, S; Sato, K; Maeda, D; Nomura, M. *Colloids & Surfaces A*, **1999**, 153, 127.
9. Nomura, M; Satpathy, U. S.; Fujita, K; Kouno, Y; *J. Polym. Sci. Part C, Polymer Letters*, **1988**, *26*, 385.

Chapter 11

Living Free Radical Miniemulsion Polymerization of Styrene

Gaofeng Pan, E. David Sudol, Victoria L. Dimonie, and Mohamed S. El-Aasser*

Emulsion Polymers Institute and Department of Chemical Engineering, Lehigh University, Bethlehem, PA 18015

TEMPO-terminated oligomers of polystyrene (TTOPS) have been investigated as a macro-initiator to initiate the miniemulsion polymerization of styrene at 125 °C. Deviations from the ideal chain extension reaction were found. These deviations may be the result of newly generated thermal free radicals and/or low molecular weight dead polymer chains. The number of polymer chains was calculated and found to increase with conversion. Molecular weights and molecular weight distributions were studied as a function of conversion. A low molecular weight dead polymer population was found in the distribution of polymers obtained from a miniemulsion polymerization initiated with TTOPS-7050 (i.e., M_n = 7050 g/mol). Significant improvements in the molecular weight distributions and numbers of polymer chains were achieved by using TTOPS-1500, a lower molecular weight (1500 g/mol) macro-initiator. A bulk polymerization using TTOPS-1500 was carried out for comparison. The resulting polymer had a narrower molecular weight distribution than that obtained by miniemulsion polymerization.

139

Emulsion polymerization has developed into a widely used process for the production of synthetic polymeric materials. Miniemulsions are submicron dispersions of one liquid in another immiscible, continuous liquid phase (*1*). Miniemulsions are prepared by an emulsification process using a combination of an ionic surfactant and a costabilizer such as a long chain alkane or fatty alcohol. In miniemulsion polymerization, monomer is the dispersed material, and water is the continuous phase. Monomer droplets can range in size from 50 to 500 nm in diameter and the distributions are typically broad. Polymerization is carried out in the stable submicron monomer droplets.

Living polymerizations are characterized by controlled molecular weights, desired end groups, and narrow molecular weight distributions. An ideal living polymerization reaction does not have any termination or transfer reactions. Until recently, living polymerizations were limited to ionic polymerizations. In free radical polymerization, it is not easy to avoid the bimolecular termination reaction between two active free radicals. Recently, several approaches were found to control free radical polymerization giving them features of living polymerizations. Living/controlled free radical polymerizations are usually divided into three categories: stable free radical polymerization (SFRP), atom transfer radical polymerization (ATRP), and reversible addition-fragmentation chain transfer polymerization (RAFT) (*2*). SFRP in bulk systems has been thoroughly studied (*3-9*). However, comparatively little has been reported using this technique in emulsion polymerization (*10-13*), or dispersion polymerization (*14*). This research focuses on the application of the stable free radical polymerization technique in miniemulsion polymerizations. The stable free radical used in this research is 2,2,6,6-tetramethylpiperidinyl-1-oxy (TEMPO). High temperature is needed for the decomposition reaction of the alkoxyamine to generate active free radicals. Usually the temperature is over 110 °C. While using a beta-phosphonylated nitroxide instead of TEMPO as the stable free radical, a living free radical miniemulsion polymerization has been reported at temperature below 100 °C (*15*).

Instead of using TEMPO/benzoyl peroxide (BPO) as initiator as most often reported in the literature, TEMPO-terminated oligomers of polystyrene (TTOPS) are used as the initiator. The purpose of using TTOPS as initiator is to simplify the system for studying the kinetics and mechanism of the polymerization. Because the initiation efficiency of benzoyl peroxide is not easily determined here, it is difficult to control the number of polymer chains in this system. By using TTOPS as the initiator, the initial number of chains can be specified and the molecular weights are readily estimated by assuming that the monomer adds only to these TTOPS chains. In addition, TEMPO is water-soluble and will partition between the water and monomer phases in the heterogeneous miniemulsion system, while TTOPS is a short chain polymer that has no water solubility. Therefore, the TEMPO will be initially restricted to the droplet phase.

Experimental

TEMPO-terminated oligomers of polystyrene (TTOPS) were prepared by bulk polymerization of styrene in the presence of benzoyl peroxide (BPO) (0.09 mol/dm^3) and TEMPO (0.108 mol/dm^3). The reactants were pre-heated for 1 hour at 90 °C followed by polymerization at 125 °C. Polymer was retrieved by precipitation in an excess of methanol, and purified by 3 dissolution/ precipitation cycles using toluene and methanol, respectively. When preparing TTOPS-7050, the styrene monomer was first cleaned by passing it over activated alumina to remove the inhibitor. The yield was 71% and the number-average molecular weight measured by gel permeation chromatography was 7050 g/mol (TTOPS-7050) with a polydispersity index (M_w/M_n) of 1.24. For preparing TTOPS-1500, the styrene was freshly distilled. The TEMPO/BPO ratio was increased to 2.1/1 and the reactant mixture was degassed by 3 freeze-thaw cycles to remove O$_2$. Bulk polymerization at 125 °C was protected by nitrogen. The polymerization was stopped at a low conversion (17%). The number-average molecular weight was 1500 g/mol (TTOPS-1500) with a polydispersity index of 1.14

The recipe for the miniemulsion polymerization is given in Table I. DOWFAX 8390 (disulfonated alkyl diphenyl oxide sodium salt; Dow Chemical Co.), an anionic surface active agent, was used as the emulsifier. Hexadecane (Aldrich) was used as the costabilizer. TTOPS-7050 and hexadecane were pre-dissolved in the styrene prior to emulsification. To prepare the miniemulsion, the reaction mixture was either sonified using a Branson sonifier for 10 minutes with stirring at a power output setting of 8 and a duty cycle of 50%, or sonified for 1 minute at a power output of 7 and a duty cycle of 50%, and then passed 10 times through the Microfluidizer (Model 110T, Microfluidics, Inc.). After degassing the miniemulsion, the polymerization was carried out in a high-pressure polymerization bottle placed in an oil bath operated at a controlled temperature of 125 ± 5 °C. The polymerization mixture was stirred with a magnetic bar at 500 rpm. Samples were removed from the bottle for analysis by needle and syringe. The conversions were measured gravimetrically and confirmed by gas chromatography (HP 5890A). Molecular weight distributions were measured by gel permeation chromatography (Waters, Styragel columns HR3, HR4, HR6; Model 410 differential refractometer). Particle size distributions of the latexes were measured by both transmission election microscopy (TEM, Phillips 400) and capillary hydrodynamic fractionation (CHDF, Model 1100, Matec Applied Sciences).

Table I. Recipe for Living Free Radical Miniemulsion Polymerization

Ingredient	Weight (g)	Concentration
	Water Phase	
Deionized Water	65.0	
Dowfax 8390	1.04	25 mM [a]
	Oil Phase	
Styrene	15.6	
Hexadecane	1.47	100 mM [a]
TTOPS	Varied	

[a] based on water phase, [hexadecane]/[Dowfax] = 4:1 mole ratio

Total final solids ~20% (based on 100% conversion)

Results and Discussion

Because of the relatively slow initiation and fast propagation rates in free radical polymerization, high molecular weight polymers are formed from the beginning of conventional free radical polymerizations, and the molecular weight does not vary significantly until high conversion is achieved. However, in living polymerizations, the molecular weight increases linearly with conversion, an important difference. In this research, miniemulsion polymerizations initiated with different concentrations of the macro-initiator TTOPS-7050 were carried out. It was found that when the TTOPS-7050 concentration was varied from 2.5% to 20% (3.55 mM to 28 mM), the molecular weights increased linearly with conversion in all cases over much of the polymerizations (Figure 1). This linear increase extended up to 80% conversion in all cases except the polymerization initiated with the lowest TTOPS-7050 concentration (2.5% or 3.55 mM), where the linear increase was only up to 40% conversion. When these conversions were exceeded, the molecular weights became lower than that expected for a linear increase. For a given conversion in the linear region, increasing molecular weights were found for decreasing TTOPS concentrations as expected since the molecular weight is inversely proportional to the initiator concentration.

As mentioned in the introduction, one advantage of using TTOPS as the macro-initiator is the possibility of tracking the number of polymer chains in the system. In ideal chain extension experiments, all TTOPS chains are living (capped by TEMPO and have the ability to propagate to a longer chain) and no new chains are generated during the polymerization. Figure 2 shows the comparison between the theoretical (ideal) molecular weights (lines) and the experimental data. All experimental values are lower than expected theoretically.

These deviations could be caused by an increasing number of polymer chains in the system resulting from the thermal generation of new free radicals and/or a population of lower molecular weight dead polymers resulting from termination reactions.
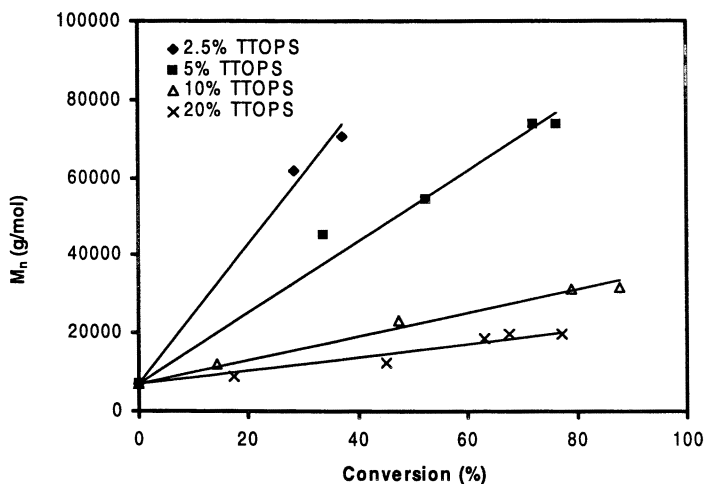
Figure 1. Number-average molecular weight as a function of conversion for miniemulsion polymerizations of styrene carried out with different TTOPS-7050 concentrations ranging from 2.5% to 20%; $T_r = 125$ °C.

Although the presence of the stable TEMPO free radical greatly limits the termination reaction, it cannot be eliminated. When irreversible termination occurs, dead polymer chains form, and dead chains, by definition, cannot grow to higher molecular weights. If there is a certain amount of low molecular weight dead polymer present in the system, which is not included in the number of chains estimated by the number of TTOPS molecules (i.e., there are extra polymer chains in the system), the number-average molecular weight will be reduced significantly.

The number of polymer chains can be calculated from the conversion and the number-average molecular weight. Figure 3 shows the evolution of the number of polymer chains with conversion for the system employing 20% TTOPS-7050. Although there is scatter in the data, it is clear that the number of polymer chains increased with increasing conversion. At the high polymerization temperature (125 °C), the styrene monomer molecules react with each other and generate free radicals (*16, 17*). These newly-generated free radicals will initiate new polymer chains other than the chains introduced by TTOPS and therefore,

the actual number of polymer chains in the system can not remain constant and will increase with time.
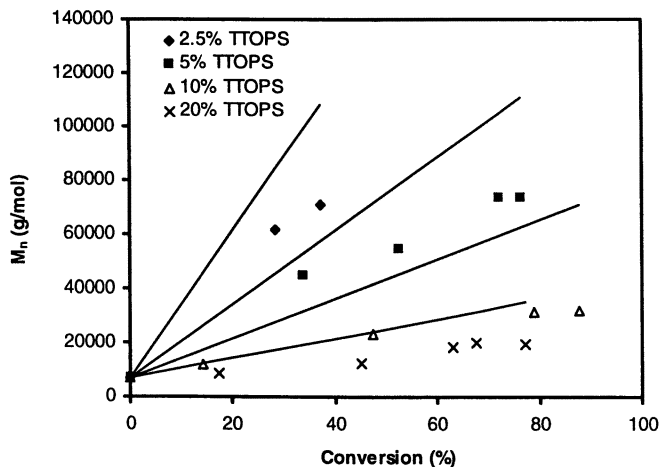
Figure 2. Experimental and theoretical number-average molecular weight as a function of conversion for miniemulsion polymerizations of styrene carried out with different TTOPS-7050 concentrations ranging from 2.5% to 20%; $T_r = 125 \,°C$.
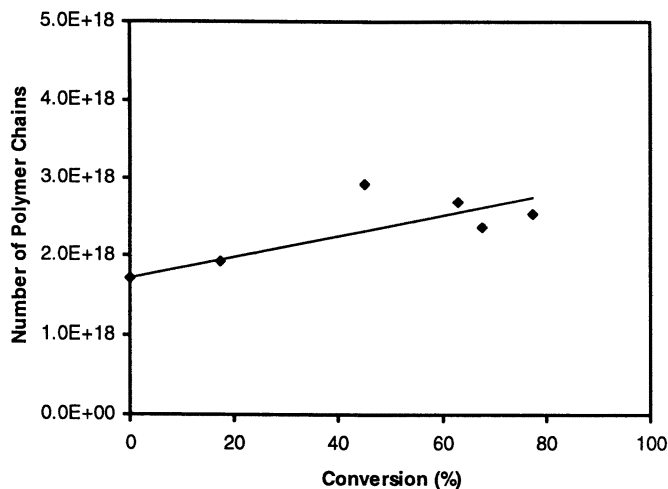
Figure 3. Number of polymer chains as a function of conversion for the miniemulsion polymerization of styrene initiated with 20% TTOPS-7050; $T_r = 125 \,°C$.

If there is a population of low molecular weight dead polymer chains in the system, it can be found as a stationary peak in the evolution of the molecular weight distribution curves with conversion. Figure 4 shows the evolution of the molecular weight distribution with conversion in the 20% TTOPS-7050 reaction. The main peak of the molecular weight distribution is shown moving to higher molecular weights with increasing conversion, while a small stationary peak remains behind with a molecular weight around 7000 g/mol. These results confirm that low molecular weight dead polymers are present in this system, which lowers the number-average molecular weights to below the ideal (theoretical) values.
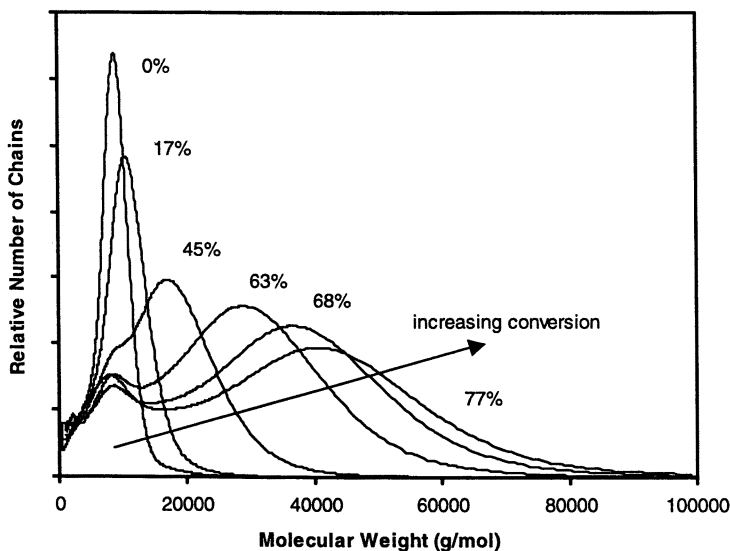
Figure 4. Evolution of molecular weight distribution with conversion in the styrene miniemulsion polymerization initiated with 20% TTOPS-7050; $T_r = 125$ °C.

Since high temperature is required for the alkoxyamine decomposition reaction, it is not possible to avoid generating thermal free radicals. Since the low molecular weight dead polymers have a molecular weight similar to the TTOPS-7050, these may originate with the TTOPS-7050 initially added to the system. That is, dead polymer may have already been present in the TTOPS-7050. In an attempt to reduce or eliminate this possibility, a new batch of TTOPS, TTOPS-1500, was synthesized under more rigorous experimental conditions as described in the experimental section. The TTOPS-1500 was used instead of TTOPS-7050 in miniemulsion chain extension experiments. Figure 5

shows the number-average molecular weights measured by GPC and the calculated number of polymer chains compared with theoretical values based on ideal chain extension. The experimental values are close to the corresponding theoretical ones up to 60% conversion. When the conversion increases beyond 60%, the molecular weight becomes lower than the theoretical value. The number of polymer chains is also close to the theoretical value (i.e., the number of TTOPS chains) at low conversions. However, since the generation of thermal radicals cannot be avoided, it increases slightly with conversion during the polymerization. When conversion exceeded 60%, the deviation became obvious. The evolution of the molecular weight distribution with conversion is shown in Figure 6. No stationary peak was found in this case. The molecular weight polydispersity index (PDI, M_w/M_n) is shown in Figure 7 as a function of conversion. All PDI are in the range of 1.1 ~ 1.5, except at 12% conversion.
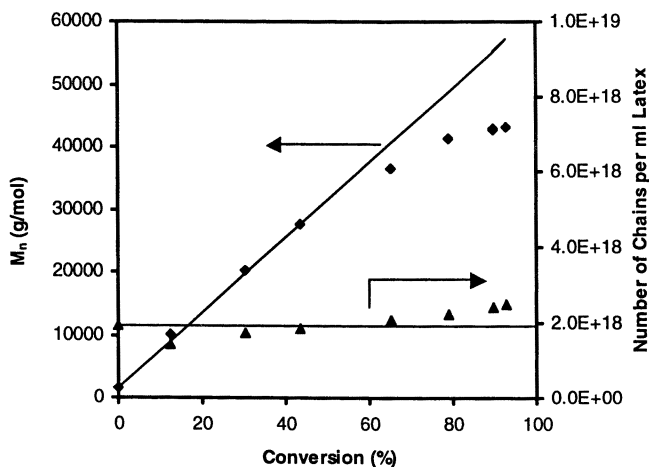
Figure 5. Evolution of number-average molecular weight and the number of polymer chains with conversion for the miniemulsion polymerization of styrene initiated with 2.5% TTOPS-1500; $T_r = 125$ °C.

The corresponding bulk polymerization using TTOPS-1500 was carried out for comparison to the miniemulsion polymerization. Similar results were found for the evolution of the number-average molecular weight and the number of polymer chains with conversion. The molecular weight distribution of the polymer obtained by bulk polymerization is narrower than that obtained from the miniemulsion polymerization. The PDIs for the bulk polymers are shown in Figure 7. All values are in the range of 1.1 ~ 1.3 and are lower than that of the miniemulsion polymerization system as expected. The molecular weight distribution curves of the bulk polymers at different conversions are given in

Figure 8. Compared with the molecular weight distribution curves of the polymers obtained from the miniemulsion polymerization, the distributions are significantly sharper.
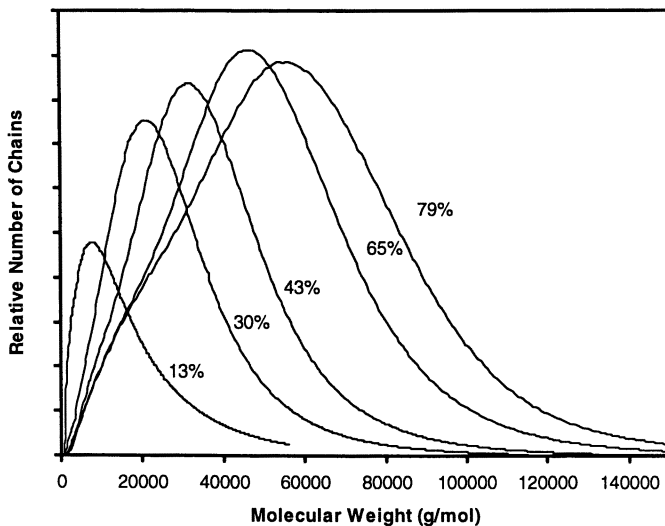
Figure 6. Evolution of molecular weight distribution with conversion in the miniemulsion polymerization initiated with 2.5% TTOPS-1500; $T_r = 125$ °C.
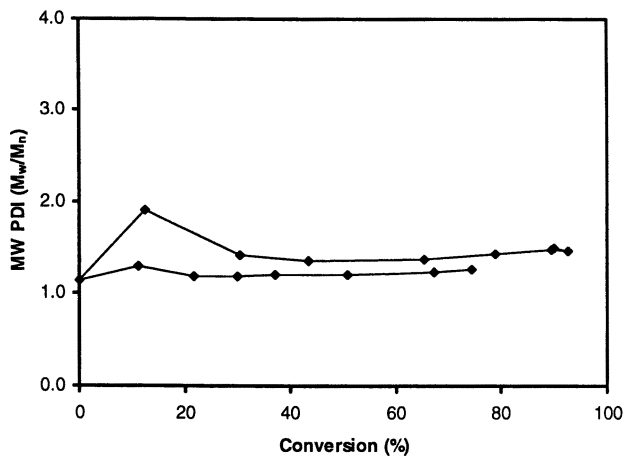
Figure 7. Molecular weight polydispersities of polymers obtained from miniemulsion and bulk polymerizations of styrene initiated with 2.5% TTOPS-1500.

A shoulder, with a molecular weight in the range of 10,000 – 20,000 g/mol can be found in the molecular weight distribution curves at higher conversions for both the miniemulsion and bulk polymers. This shoulder is much smaller in the bulk polymers than in the miniemulsion polymers. These shoulders indicate that a certain amount of low molecular weight polymers become significant at higher conversions. These could be terminated polymer chains with low molecular weight (dead chains) and/or new polymer chains initiated by thermal radicals (living chains). The heterogeneous nature of the miniemulsion system may be the main reason that the miniemulsion polymers having a larger shoulder than the bulk polymers. Although styrene is a much better solvent for TEMPO than water, TEMPO radicals will partition between the phases in a miniemulsion. When TTOPS is used as the macro-initiator, TEMPO molecules are initially restricted in the droplet phase as they are bound to the TTOPS, which is not water-soluble. However, when the temperature is raised, TEMPO radicals dissociate from the polymer/oligomer chains, and thus have a chance to exit the droplet/particle and enter the water phase. This can lower the TEMPO concentration in the monomer/polymer phase, resulting in less control of the active free radicals and more deviations from ideal living polymerization.
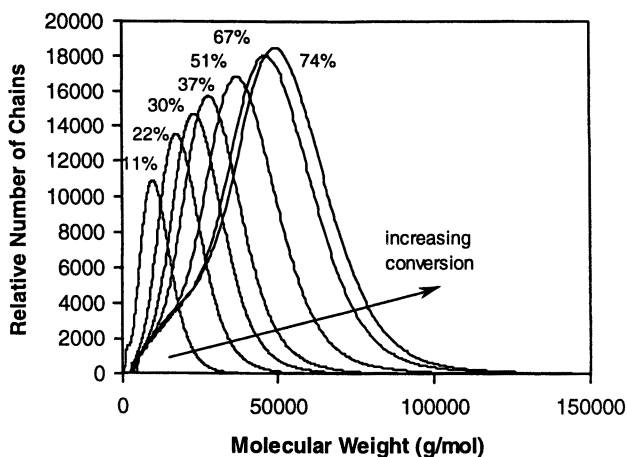
Figure 8. Evolution of molecular weight distribution with conversion in the bulk polymerization of styrene initiated with 2.5% TTOPS-1500; T_r = 125 °C.

Another possible contribution to the larger low molecular weight shoulder of the miniemulsion polymers is the continuous nucleation that occurs during the miniemulsion polymerization. It was found that the number of particles increases with increasing conversion up to 90% conversion (Figure 9). Since the TTOPS is

water-insoluble, there are no TTOPS chains in the newly nucleated particles. Therefore, the polymer chains in these new particles must be initiated by thermal radicals and are expected to be shorter than those living chains grown from the TTOPS. The newly initiated polymer chains having low molecular weights are particularly significant at higher conversions compared with other chains having about 500 or more monomer units (molecular weight larger than 50,000 g/mol). Although no TTOPS is present in the newly nucleated particles, it can be found from the molecular weight distribution curve that few polymer chains have a molecular weight larger than 200,000 g/mol. This indicates that the polymerization in these newly nucleated particles is still well-controlled by TEMPO. As mentioned before, TEMPO will partition between the aqueous and organic phases. Therefore, the TEMPO radicals in the aqueous phase diffuse to the new particles to control the polymerization.
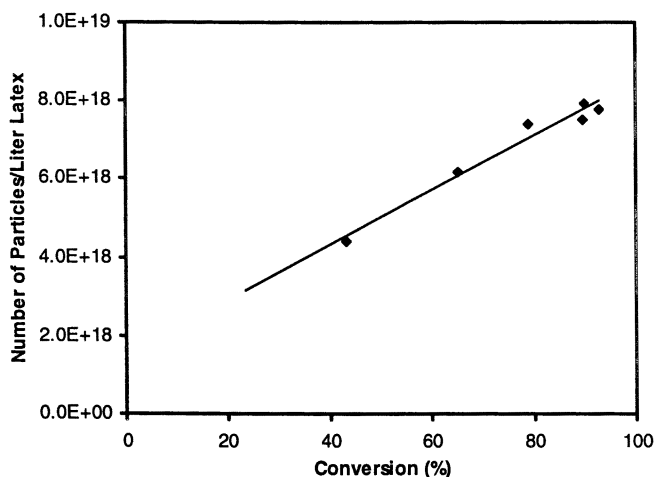
Figure 9. Evolution of number of particles with conversion in the styrene miniemulsion polymerization initiated with TTOPS-1500; $T_r = 125\,°C$.

Conclusions

Two different molecular weight TTOPS (TTOPS-7050, TTOPS-1500) were synthesized and used successfully as macro-initiators to initiate miniemulsion polymerizations of styrene. The effect of varying TTOPS-7050 concentration was studied. In each case, the number-average molecular weight was found to increase linearly up to a certain conversion after which it deviated from linearity.

Higher TTOPS concentrations resulted in lower molecular weights at the same conversion. By assuming ideal chain extension conditions, the theoretical molecular weights were calculated for comparison. Experimentally measured molecular weights of the polymers obtained from miniemulsion polymerizations initiated by TTOPS-7050 were lower than the corresponding theoretical values. The number of polymer chains increased with conversion. A stationary peak, which indicates a population of dead polymer chains, was found in the molecular weight distribution curves of polymers obtained from polymerizations initiated with TTOPS-7050. Using TTOPS-1500, the stationary peak did not appear and significantly more ideal molecular weights and number of polymer chains were obtained. Compared to the bulk polymer initiated by TTOPS-1500, the miniemulsion polymers had broader distributions and a more significant low molecular weight shoulder. These results are considered to be caused by the partitioning of TEMPO radicals between the phases.

Acknowledgment

References

1. Ugelstad, J.; El-Aasser, M. S.; Vanderhoff, J. W. *J. Polym. Sci., Polym. Lett.*, **1973**, *11*, 503.
2. Gaynor, S.; Greszta, D.; Shigemoto, T.; Mardare, D.; Matyjaszewski, K. *Macromol. Symp.*, **1995**, *98*, 73.
3. Veregin, R. P. N.; Georges, M. K.; Kazmaier, P. M.; Hamer, G. K. *Macromolecules*, **1993**, *26*, 5316.
4. Veregin, R. P. N.; Odell, P. G.; Michalak, L. M.; Georges, M. K. *Macromolecules*, **1996**, *29*, 2746.
5. Fukuda, T.; Teauchi, T.; Goto, A.; Ohno, K.; Tsujii, Y.; Miyamoto, T. *Macromolecules*, **1996**, *29*, 6393.
6. Greszta, D.; Matyjaszewski, K.; Priddy, D.; Li, I.; Howell, B. A. *Polymer Preprints, Division of Polymer Chemistry, ACS*, **1996,** *37*, 519.
7. Goto, A.; Fukuda, T. *Macromolecules*, **1997,** *30*, 4272.
8. Han, C. H.; Butz, S.; Schmidi-Naake G. *Die Angewandte Makromolekulare Chemie*, **1999**, *265*, 69.
9. Goto, A.; Fukuda, T. *Macromolecules*, **1999,** *32*, 618.
10. Bon, S. A.; Bosveld, M; Klumperman, B.; German A. L. *Macromolecules*, **1997,** *30*, 324.

11. Gabaston, L. I.; Jackson, R. A.; Armes, S. P. *Macromolecules*, **1998**, *31*, 2883.
12. Prodpran, T.; Dimonie, V. L.; Sudol, E. D.; El-Aasser, M. S. *Macromol. Symp.* **2000,** *155,* 1.
13. Pan, G.; Dimonie, V. L.; Sudol, E. D.; El-Aasser, M. S. *Macromolecules*, **2001**; *34,* 481.
14. Buback, M.; Gilbert, R.; Hutchinson, R.; Klumperman, B.; Kuchta, F.; Manders, B.; O'Driscoll, K.; Russell, G.; Schwer, J. *Macromol. Chem. Phys.*, **1995,** *196*, 3267.
15. Lansalot, M; Farcet, C.; Charleux, B.; Vairon, J.-P.; Pirri, R.; Tordo, P. In *Controlled/Living Radical Polymerization;* Matyjaszewski, K., Ed.; ACS Symposium Series 768; American Chemical Society: Washington DC, 2000, p 138.
16. Buzanowski, W.; Graham, J.; Priddy, D.; Shero, E. *Polymer*, **1992**, *33*, 3055.
17. Mayo, F. R. *J. Am. Chem. Soc.,* **1968**, *90*, 1289.

Chapter 12

Dispersed Condensation Polymerization in Supercritical Fluids

K. N. Lee, H. J. Lee, J. Y. Lee, Y. J. Suh, and J. H. Kim*

Nanosphere Process and Technology Laboratory, Department of Chemical Engineering, Yonsei University, Seoul 120-749, Korea

It was an objective of the present paper to describe the development of condensation polymers in the form of microspheres using a new method which is capable of avoiding the existing process which requires very high temperature and vacuum to allow the removal of the condensate molecule from the polymer melt. The removal of the condensate molecule is facilitated by the ability of supercritical CO_2 to act as a plasticizing agent for the polymer phase. In this approach, phenolic (P) /furfural (F) /alcohol mixtures were dispersed in supercritical CO_2. The solubility of alcohol in supercritical CO_2 varied with the temperature and pressure of the system. As the process conditions were varied, P/F gel particles could be successfully prepared. The reactants were heated to 80 °C to form the gel particles. The alcohol in the P/F gel particles was continuously exchanged with supercritical CO_2 at 40 °C, after which they were supercritically dried. PDMS was used as the stabilizer in this system. The spherical polymer particles were isolated by simply venting the supercritical CO_2 from the reaction mixture. SEM analysis showed that the product consisted of spheres in the micrometer size range.

Organic aerogels have continuous porosity, an ultrafine cell/pore size (≤ 50 nm), high surface area (400-1000 m^2/g), and a solid matrix composed of interconnected colloidal-like particles or polymeric chains with characteristic diameters of 10 nm (*1*). This ultrastructure and the low Z (atomic number) composition are responsible for the unique optical, thermal, electrical, and acoustic properties of organic aerogels (*2-5*).

The aqueous polycondensation of resorcinol with formaldehyde (R/F) (*1,6*) and melamine with formaldehyde (M/F)(*1*) are two proven synthetic routes for the formation of organic aerogels. The synthetic processes used to prepare these aerogels were carried out in two steps: (a) polymerization in a glass reactor at 80 °C, under atmospheric conditions and acetone exchange, which replaces alcohol within the organic gel with acetone (compatible with CO_2), and (b) solvent exchange in a high-pressure vessel by addition of CO_2 (*6*). The processes were so complicated that the process time was very long. We have found a new process to circumvent the energy-saving concerns about the synthetic route for organic aerogels by preparing these technologically important organic aerogels in one-step. Figure 1 shows a schematic diagram of the principal reactions for phenolic novolac with furfural (P/F) under conditions used in this study. Phenolic/furfural (P/F) aerogels have a major advantage over previous organic aerogels: the P/F mixtures have the ability to be formed directly in an organic solvent (i.e., alcohol) that is compatible with supercritical CO_2, and therefore, the synthetic process of a P/F aerogel is simpler than that of other organic aerogels because the acetone exchange prior to supercritical drying has been eliminated (*7,8*). The primary differences between the process for producing new P/F aerogel microspheres and the prior process for producing R/F aerogel microspheres are shown in Figure 2.

Herein, we describe the use of supercritical CO_2 as a continuous phase for the manufacture (and processing) of organic aerogels. The environmental supercritical CO_2-based reaction removes the need to wash the resultants and excludes the solvent (*9,10*). This paper focuses on the design of a direct process for producing P/F aerogel microspheres in supercritical CO_2 by sol-emulsion-gel polymerization (*11-14*) which is much more suitable for handling and which can be used in a variety of applications. In the sol-emulsion-gel method, droplets are dispersed and stabilized in a continuous medium by addition of an appropriate stabilizer, which forms a stable organic gel microspheres consisting of a dispersion phase in supercritical CO_2 continuous phase (*15*). The emulsion droplets serve as microreactors during gelation (*16*). P/F gel microspheres produced by sol-emulsion-gel polymerization are usually stabilized by a "steric" mechanism as compared with an electrostatic mechanism that is common to colloidal stabilization in aqueous environments (*17-19*). The P/F gel microspheres were exchanged into supercritical CO_2 several times, after which it was supercritically dried. This procedure allows for the synthesis of organic

aerogels in the form of micrometer-sized microspheres with high surface area by a direct method. In this paper, we focus on the process of synthesizing P/F aerogel microspheres in supercritical CO_2 by sol-emulsion-gel polymerization. A direct process of organic aerogel microspheres, based on the P/F reaction, has many advantages such as: (1) an environmentally friendly supercritical CO_2-based reaction is used, (2) the sol-emulsion-gel reaction, and (3) the possibility of modifying P/F gel microspheres to P/F aerogel microspheres simply by varying the temperature and pressure of the system. The following experiments were carried out to investigate the properties of P/F aerogel microspheres.

Experimental

Synthesis

Phenolic novolac (Kangnam Chemical Co., M_n = 800 g/mol), furfural (Acros Organics), p-toluenesulfonic acid (Junsei Chemical Co.), heptyl alcohol (Junsei Chemical Co.), and PDMS (polydimethylsiloxane, Dow Corning Co., M_n = 10,000 g/mol) were used as received. Phenolic novolac and furfural were mixed and p-toluenesulfonic acid was added as an acid catalyst. Alcohol was added in order to adjust the overall reactant concentration. CO_2-soluble PDMS

Phenolic novolac   Furfural
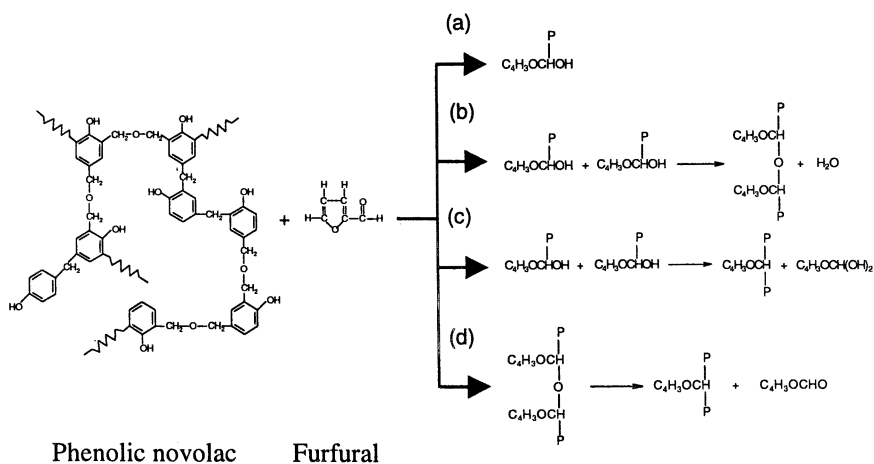
Figure 1. P/F gelation mechanisms: (a) addition polymerization, (b) and (c) condensation polymerization, and (d) disproportionation termination.

(a)

R/F aqueous solution	
Sol-emulsion-gel polym. (W/O emulsion)	Conducted in a glass reactor at 80 °C for 24 hours
Acetone exchange	Conducted in a glass reactor for a week
Liquid CO_2 exchange	Conducted in a high-pressure vessel at 12 °C and 1200 psi several times
Supercritical drying	Conducted in a high-pressure vessel at 40 °C and 1500 psi for 2 hours and vented supercritical CO_2 for 1 hour

(b)

P/F organic solution	
Sol-emulsion-gel polym. (O/CO_2 dispersion)	Conducted in a high-pressure reactor at 80 °C and 1200 psi for 24 hours
Supercritical CO_2 exchange	Conducted in a high-pressure vessel at 40 °C and 1800 psi several times
Supercritical drying	Conducted in a high-pressure vessel at 40 °C and 1800 psi for 2 hours and vented with supercritical CO_2 for 1 hour

Figure 2. Synthetic process for organic aerogel microspheres: (a) existing process for R/F aerogel microspheres, (b) new one-step process for P/F aerogel microspheres.

was used to disperse P/F alcohol solution in supercritical CO_2. As shown in Table I, a set of experiments was carried out to assess the effects of solids content and P/C weight ratio on particle size and particle size distribution of P/F aerogel microspheres. In a typical sol-emulsion-gel polymerization reaction of P/F mixture, phenolic novolac, furfural, p-toluenesulfonic acid, alcohol, and PDMS were put into a 100 mL high-pressure reaction vessel. The cell was purged with nitrogen for ~ 10 min and then filled with CO_2. The cell was heated to 80 °C and the pressure was increased to 1200 psi (CO_2 density = 0.1678 g/mL). The polymerization was continued under these conditions for 24 h. The emulsion was stirred with 6-blade turbine impeller in the stirring rate of 300 rev/min. The reaction cell was fitted with two sapphire windows 2 cm in diameter and 1 cm thick. At the end of the polymerization, the cell was cooled to 40 °C. But the pressure was increased to 1800 psi (CO_2 density = 0.7305 g/mL) by the addition of more CO_2 (conducted by pressure generator). The overall experiment proceeded by a one-step process. The solubility of alcohol in supercritical CO_2 varies with temperature and pressure of the system. As a result, the solubility of heptyl alcohol in supercritical CO_2 at 80 °C and 1200 psi was so low that the polymerization was conducted heterogeneously. After the sol-emulsion-gel polymerization, the solubility change of heptyl alcohol in supercritical CO_2 causes the heptyl alcohol to be miscible with the supercritical CO_2 at 40 °C and 1800 psi (Figure 3) (20). The solvent in the crosslinked gels is extracted in the transition state and supercritical drying step. The solvent in the gel was exchanged into supercritical CO_2, after which it was supercritical dried. The heptyl alcohol including PDMS in this step is eliminated by venting of the supercritical CO_2. As the process conditions were varied, P/F aerogel microspheres were successfully prepared. The overall experimental procedure for a direct process is shown in Figure 4.

Characterization

An essential requirement for experimental investigation of P/F aerogel microspheres is the accurate measurement of the time dependence of conversion. The gravimetric method was carried out in this study. Processed P/F aerogel microspheres were withdrawn from the high-pressure vessel after constant time, then dried at vacuum oven (40 °C), and weighed. Scanning electron microscopy (SEM) and nitrogen adsorption measurements showed that the P/F aerogel microspheres synthesized in supercritical CO_2 by the one-step process were identical to the R/F aerogel microspheres made in VOCs. The average particle

size and size distribution were quantified from SEM micrographs using an Escan 4000 image analysis system. In this technique, the SEM image was converted to a binary image, which was then processed to separate all particles at the set detection level of gray shades, while preserving their sizes. The computer then calculated eight different chords (or diameters) from each aerogel by a dilation/erosion procedure. From these chords, a mean diameter for each aerogel microsphere was calculated. The mean diameter for each aerogel microsphere visible on the micrograph was calculated. Specific BET surface area and pore size distribution of P/F aerogel microspheres is evaluated by BET (Brunauer-Emmett-Teller) from nitrogen adsorption isotherms at 78 K.

Table I. Recipe and Characterization for P/F Aerogel Microspheres used in this Study

Runs[1]	Components					Solids cont. [wt%]	P/C weight ratio	D_n [μm]	Surf. Area [m²/g]
	Phenolic novolac (g)	Furfural (g)	PTSA[2] (g)	Heptyl alc. (g)	PDMS[3] [wt%]				
A	1.52	1.52	0.31	30.0	20	10	20	2.15	775
B	2.27	2.27	0.46	28.3	20	15	20	3.28	635
C	3.03	3.03	0.61	26.7	20	20	20	3.55	579
D	4.53	4.53	0.93	23.3	20	30	20	3.72	539
E	3.0	3.0	0.15	15.4	20	20	20		375
F	3.0	3.0	0.30	14.7	20	20	10		451
G	3.0	3.0	0.60	14.4	20	20	5		539

[1]The polymerization was continued at 80 °C and 1200 psi for 24 hours. The supercritical CO_2 exchange was conducted at 40 °C and 1800 psi over 10 times.

[2] p-Toluene sulfonic acid

[3] Poly(dimethylsiloxane) is based on the dispersion phase (phenolic novolac + furfural + p-toluenesulfonic acid + heptyl alcohol).
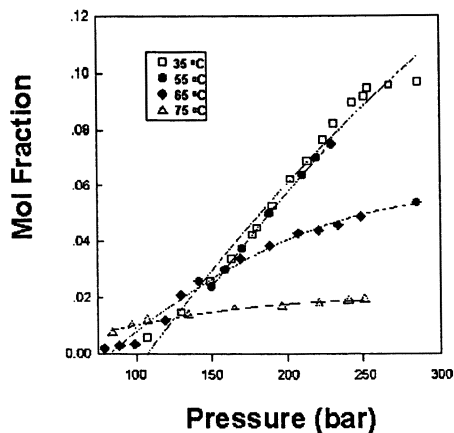
Figure 3. Solubility of heptyl alcohol in supercritical CO_2 as a function of pressure (20).
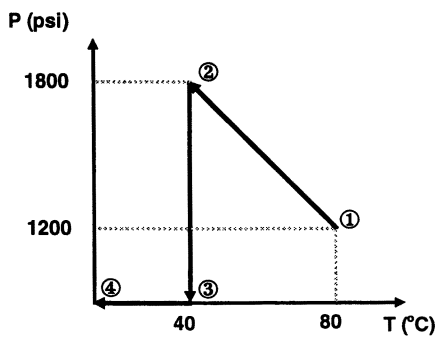
Figure 4. Overall experimental conditions: ① sol-emulsion-gel polymerization,② solvent exchange, ③ supercritical drying, ④ temperature quench.

Results and Discussion

Synthesis of P/F Aerogel Microsphere

In this study, a synthetic process for organic aerogels based upon the P/F reaction was discovered. The process has many advantages as follows. First, the environmentally-friendly supercritical CO_2-based reaction removes the need to wash the resultant and to exclude the solvent. Second, P/F gel microspheres were produced by a sol-emulsion-gel technique. Third, the resultant P/F gel particles were modified to P/F aerogel microspheres simply by varying the temperature and pressure of the system owing to temperature-dependent, pressure-dependent solubility of P/F alcohol solution to supercritical CO_2. Micron-sized P/F aerogel microspheres were successfully produced by a direct process. The conversion-time behavior for P/F aerogel microspheres is shown in Figure 5. The P/F reaction was monitored through weighing free furfural as a function of reaction time using gravimetry. The conversion of the reaction increased sharply during the initial 3 hours of the reaction. The conversion at 3 hrs shows that approximately 50 % of the original furfural has been consumed, and it probably represents the point at which the majority of the P/F "clusters" have been formed. The reaction then depends primarily upon the crosslinking of these "clusters" to form a gel. The latter reaction would be expected to be slow, and the rate-determining step for gelation.
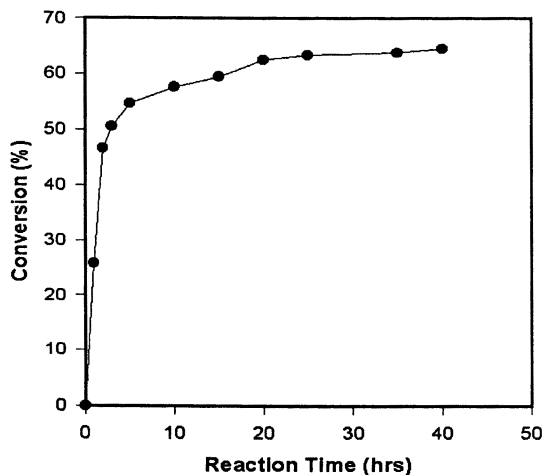
Figure 5. Conversion of P/F microsphere aerogel vs. reaction time.

Particle Size and Particle Size Distribution

Figure 6 shows SEM micrographs of P/F aerogel microspheres at different solids contents. SEM examination showed no significant differences in the spherical morphology of the P/F aerogel microspheres as the solids content was varied in the range of 10 wt% to 30 wt% (runs A ~ D). Figure 6 and Table I reveal that the particle size range of the P/F aerogel microspheres is 1-6 μm in diameter. The particle size was found to increase with increasing the solids content at a constant stabilizer content.
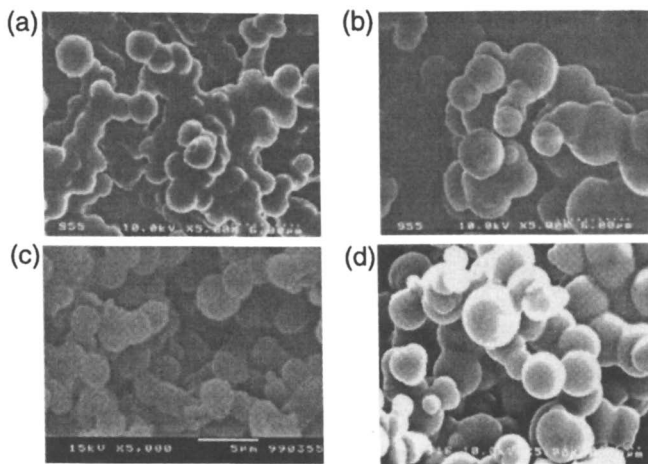
Figure 6. SEM micrographs of P/F aerogel microspheres at different solids contents: (a) run A, 10 wt%, (b) run B, 15 wt%, (c) run C, 20 wt%, and (d) run D, 30 wt%.

At a solids content of 10 wt% (run A), the surfaces of the particles were not smooth owing to the presence of a few small dents, which may have been created by partial melting of the sample under the electron microscope beam. As the solids content was increased to more than 10 wt%, the surfaces of the particles appeared to be smooth. In the present gelation process, the stabilizer prevented the formation of deformed spheres by controlling the sol-supercritical CO_2 interfacial tension (21-23). CO_2-soluble PDMS was used to stabilize a sol-emulsion-gel polymerization in supercritical CO_2 (24-25). In the absence of PDMS, no P/F aerogel microsphere formation was found. Although a relatively small amount of PDMS considerably increased the yield of the P/F aerogel microspheres obtained, larger amounts of PDMS were necessary to adequately

stabilize the sol-emulsion-gel polymerization of P/F in supercritical CO_2. It was assured that PDMS was effective in stabilizing the sol-emulsion-gel polymerization of P/F in supercritical CO_2.

Surface Area

As shown in Figure 7(a) and Table I, the surface area of the P/F aerogel microspheres increased as the [phenolic]/[catalyst] P/C weight ratio was lowered. The surface areas for P/F aerogel microspheres (runs E ~ G) were 375, 451, and 539 m^2/g, respectively. The P/C weight ratio is the dominant factor which affects the surface area. Under high catalyst conditions (i.e., run G; P/C=5), the interconnected particles have diameters of 10-50 nm and are joined together with large necks. From these data, P/F aerogel microspheres can be explained in terms of the better interparticle connections in the 'polymeric' aerogel microspheres as compared with the 'colloidal' aerogel microspheres. This relationship suggests that there are differences in the size, distribution, interpenetration, and chemical linkage of the P/F 'clusters' depending upon reaction conditions (*1*).

Figure 7(b) and Table I show the surface area of P/F aerogel microspheres as a function of solids content. The surface area of P/F aerogel microspheres decreased as the solids content increased. The surface areas for 10 wt% through 30 wt% (runs A ~ D) were 775, 635, 579, and 539 m^2/g, respectively. Obviously, the density is the main parameter that determines the surface area. These data imply that there are subtle differences in the morphologies of P/F aerogel microspheres. As shown in Figure 8, P/F aerogel microspheres possess a 'string of pearls' morphology (*26*). Five typical features can be identified: (a) a mesopore that spans the distance between chains of interconnected particles, (b) a micropore sandwiched between particles, (c) an individual particle, (d) micropores within the particles, and (e) a neck region between contiguous particles.

Inner Structure

The aerogel microspheres have been described as 'polymeric' (under high catalyst conditions) and 'colloidal' (under low catalyst conditions), respectively. As a result of removal of the solvent by evaporation, large capillary forces at the liquid-vapor interface cause the aerogel microspheres to shrink. The surface area of the P/F aerogels increased as the shrinkage level was higher. The amount of shrinkage was dependent upon the catalyst level used to prepare the P/F aerogel microspheres. The small interconnected particle size of the aerogel microspheres necessitates high catalyst conditions.
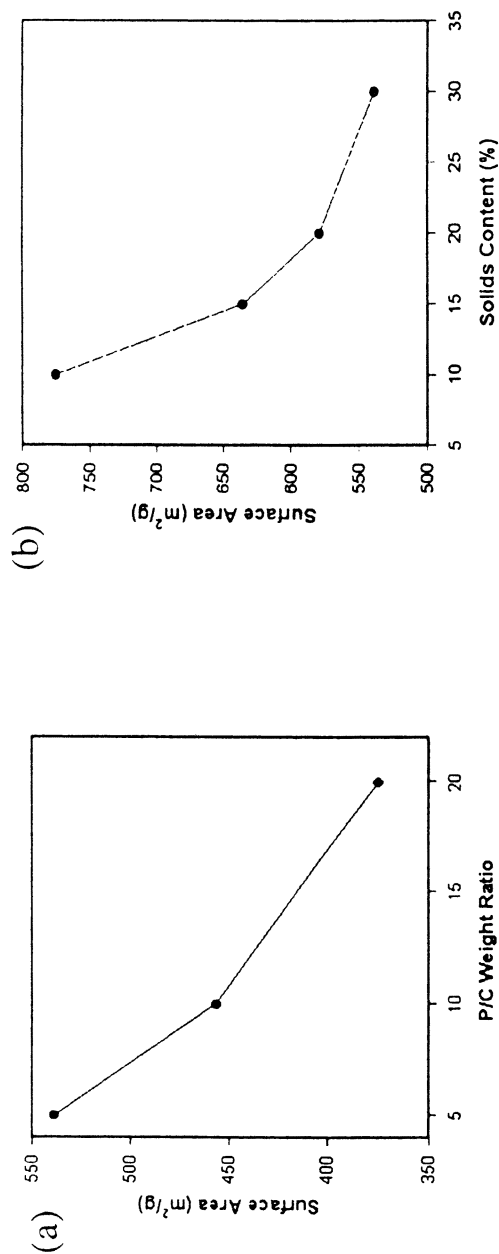
Figure 7. Surface area of P/F aerogel microspheres as a function of: (a) P/C weight ratio (runs E ~ G) and (b) solids content (runs A ~ D).
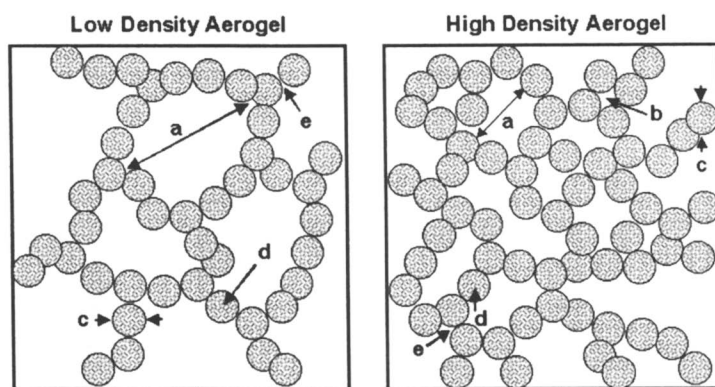
Figure 8. Schematic diagram showing the features of the P/F aerogel microstructure as a function of the bulk density.

Characteristics of the polymeric aerogel microspheres include substantial shrinkage during supercritical drying, small interconnected particle size, and high surface area. In contrast, the colloidal aerogel microspheres exhibit little shrinkage upon supercritical drying, a relatively large interconnected particle size and lower surface area (*6*). Figure 9 (run G) shows SEM micrographs of P/F aerogel microspheres (Figure 9a) and their fractured surfaces (Figure 9b and 9c). This figure shows a morphology of 'polymeric' aerogel microspheres with the high catalyst loading and a morphology common to all of the formulations, namely an open-celled structure with continuous porosity and cell sizes less than 100 nm. The P/F 'polymeric' aerogel microspheres have an interconnected particle structure in the range of 10 ~ 50 nm in diameter. Intuitively, these data can be explained in terms of the better interparticle connections in the polymeric aerogel microspheres as compared with the colloidal aerogel microspheres. This structure is analogous to that reported for R/F aerogel microspheres produced with a base catalyst (*6*).
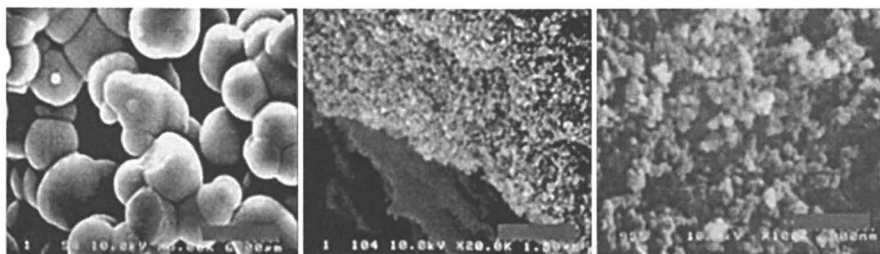
Figure 9. SEM micrographs (run G) of P/F aerogel microspheres (✕5000, a) and their fractured surfaces (✕20,000, b and ✕100,000, c).

Figure 10 shows the pore size distribution (PSD) of P/F aerogel microspheres. PSD is presented as dV/dR plots so that the integrated area under the plot directly corresponds to the pore volume. In this expression dV is the change of volume and dR is the change of radius of P/F aerogel microspheres. The pore size of P/F aerogel microspheres is predominantly about 10 nm, which are responsible for much of the surface area.
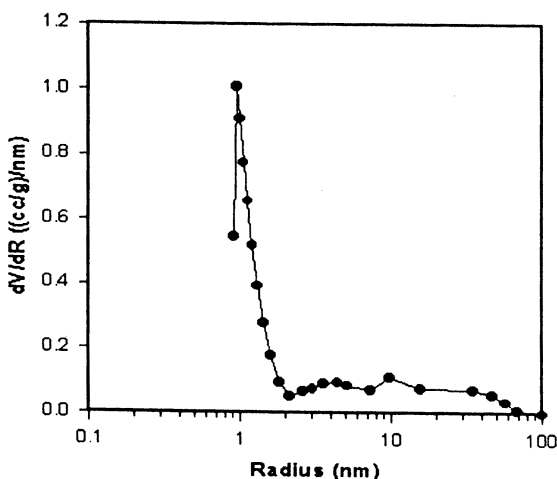
Figure 10. Pore size distribution of the P/F aerogel microspheres.

Conclusions

Micrometer-sized P/F aerogel microspheres were produced in supercritical CO_2 medium by the sol-emulsion-gel technique that is capable of altering the existing process. The process of preparing organic aerogel microspheres based on the P/F reaction represents an advance in organic aerogel microspheres because of: (1) environmental supercritical CO_2-based reaction, (2) the sol-emulsion-gel polymerization, (3) the possibility of modifying P/F gel microspheres to P/F aerogel microspheres simply by varying the temperature and pressure of the system, and (4) the sol-emulsion-gel polymerization and subsequent supercritical drying in one-step process that is an excellent alternative to the existing process. PDMS stabilizer was used to disperse the P/F solution in supercritical CO_2. PDMS was effective in stabilizing the sol-emulsion-gel polymerization of P/F in supercritical CO_2. Spherical morphology of P/F aerogel microspheres was confirmed by SEM. P/F aerogel microspheres have average particle sizes in the range of 1-6 μm. The average particle size increased with increasing solids content. Under the conditions used here, we have prepared P/F aerogel microspheres with high surface area (400-700 m^2/g) similar to other organic aerogels. In this system, It is possible to synthesize aerogel microspheres derived from multifunctional organic monomers in a heterogeneous fashion in supercritical CO_2.

Acknowledgment

References

1. Pekala, R. W.; Alviso, C. T.; Kong, F. M.; and Hulsey, S. S. *J. Non-Cryst. Solids,* **1992,** *145,* 90.
2. Fricke, J.; Emmerling, A. *J. Am. Chem. Soc.,* **1992,** *75,* 2027.
3. Lu. X.; Arduini-Schuster, M. C.; Kuhn, J.; Nilsson, O.; Fricke, J.; Pekala, R. W. *Science,* **1992,** *255,* 971.
4. Fricke, *J. Aerogels*; Springer: New York, **1986.**
5. Hair, L. M.; Pekala, R. W.; Stone, R. E.; Chen, C.; Buckley, S. R. *J. Vac. Sci. Technol. A,* **1988,** *6,* 2559.
6. Pekala, R. W. *J. Mater. Sci.,* **1989,** *24,* 3221.
7. Pekala, R. W. U.S. Patent 5, **1998,** *744,* 510.
8. Pekala, R. W.; Alviso, C. T.; Lu, X.; Gross, J.; Fricke, J. *J. Non-Cryst. Solids,* **1995,** *188,* 34.
9. Canelas, D. A.; DeSimone, J. M. *Adv. Polym. Sci.,* **1997,** *133,* 103.
10. Lee, K. N.; Kim, J. H. *Chem. Ind. & Tech. (Korea),* **1998,** *16,* 352.
11. DeSimone, J. M.; Maury, E. E.; Menceloglu, Y. Z.; McClain, J. B.; Romack, T. R.; Combes, T. R. *Science,* **1994,** *265,* 35.
12. Ponthieu, E.; Payer, E.; Grimblot, J. *J. Non-Cryst. Solids,* **1992,** *147&148,* 598.
13. Chatterjee, M.; Ray, J.; Chatterjee, A.; Ganguli, D. *J. Mater. Sci. Lett.,* **1993,** *28,* 2803.
14. Chatterjee, M.; Siladitya, B.; Ganguli, D. *Mater. Lett.,* **1995,** *25,* 261.
15. Mayer, S. T.; Kong, F. M.; Pekala, R. W.; Kaschmitter, J. L. U.S. Patent 5, **1996,** *508,* 341.
16. Baraton, M. I.; Merle-Mejean, T.; Quintard, P.; Lorenzelli, V. *J. Phys. Chem.,* **1990,** *94,* 5930.
17. Shen, S; Sudol, E. D.; El-Aasser, M. S. *J. Polym. Sci., Part A,* **1994,** *32,* 1087.
18. Napper, D. H. Polymeric Stabilization of Colloidal Dispersions; Academic Press Inc.: London, 1983.
19. Fitch, R. M. Polymer Colloids: A Comprehensive Introduction; Academic Press, Inc.: San Diego, 1997.
20.. Bartle, K. D; Clifford, A. A.; Jafar, S. A.; Shilstone, G. F. *J. Phys. Chem. Ref. Data.,* **1991,** *20,* 713.

21. Yates, M. Z.; Shah, P. S.; Johnston, K. P.; Lim, K. T.; Webber, S. E. *J. Colloid Interface Sci.* **2000**, 227, 176.
22. Harrison, K. L.; daRocha, S. R. P.; Yates, M. Z.; Johnston, K. P.; Canelas, D.; DeSimone, J. M. *Langmuir,* **1998**, *14*, 6855.
23. O'Neill, M. L.; Yates, M. Z.; Harrison, K. L.; Johnston, K. P.; Wilkinson, S. P.; Canelas, D. A.; Betts, D. E.; DeSimone, J. M. *Macromolecules,* **1997**, *30*, 5050.
24. Zhao, X.; Watkins, R. and Barton, S. W. *J. Appl. Polym. Sci.*, **1995**, 55, 773.
25. Garg, A, Gulari, E. and Manke, C. W. *Macromolecules,* **1994**, 27, 5643.
26. Fung, A. W. P.; Reynolds, G. A. M.; Wang, Z. H.; Dresselhaus, M. S.; Dresselhaus, G.; Pekala, R. W. *J. Non-Cryst. Solids,* **1995**, *186*, 200.

Chapter 13

Improving Latex Performance by Using Polymerizable Surfactants

Esteban Aramendia[1], Maria J. Barandiaran[1], Jose C. de la Cal[1], Jo Grade[2], Trevor Blease[2], and Jose M. Asua[1,*]

[1]**Institute for Polymer Materials (POLYMAT) and Grupo de Ingeniería Química, Departamento de Química Aplicada, Facultad de Ciencias Químicas, The University of the Basque Country, Apdo. 1072, ES-20080 Donostia-San Sebastián, Spain** [2]**Uniqema, Everslaan 45-B-3078 Everberg, Belgium**

Latexes with superior properties were produced by using a new alkenyl-functional polymerizable surfactant (surfmer). These latexes have a better freeze-thaw stability, and form films with less water absorption and lower vapor and water permeability. These improvements were due to the chemical bonding of the surfmer to the polymer that minimized its migration. Results obtained by using a mathematical model show that the reactivity ratio of the monomer with respect to the surfmer is the key parameter for an adequate incorporation of the surfmer and such a value should be between 1 and 5.

Surfactants play a crucial role in the production of emulsion polymers. They are very important for the nucleation of latex particles, emulsification of the monomers and stabilization of the polymer particles during the polymerization and shelf life of the product. However, they can also have an adverse effect during application. For example, when the latex is coated at high application speeds the surfactant may desorb and cause destabilization, and when mixed

168 © 2002 American Chemical Society

with pigments in paints the surfactant may migrate to the pigments destabilizing the latex particles. The presence of the surfactant can also have adverse effects on the film properties, as the surfactant may migrate through the film to the film-air interface affecting gloss and to the film-substrate interface reducing adhesion. Also it can concentrate in pockets increasing the percolation by water. In polymer recovery by coagulation the surfactants can have negative effects, for example, in waste-water treatment.

These drawbacks are due to the mobility of the surfactant molecules during the film formation process. Therefore, a promising way to reduce the negative effects of surfactants is to use polymerizable surfactants (surfmers). A surfmer is a surfactant with a polymerizable double bond in its structure. Upon polymerization, these compounds become bound covalently to the polymer material so that desorption from the polymer particle and migration through the polymer film is impeded.

Surfmers have attracted much attention in both open (*1-14*) and patent (*15-20*) literature as improvements in product quality by using surfmers have been reported (*16-31*). Asua and Schoonbrood (*32*) have recently reviewed the publications concerning the use of surfmers in heterophase polymerization in terms of the mechanisms relevant in the process. The authors concluded that there is no general formula for a conventional emulsifier that works well in every system and gave general guidelines to choose or design a specific surfmer and to apply it in an appropriate way. In particular, they proposed that the reactivity ratio of the surfmer with respect to the monomers should be close to zero to avoid surfmer homopolymerization, and the reactivity ratios of the monomers with respect to the surfmer should be between 0.5 and 10 to avoid early polymerization of the surfmer, which would otherwise result in burying of the surfmer, and to achieve a high degree of incorporation at the end of the process. The authors stressed that these were rough guidelines because other factors may affect the observed reactivity.

This paper addresses two important aspects of surfmer technology. The first one deals with latex performance improvements achieved using a new nonionic surfmer. The second is related to the choice of the reactive group of the surfmer.

Improvement of Latex Performance

The performance of latexes prepared using a new alkenyl-functional nonionic surfmer (Maxemul 5011, Uniqema) was compared with that of the latexes prepared with the same monomers but stabilized with conventional nonyl phenol ethoxylated nonionic surfactants (NP20 and NP30).

50 wt% solids vinyl acetate / butyl acrylate (85/15 by weight) latexes were prepared through semicontinuous emulsion copolymerization with both Maxemul 5011 and NP20 using the recipe given in Table I. The latexes were subjected to freeze-thaw cycles (-20 °C, 11 hrs / 1 hr heating, 23 °C, 11 hrs, 1 hr cooling). It was found that the latexes prepared with Maxemul 5011 resisted 5 freeze-thaw cycles whereas those prepared with NP20 failed after 2 cycles. A possible reason for the superior performance of the latex stabilized with the surfmer is that during the freezing process as ice crystals are formed, the polymer particles are restricted in a smaller volume, and hence they are in close contact. The pressure created by the ice forces the interpenetration of the hairy layers formed by the surfactant covering the polymer particles. The interpenetration of the hairy layers increases the energy of the system causing the repulsion of the polymer particles, and hence maintaining their stability. However under conditions occurring during the freezing process, the pressure created by the ice may be sufficient to displace the conventional surfactant along the surface of the particles, leaving uncovered zones that are closer to other particles. This results in particle coagulation. When the latex is stabilized by the polymerizable surfmer, the surfmer cannot be displaced along the particle surface because it is bound to the polymer. Therefore, no parts of the polymer particle are left unprotected and the particles remain stable.

Table I. Formulation Used to Prepare the Vinyl Acetate / Butyl Acrylate Latexes[a]

Initial charge	Water	99.30
	VAc/BA	12.50
	KPS	0.63
	K_2CO_3	0.25
	Nonionic surfactant / Maxemul 5011	12.51
Pre-emulsion	Water	268.97
	VAc/BA	437.50
	Maxemul 5011	18.93
Initiator stream	KPS	1.80
	K_2CO_3	1.80
	Water	120.00
Mop-up	Water	25.00
	t-BHP	0.45
	SFS	0.36

[a] All amounts are in grams

Films with a wet thickness of 200 μm were cast from these latexes on polyester and allowed to dry for 7 days at 21°C and 50% relative humidity (R.H.). The films were compared for water absorption upon immersion in water. Figure 1 shows that the film cast from the latex stabilized with Maxemul 5011 showed much better water resistance than that cast from the latex containing the conventional emulsifier. The difference increased with the time of immersion in water. The higher water sensitivity showed by the film stabilized with the conventional emulsifier may be due to the migration of the emulsifier during the film formation that results in both channels through which the water can percolate and segregated pockets of emulsifier where water can accumulate.
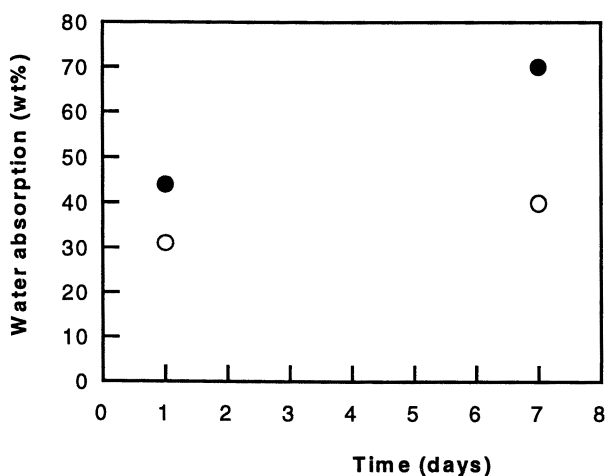
*Figure 1. Water absorption of the vinyl acetate / butyl acrylate copolymer films.
(O) Maxemul 5011; (●) NP20*

50 wt% solids methyl methacrylate / butyl acrylate (50/50 by weight) latexes were prepared by semicontinuous emulsion copolymerization using the recipe given in Table II. Both Maxemul 5011 and NP30 were used in these polymerizations. Films from these latexes were cast onto a glass surface and kept at room temperature overnight. The films were observed by atomic force microscopy (AFM, NanoScope IIIa), working in contact mode. Figure 2 presents the AFM micrographs of the film produced from the latex stabilized with NP30. The untreated film (Figure 2a) shows the presence of large amounts of surfactant that migrated to the film-air interface during the film formation. This emulsifier disappeared when the film was rinsed with water (Figure 2b). Figure 3 shows the AFM micrographs of the film cast from the latex stabilized by Maxemul 5011.

No evidence of surfactant migration was observed in the untreated film (Figure 3a) and no significant differences were found after rinsing with water (Figure 3b).

Table II. Formulation Used to Prepare the Methyl Methacrylate / Butyl Acrylate Latexes[a]

SEED	Water	1485.01
	MMA	68.91
	BuA	68.91
	AA	1.76
	KPS	6.00
	NaHCO$_3$	0.90
	Anionic surfactant	17.16
SEEDED POLYMERIZATION		
Initial Charge	Seed	156.50
	Water	59.27
	MMA	11.28
	BuA	11.28
	KPS	0.056
	Nonionic Surfactant / Maxemul 5011	0.67
Feed 1	MMA	212.71
	BuA	212.71
	AA	8.98
Feed 2	KPS	0.91
	Nonionic surfactant / Maxemul 5011	12.79
	Water	143.75
Feed 3	Water	100.00
	Na$_2$S$_2$O$_5$	0.69

[a] All amounts are in grams

The methyl methacrylate/butyl acrylate copolymer films were also compared for vapor and liquid water permeability. In order to measure the vapor permeability, the films were used to close a small chamber (the lower part is about 2 cm^3, while the whole system is about 4 cm^3) containing 1.2 cm^3 of water. The chamber was placed on a balance and the loss of weight due to vapor diffusion through the film was recorded. Data were normalized by means of the following equation:

$$WVTR = \frac{B \times L}{A(1 - RH)} 8.64 \times 10^5 \qquad (1)$$

where *WVTR* represents the water or vapor transmission rate (g mm/m^2 day), *B* is the slope of the weight loss vs time curve, *L* the film thickness, and *A* the area of the cell.
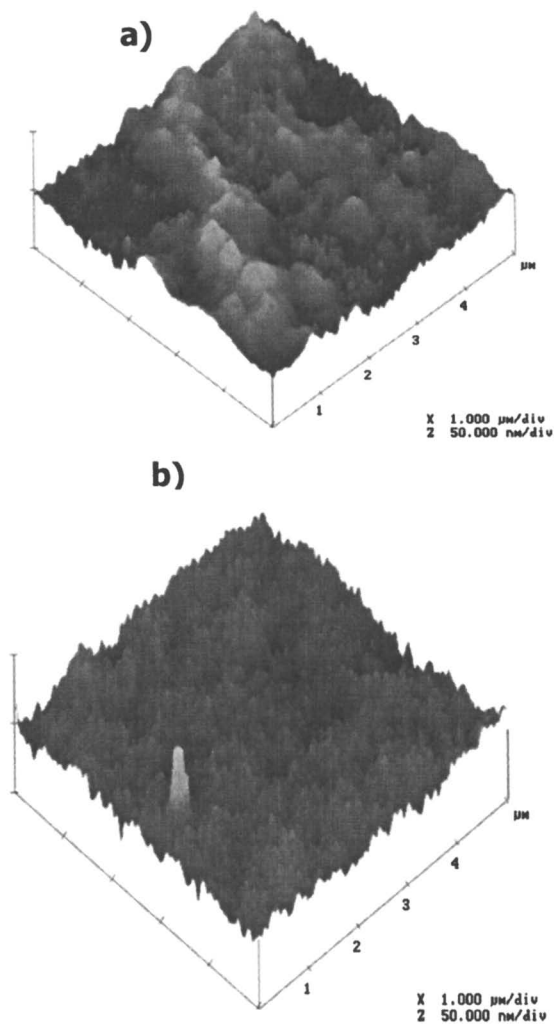
Figure 2. AFM micrographs of the film produced from methyl methacrylate / butyl acrylate latex stabilized with NP30. (a) untreated film; (b) film rinsed with water.
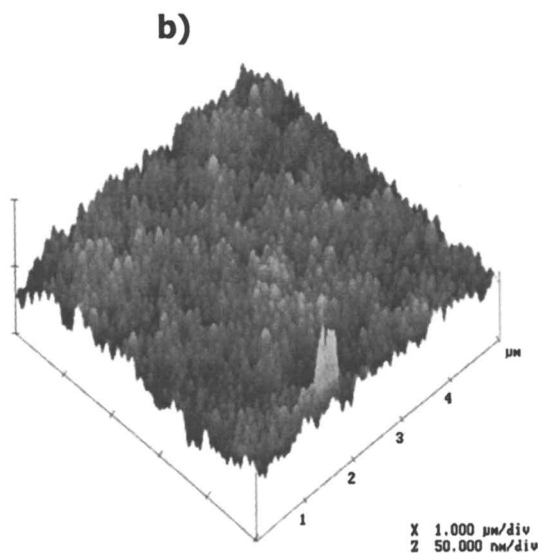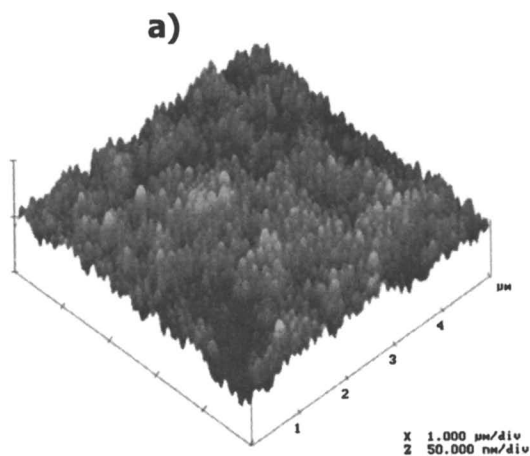
Figure 3. AFM micrographs of the film produced from methyl methacrylate / butyl acrylate latex stabilized with Maxemul 5011. (a) untreated film; (b) film rinsed with water.

Each measurement was carried out three times and the data were found to be reproducible within 10%. The main source of error in these kinds of experiments is related to the thickness of the films.

Table III. Permeability of MMA/BuA Films

Surfactant	WVTR	VTR
NP30	17.21	183.50
Maxemul 5011	14.12	34.31

Film permeability by liquid water (WTR) was determined in a similar way, but placing the chamber upside down, maintaining the film in direct contact with the water. In this system, the loss of weight was due to the evaporation at the external surface of the film of the water that diffused through the film. Table III shows that both vapor and liquid water permeability were higher for the film cast from the latex stabilized by the conventional surfactant, the difference being enormous for the liquid water permeability. The formation of percolation channels and segregated surfactant pockets is the reason for the higher liquid and vapor permeability of the film containing the conventional surfactant. It is worth pointing out that a high water penetration is a serious drawback for using these latexes for exterior paints because they will not protect the substrate.

Choice of the Reactive Group of the Surfmer

In the previous section it has been shown that the use of surfmers can lead to latexes of superior performance. The advantages of these latexes are related to the fact that the surfmer is bound to the polymer, namely to its lack of mobility. However, the lack of mobility may be a serious drawback during the polymerization process. Thus, if the surfmer reacts early in the process it may become buried inside the polymer particle as the polymer particle grows. Ideally, the surfmer should not react early in the process to avoid being buried, but complete incorporation into the polymer at the end of the process is desired (*32*). The key parameter controlling the polymerization of the surfmer is its intrinsic reactivity. Asua and Schoonbrood (*32*) gave a rough guideline for the reactivity ratios of the surfmer and monomers ($r_{SM} \sim 0$ and $0.5 < r_{MS} < 10$). This guideline was mostly based on scattered experimental results and there are indications that they may not be accurate (*33*). In order to check the recommended values for the reactivity ratios, a mathematical model was developed for emulsion

polymerization involving surfmers. The model incorporates the following mechanisms:

i) The surfmer adsorbs on the surface of the polymer particles according to an adsorption equilibrium isotherm.

ii) The surfmer polymerizes in an outer shell of thickness δ_1, that is a parameter of the model.

iii) Due to particle growth, the polymerized surfmer may become buried. The polymerized surfmer may resist burying by migrating towards the particle surface. The driving force for this migration is the water affinity of the hydrophilic part of the surfmer. Viscous drag is the resistance to migration. The relative rates of particle growth and surfmer migration determine the fate of the polymerized surfmer. These considerations are accounted for in the model by considering that the surfmer does not migrate but that all of the polymerized surfmer located in an outer shell of thickness δ_2 is active in stabilizing the polymer particles. A small value of δ_2 (in the range of 0.5 nm) means that the polymerized surfmer does not migrate towards the surface. On the other hand, a value in the range of 5 nm represents an important migration.

iv) Stability is provided by both the adsorbed unreacted surfmer and by the polymerized surfmer located in an outer shell of thickness δ_2.

v) A radial concentration profile may exist in the polymer particle due to the surface anchoring effect (34,35).

Table IV. Parameters of the Model

$dp_{seed}= 40$ nm	$k_{t1}= 7 \times 10^{10}$ cm^3 mol^{-1} s^{-1}
$\delta_1= 2$ nm	$k_{t2}= 6.5 \times 10^9$ cm^3 mol^{-1} s^{-1}
$\delta_2= 0.5$ nm	$r_{12}= 0.75$
$m_1= 1624$	$r_{21}= 0.2$
$m_2= 480$	$k_{p11}=2.75 \times 10^5$ cm^3 mol^{-1} s^{-1}
$k_a= 1 \times 10^9$ cm^3 mol^{-1} s^{-1}	$k_{p22}= 5 \times 10^6$ cm^3 mol^{-1} s^{-1}
$k_d= 8 \times 10^{-4}$ s^{-1}	$k_{pss}= 1 \times 10^4$ cm^3 mol^{-1} s^{-1}
$k_I=1 \times 10^{-6}$ s^{-1}	

Figure 4 presents the monomer and surfmer conversions predicted by the model when surfmer and monomer reactivity ratios were varied (the values of the parameters of the model are given in Table IV). It can be seen that the reactivity ratios did not affect monomer conversion. On the other hand, surfmer conversion was only moderately affected by the reactivity ratios of the surfmer with respect to the monomers, namely, it is unlikely to find two adjacent surfmer molecules in the same chain. The key parameter affecting surfmer conversion is the reactivity ratio of the monomers with respect to the surfmer. Figure 4 shows

that the range of reactivity ratios proposed by Asua and Schoonbrood (*32*) is too broad because $r_{MS} = 10$ resulted in a poor incorporation of the surfmer into the polymer chains and $r_{MS} = 0.5$ yielded early incorporation of the surfmer, and likely buried surfmer. Figure 4 suggests that the monomer reactivity ratio should be between 1 and 5. It is worth pointing out that other aspects such as surface properties of the surfmer and particle size also affect surfmer conversion (*36*).
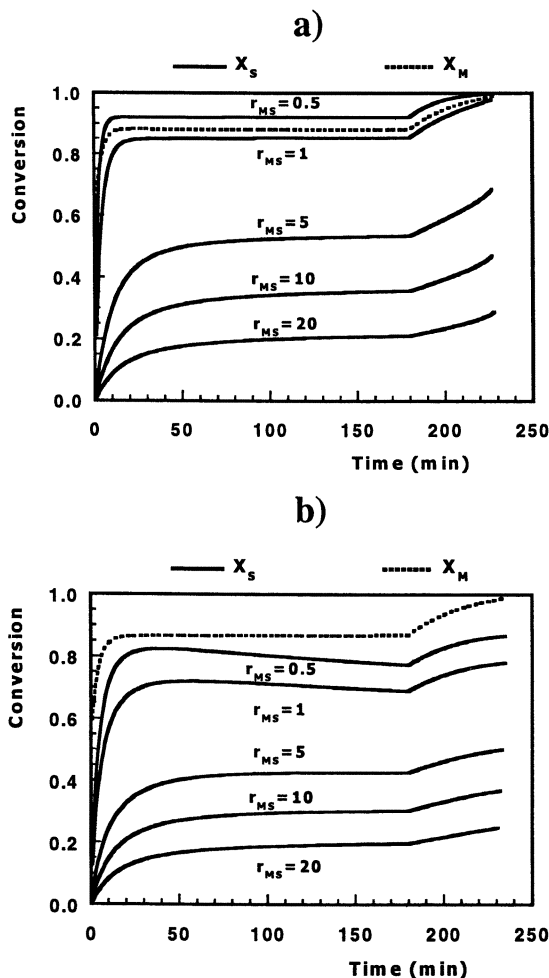
Figure 4. Effect of reactivity ratios on monomer and surfmer conversion. (a) $r_{SM}=0.001$;(b) $r_{SM}=0.5$.

Conclusions

In the foregoing it has been shown that latexes with superior properties can be produced by using a new alkenyl-functional nonionic surfmer. These latexes have a better freeze-thaw stability and form films with less water absorption and lower vapor and liquid water permeability. The films prepared from latexes stabilized with the surfmer showed no trace of surfactant migration whereas those obtained from the latex stabilized by the conventional surfactant presented large aggregates of surfactant at the film-air interface. The choice of the reactive group of the surfmer was investigated by using a mathematical model for the process. It was found that, for small values of r_{SM}, the reactivity ratio of the monomer with respect to the surfmer is the key parameter for an adequate incorporation of the surfmer. A monomer reactivity ratio between 1 and 5 gives the best results.

Acknowledgment

References

1. Tsaur, S. L.; Fitch, R. M. *J. Colloid Interface Sci.* **1987**, *115*, 450.
2. Nagai, K.; Satoh, H.; Kuramoto, N. *Polymer*, **1993**, *34*, 4969.
3. Joynes, D.; Sherrington, D. C. *Polymer* **1997**, *38*, 1427.
4. Charleux, B.; Pichot, C.; Llauro, M. F. *Polymer* **1993**, *34*, 4352.
5. Urquiola, M. B.; Dimonie, V. L.; Sudol, E. D.; El-Aasser, M. S. *J. Polym. Sci., Part A: Polym. Chem.* **1992**, *30*, 2631.
6. Urquiola, M. B.; Dimonie, V. L.; Sudol, E. D.; El-Aasser, M. S. *J. Polym. Sci., Part A: Polym. Chem.* **1992**, *30*, 2619.
7. Urquiola, M. B.; Dimonie, V. L.; Sudol, E. D.; El-Aasser, M. S. *J. Polym. Sci., Part A: Polym. Chem.* **1993**, *31*, 1403.
8. Lacroix-Desmazes, P.; Guyot, A. *Colloid Polym. Sci.* **1996**, *274*, 1129.
9. Unzué, M. J.; Schoonbrood, H. A. S.; Asua, J. M.; Montoya-Goñi, A.; Sherrington, D. C.; Stähler, K.; Goebel, K.-H.; Tauer, K.; Sjöberg, M.; Holmberg, K. *J. Appl. Polym. Sci.* **1997**, *66*, 1803.
10. Schoonbrood, H. A. S.; Unzué, M. J.; Beck, O. J.; Asua, J. M.; Montoya-Goñi, A.; Sherrington, D. C. *Macromolecules* **1997**, *30*, 6024.
11. Schoonbrood, H. A. S.; Unzué, M. J.; Amalvy, J. I.; Asua, J. M. *J. Polym. Sci., Part A: Polym. Chem.* **1997**, *35*, 2561.

12. Lam, S.; Hellgren, A. C.; Sjöberg, M.; Holmberg, K.; Schoonbrood, H. A. S.; Unzué, M. J.; Asua, J. M.; Tauer, K.; Sherrington, D. C.; Montoya-Goñi, A. *J. Appl. Polym. Sci.* **1997**, *66*, 187.
13. Schoonbrood, H. A. S.; Asua, J. M. *Macromolecules*, **1997**, *30*, 6034.
14. Amalvy, J. I.; Unzué, M. J.; Schoonbrood, H. A. S.; Asua, J. M. *Macromolecules* **1998**, *31*, 5631.
15. Heilier, L.; Schmidt, A.; Probst, J. *DE 4202050 A1.*
16. Onodera, S.; Yamamoto, S.; Tamai, T.; Takahashi, H. *Jpn Pat.* 6,239,908, **1994**.
17. Tang, R. H. and Chakrabarti, P. M. *US Pat.*, US 5,296,627, **1994**.
18. Kinoshita, K.; Fukakusa, K.; Fukuzumi, T.; Takahata, N. *Jpn. Pat.*, 6049108, **1994.**
19. Yokota, K.; Ichihara, A.; and Shinike, H. *US Pat.*, US 5,324,862, **1994**.
20. Usui, S. *Jpn. Pat.*, 6065551, **1994**.
21. Greene, B. W.; Sheetz, D. P.; Filer, T. D. *J. Colloid Interface Sci.* **1970**, *32*, 90.
22. Greene, B. W.; Sheetz, D. P. *J. Colloid Interface Sci.* **1970**, *32*, 96.
23. Hatala, R. J. *Org. Coatings Plastic Chem. Preprints of Papers presented at the Philadelphia Meeting of the American Chemical Society,* **1964**.
24. Muroi, S. *Kogyo Kagako Zasshi* **1965**, *68*, 1790.
25. Greene, B. W.; Saunders, F. L. *J. Colloid Interface Sci.* **1970**, *33*, 393.
26. Leary, B.; Lyons, C. J. *Aust. J. Chem.* **1989**, *42*, 2055.
27. Palluel, A. L. L.; Wesby, M. J.; Bromley, C. W. A.; Davies, S. P.; Backhouse, A. J. *Makromol. Chem., Macromol. Symp.* **1990**, *35/36*, 509.
28. Biale, J. *US patent 5,326,814* to Rohm and Haas Co., **1994**.
29. DE Patent 3,239,527 to Rohm GmbH, **1984**.
30. GB Patent 1,427,789 to Bayer AG, **1982**.
31. Cochin, D.; Laschewsky, A.; Nallet, F. *Macromolecules* **1997**, *30*, 2278.
32. Asua, J. M.; Schoonbrood, H. A. S. *Acta Polym.*, **1998**, *49*, 671.
33. Roy, S.; Favresse, P. A.; Laschewsky, A.; de la Cal, J. C.; Asua, J. M. *Macromolecules* **1999**, *32 (18)*, 5967.
34. Chern, C. S.; Poehlein, G. W. *J. Polym Sci., Polym. Chem. Ed.* **1987**, *25*, 617.
35. de la Cal, J. C.; Urzay, R.; Zamora, A.; Forcada, J.; Asua, J. M. *J. Polym. Sci., Polym. Chem. Ed.* **1990**, *28*, 1011.
36. de la Cal, J. C.; Asua, J. M. Submitted to *J. Polym. Sci., Polym. Chem. Ed.*

Chapter 14

Characterization of Latexes Synthesized Using a Reactive Surfactant and Its Polymeric Counterpart

Xiaoru Wang, E. David Sudol, and Mohamed S. El-Aasser*

Emulsion Polymers Institute and Department of Chemical Engineering, Lehigh University, Bethlehem, PA 18015

Emulsion polymerizations of styrene using the reactive surfactant TREM LF-40, and its polymeric counterpart, poly(TREM), have been previously investigated regarding the extent of bonding of the surfactants on the surface of the polymer particles. In this paper, additional characterization of these latexes was performed. The aqueous phase was found to contain oligomers of TREM LF-40 and copolymers of TREM LF-40 with styrene. A substantial amount of buried surfactant was also found. Characterization of the molecular weights of the final latex polymers revealed a decrease in M_n with increasing TREM LF-40, indicating that a significant amount of chain transfer to TREM LF-40 occurred during the reactions. The hydrophobicity of the latex films was increased by incorporation of these surfactants. AFM examination showed that the TREM LF-40 and poly(TREM) surfactants remained primarily on the polymer particles both before and after cleaning the latexes. These characterization results are consistent with the mechanism of the emulsion polymerization as proposed based on the kinetic studies.

Emulsion polymerization is an important technique for synthesizing various industrial-based polymers used in coatings and paints, adhesives, toners, inks, drug delivery and other applications (*1*). Surfactants play major roles in the particle nucleation and growth stages of an emulsion polymerization, having direct impact on the latex particle size, size distribution and polymerization rate. Some variations on the conventional emulsion polymerization process include the replacement of conventional surfactants by functional monomers, such as acrylic acid, sodium styrene sulfonate, acrylamide, and the use of polymeric and reactive surfactants. Polymeric surfactants, such as block copolymers, can be adsorbed and/or grafted on the particle surface. Reactive surfactants can be classified as: (1) surfactants with an initiating moiety (inisurfs); (2) surfactants with a moiety capable of chain transfer (transurfs); or (3) surfactants with a group capable of copolymerization (surfmers). Reactive surfactants can be chemically bound to the particles and thus increase the stability of the latex, decrease the foaming of the latex, and increase the water resistance of the latex film by preventing surfactant migration during film formation or on exposure to water. Reactive surfactants and polymeric surfactants have recently been widely used and studied in emulsion polymerization due to these significant advantages. The kinetics and mechanism of emulsion polymerization of styrene using the reactive surfactant TREM LF-40 and its polymeric counterpart, poly(TREM), have been studied (*2-8*). The results revealed significant differences between a conventional surfactant (SLS) and the reactive surfactant and its polymeric counterpart. Deviations from Smith-Ewart kinetics (case 2) (*9*) were attributed to the chemical reactions involving the surfactant. Using poly(TREM), particle nucleation in the emulsion polymerization of styrene was dominated by homogeneous nucleation with only a small component attributed to micellar nucleation. This was in contrast to polymerizations with the conventional (*10-12*) and the monomeric surfactants, which both were characterized by substantial amounts of micellar nucleation along with homogeneous nucleation (*8*). Further detailed characterization of the latexes is reported in this paper.

Experimental

Materials

Styrene (Aldrich) was washed with a 10 wt% aqueous NaOH (Fisher Scientific) solution and deionized water, and purified by distillation under vacuum prior to use. Buffer (NaHCO$_3$, Aldrich) and initiator (Na$_2$S$_2$O$_8$, FMC Corporation) were analytical grades. TREM LF-40 (Cognis Corp.) was used as received. A monodisperse polystyrene seed latex (92 nm, LS 1039E, Dow Chemical Company) was used both before and after cleaning. Ion-exchange

resins (AG 1-X4, AG 50W-X4, 20~50 mesh, Bio-Rad Laboratories) were used to clean the latexes (*13*). HPLC grade THF (Mallinckrodt Baker) was used in the GPC and titration experiments. Deionized (DI) water was used throughout.

Synthesis of TREM LF-40 Homopolymer

The homopolymer of TREM LF-40, poly(TREM), was prepared via solution polymerization using sodium persulfate ($Na_2S_2O_8$) as initiator. The reaction was carried out at 60 °C for 12 hrs followed by 9 hrs at 90 °C, using the recipe containing 7.8 wt% TREM LF-40, 10 mM $NaHCO_3$, and 16 mM $Na_2S_2O_8$ in DI water (360 g). The resulting polymer had a number-average molecular weight of 6000 ± 300 g/mol (estimated by vapor pressure osmometry, VPO) indicating an average of 14 mers per chain. This poly(TREM) was used without further purification.

Synthesis of the Latexes

Emulsion polymerizations were carried out in the Mettler RC1 reaction calorimeter equipped with a one liter medium pressure reactor (MP10), a pitched blade impeller, and baffle (*10*). The reactor was first charged with 420.0 g of water, buffer ($NaHCO_3$, 4 – 10 mM), and surfactant (20 – 50 mM), followed by 218.4 g of styrene monomer. The reactor was flushed with nitrogen (Zero grade, Airgas/JWS Technologies Inc.) for about 20 minutes and sealed. After the temperature was ramped to the reaction temperature (T_r = 60 °C), the initiator ($Na_2S_2O_8$) solution (4 – 10 mM) was added to start the reaction. When the reaction was completed (conversion > 95%), an aqueous solution (1 wt%) of hydroquinone (Aldrich) was added to the latex. The final latexes were stored at room temperature.

Incorporation of the Surfactants

The characterization of the latex particles for the presence of strong acid groups derived from the surfactant and initiator fragments was carried out by desorption (serum replacement) and ion-exchange/conductometric titration (*14*). The desorption method was used to estimate the amount of surfactant incorporated into the particles both on the surface and buried inside. This was done by measuring the amount of surfactant not bound to the particles. DI water was continuously flushed through a serum replacement cell containing a sample of latex until the water flowing out of the cell had the same conductivity as the

DI water. The concentration of the surfactant in the effluent (assumed to be the only significant component) was determined by gravimetry ($\pm 1\%$ error). The amount of incorporated surfactant was calculated by subtracting the amount of the surfactant in the effluent from the initial amount of surfactant used to prepare the latex. To determine the amount of surfactant chemically bound to the surface of the particles, the latex cleaned by serum replacement was ion-exchanged and titrated conductometrically.

The ion-exchange resins (both cationic and anionic, in their OH^- and H^+ forms, respectively) were separately washed with DI water until the wash water had the same conductivity as DI water. The resins were then mixed (1:1 wt ratio) and washed again. The latexes were diluted to 5 wt% solids and then cleaned using the mixed bed resins employing a 1:1 weight ratio of latex polymer to resin. The latexes and mixed bed resins were mixed together for two hours and then the resins were removed by filtration. Ion-exchange was repeated until two successive ion-exchange cycles resulted in the same latex conductivity. The cleaned latexes (~1 g polymer) were then titrated with 0.02 N NaOH (Fisher Scientific) and the conductivity monitored. The amount of strong acid groups was calculated from the end-point (change in slope), which represents the amount of chemically-bound surfactant, plus a minor amount of SO_4^- from the initiator fragments ($\leq 1\%$), on the surface of the polymer particles.

The possible burial of the surfactant within the polymer particles was first examined by dissolving the latex in 10 times its volume of dioxane/water (95:5), and then ion-exchanging three times. However, this treatment resulted in the precipitation of the polystyrene. An alternative method was devised in which the ion-exchanged polystyrene latex particles were first swollen by adding THF (20 wt% based on the polymer). Then an excess of NaOH was added to this latex, which could then diffuse into the particles. Afterwards, a back titration (0.02 N HCl) was performed to measure the amount of strong acid present in the latex. This procedure was further modified whereby the same cleaned PS latex containing THF was ion-exchanged with mixed bed resins to replace ions exposed by the swelling procedure. Conductometric titration to determine the quantity of the buried plus surface groups was then carried out. The amount of strong acid groups was calculated from the titration, which represents the amount of chemically-bound surfactant on the surface and inside the particles, plus a negligible amount due to the initiator fragments.

Molecular Weights

The latex was dried at room temperature and then dissolved in THF. The

polymer solution (1 wt%) was then filtered through a 0.45 μm filter before injection into the gel permeation chromatography instrument (GPC, Millipore-Waters). The number-average molecular weight (M_n), weight-average molecular weight (M_w), and polydispersity index (PDI) were obtained from the chromatograms based on a calibration using polystyrene standards (Polymer Laboratories, Ltd.).

Serum Phase Analysis

Filtration and ultracentrifugation were used as two separate means to separate the serum phase. FTIR (Mattson Sirius Model 100 FTIR spectrophotometer) and NMR (Bruker spectrometer) were used to qualitatively study the composition of the non-volatile components of the aqueous phase of the serum. Ultracentrifugation was carried out at 30,000 rpm and 4 °C for 7 hours using a Beckman L50 ultracentrifuge with swinging buckets. In the FTIR spectrum of TREM LF-40, the characteristic peak, corresponding to the S–O stretch of the sulfonate salt is at $\nu = 1052$ cm^{-1}, and the peak at $\nu = 927$ cm^{-1} was used to identify the C=C component in TREM LF-40. For styrene, the characteristic peaks are at $\nu = 3000, 3022, 3060, 3080,$ and 3100 cm^{-1}.

Film Characterization

Two continuous (coalesced) films were formed in aluminum pans for each latex sample. The first film was formed at 180 °C (T_g PS = 104 °C), while the second film was formed at room temperature after lowering the T_g by swelling the latex with 10 wt% toluene (based on polymer).

The hydrophilicity of the films was characterized by measuring the contact angle (advancing) of DI water on the surface of the films before and after equilibrium, using a computerized goniometer. Both the film/air and the film/substrate surfaces were examined. Data were obtained before (as soon as the water droplet was placed on the surface) and after equilibrium (1 minute) was established for a water droplet placed on the surface.

The film surface morphology of the latexes dried at room temperature (i.e., not coalesced) was examined using an atomic force microscope (AFM) (Park Scientific Instruments, BioProbe Electronics Module).

Results and Discussion

Chemical Incorporation of TREM LF-40 and Poly(TREM)

As reported in detail elsewhere (*6-8*) the results obtained by ion-exchange/ conductometric titration showed that for the polystyrene latexes prepared with increasing TREM LF-40 concentration, the amount of chemically-bound surfactant (grams TREM LF-40 per gram polystyrene) increased, while the fraction bound to the polymer particles decreased. At the same time, the particle size decreased with increasing surfactant concentration, as expected. The characterization results also showed that both the chemically-bound surfactant and the fraction incorporated were larger as measured by serum replacement (e.g., 30 mM [TREM LF-40] and 8 mM [I], 62 wt%) than the comparable results obtained by ion-exchange/conductometric titration (35 wt%). This indicated that among the chemically-bound surfactant, some had to be buried inside the particles (i.e., inaccessible in the titrations). Also, the results showed that with increasing initiator concentration, both the amount and fraction of the TREM LF-40 incorporated increased significantly. Again, the particle size decreased with increasing initiator concentration as expected. It was concluded that the most obvious way to increase the amount of chemically-bound TREM LF-40 was to decrease the surfactant concentration and to increase the initiator concentration.

Although the two measurements described above should by mass balance give the amount of buried surfactant (e.g., 27% in the preceding example), a more direct measurement was sought to confirm this. In order to determine the amount of buried surfactant, THF was used to partially swell the particles as described in the experimental section. For the same latex (30 mM [TREM LF-40], 8 mM [I]), it was found that after swelling with THF (without the second ion-exchange step) and carrying out the conductometric titration, 40% of the surfactant remained in the latex. This is about the same value as obtained by difference based on the serum phase analysis (38%). This method apparently failed to reveal any buried groups because the counterions to the buried groups had not been replaced with H^+ in the initial ion-exchange treatment. When the THF-swollen latex was subsequently ion-exchanged a second time and then titrated, it was found that 60% of the surfactant was bound to the polymer particles. These results indicate that about 20% of the surfactant was buried inside the particles. This buried fraction may be the result of the partitioning of the TREM LF-40 surfactant into the styrene monomer including the monomer-swollen particles, followed by its copolymerization there. It could also result from homogeneous/coagulative nucleation, which is also considered to occur in this system (*6*).

The combination of all the above results can be used to quantitatively explain the unusual kinetics of the emulsion polymerization of styrene using TREM LF-40 as the surfactant (*8*). The lack of the one-to-one relationship found between R_p and N_p ($R_p \propto N_p^{0.67}$) is proposed to be caused by a combination of the following: (1) copolymerization between TREM LF-40 and styrene; (2) chain transfer to TREM LF-40 during the polymerization of styrene; and (3) possibly reduced radical entry into the particles because of the existence of a "hairy" layer formed by the polymeric surfactant (formed in situ), poly(TREM) or poly(TREM-co-styrene), on the surface of the particles.

In the case where poly(TREM) was used as the surfactant, however, significantly higher amounts of the surfactant were bound to the latexes (e.g., 30 mM [poly(TREM)] and 8 mM [I], 83% by serum replacement and 76% by ion-exchange/conductometric titration) (*6*). As for the TREM LF-40 system, the increasing poly(TREM) concentration lead to a decreasing particle size, increasing amounts of bound surfactant (g/g) but a decreasing fraction bound to the polymer particles. With increasing initiator concentration (decreasing particle size), both the amount incorporated and the bound fraction of the poly(TREM) increased significantly. The exact mechanism by which the poly(TREM) becomes bound to the polymer particles is not known; however, grafting of polystyrene onto the poly(TREM) is considered to be likely. Some entrapment is also possible through the homogeneous/coagulative nucleation process. Another possible contribution is some irreversible adsorption of the longer polymeric surfactant chains through multiple anchoring sites. The possibility or extent of these was not determined, however.

Serum Phase Analysis of Latex

To gain an additional understanding of what is happening in these emulsion polymerizations, the serum phase of the latexes was analyzed. The purpose of this analysis was to determine the fate of the surfactant that is not chemically bound to the particles as it exists in the serum phase. The TREM LF-40 that was not chemically bound to the surface or inside the particles could either be adsorbed on the surface of the polymer particles or remain free in the aqueous phase as monomer, homopolymer or copolymer oligomers. To investigate the chemical structure of this material, the first step was to separate it from the latex and then apply FTIR or NMR to analyze it.

The serum was collected by two means; ultracentrifugation of the latex and filtration via a serum replacement cell. For the serum decanted after ultracentrifugation, both surfactant and styrene were found from their characteristic peaks in the FTIR and NMR spectra. In the FTIR spectrum, only a small C=C peak could be seen representing unreacted TREM LF-40 (927 cm^{-1}).

This implies that most of the TREM LF-40 present in the serum is in the form of homopolymer or copolymer oligomers. However, no definite conclusion can be drawn from these results regarding the presence of the styrene peaks. This is because these peaks could be due to the presence of not only water-soluble copolymer of styrene and TREM LF-40 but also small polystyrene particles. These were confirmed by analyzing the serum by dynamic light scattering (DLS) (Nicomp Submicron Particle Sizer, Model 370), which indicated the presence of particles on the order of 30 nm in diameter. Therefore, ultracentrifugation was not a suitable method for separating the water-soluble components from the PS latex.

For the samples separated using filtration, no small particles were found in the serum phase (by DLS). FTIR spectra of the sera of the same two samples are given in Figure 1. The top figure shows that the main component in the serum phase is the surfactant, which is represented by the peak at 1052 cm^{-1}. The C=C group, indicative of unreacted TREM LF-40, can hardly be seen by the peak at 927 cm^{-1} (as compared to the spectrum of TREM LF-40 itself (not shown)), indicating that most of the TREM LF-40 had polymerized. For comparison, the spectrum of the serum extracted from the latex prepared with poly(TREM) is also given (bottom), showing a strong peak at 1052 cm^{-1} and no peak at 927 cm^{-1}. There is some trace of styrene as indicated by the peaks at 3000 – 3100 cm^{-1}; however, the amount is small. These results show that besides the chemical incorporation of TREM LF-40 into the polymer particles, TREM LF-40 forms either homopolymer (mainly) and copolymer oligomers, or remains as unreacted monomer, being adsorbed on the particles in equilibrium with that in the aqueous phase.

AFM was also used to examine the dried serum phase separated by serum replacement from the latex synthesized using 30 mM TREM LF-40 and 5 mM Na$_2$S$_2$O$_8$. No small polymer particles were noted, which agrees with the DLS data. There were some aggregates, however, representing the water-soluble components (i.e., TREM LF-40 monomer, homopolymer or copolymer oligomers of the surfactant).

Molecular Weights

As indicated above, both the reactive surfactant, TREM LF-40, and its polymeric counterpart, poly(TREM), were found to be irreversibly bound to the polymer particles in significant quantities (30 wt% – 60 wt%). TREM LF-40 is incorporated due to its ability to react (copolymerize, chain transfer) during the emulsion polymerization. As mentioned previously, grafting of styrene onto the poly(TREM) is considered at least partially responsible for its bound component. Besides this, it seems likely that there is irreversible adsorption of some of the
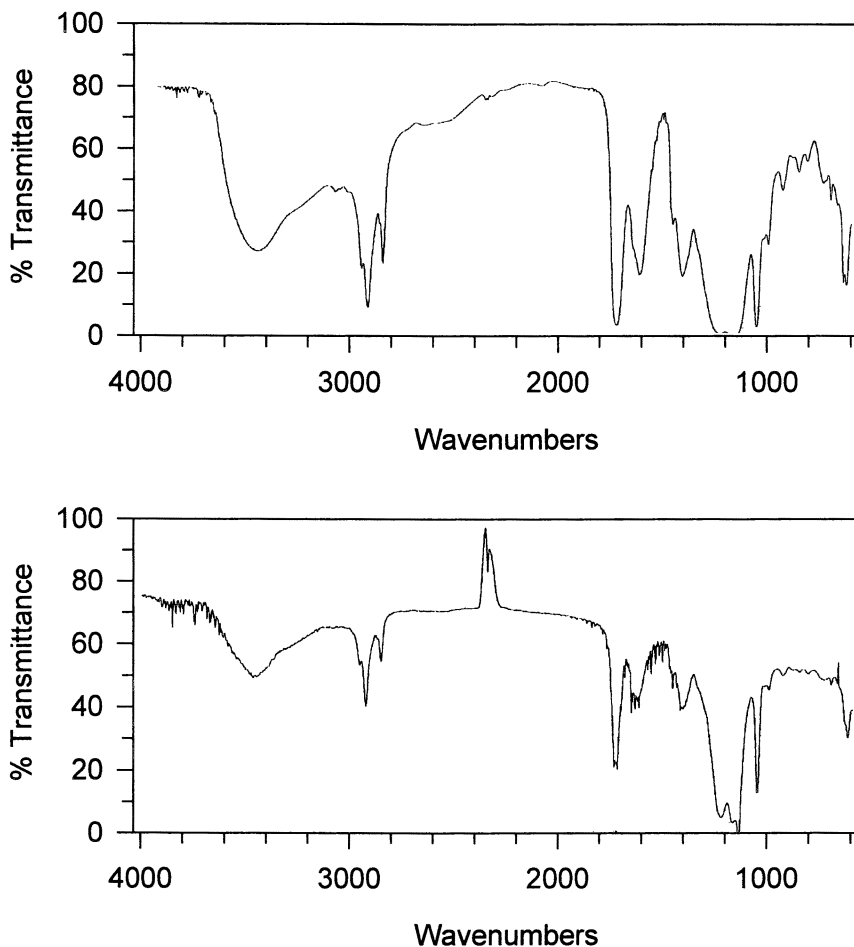
Figure 1. FTIR spectra of the serum phase of the latexes separated by serum replacement, (top) 30 mM [TREM LF-40], 5 mM [I]; (bottom) 30 mM [poly(TREM)], 5 mM [I].

polymeric surfactant (higher molecular weights) on the particle surfaces. However, during emulsion polymerization using TREM LF-40, the relative contributions of copolymerization and chain transfer to the chemical bonding of the surfactant to the particles remains unknown. It would, therefore, be of interest to determine the quantities of TREM LF-40 that are consumed by copolymerization and chain transfer, respectively. To further investigate the likelihood of these mechanisms occurring in the emulsion polymerization, the

molecular weights of some of the latexes synthesized using TREM LF-40 and poly(TREM) were measured by GPC.

First, the molecular weights and the particle sizes (or the particle numbers) of the polystyrene latexes synthesized using TREM LF-40 are compared to those prepared using poly(TREM). The results are reported in Figure 2 and Table I. Three TREM LF-40 and poly(TREM) concentrations are represented along with three initiator concentrations (4, 5, 8 mM $Na_2S_2O_8$) for TREM LF-40 and one (5 mM) for comparison used with poly(TREM). First, it can be seen that the number-average molecular weight (M_n) decreased with increasing concentration of TREM LF-40 while it increased with increasing poly(TREM). The latter is the more usual behavior in emulsion polymerization. As expected, M_n also decreased with increasing initiator concentration. In addition, higher molecular weights were obtained using TREM LF-40 compared to poly(TREM) at the same initiator and surfactant concentrations. These results can be partially explained by the smaller particle size or larger particle number (other conditions being the same) obtained with the reactive surfactant. A larger number of particles being
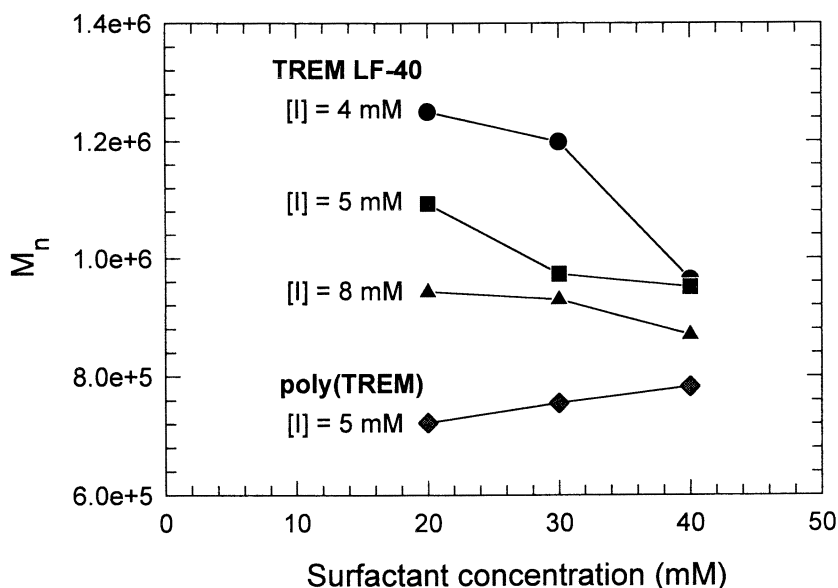
Figure 2. Number-average molecular weight of polystyrene latexes as a function of the surfactant (TREM LF-40 or poly(TREM)) and initiator concentrations; note: poly(TREM) concentration based on the monomeric TREM LF-40 molecular weight.

grown under conditions with the same radical production rate as compared to a system with a smaller number of particles, will result in a lower radical entry rate per particle, which, in turn, results in higher molecular weight chains (termination being less frequent).

From the theory of free radical polymerization, the molecular weight follows equations (1) and (2) (*15*). The Smith-Ewart theory for a classical emulsion polymerization system, such as styrene, predicts the dependencies given in equation (3):

$$\frac{1}{\overline{X}_n} = \frac{R_i}{R_p} + C_M + C_S \frac{[S]}{[M]} + C_I \frac{[I]}{[M]} \tag{1}$$

$$\frac{1}{\overline{X}_n} = \frac{k_t R_p}{k_p^2 [M]^2} + C_M + C_S \frac{[S]}{[M]} + C_I \frac{k_t R_p^2}{k_p^2 f k_d [M]^3} \tag{2}$$

$$\overline{X}_n = K[M][I]^{-0.6}[E]^{0.6} \tag{3}$$

Table I. Molecular Weight and Particle Size Data for Latexes Synthesized Using TREM LF-40 and Poly(TREM)

Latex			M_n (g/mol)	PDI	D_v (nm)	N_p (×10^{18} dm^{-3} H_2O)
Surfactant	[I] mM	[E] mM				
TREM LF-40	4 mM	20	1,250,000	2.92	88.5	1.29
		30	1,198,700	2.88	84.0	1.52
		40	963,300	3.29	81.2	1.68
TREM LF-40	5 mM	20	1,093,230	2.72	89.0	1.27
		30	973,000	2.75	84.0	1.52
		40	951,000	2.85	77.6	1.92
TREM LF-40	8 mM	20	943,200	2.73	83.1	1.57
		30	929,712	2.82	76.7	1.99
		40	870,100	3.10	73.4	2.27
Poly(TREM)	5 mM	20	722,000	2.91	96.4	1.00
		30	755,000	3.19	88.8	1.28
		40	783,000	3.03	86.9	1.37

where $\overline{X}_n$ is the average degree of polymerization, R_i is the initiation rate, R_p is the polymerization rate, C_M is the chain transfer constant to monomer, C_S is the chain transfer constant to chain transfer agent, which is TREM LF-40 in this case, [S] and [M] are the concentrations of chain transfer agent and monomer, respectively, C_I is the chain transfer constant to initiator, k_t is the termination rate constant of polymerization, k_p is the propagation rate constant, k_d is the decomposition constant of the initiator, [I] is the initiator concentration, [E] is the surfactant concentration, and K is a constant. With increasing surfactant concentration, all other conditions being constant, the latex molecular weight is, therefore, expected to increase when no chain transfer to the surfactant occurs. The resulting molecular weights of the latexes prepared using poly(TREM) (Figure 2) show the expected results. Even though grafting reactions to poly(TREM) are expected to occur during emulsion polymerization, the effect on the molecular weight of the latex is small. This is probably due to both the small amount of poly(TREM) that was used (only 1/14 the molar amount of TREM LF-40), and the incorporation of the poly(TREM) by entrapment and irreversible adsorption on the polymer particles. In contrast to these results, the latexes prepared using TREM LF-40 have a decreasing molecular weight with increasing surfactant concentration. Based on eq (3), the molecular weight is expected to increase with increasing surfactant concentration. However, if the surfactant also acts as a chain transfer agent, the molecular weight can decrease with increasing TREM LF-40 concentration. Finally, the molecular weight depends on the relative weighting of these opposing effects. Chain transfer to TREM LF-40 apparently increases with its increasing concentration and this is likely to be brought about by the increased surface area generated, which acts as the major site for the chain transfer. As would normally be expected, the molecular weight (M_n) decreased with increasing initiator concentration using TREM LF-40 as shown in Figure 2.

The dependencies of the molecular weight (M_n) on the surfactant concentration ($M_n \propto [E]^y$) were estimated for both TREM LF-40 and poly(TREM) from the above data and are summarized in Table II. The dependence for the poly(TREM) system (0.2) is much lower than the classical theory (0.6). One possible reason is the grafting reaction to poly(TREM) that occurs during the emulsion polymerization of styrene. Increased chain transfer to polymer (i.e., poly(TREM)) could cause the molecular weight to increase to a lesser extent with increasing [E] leading to the lower dependence. Another reason is the lower dependence of R_p and N_p on [E] in the emulsion polymerization of styrene ($R_p \propto [E]^{0.5}$ and $N_p \propto [E]^{0.5}$ for [I] = 5 mM) compared to the classical theory (0.6), which can lead to a lower dependence of M_n on [E]. In addition, the effect of the adsorbed polymer layer on the entry of free radicals (i.e., possible reduction) could also play a role here.

Table II. Dependencies of Molecular Weight on Surfactant Concentration
for Latexes Synthesized Using TREM LF-40 and Poly(TREM)

Reaction	Dependencies $(M_n \propto [E]^A)$
TREM LF-40 (20 – 30 mM), [I] = 4 mM	– 0.36
TREM LF-40 (20 – 30 mM), [I] = 5 mM	– 0.21
TREM LF-40 (20 – 30 mM), [I] = 8 mM	– 0.11
Poly(TREM) (20 – 30 mM), [I] = 5 mM	+ 0.20

The dependencies of M_n on [E] for the TREM LF-40 system are negative as expected. The absolute values of these dependencies decreased with increasing initiator concentration. This was attributed to the increasing role of copolymerization during the emulsion polymerization relative to chain transfer.

Film Formation and Contact Angles

Films were prepared to obtain information regarding the migration of surfactant during the film formation process. For a polystyrene (PS) latex, the film formation temperature needs to be high owing to the high T_g (104 °C). The films were, therefore, formed at 180 °C in an oven. As an alternative, the latexes were first swollen with 10% toluene (based on the polymer) to reduce the T_g and then dried at room temperature. Both methods produced clear, smooth, and continuous films.

Several latexes were cast into films: (1) cleaned PS latex (monodisperse, 92 nm, LS 1039E, Dow Chemical Co.); (2) PS latex synthesized using TREM LF-40; (3) PS latex synthesized using poly(TREM); (4) cleaned PS latex (1) blended with TREM LF-40; and (5) cleaned PS latex (1) blended with poly(TREM). If there is no surfactant migration during film formation, the film surface will be relatively hydrophobic and a water droplet will remain on the film surface with a high contact angle. However, if surfactant migration to the film surface occurs during the film formation process, the surface will be relatively hydrophilic and a water droplet will spread on the film with a low contact angle.

The results of the contact angle measurements on the various films are given in Table III. Each film has two surfaces: film/air and film/substrate (i.e., aluminum pan). The contact angles on both surfaces of the films were tested. In general, the contact angle was greater on the film/substrate surface for the films prepared at 180 °C while little difference is seen for the films prepared from the swollen latexes. In addition, the contact angles were slightly smaller when the

measurement was made after one minute of equilibration (a*) as compared to the immediate result (b*).

Table III. Contact Angles of Water on Polystyrene Latex Films

Latex	Film formed at 180 °C				Film formed from toluene-swollen latex at 25 °C			
	film/air		film/substrate		film/air		film/substrate	
	b*	a*	b*	a*	b*	a*	b*	a*
Cleaned PS	73	68	82	79	100	86	98	85
PS (TREM LF-40 30 mM)	42	41	46	45	72	65	73	64
PS + TREM (blend, 30 mM)	< 5	< 5	< 5	< 5	< 5	< 5	< 5	< 5
PS (poly(TREM))[1] 30 mM)	70	63	80	75	93	84	91	86
PS + poly(TREM)[1] (blend, 30 mM)	19	17	22	19	23	20	21	20

note: error on measurements range from ± 1° to ± 3°
b* immediate measurement
a* after one minute
[1] based on monomeric TREM LF-40; actual concentration obtained by dividing by 14

The contact angle is expected to be the largest for the film cast from the cleaned PS latex because of the absence of any surfactant. In contrast, the contact angle is expected to be the smallest for the latex synthesized using a conventional surfactant such as SLS (which would be similar to the cleaned PS latex blended with TREM LF-40), due to the surfactant migration to the surface of the film. The results in Table III are in agreement with these expectations. As a reference, a literature value of 91° is reported for the contact angle of water on polystyrene (*16*). This value is higher than that reported for the cleaned PS (73°). This is considered to be due to the initiator fragments of (SO_4^-) present on PS chains in the latex, which are hydrophilic. By comparing the contact angles of the films cast from latexes prepared using 30 mM TREM LF-40 (42°) or poly(TREM) (70°) to those where equivalent amounts were added to the cleaned PS latex, it can be seen that little surfactant migration occurred in the former as indicated by the relatively high contact angles. The high contact angle on the PS latex film synthesized using poly(TREM) can be partially explained by the high

contact angle on poly(TREM) itself (16°); while the contact angle on TREM LF-40 is very low (< 5°). The film prepared from the cleaned PS latex blended with poly(TREM) had a larger contact angle (21°) than poly(TREM), which could indicate that some of the poly(TREM) is irreversibly adsorbed on the polymer particles.

These contact angle measurements provide additional evidence of incorporation of both the reactive surfactant TREM LF-40 and poly(TREM) during the emulsion polymerizations. The results are consistent with the previous surface characterization results of the latexes (6), which showed that 30 – 60 wt% of the TREM LF-40 and 70 – 90 wt% of the poly(TREM) were permanently bound to the polymer particles. Comparing the results for the films prepared by the two methods, at 180 °C and from toluene-swollen latexes at room temperature, the latter have higher contact angles. This could be caused by some residual toluene being present in the glassy polymer film or by some surface reconstruction occurring during the film formation process whereby hydrophilic groups are oriented away from the film/air interface. Despite these differences, the trends are the same. Overall, these results provide corroborating evidence for the binding of the surfactants to latex particles and support the mechanistic explanations given for the emulsion polymerizations using reactive and polymeric surfactants as discussed elsewhere (6).

AFM

The room temperature dried latexes (opaque, white, and friable) were examined by AFM to determine any difference in surface morphology. Three different latexes were studied before and after cleaning by ion-exchange: (1) the latex synthesized using 30 mM TREM LF-40 (5 mM $Na_2S_2O_8$); (2) the latex synthesized using 30 mM poly(TREM) (5 mM $Na_2S_2O_8$), and (3) a monodisperse polystyrene latex (92 nm diameter, LS 1039E, Dow Chemical Co.). Although the specific surfactant content of the Dow latex is not known, it is expected to have been prepared using a conventional anionic surfactant. The AFM images of these latexes are shown in Figure 3. It can be seen that the Dow latex is readily cleaned of its surfactant content as no surfactant appears between the particles after ion-exchange. This was also indicated by the contact angle results. However, both latexes prepared with TREM LF-40 and poly(TREM) show that surfactant is present on their surfaces both before and after the cleaning process. This is further evidence of the irreversible incorporation of these surfactants onto the surface of the particles, whether it is by chemical reaction (copolymerization and chain transfer for TREM LF-40; grafting of poly(TREM)) or irreversible adsorption (poly(TREM-co-styrene) or poly
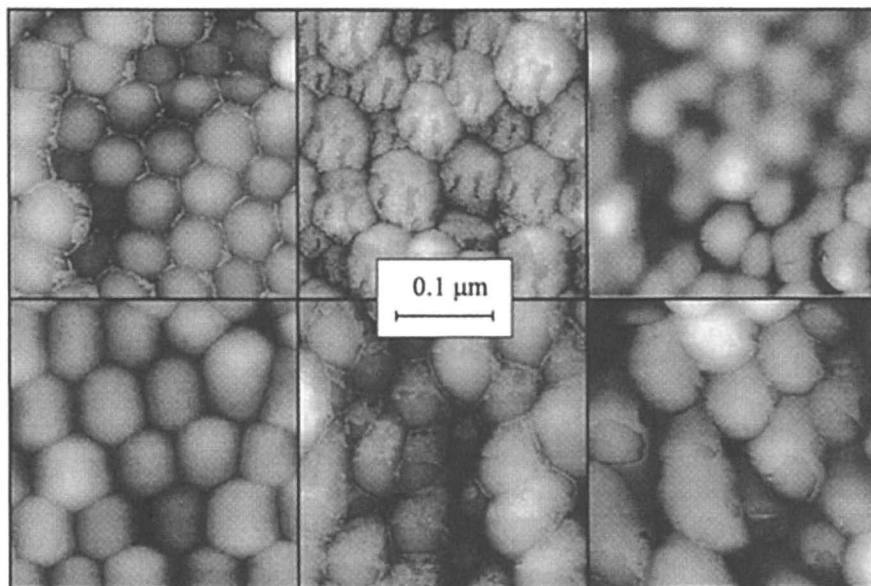
Figure 3. AFM images of: conventional polystyrene (PS) latex (left); (2) PS latex synthesized using TREM LF-40 (30 mM [E], 5 mM [I]) (middle); and (3) PS latex synthesized using poly(TREM) (30 mM [E], 5 mM [I]) (right); before (top) and after (bottom) cleaning by ion-exchange.

(TREM)). These results are consistent with all of the proceeding characterization results.

Conclusions

In the present work, additional characterization of the latexes synthesized using TREM LF-40 and poly(TREM) was performed to gain a further understanding of the emulsion polymerizations performed using these surfactants. The molecular weight of the latexes increased with increasing poly(TREM) concentration, while the molecular weight decreased with increasing TREM LF-40 concentration. This opposite behavior for TREM LF-40 is considered to be caused by the chain transfer to TREM LF-40, which is consistent with its C_S value (111×10^{-4}) (8) and the characterization of the latex in terms of the amount of chemical incorporation (30 – 60 wt%). The serum replacement method was found to be a better method to separate the serum phase from the latex particles than ultracentrifugation. The latter technique could not

separate the smallest polymer particles from the serum phase. The serum phase analysis of the latex showed it to be mainly comprised of surfactant homopolymer or copolymer oligomers containing a trace of styrene.

Both coalesced and non-coalesced films were prepared from the latexes and examined by contact angle and AFM, respectively. Contact angles showed that the film prepared from the latex containing an adsorbed-only surfactant (PS blended with TREM LF-40) had the smallest contact angle, i.e., the greatest hydrophilicity of the film surface. The film cast from the latex prepared with the reactive surfactant (TREM LF-40) had a much higher contact angle, which was still higher for the latex prepared using poly(TREM), indicating increased hydrophobicity of the film surface. AFM images showed that the conventional surfactant was found between the particles in the dried latex, and could be completely removed by ion-exchange. The reactive surfactant was found on the polymer particle surface, and much remained on the particle surface even after cleaning, indicating that it is chemically bound to the particles. The polymeric surfactant was also found on the particle surface and much remained after the cleaning process. This is attributed to grafting and/or irreversible adsorption of poly(TREM) on the particles. These studies indicate that the envisioned advantages of employing a reactive surfactant in emulsion polymerizations are achievable.

Acknowledgment

References

1. El-Aasser, M. S. In *Advances in Emulsion Polymerization and Latex Technology*, Short Course Notes, Emulsion Polymers Institute, Lehigh University, 1991.
2. Urquiola, M. B.; Dimonie, V. L.; Sudol, E. D.; El-Aasser, M. S. *J. Polym. Sci., Part A: Polym. Chem.* **1992**, *30*, 2619.
3. Urquiola, M. B.; Dimonie, V. L.; Sudol, E. D.; El-Aasser, M. S. *J. Polym. Sci., Part A: Polym. Chem.* **1992**, *30*, 2631.
4. Urquiola, M. B.; Dimonie, V. L.; Sudol, E. D.; El-Aasser, M. S. *J. Polym. Sci., Part A: Polym. Chem.* **1993**, *31*, 1403.
5. Wang, X.; Sudol, E. D.; El-Aasser, M. S. "Emulsion Polymerization Styrene Using a Reactive Surfactant and its Polymeric Counterpart: Kinetic Studies", submitted.

6. Wang, X.; Sudol, E. D.; El-Aasser, M. S. "Mechanism of Emulsion Polymerization of Styrene Using a Reactive Surfactant", submitted.
7. Wang, X.; Sudol, E. D.; El-Aasser, M. S. "Emulsion Polymerization Styrene Using the Polymeric Version of a Reactive Surfactant", submitted.
8. Wang, X. *Ph.D. Dissertation,* **2000**, Lehigh University.
9. Smith, W. V.; Ewart, R. W. *J. Chem. Phys.* **1948**, *16*, 592.
10. Varela de la Rosa, L.; Sudol, E. D.; El-Aasser, M. S.; Klein, A. *J. Polym. Sci., Part A: Polym. Chem.* **1996**, *34*, 461.
11. Varela de la Rosa, L.; Sudol, E. D.; El-Aasser, M. S.; Klein, A. *J. Polym. Sci., Part A: Polym. Chem.* **1999**, *37*, 4066.
12. Varela de la Rosa, L.; Sudol, E. D.; El-Aasser, M. S.; Klein, A. *J. Polym. Sci., Part A: Polym. Chem.* **1999**, *37*, 4073.
13. Ahmed, S. M.; El-Aasser, M. S.; Pauli, G. H.; Poehlein, G. W.; Vanderhoff, J. W. *J. Colloid Interface Sci.* **1980**, *73*(2), 388.
14. van den Hul, H. J.; Vanderhoff, J. W. *J. Electroanal. Chem.* **1972**, *37*, 161.
15. Odian, G. *Principles of Polymerization,* John Wiley & Sons, Inc., New York, 1983.
16. Shafrin, E. G. and. Zisman, W. A. *Upper Limits of Contact Angles on Solids*, N.R.L. Report 5985 (1963).

Chapter 15

Stabilization Mechanisms in Vinyl Acetate Emulsion Polymerization Stabilized by Poly(vinyl alcohol)

St. Carrà[1], L. Malcovati[2], A. Sliepcevich[2], G. Storti[3], and S. Carrà[3]

[1]Mapei SpA, Research and Development Center, Via Cafiero, 22, 20158, Milano, Italy
[2]Dipartimento di Chimica Fisica Applicata, Politecnico di Milano, Via Mancinelli 7, 20131, Milano, Italy
[3]Laboratorium für Technische Chemie, LTC, ETH Zentrum, CAB C40, Universitätstrasse 6, CH-8092, Zürich, Switzerland

Stabilization mechanisms in vinyl acetate emulsion polymerization protected by poly(vinyl alcohol) were studied by combining kinetics and rheology. A series of polymerizations was performed using different types of poly(vinyl alcohol), in order to validate a kinetic model that was then used to predict the set of microscopic properties that might determine the flow behavior of the latex. Rheology was, then interpreted by describing the dispersion as being formed by fractal aggregates of particles, generated by bridging flocculation mechanisms. Furthermore equilibrium flocculation was modeled through an analytical theory based on the Percus-Yevick solution of the sticky-hard sphere potential, where the adhesive energy between the particles and the protective colloid was used as the only adaptive parameter. An estimate of the adhesive energy was also derived from the flow curves of the dispersions, evaluating the force required for particle desegregation that is a function of the critical shear stress for shear thinning. Also an interpretation of the evolution of the

© 2002 American Chemical Society

viscosity of the system during the course of the polymerization was proposed.

Poly(vinyl alcohol) (PVA) is widely used as a protective colloid for vinyl acetate (VAc) emulsion polymerization, particularly in the production of latexes for adhesive applications, where PVA is capable of imparting desirable properties such as superior water and heat resistance, improved stability in a formulation, better high shear behavior and robust stability over long periods of time at high solids contents. PVA is also an effective viscosity builder. At the same time, PVA plays a critical role in emulsion polymerization mechanisms since it partakes in grafting reactions with VAc. PVA influences both particle nucleation and stabilization in a way that is not completely understood yet, but that certainly has a major impact on most application properties of poly(vinyl acetate) (PVAc) latexes. At the same time the effect of PVA is often scarcely controllable since its industrial grades often present wide variations in scatter of macromolecular properties, particularly stereoregularity, intermolecular distribution of acetyl content, degree of blockiness, broadness of molecular weight distribution, and frequency of long-chain and short-chain branching (*1*) This extreme variability also manifests itself in the scientific literature where it is impossible to find any agreement among researchers about the power law dependence of the rate of polymerization, R_p, and the number of particles, N_p, on the emulsifier and initiator concentration, demonstrating, if nothing else, that the effects of PVA are erratic. Experiments and theory support a homogeneous/coagulative mechanism, similar to the one suggested for ionically-stabilized systems, and a detailed description has been recently proposed (*2*). The formation of PVA pseudo-micelles and grafting onto PVA can alter the kinetics, and also radical mobility (absorption into/desorption from polymer particles) can be reduced by the formation of a thick stabilizer layer at the particle surface (*3*).

The use of a protective colloid also evidently influences stabilization mechanisms and many fundamental application properties of the latex, mostly those that have been listed as the most enticing traits of PVA-stabilized dispersions. A convenient operative strategy to approach the problem could be represented by the combination of kinetic and rheological investigations of the system. Kinetic data can be interpreted by a mechanistic detailed model also capable of predicting the set of microscopic properties that determine the flow behavior of the latex. The rheology of a latex is not only a fundamental application property by itself, but it also carries the fingerprints of the microstructure of the dispersion and of the forces acting between the particles.

Theory

Kinetic Model

In order to simulate the reaction process, we developed a mathematical model and validated it by comparison with experimental data. The kinetics of the emulsion polymerization of VAc in the presence of PVA has been analyzed by different authors (4). The model developed in the present paper can be somehow considered a simplification of the detailed model proposed by [3]. In the next paragraphs, after a short account of the main underlying assumptions, the equations of the model are briefly summarized.

Model Assumptions

(a) Supposing that no micelles are formed even at large stabilizer concentrations, a homogeneous nucleation mechanism has been considered. A polymer chain growing in the aqueous phase is considered to become insoluble above a certain critical chain length, j_{cr}. When active or terminated chains with a length larger than this critical value are formed, they aggregate to form unstable nuclei, N^*, which by subsequent coagulation could form stable, mature particles, N_p. The difference between these two particle types is in terms of stability, the nuclei being extremely unstable and forming the stable particles by coagulation. (b) The adsorption of PVA on the particle surface is effectively described as an "incorporation" of the stabilizer by the growing particle. Since a kind of polymer network is likely to be formed in aqueous solution at the PVA concentrations used in the recipes, this incorporation could be considered as an effective approach to simulate the stabilizer adsorption in this highly concentrated system. Moreover, the grafting reactions are not accounted for and it is assumed that the incorporated stabilizer is irreversibly linked to the particle surface in the form of a compact surface layer of pure PVA. (c) The quasi-steady-state assumption (QSSA) is applied to active and terminated species both in the aqueous and particle phases. Moreover, only the desorption of active radicals of unit length only is considered, *i.e.*, the monomeric radicals just formed by chain transfer to monomer. Concerning radical entry, chains of any length between 1 and j_{cr} are assumed to be captured by the particles, thus considering all chains to have enough hydrophobic character independent of their degree of polymerization. (d) The reactor is assumed perfectly mixed and isothermal.

Kinetic Scheme

A classical set of reactions is considered, including initiation by thermal decomposition of the initiating species (potassium persulfate, I_2; rate constant k_d), propagation (k_p), chain transfer to monomer (k_{fm}) and bimolecular termination (k_t). Apart from initiation, confined to the aqueous solution, all these reactions take place in both aqueous and particle phases. In addition to these standard reactions, the interphase transport by radical entry (k_e) and desorption (k_{des}) are also included, based on the following rate laws:

$$\text{entry rate}: \rho = k_c R_W^{\bullet} N_A \tag{1}$$

$$\text{desorption rate } (5): k_{des} = k_{fm} M_p \frac{K_0}{\beta K_0 + k_p M_p} \tag{2}$$

In the desorption rate law a value $\beta = 1$ was assumed, corresponding to the limit where all desorbed radicals react in the aqueous phase.

The entry rate is effectively described as a first order rate with respect to the active chain concentration in the aqueous phase, $R^{\bullet}_W$, thus neglecting any dependence on the particle size. The desorption rate proposed by Nomura (6) was used, with M_p being the monomer concentration in a particle and K_0 defined as $12 D_W / [md_p^2 (1 + 2 D_W / m D_p)]$, m being the partition coefficient of the monomer between the particle and aqueous phases, D_W and D_p the diffusion coefficients of the same species in the aqueous and particle phases.

Constitutive Equations. The material balances of the various species are reported below separately for each phase.

Aqueous Solution.

Initiator and Initiating Radicals:

$$\frac{dI_2}{dt} = -k_d I_2 ; \qquad I^{\bullet} = \frac{2 f k_d I_2}{k_p M_W} \tag{3}$$

Active and terminated chains:

$$R^{\bullet}_{W,1} = \frac{k_p M_W I^{\bullet} + k_{des} \bar{n} N_p / N_A}{k_p M_W + k_t R^{\bullet} + k_c N_p} \tag{4}$$

$$R_{W,n}^{\bullet} = \left(\frac{k_p M_W}{k_p M_W + k_t R_W^{\bullet} + k_e N_p} \right)^{n-1} R_{W,1}^{\bullet} \quad (1 < n < j_{cr}) \tag{5}$$

$$P_{W,n} = \frac{k_t \sum_{i=1}^{N} R_{W,i}^{\bullet} R_{W,n-i}^{\bullet}}{k_e N_p} \qquad (N = n/2 \text{ or } (n-1)/2) \tag{6}$$

where $R_{W,n}^{\bullet}$ and $P_{W,p}$ indicate the concentrations of active and terminated chains of length n, respectively, f the initiator efficiency, M_W the monomer concentration in aqueous phase, $I^{\bullet}$ the concentration of the initiating radicals, $\bar{n}$ the average number of active chains per particle and N_p the particle concentration. Using the previous expressions, the rate of nuclei formation, Rn, is evaluated as:

$$Rn = k_p M_W R_{W,J_{cr}-1}^{\bullet} + k_t \sum_{i=1}^{j_{cr}-1} \sum_{n=j_{cr}-1}^{i} R_{W,i}^{\bullet} R_{W,n}^{\bullet} \quad (i = j_{cr}/2 \text{ or } (j_{cr}+1)/2) \tag{7}$$

Polymer Particles

Nuclei and Particle Number

$$\frac{dN^*}{dt} = Rn\, N_A - \beta_1 N^{*2} - \frac{\beta_2}{2} N^* N_p; \qquad \frac{dN_p}{dt} = \frac{\beta_2}{2} N_p^2 \tag{8}$$

where the coagulation coefficients between two nuclei β_1, and between a nucleus and a particle, β_2, are evaluated using the well-known Smoluchowsky expression:

$$\beta_1 = \frac{8}{3}\left(\frac{kT}{W_1 \eta} \right); \qquad \beta_2 = \frac{2}{3}\left(\frac{kT}{W_2 \eta} \right)(r^* + r_p)\left(\frac{1}{r^*} + \frac{1}{r_p} \right) \tag{9}$$

where W_i is the so-called Fuchs stability ratio (a value of one indicates no barrier to interparticle coagulation, whose rate becomes diffusion limited), η indicates the viscosity of the suspending medium, and r^*, r_p the radii of a nucleus and a particle respectively.

Polymer Volume

$$\frac{dV_{pol}}{dt} = k_p M_p \frac{\bar{n} N_p}{N_A} \frac{MW_m}{\rho_p} \tag{10}$$

MW_m being the molecular weight of the monomer and ρ_p and density of the polymer. From the polymer volume, the overall particle volume is readily evaluated as $V_p = V_{pol}/(1-\phi_m)$, where ϕ_m is the volume fraction of the monomer inside the particles, defined as $M_p MW_m / \rho_m$, with ρ_m being the density of the monomer. From these values, the particle size is readily estimated assuming spherical shape. The monomer partitioning between the aqueous and particle phase is described in terms of oversimplified, linear laws, with the corresponding partition coefficient, m, equal to the ratio between the monomer solubility in the aqueous phase, M^*_W, and that in the polymer phase, M^*_p. Note that equilibrium conditions are always assumed all along the reaction, thus neglecting any mass transport resistance for the monomer. The calculation of the growth rate of the particles by equation (10) requires the average number of active chains that was calculated from the analytical solution of the steady-state equations of Smith and Ewart (7).

Poly(vinyl alcohol) distribution. According to the model assumption (b), the amount of stabilizer in the particle surface layer, A_p is calculated associating the following two equations

$$A_{tot} = A_0 = A_W V_W + A_p V_p \qquad A_p V_p = A^* S_p \delta = \int_0^{V_p} A_W dV_p \tag{11}$$

where A_i indicates the PVA concentration in phase i and A^* is the concentration of the alcohol in the surface layer (assumed equal to the molar density of the pure component) and δ the corresponding thickness.

Rheology

In general, a successful emulsion polymerization is subordinate to an effective stabilization of colloidal-sized particles in a continuous phase. The emulsifier adsorbs onto the surface of the particles to form a layer that prevents coagulation. Stabilization through a protective colloid clearly requires a good solvent for the stabilizer and a repulsion of sufficiently long range to mask the dispersion forces, *i.e.*, a minimum layer thickness. The most effective polymeric stabilizers are amphipathic block, comb or graft copolymers (8). Random

copolymers are usually less effective stabilizers than block copolymers. Direct grafting to the particle is particularly effective but it requires a chemistry specific to the particle; PVA is particularly suited to the emulsion polymerization of vinyl acetate since both the stabilizer and the latex particles contain pVAc. PVA usually used in emulsion polymerization recipes is partially hydrolyzed, with an 82% degree of hydrolysis, but its degree of blockiness might vary. Hydrophobic pVAc blocks anchor the polymer onto the particle surface, while hydrophilic PVA blocks impart steric stability. Extensive evidence supports grafting as a primary mean of attachment in PVA-stabilized emulsion polymerization, but adsorption can also be important. A lattice model provides the basic picture to predict layer structures of adsorbed polymers (9, 10) and forces and potentials between surfaces (11, 12, 13). According to this approach surfaces sparsely loaded with adsorbing polymer in a theta solvent at restricted equilibrium potentials exhibit an attraction that begins near $2R_g$, reaching a minimum at $0.5R_g$, where R_g is the radius of gyration of the polymer. This case roughly corresponds to irreversible bridging that occurs when colloidal particles covered with adsorbed polymer layers are added to a suspension consisting of uncovered particles, inducing flocculation through the long loops extending from the covered to the bare particles (14). If more polymer is added to the surface, the attractive minimum diminishes and becomes longer range, until the interaction becomes purely repulsive. This case corresponds to what is called steric stabilization. At extremely high surface coverage, adsorption sites are scarce and hydrophobic groups extend into the water phase. Under these conditions bridging can occur through the lateral interactions between the hydrophobic groups (or blocks) extending from different particles in order to reduce the surface energy (15).

The nature and type of interparticle potentials depend on the thermodynamic interactions among three constituents, polymer, solvent and the particle surface. All three interaction regimes are possible in principle in PVA-stabilized latexes, depending on a series of factors, particularly: (1) the latex solids content; (2) pVAc particle size and particle size distribution; (3) the molecular characteristics of PVA; (4) the total quantity of PVA used in the recipe, its grafted, adsorbed fractions and the amount that remains free in the water phase; and (5) temperature.

Although the forces between particles are attractive in the first and third regime, the lifetime of a particle bond is very different in the two cases. In bridging flocculation induced by polymer adsorption, polymer bridges are not broken down by thermal energy, while associations between hydrophobic groups in the water phase are constantly forming, breaking, and reforming in a quiescent state causing a reversible flocculation that may well be an equilibrium phenomenon. A detailed and direct investigation of the nature and magnitude of interaction mechanisms in PVA-stabilized emulsion polymerization is extremely

difficult given the multiplicity of factors that influence them and the quantity of sources of uncertainty that might affect them. Most methods for latex characterization can offer information on the nature of the particles and of the polymers they are made of, but they do not provide us with any direct appreciation about the way particles interact. In these conditions it is probably wise to infer the fluid structure and interaction mechanisms from rheological measurements, rather than the other way around.

The rheological behavior of polymerically-stabilized dispersions has been the subject of much interest and work in recent years and in fact the literature abounds with examples displaying a phenomenology that is often unusual and complex. In general the shear viscosity of a polymer colloid depends on hydrodynamic, Brownian, and direct particle interactions. A grafted layer of thickness δ increases the effective size of a colloidal particle. In a purely steric regime these dispersions behave as non-Newtonian fluids with low and high-shear limiting relative viscosities η_0 and η_∞, and a dimensionless critical shear stress equal to $r_p \sigma_c / kT$, σ_c being the shear stress at which thinning arises that depends on the effective volume fraction $\phi_{\text{eff}} = \left(1 + \delta/r_p\right)^3 \phi$. The flow behavior of flocculated suspensions shows more peculiar and diverse characteristics. For attractions that are not too strong, the dispersion remains a fluid at rest and exhibits a steady shear viscosity with low and high shear Newtonian plateaus. The former increases exponentially with the strength of attraction (*16*), while the latter remains comparable to that of hard spheres. The normalized viscosity (*η/η_0*) superimpose if plotted against the shear stress σ scaled on the strength ε and the range Δ of the interparticle attraction for particles of radius r_p as $r_p^2 \Delta \sigma / \varepsilon$ (*17*). Otsubo obtained a significant mass of experimental results on flocculating systems in the three regimes (*18*).

The mechanisms of floc growth has attracted much interest in recent years. Experimental studies by light scattering (*19*) show that the radius a_S of a cluster containing S particles scales as a power law with S: $a_S/a \approx S^{1/D}$. Growth has been explained in terms of diffusion and sticking. Because of wide variation in the kinetics, the geometrical aspect of the flocs is very complicated. Many numerical simulations and experiments suggest that aggregates behave as fractals on a scale larger than the primary particle size (*20*). The development of predictive models of dispersion microstructure is a challenging issue, but qualitative trends have been identified (*21*): (i) the thermodynamic tendency to flocculate depends on the solvent-particle and particle-particle interactions; (*ii*) aggregates growing far from equilibrium satisfy the "diffusion-limited" model that generates open fractal structures. On the other side, if particle sticking is not irreversible, instead, flocs develop into more compact structures, compatible with the "reaction-limited" model. The structure of fractals is defined in terms of

a fractal dimension, D, typically in the range of 2.0 - 2.2 for the "reaction-limited" model, and close to 1.75 for the "diffusion-limited" model; (*iii*) flocs disintegrate into their component particles under shear flow when the shear stress σ is sufficiently large (*22*). The value of this critical shear stress reflects the magnitude of the attractive interparticle energy. This leads to a strong shear-thinning behavior. Vice versa flocs can form at low shear due to increased collision frequency between the particles, leading to shear thickening. Flocs may or may not reform after the external perturbation is removed. The breakdown of flocs held together by weak interparticle forces is usually more reversible than the destruction of flocs held together by strong attractions; (*iv*) As a floc grows its porosity increases and the volume fraction of solids in a floc, ϕ_S, containing S particles decreases with increasing S: $\phi_S = \left(a_S/a\right)^{D-3} = S^{(D-3)/D}$. The volume fraction of solution flocs encompass hence increases. Once the volume fraction occupied by the flocs fills the entire system, the flocs connect together to form a percolating network. This corresponds to gelation and it occurs when the floc size S reaches a value S^* such that the volume fraction in the floc equals the volume fraction of particles in solution, corresponding to the condition: $S^* = \phi^{-D/(3-D)}$.

Several authors have recently proposed microrheological models accounting for fractal aggregation. Many have suggested use of a universal expression for the relative viscosity, η_r, as a function of ϕ, the solid volume fraction, and ϕ^*, the critical volume fraction relative to the transition threshold between the fluid and the solid state. This can be extended to aggregated dispersions simply assuming for ϕ^* the maximum packing fraction of cluster, that varies with the solid volume fraction. Bicerano et al. (*21*) proposed the following general expression for dispersion viscosity:

$$\eta_r = \frac{\eta(\phi,\sigma)}{\eta_c} = \left(1 - \frac{\phi}{\phi^*}\right)^{-2}\left[1 - 0.4\left(\frac{\phi}{\phi^*}\right) + 0.34\left(\frac{\phi}{\phi^*}\right)^2\right] \qquad (12)$$

and showed that the effects of fractal aggregation can be incorporated in equation (12) if the reducing volume fraction variable ϕ^* is modified appropriately in order to account for the effectiveness of the aggregate to screen its interior from hydrodynamic interactions. Russel and Sperry (*23*) proposed a value for ϕ^* equal to $\phi_{mp}S^{1-(3/D)}$ where ϕ_{mp} is the maximum packing fraction in the absence of aggregation (typically 0.64 for monodisperse spheres). Aggregates with a radius above the maximum stable size are destroyed by shear stresses, breaking up into approximately equal parts or individual particles are split off small clusters one by one. The radius and shape of particles, the energy

of links and both the type and strength of flow influence cluster break-up (24) Experimental work (25, 26) and computer simulations (27) suggest that the equilibrium radius $R_F(\sigma)$ of an isolated fractal cluster decreases with increasing shear stress, τ, in the form of a power law without dependence on the mean particle density in the aggregate as $R_F(\sigma)/r_p \approx 1+(\sigma*/\sigma)^m$, where the value of the exponent m depends mainly on the reversibility of cluster deformation under the action of external stresses, while the characteristic shear stress, $\sigma*$, can be related to the surface adhesive energy, Γ, since $\sigma* = \Gamma/r_p$

One of the simplest ways of modeling flocculation and network formation in a colloidal dispersion containing polymer is to schematize it as a binary mixture of large spheres, representing the colloidal particles, and small spheres, representing polymer molecules (28). This system can be described employing an analytical theory based on a reliable statistical description of the liquid state such as the Percus-Yevick solution of the so-called "sticky-hard sphere" model. Considering a binary system consisting of a mixture of large particles of diameter d_A and small spheres of diameter d_B and assuming that the "like" interactions A-A and B-B follow the simple hard-potential form:

$$u_{ii}(r) = \begin{cases} \infty & (r \leq d_i) \\ 0 & (r > d_i) \end{cases} \tag{13}$$

while the "unlike" pairs A-B interact through a sticky hard-sphere potential:

$$\exp[u_{AB}/kT] = \begin{cases} (d_{AB}/12\tau_{AB})\delta(r - d_{AB}) & r \leq d_{AB} \\ 1 & r > d_{AB} \end{cases} \tag{14}$$

where k is the Boltzmann's constant, T is the temperature, δ is the Dirac delta function, $d_{AB} = (d_A + d_B)/2$ is the unlike hard-sphere diameter, and τ_{AB} is a parameter whose reciprocal is a measure of the strength of the stickiness of the A-B interaction. This schematization will allow us to describe the formation of clusters of particles by bridging induced by PVA, where the strength of sticking is an effect of the interaction caused by grafting/adsorption of PVA on polymer particles. Since the objective here is to describe "reversible bridging", where hydrophobic groups from the polymer chains associate in the water phase to flocculate the particles, a model accounting also for B-B physical association would better capture the physics of the phenomenon, but its analytical solution would be much more complicated. In any case it is the A-B interaction that is discriminating for the formation of the bridge and that characterizes the

specificity of the alcohol and of the reaction since it is a function of complex adsorption phenomena that are both physical and chemical in nature.

Based on the solution of the Percus-Yevick integral for the system described by equations (13) and (14), an expression for the average cluster size S has been derived:

$$S = \left[x_A(1 + \phi_B \lambda_{AB} d_A d_B^{-3} d_{AB}^2)^2 + x_B(1 + \phi_A \lambda_{AB} d_B d_A^{-3} d_{AB}^2)^2 \right] / D^2 \tag{15}$$

where

$$D = 1 - \phi_A \phi_B (\lambda_{AB} d_{AB}^2 / d_A d_B)^2 \tag{16}$$

x_A and x_B are the mole fractions of A and B, while ϕ_A and ϕ_B are the volume fractions defined by $\phi_i = \pi \rho_i d_i^3 / 6$ where ρ_i is the number density of species i. The coefficient λ_{AB} is related to τ_{AB} by:

$$\lambda_{AB} = \frac{K_1}{\tau_{AB} + K_2} \tag{17}$$

where:

$$K_1 = \frac{1}{(1-\phi)} + \frac{3\xi d_A d_B}{2(1-\phi)^2 d_{AB}}; \qquad K_2 = \frac{\xi d_{AB}}{2(1-\phi)}$$

$$\xi = \frac{\phi_A}{d_A} + \frac{\phi_B}{d_B}; \qquad \phi = \phi_A + \phi_B \tag{18}$$

The theory described by equations (15)-(18) has been used in the literature to model clustering and gelation in binary systems (29). An important result resides in the circumstance that weak attractions can also lead to the formation of network structures (28).

Experimental

A series of pVAc latexes was synthesized via PVA-stabilized emulsion polymerization with different recipes and characterized by measuring conversion, particle size, free PVA content, and viscosity. Latexes were

produced in a batch process, in a 3 liter glass reactor, equipped with stirrer, reflux condenser, sampling device and inlet systems for nitrogen and reactants. The reactor was operated automatically, using in-house developed software. PVA solutions, prepared the day before the polymerization, were charged into the reactor and heated up to the polymerization temperature. The reactor was then purged for some time with N_2 to eliminate O_2. Afterwards, the monomer and the initiator solution were fed to start the polymerization. The polymerization recipe was: 1800 g of water, 0.5 g of potassium persulfate, 100 to 240 g of VAc, 48 to 120 g of PVA, a temperature of 60 °C and a reaction time between 1.5 and 4 hours. The monomer manufactured by BP, was used as received. Different commercial types of PVA were employed in order to verify and study their effects on the rheological behavior of the latex. In this paper we, will refer to the results obtained using three different types of PVAs, all with a degree of hydrolysis equal to 88%: Airvol 823, manufactured by Air Products, with a molecular weight around 72,000 g/mol; Erkol, same characteristics as Airvol; Fluka 100 that, unlike the first two, is a laboratory reactant, not used for industrial reactions, and has a higher molecular weight, around 100,000 g/mol. An index of blockiness of the various PVAs was determined by colorimetry of the complex formed with iodine. Samples were prepared by mixing 3 mL of a 1% by weight PVA solution, 6 ml of a N/1000 I_2 solution and 21 ml of distilled water. At the same time a reference was prepared by mixing 6 ml of the same I_2 and 24 ml of distilled water. The absorbance of the sample was then measured at 490 nm on a JASCO 7800 spectrophotometer. The absorbance measured in this way is also called the "iodine index", and it increases with blockiness, and it was higher for Erkol, equal to 1.04, than for Fluka (0.559) and Airvol (0.509).

The amounts of free PVA in the final latex, the fraction of PVA that was not adsorbed onto the polymer particles and was still free in the water phase, were measured by colorimetry of the complex with boric acid and iodine. Prior to the analysis, a reference adsorbance/concentration curve had been constructed by preparing solutions at different PVA contents. Latex samples were ultracentrifuged in order to separate the particles from the serum. The particles take with them the adsorbed PVA, while the free fraction remains in the water phase. The adsorbance of the serum is then measured and compared to the values reported on the reference curve to estimate the amount of free PVA.

Particle size of the latexes was measured by light scattering, using a Coulter N4. Viscosity measurements were performed both on a Haake Viscotester VT5, using a type R spindle, and on a stress-controlled rheometer by Rheometrics, with a cone and plate set up, applying shear rates between 0.025 and 10^3 s^{-1}.

Adsorbed layer thickness, δ, was determined estimating the difference between hydrodynamic radii of PVA-coated and bare pVAc particles. Coated particles were produced by PVA adsorption onto bare particles, performed by equilibrating dilute mixtures of polymer and latex overnight. Bare particles were

obtained by producing monodisperse pVAc latexes by sodium lauryl sulfate-stabilized emulsion polymerization and then cleaning the latex by dialysis.

During the course of the polymerization on-line measurements of the torque on the stirrer motor were acquired, providing indications on the variations of viscosity in the emulsion over the course of the reaction. Often the viscosity, η, is assumed proportional to the torque T as $T = k\eta\omega$. k is a characteristic constant of the stirrer and ω is the radial velocity, but this, in principle, is a crude approximation since it neglects second-order hydrodynamic interactions and the fact that the fluid is actually heavily perturbed by the action of the stirrer, and does not even maintain a flat surface. However, a calibration performed on different aqueous solutions of PVA confirmed that the linear approximation is acceptable. The obvious, and important, limitation when polymerizations are performed resides in the fact that latexes, unlike PVA solutions, are heavily non-Newtonian. For this reason, torque measurements can only provide an indication on the flow characteristics of emulsions over the course of the polymerization.

Results

Kinetic Model

The validation of the kinetic model was performed by comparing predictions and experiments for a large set of batch reactions in the range of recipes described in the last section, using the three PVAs. A huge number of physico-chemical parameters is involved. To assure a modeling tool with reasonable reliability, a special effort was made to evaluate most of the parameters independently, while minimizing the number of those evaluated by fitting the reaction experiments. The values of most model parameters are summarized in Table I, along with the corresponding literature source. Only two have been evaluated by fitting, the Fuchs' stability ratios W_1 and W_2, whose values are reported in Table II. The same values were obtained for Airvol and Fluka, but a considerable variation was necessary to simulate Erkol-stabilized polymerizations.

A data-simulation comparison is shown in Figure 1 for a recipe with 240 g of VAc and 48 g of PVA Airvol, in terms of conversion and particle diameter, showing a good agreement. In particular, the continuous growth in particle number is well described, thanks to the homogeneous nucleation mechanism, which remains operative all along the polymerization. It is also worth mentioning that the calculated $\bar{n}$ remains well below 0.5 for most of the reaction, due to the relevance of desorption in VAc emulsion polymerization. A satisfactory agreement between theory and experiments was also found for Airvol and Erkol-stabilized polymerizations, although the results are not shown here for the sake of brevity. As reported in Table II, the values of the adaptive parameters W_1 and W_2 had to be changed significantly in order to simulate the polymerizations stabilized by PVA Erkol. This seems to indicate that this stabilizer is much less

Table I. Model Parameters and their Literature Sources

Parameter	Numeric Value	Ref.
k_p (propagation constant)	3.53×10^5 [l/mol/s]	(30)
k_{fm} (chain transfer to monomer)	2.1 [l/mol/s]	(31)
k_t (termination)	9.37×10^7 [l/mol/s]	(32)
k_i (initiation $K_2S_2O_8$)	5.35×10^{-6} [1/s]	(33)
k_e (entry)	2×10^{-16} [1/s]	(34)
D_p (particle diffusion)	1×10^{-7} [cm^2/s]	(32)
D_w (water diffusion)	1.86×10^{-6} [cm^2/s]	(35)
A_p^* (saturation solubility in the particle)	8.95 [mol/l]	(35)
A_w^* (saturation solubility in water)	0.33 [mol/l]	(35)

Table II. Values Assumed for the Adaptive Parameters W_1 and W_2

Parameter	Airvol	Erkol	Fluka
W_1	6 E+09	6 E+13	2.5 E+11
W_2	2 E+06	6.25 E+06	2.E+06

effective in particle nucleation as indicated by the smaller values of the coagulation rate constants that could be ascribed to a low homogeneity of this PVA, resulting in a smaller water solubility and reduced emulsifier action.

Rheology

We measured the latex viscosity at the end of every reaction. Figure 2 displays data for a series of polymerizations performed with constant amount and type of PVA (72 g of Airvol) and increasing amounts of VAc, reported as a function of the solid volume fraction, calculated from the final conversion.

The graph shows that, even though the average particle diameter remains relatively constant in the different reactions, the relative viscosity increases very much with increasing solids content. As a reference, we report in the graph also the theoretical curve calculated using the classical hard-sphere equation as developed by Batchelor (36), $\eta = \eta_c \left(1 + 2.5\phi_{eff} + 6.2\phi_{eff}^2\right)$, that describes sufficiently well the rheological behavior of "sterically-stabilized" particles, with a sufficiently thin ($\delta << d$) surface layer (37), that predicts viscosity much lower than those actually measured, hence demonstrating that, in PVA-stabilized latexes, rhelogical behaviour is completely different from that of suspensions of hard-spheres. In these calculations, and in those that will follow, the viscosity of the continuous phase, η_c, was estimated using an empirical equation $\eta_c = \eta_{H_2O}(T)\exp(A\phi_{PVA})$, derived performing viscosity measurements on PVA solutions. A is essentially a function only of the molecular weight of PVA. The volume fraction of PVA, φ_{PVA}, was calculated from the moles of free PVA, A_w, as estimated by the model in equation (11), being $\phi_{PVA} = A_w/\bar{\rho}_{PVA}$.

Figure 3 shows, for latexes stabilized by Erkol and Airvol, a graph where S, the average cluster dimension, is represented as a function of ϕ_{PVA}. Experimental data have been estimated using equation (12) on the basis of experimental viscosity measurements, using a value of D equal to 2, a hypothesis justified by the fact that flocs here are probably reversible and their growth is of the "reaction limited" type. Continuous curves are calculated using equations (15)-(18), taking for d_A the average particle diameteras calculated from the kinetic model, and for d_B the radius of gyration of PVA as estimated from solution viscosity ($d_A \cong 6d_B$ for Erkol, $d_A \cong 5d_B$ for Airvol). The only adaptive parameter in these calculations is $(\tau_{AB})^{-1}$ assumed equal to 2 for Erkol and to 2.5 for Airvol. The sticky hard sphere potential is attractive at extremely short range that can be corrected introducing a square-well potential defining a square well width W and a square well depth ε. In this case it is (29): $\tau_{AB}^{-1} = 4\left\{1 - \left[W^3 - (W^3 - 1)\exp(\varepsilon/kT)\right]\right\}$.

Assuming $W = 1.1$, one calculates $\varepsilon \approx kT$ for both Airvol and Erkol.
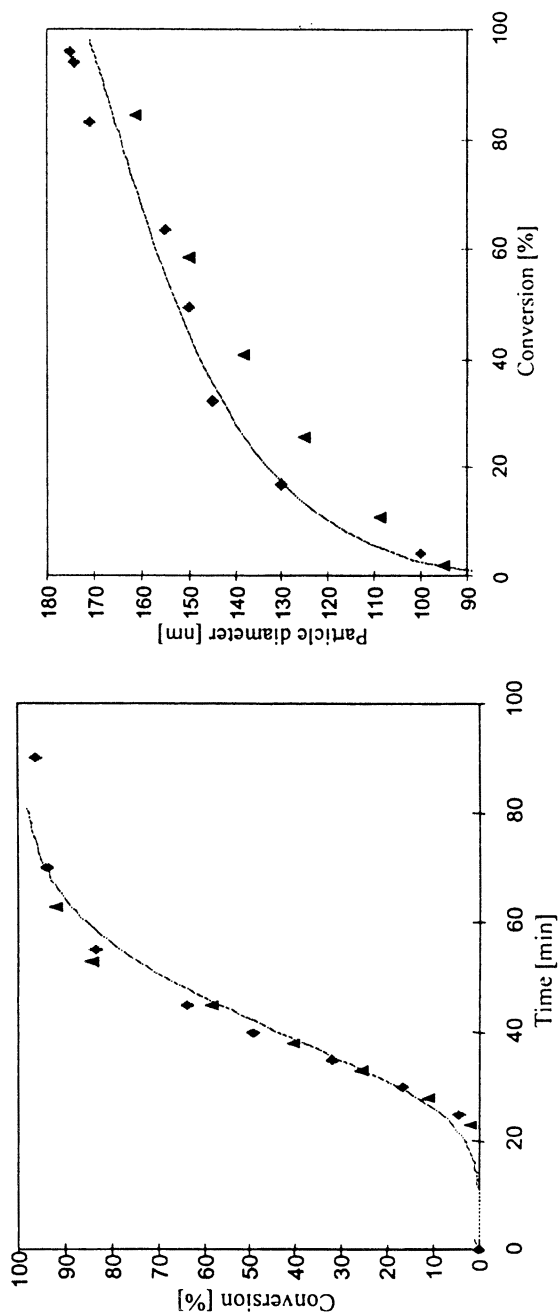
Figure 1. Data-simulations comparison in terms of conversion and particle diameter vs. time for a batch reaction employing 48 g of Airvol and 240 g of VAc.
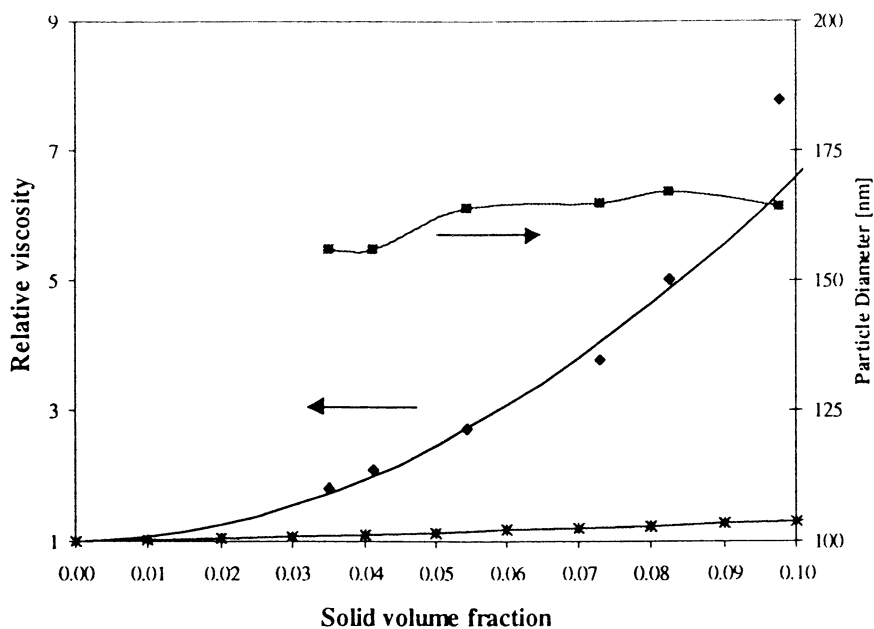
Figure 2. Relative viscosity and average particle diameter vs. solid volume fraction for a series of latexes produced with constant concentration and type of PVA (72 g of Airvol). The figure also shows (*) hard-sphere relative viscosity.
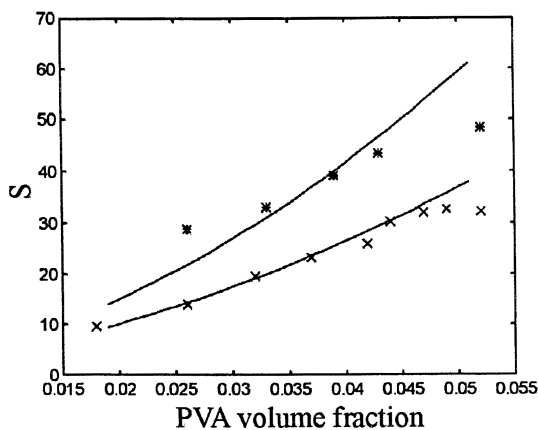
*Figure 3. S vs. PVA volume fraction for the series of polymerizations: (*)
stabilized by Erkol, (×) stabilized by Airvol 823.*
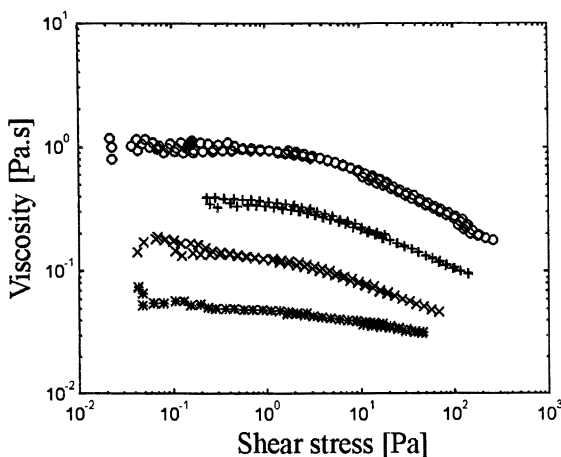
*Figure 4. Rheograms (η vs. σ) for a series of latexes stabilized by Airvol;
(*) = 120 g of VAc, 72 g of PVA; (×) = 240/72, (+) = 240/96,(○) = 240/120.*

Figure 4 shows the rheograms (η vs. σ) for a series of latexes stabilized by Airvol. The samples always display a Newtonian plateau followed by a shear-thinning region (unfortunately we have not been able yet to verify the existence of a high-shear plateau, η_∞). The critical shear stress is approximately constant in the different latexes (around 1 - 2 Pa) from which it is possible to estimate a $\Gamma \cong 5 \times 10^{-8}$ N/m, that corresponds again to an energy on the order of kT.

A last problem tackled in this paper consists of the prediction of the variation of the viscosity of the latex over the course of the polymerization. As explained in the experimental section, only a rough indication of the viscosity during the process is available, through torque measurements. A typical torque vs. time curve is shown in **Figure 5** for a polymerization stabilized by 100 g of PVA Fluka, where also three values of viscosity measured off-line on samples withdrawn from the reactor are reported.

A prediction of viscosity vs. time can be attempted by using the kinetic and rheological models together. In particular, Dickinson's model (15)-(18) can be used to predict S at intermediate conversions adopting the values of ϕ_A, ϕ_B, x_A, x_B predicted by the kinetic model as a function of time. Figure 6 shows the predictions obtained in this way for three reactions with different quantities of Airvol. Indeed, a peak at the end of Interval II is forecast, due in this case to the effect of the swollen particle diameter. The model is very sensitive to the particle diameter, and in fact it even overestimates the peak, since values of S above ca. 60 surpass the gelation threshold that corresponds to the occurence of a yield stress, a circumstance that is not likely at such low solid contents.

Conclusions

An approach combining kinetic and rheological modeling was proven useful to understand and interpret stabilization mechanisms in VAc emulsion polymerization stabilized by PVA. The kinetic model was capable of predicting vs. time the fundamental microstructural properties of the latex, particularly the evolution of the average particle diameter, the partition of PVA among the adsorbed/grafted and the "free" fraction. These properties can be used in a model describing the flow behavior of the dispersion. Stabilization mechanisms play a crucial role here, since they determine interparticle potentials that, in these systems, depend on the thermodynamic interactions among solvent, protective colloid, and particle surface. Describing the dispersion as reversibly flocculated by bridging, an hypothesis compatible with the relative concentrations of particles and polymer, we combined an expression for the shear viscosity of a flocculated system with an analytical theory based on a reliable schematization of the liquid state to obtain a model that is a function of the solids content, of the polymer volume fraction, of the average particle diameter, and of the radius of gyration of the polymer, and that contains a single adaptive parameter, indicative
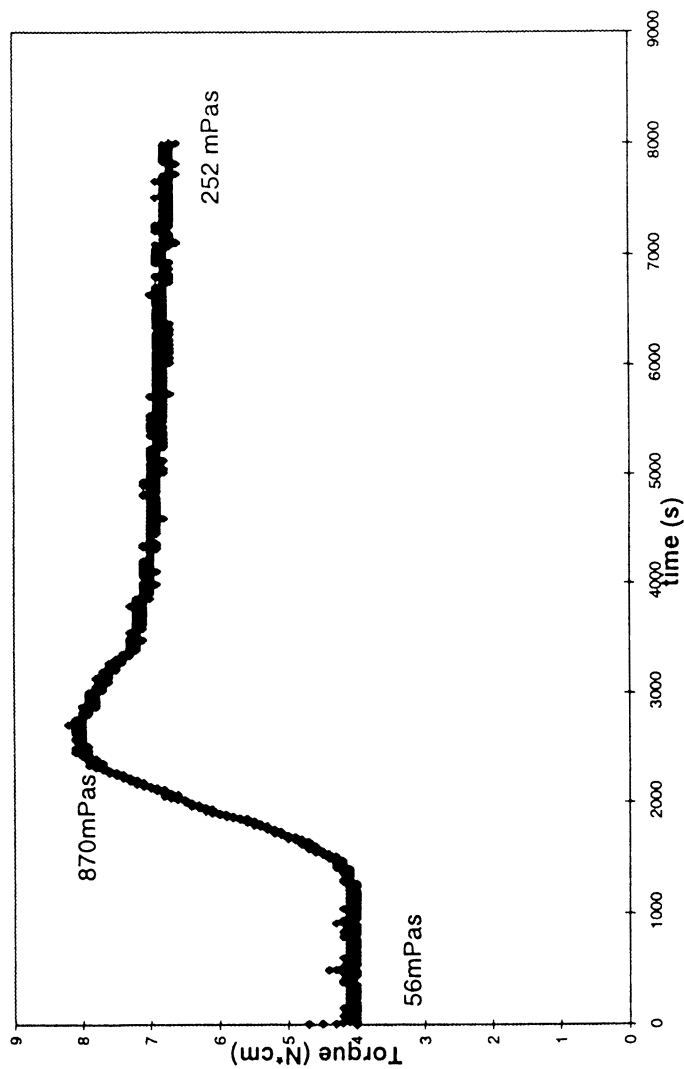
Figure 5. Torque vs. time for a polymerization with 100 g of Fluka PVA. The graph also reports three off-line viscosity values measured on samples withdrawn from the reactor.
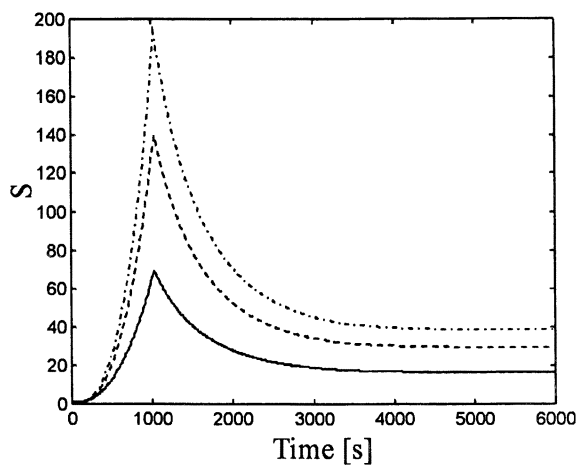
Figure 6. Predicted average cluster size vs. time for three different quantities of PVA Airvol (-) = 40 g, (- -) = 60 g, (• –) = 72 g.

of the strength of the interaction between the polymer and the particle. The interpretation was further verified from the flow curves of the latex that provide another means to evaluate the energy content of the interactions in flocculated systems. The model was also proved to be capable of predicting, at least qualitatively, the typical behavior of viscosity *vs.* over the course of emulsion polymerization that always displays a maximum at intermediate conversions.

References

1. Dunn, A. S. in *11ᵗʰ Annual Short Course Notes: Advances in Emulsion Polymerization and Latex Technology, Vol II,* El-Aasser, M. S., Ed.; Emulsion Polymers Institute, Lehigh University, 1980.
2. Budhlall, B. M. *Ph.D. Dissertation,* Lehigh University, Bethlehem, PA, 1999.
3. Gilmore, C. M.; Poehlein, G. W.; Schork, F. J. *J. Appl. Polym. Sci.,* **1993,** *48,* 1449.
4. Moritz, H. -U.; Taylor T. W.; Reichert K. -H. *Polymer Material Science and Engineering,* **1985,** *53,* 524.
5. Asua, J. M.; Sudol, E. D.; El-Aasser, M. S. *J. Polym. Sci.: Part A: Polym. Chem,* **1989,** *27,* 3303.
6. Nomura, N. in *Emulsion Polymerization,* Piirma, I., Ed.; Academic Press, New York, NY, 1982, 191.
7. Smith, W. V ; Ewart, R. W. *J. Chem. Phys.,* **1948,** *16,* 592.
8. Napper, D. H. *Polymeric Stabilization of Colloidal Dispersions,* Academic Press, New York, NY, 1983.
9. Schutjens, J. M. H. M. ; Fleer, G. J. *J. Phys. Chem,* **1979,** *83,* 1619.
10. Schutjens, J. M. H. M. ; Fleer, G. J. *J. Phys. Chem,* **1980,** *84,* 178.
11. Fleer, G. J.; Schutjens, J. M. H. M. *J. Colloid Interface Sci.,* **1982,** *86,* 361.
12. Schutjens, J. M. H. M. ; Fleer, G. J. *Macromolecules,* **1985,** *18,* 1882.
13. Fleer, G. J.; Schutjens, J. M. H. M. *J. Colloid Interface Sci.,* **1986,** *111,* 504.
14. Fleer, G. J.; Lyklema, J. *J. Colloid Interface Sci.,* **1974,** *46,* 1.
15. Somasundaran, P.; Healy, T. W.; Furstenau, D. W. *J. Colloid Interface Sci.,* **1966,** *22,* 599.
16. Buscall, R.; McGowan, J. I.;. Morton-Jones, A. J. *J. Rheol.,* **1993,** *37,* 621.
17. Woutersen , A. T. J. M.; de Kruif, C. G. *J. Chem. Phys.,* **1991,** *94,* 5739.
18. Otsubo, Y. *Het. Chem. Rev.,* **1996,** *3,* 327.
19. Schaefer, D. W.; Martin, J. E.; Wiltzius, P.; Cannell, D. S. *Phys Rev. Lett.,***1984,** *52,* 2371.
20. Torres, F. R.; Russel, W. B.; Schowalter, W. B. *J. Colloid Interface Sci.,* **1991,** *145,* 51.
21. Bicerano, J.; Douglas, J. F; Brune, D. A. *Rev. Macromol. Chem. Phys.,* **1999,** *C39(4),* 561.
22. Casson, N. in *Rheology of Dispersed Systems,* Mills, C.C., Ed., Pergamon (1959).

23. Russel, W. B.; Sperry, P. R. *Prog. in Org. Coat.*, **1994**, *23*, 305.
24. van de Ven, T. G. M. *Colloidal Hydrodynamics*, Academic Press , New York, NY, 1989.
25. Sonntag, R. C.; Russel, W. B. *J. Colloid Interface Sci.*, **1989**, *115*, 378.
26. Torres, F. R.; Russel, W. B.; Schowalter, W. B.; *J. Colloid Interface Sci.*, **1991**, *45*, 73.
27. Potanin, A. *J. Colloid Interface Sci.*, **1993**, *157*, 399.
28. Dickinson, E. *J. Chem. Soc. Faraday Trans.*, **1995**, *91*, 4413.
29. Chiew, Y. C.; Glandt, E. D.; *J. Phys A*, **1989**, *22*, 3969.
30. Hutchinson, R. A ; Paquet, D. A.; McMinn, J. H.; Beuermann, S.; Fuller, R. E.; Jackson, C. in *5th International Workshop on Polymer Reaction Engineering*, DECHEMA, VCH: Weinheim (Germany), 1995, vol. 131, 467.
31. Harriott, P. *J. Polym.Sci.*, **1971**, *A-1 (9)*, 1153.
32. Friis, N.; Nyahagen, L. , *J.Applied Polym.Sci.*, **1973**, *17*, 2311.
33. Kolthoff, I. M.; Miller, I. K. *J. American Chem. Soc.*, **1951**, *73*, 3055.
34. Ghielmi, A.; Storti, G.; Morbidelli, M. *Chem. Eng. Sci.*, accepted for publication, **2000**.
35. Nomura, M.; Harada, M.; Eguchi, W.; Nagata S. in *Emulsion Polymerization*, Piirma, I.; Gardon, J. L., Eds.; ACS Symp. Ser. No. 24, American Chemical Society: Washington DC, 1976, 102.
36. Batchelor, G. K.; *J. Fluid Mech*, **1977**, *83*, 97.
37. Mewis, J; Frith, W. J.; Strivens, T. A. ; Russel, W. B.; *AIChE J.*, **1989**, 35, 415
38. Miller, C. M.; Olesen, K. R.; Shay, G.D.; in *Associative Polymers in Aqueous Media*, Glass, J. E., Ed; *ACS Symp. Ser.,* American Chemical Society: Washington DC, in press, 2000.

Chapter 16

Modeling of Young's Modulus of Latex Blend Films as a Function of the Carboxyl Group Concentration on the Latex Particles

Jiansheng Tang, Eric S. Daniels, Victoria L. Dimonie, Andrew Klein, and Mohamed S. El-Aasser

Emulsion Polymers Institute and Department of Chemical Engineering, Lehigh University, 111 Research Drive, Bethlehem, PA 18015

The mechanical behavior of polystyrene [PS]/poly(*n*-butyl methacrylate-co-*n*-butyl acrylate) [P(BMA/BA)] latex blend films have been modeled using modified Nielsen and Takayanagi equations which correlate Young's modulus to the volume fraction of the PS phase (both unmodified and modified with carboxyl functional groups). Carboxyl groups were incorporated into the PS latex particles in order to alter their surface properties. It was found that the presence of carboxyl groups on the PS latex particles enhanced the Young's modulus of these films. This enhancement in mechanical properties resulted from the formation of hydrogen bonds between the carboxyl groups on the PS particles and the carbonyl groups in the P(BMA/BA) matrix. The predicted moduli that were obtained using a proposed equivalent high T_g interphase volume model match the experimental data well.

A high T_g/low T_g latex blend film provides an excellent example of a two-phase system with one continuous phase and one dispersed phase. The mechanical properties of these composite materials are determined by the

221

properties of the components, the shape of the filler phase, the morphology of the system, the nature of the interface between the phases, and the composition of each component. Research on the prediction of the mechanical properties of two-phase mixtures using theoretical models began long ago (*1-7*). However, the theoretical models that were developed in this area are still incomplete. The main parameters which were considered in the majority of these predictive models are the mechanical properties of the component materials and the composition of the two-phase mixtures. As latex blending has been found to be a good strategy to eliminate volatile organic compounds (VOC's) from polymer coatings, theoretical predictions of the mechanical properties of latex blend films are demanded. Thus, research in this area has been triggered. Again, the quantitative predictions up to now have focused on the volume fraction of the filler particles in latex blend films (*8-10*), although some qualitative or semi-quantitative approaches have been developed which consider the interfacial properties (*11-14*).

In this paper, Young's moduli of PS/P(BMA/BA) latex blend films were examined with an emphasis on the surface properties of the latex particles, which were altered by the inclusion of carboxyl groups. Polystyrene latex particles served as the high T_g component, while poly(*n*-butyl methacrylate-co-*n*-butyl acrylate) latex particles represented the low T_g component in the two-phase material. An approach has been developed to quantitatively predict the Young's modulus of the PS/P(BMA/BA) latex blend films taking into account the surface concentration of the carboxyl groups that were present in the PS latex particles, while keeping all other variables such as the phase volume ratio and particle size unchanged.

Experimental

Materials

n-Butyl methacrylate (BMA), *n*-butyl acrylate (BA), styrene (St), and methacrylic acid (MAA) monomers (Aldrich; reagent grade) were purified by passing them through columns filled with an appropriate inhibitor removal packing material (Aldrich). Sodium dodecyl sulfate (SDS; Fisher Scientific; reagent grade) and potassium persulfate (KPS; Aldrich; reagent grade) were used as received. Carboxylated and non-carboxylated PS and non-carboxylated P(BMA/BA) model latex particles were synthesized, cleaned, and characterized according to the methods published earlier (*15*). Table I shows the characteristics of the latex particles that were used in this study.

Preparation of Latex Films

Films were cast from latex blends consisting of cleaned PS and P(BMA/BA) latex particles (vol% PS varied from 0 to 60%) to eliminate any possible influence of water-soluble oligomers, surfactant, or other additives on the properties of the resulting films. An initial solids content of 6 wt% was utilized and the latex blends were dried under controlled conditions (temperature = 22 ± 0.5 °C; relative humidity = 50 ± 0.5%) on poly(vinyl fluoride) films (Tedlar; DuPont) for ten days. The thickness of these films ranged from 0.20 to 0.25 mm.

Table I. Characteristics of the High T_g and Low T_g Latex Particles

	P(BMA /BA)[e]	Polystyrene (PS)						
D_n (nm)[a]	122.9	123.1	123.2	125.8	128.8	127.5	125.8	125.3
D_w (nm)[b]	126.2	127.4	126.6	127.5	130.2	129.8	129.6	128.6
PDI[c]	1.027	1.035	1.028	1.014	1.011	1.018	1.030	1.026
Wt% MAA	0.0	0.0	0.85	1.82	3.13	4.67	5.34	6.10
σ_{COOH}[d] (%)	0.0	0.0	7.6	12.9	19.1	29.7	43.0	65.8
T_g (°C)	0	105	105	105	105	105	105	105

[a] Number-average diameter
[b] Weight-average diameter
[c] Polydispersity index ($= D_w/D_n$)
[d] The particle surface area covered by carboxyl groups, choosing the cross-sectional area of each carboxyl group as 9 Å^2 based on a theoretical calculation (16)
[e] Statistical copolymer consisting of 75 wt% BMA and 25 wt% BA

Tensile Testing

The latex blend films were cut into dumbbell-shaped specimens according to ASTM Standard D1708-96 and tensile tests were carried out using an Instron Universal Testing Machine (Model 5567) with a crosshead speed of 200 mm/min. A 500 N load cell was used in all experiments. Young's moduli were calculated based on the initial portion of the stress-strain curves. At least five specimens were tested for each film and the results were averaged.

Results and Discussion

Influence of the Volume Concentration of High T_g PS Latex Particles on Young's Modulus

Young's modulus is one of the most important physical properties of a material. Probably the most widely used method to determine Young's modulus is the tensile stress-strain test (17, 18). Young's modulus is represented by the initial slope of the stress vs. strain curve. Similar to the yield strength (19), the Young's modulus of the PS/P(BMA/BA) latex blend films increased as the volume concentration of the PS particles increased (Figure 1). Many equations have been proposed to predict the Young's modulus of two-phase mixtures with one continuous phase and one dispersed phase as the volume fraction of the high T_g phase changes (1-7, 20-23). However, each of the numerous equations describes a specific two-phase mixture system. Nielsen proposed a more generalized equation to predict the elastic modulus of many two-phase composite materials (24,25). The theory used to predict the modulus as a function of the volume fraction of the dispersed phase on the composite materials in which the dispersed phase is the high T_g component is described by equations 1, 2, and 3.
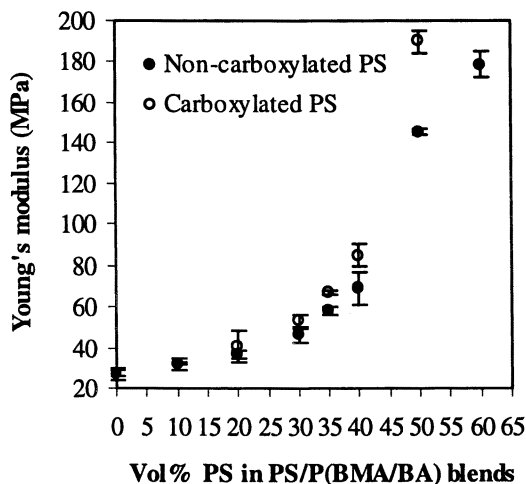
Figure 1. Young's modulus vs. the volume concentration of high T_g latex particles in PS/P(BMA/BA) latex blend films: (●): neither PS nor P(BMA/BA) particles contain carboxyl groups; (○): carboxyl group coverage on the PS particles = 12.9%, no carboxyl groups present on P(BMA/BA) latex particles.

$$E = E_1 \frac{1 + AB\phi_2}{1 - B\psi\phi_2} \tag{1}$$

$$B = \frac{\dfrac{E_2}{E_1} - 1}{\dfrac{E_2}{E_1} + A} \tag{2}$$

$$\psi = 1 + \left(\frac{1 - \phi_m}{\phi_m^2}\right)\phi_2 \tag{3}$$

where E is the modulus of the composite material, E_1 and E_2 are the moduli of the continuous phase and the dispersed phase, respectively, ϕ_2 is the volume fraction of the dispersed phase, ϕ_m is the maximum packing fraction of the high T_g dispersed phase, A and B are constants, and ψ is the factor that enables one to use a reduced concentration scale to take into account the existence of the maximum packing fraction of the particles.

The constant A takes into account such factors as the geometry of the filler phase and Poisson's ratio of the matrix in the two-phase system (25). The value of A varies for different two-phase systems. Based on the experimental data plotted in Figure 1, the constant A for the PS/P(BMA/BA) latex blend films can be obtained by fitting the experimental data (non-carboxylated latex blend films shown in Figure 1) into Nielsen's equations. The fitted A value for this system is 0.39 if ϕ_m is chosen as 0.60. By applying the fitted constant A into Nielsen's equations (equations 1 to 3), and calculating the modulus of the non-carboxylated PS/P(BMA/BA) latex blend films, the theoretical curve fit the experimental data very well except for the point at 60 vol% PS. At this point, the high T_g PS phase in the PS/P(BMA/BA) latex blend film is no longer a separate phase (i.e., above the critical pigment volume concentration, CPVC, or the PS particles contact each other; see next paragraph) and the equations can not be applied (Figure 2) (19). Table II shows the values used for this calculation.

The reason for choosing $\phi_m = 0.60$ is based on the determination of the CPVC for this system (19). The CPVC of the non-carboxylated PS/P(BMA/BA) latex blend system is between 50 and 60 vol% PS latex particles, which implies that the maximum packing fraction of the PS particles would be close to the upper limit of this range. Table III shows some of the ϕ_m values which were derived from calculations of the maximum packing fraction of spherical particles for different types of packing (25). By comparing the CPVC results and the value given for ϕ_m in Table III, it is reasonable to assume that the packing type of the non-carboxylated PS latex particles in the PS/P(BMA/BA) latex blend films is body-centered cubic or random-loose packed at their maximum packing state.

Table II. Parameter Values used for the Calculation of the Theoretical Moduli of PS/P(BMA/BA) Latex Blend Films

Parameter	E_1	E_2	ϕ_m	A	D_v	T
Value	27.02 MPa[a]	3200 MPa[b]	0.60	0.39	125 nm	0.13

[a] Measured by Instron Testing Machine using the pure P(BMA/BA) latex films
[b] Value from literature (26)
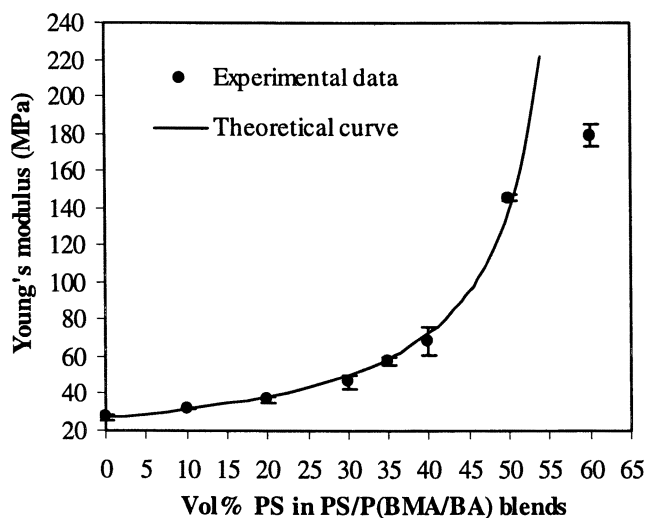
Figure 2. Young's modulus vs. the volume concentration of PS latex particles in PS/P(BMA/BA) latex blend films: neither high T_g PS nor low T_g P(BMA/BA) latex particles were carboxylated; the theoretical curve was calculated using equations 1, 2 and 3.

Table III. Maximum Packing Fractions (ϕ_m) for Spherical Particles (25)

Type of Packing	ϕ_m
Hexagonal close packing	0.74
Face-centered cubic packing	0.74
Body-centered cubic packing	0.60
Simple cubic packing	0.52
Random close packing	0.64
Random loose packing	0.60

Influence of Carboxyl Groups on the PS Latex Particles on Young's Modulus

Young's modulus as a function of vol% PS was also plotted in Figure 1 for the PS/P(BMA/BA) latex blend films containing carboxylated PS latex particles. It was found that the modulus of the carboxylated latex blend film is higher than that of the non-carboxylated latex blend films if they have the same vol% PS, indicating that the modulus of the carboxylated PS/P(BMA/BA) latex blend film is higher than the value predicted by Nielsen's equation. This occurs because this equation does not consider the surface properties of the latex particles which are altered by the presence of the carboxyl groups. Thus, a modification of this equation is necessary to take the surface properties of the particles into consideration.

As discussed previously (19), the presence of the carboxyl groups on the PS latex particles increased the yield strength of the latex blend films resulting from the formation of hydrogen bonds between the carboxyl groups on the PS particles and the carbonyl groups present in the copolymer matrix. However, all the moduli were measured before the yield point was reached. Thus, the enhanced interfacial adhesion may not be the most important factor which increases the Young's modulus. The modulus may be enhanced by another mechanism. The mechanism proposed here is the formation of an equivalent high T_g interphase. This interphase is formed between the PS particles and the P(BMA/BA) copolymer matrix because of the formation of hydrogen bonds, which is illustrated in Figure 3. The carboxyl groups present on the PS latex particles form hydrogen bonds with the carbonyl groups that are in the P(BMA/BA) copolymer matrix. Domains resulting from the formation of the hydrogen bonds would be formed around each PS particle (Figure 3A). In each of the domains, the P(BMA/BA) molecular chains are "cross-linked" by these hydrogen bonds, resulting in a higher modulus than that of the P(BMA/BA) copolymer matrix. These domains may serve as high T_g fillers and increase the Young's modulus of the PS/P(BMA/BA) latex blend films. To simplify the
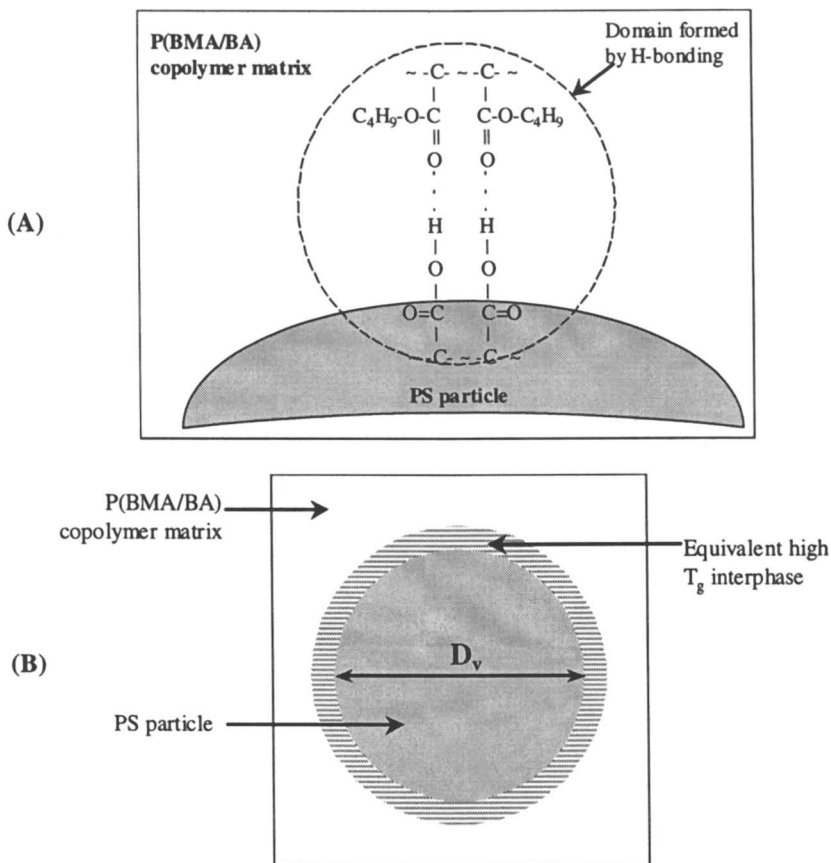
Figure 3. Schematic representations of: (A) high T_g domain resulting from the formation of hydrogen bonds between the carboxyl groups on the PS particle and the carbonyl groups in the P(BMA/BA) copolymer matrix; and (B) an equivalent high T_g interphase which forms between the PS latex particles and the P(BMA/BA) copolymer matrix resulting from the formation of hydrogen bonds.

calculation, an equivalent volume of each of the domains (v) is defined as the volume of the PS phase that contributes to the increase in the Young's modulus of the latex blend films the same as each of the domains. Then, the total equivalent volume of the domains around each of the PS latex particles (Σv) can be expressed as equation 4 (Figure 3B):

$$\Sigma v = v \cdot \frac{S \cdot \sigma_{COOH}}{a_{COOH} \cdot n} \tag{4}$$

where S is the surface area of each PS particle, σ_{COOH} is the fraction of the PS particle surface area covered by carboxyl groups, a_{COOH} is the cross-sectional area of each carboxyl group (which is 9 Å^2 from the literature (16)), and n is the average number of carboxyl groups in each of these domains.

Equation 5 defines another parameter T. The total volume of the equivalent high T_g interphase in the entire PS/P(BMA/BA) latex blend film (ΔV_2) can then be calculated using equation 6.

$$T = \frac{v}{n \cdot a_{COOH}} \tag{5}$$

$$\Delta V_2 = T \cdot S \cdot \sigma_{COOH} \cdot N_{p, \text{high } T_g} \tag{6}$$

where $N_{p,\text{high } T_g}$ is the total number of PS particles present in the latex blend film. T is a coefficient which could be assumed to be a constant because the larger the number of carboxyl groups present in each of these domains, the larger the equivalent volume of this domain (v).

S and $N_{p,\text{high } T_g}$ can be expressed by equations 7 and 8, respectively. Substituting these values into equation 6 results in equation 9.

$$S = \pi \cdot D_v^2 \tag{7}$$

$$N_{p, \text{high } T_g} = \frac{6 \cdot V_2}{\pi D_v^3} \tag{8}$$

$$\Delta V_2 = \frac{6 \cdot T \cdot \sigma_{COOH} \cdot V_2}{D_v} \tag{9}$$

where D_v is the volume-average diameter of the PS particles and V_2 is the volume of the PS phase.

Now the increased volume fraction of the high T_g phase (including the equivalent high T_g interphase) of the latex blend films can be calculated by equation 10:

$$\phi_2' = \frac{V_2 + \Delta V_2}{V} = \left(1 + \frac{6 \cdot T \cdot \sigma_{COOH}}{D_v}\right)\phi_2$$

(10)

where V is the total volume of the latex blend.

From the assumption that an equivalent high T_g interphase is formed because of the formation of hydrogen bonds between the high T_g PS particle and the low T_g P(BMA/BA) copolymer matrix, the actual volume fraction of the PS phase in the latex blend films consisting of carboxylated PS particles should be ϕ'_2 instead of ϕ_2. Thus, to model the modulus of the carboxylated PS/P(BMA/BA) latex blend films, ϕ_2 in equations 1 and 3 should be substituted by ϕ'_2 in equation 10, yielding equation 11. By fitting equation 11 to the experimental data for the carboxylated latex blend films plotted in Figure 1, the coefficient T can be calculated for each experimental point (Table IV). Table IV shows that T is basically constant, indicating that the assumption of a constant ratio between the equivalent volume of each of the domains and the average number of carboxyl groups present in the same domain is reasonable. The averaged T value, which is 0.13, is used as the constant in equation 11. The prediction of the modulus by equation 11 using the values given in Table II is also very good (Figure 4).

$$E = E_1 \cdot \frac{1 + A\left(\dfrac{E_2/E_1 - 1}{E_2/E_1 + A}\right)\left(1 + \dfrac{6T\sigma_{COOH}}{D_v}\right)\phi_2}{1 - \left(\dfrac{E_2/E_1 - 1}{E_2/E_1 + A}\right)\left[1 + \left(\dfrac{1 - \phi_m}{\phi_m^2}\right)\left(1 + \dfrac{6T\sigma_{COOH}}{D_v}\right)\phi_2\right]\left(1 + \dfrac{6T\sigma_{COOH}}{D_v}\right)\phi_2}$$

(11)

Table IV. Determination of the T Value in Equation 11

ϕ_2	0.00	0.10	0.20	0.30	0.35	0.40	0.50
E	27.02	31.95	40.35	53.00	66.80	84.82	189.90
T	--	0.124	0.171	0.104	0.142	0.122	0.093
						Averaged $T = 0.13$	

$\sigma_{COOH} = 13$ (%); $D_v = 125$ nm; $E_1 = 27.02$ MPa; $E_2 = 3200$ MPa; $A = 0.39$; $\phi_m = 0.60$
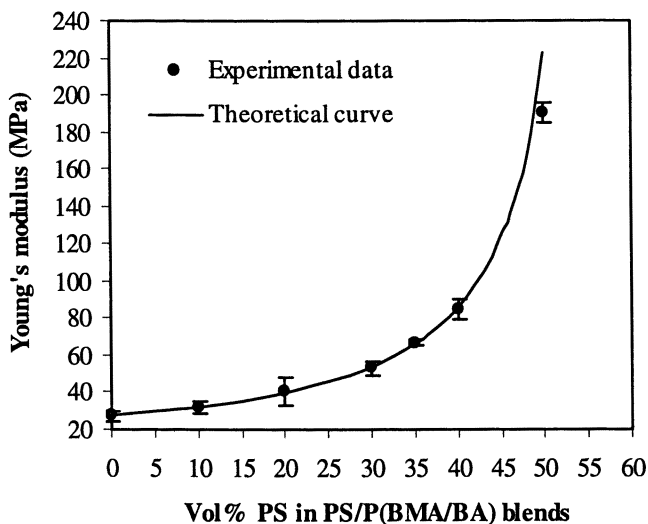
Figure 4. Young's modulus vs. the volume concentration of PS latex particles in PS/P(BMA/BA) latex blend films; the carboxyl group coverage on the PS particles = 12.9%; no carboxyl groups are present on the P(BMA/BA) latex particles; the theoretical curve was calculated using equation 11.

The results shown in Figure 1 demonstrate that the presence of the carboxyl groups on the high T_g PS latex particles significantly influence the modulus of the latex blend film. Thus, further experiments are needed to investigate the influence of the carboxyl groups on the modulus over a larger range. Figure 5 and Table V show these results. A general trend is noted in which the modulus first increased as the carboxyl group coverage on the PS latex particles increased. However, this was followed by a sudden drop in the modulus between 12.9% and 19.1% carboxyl group coverage on the PS particles. The predicted curve obtained from equation 11 (theoretical curve 1; Figure 6) shows that it matches the experimental data very well at or before the point where there is 12.9% carboxyl group coverage on the PS latex particles (Figure 6). However, the experimental data obtained after this point show large deviations from the theoretical curve 1. The investigation of the film morphology and surface properties described in earlier publications (*19, 27*) also showed sudden changes in the morphology and surface properties of the latex blend films after the point where the surface carboxyl group coverage on the PS latex particles was 12.9%. These findings suggest that there should be a change in the type of packing of the PS particles after this point. As discussed above, the maximum packing of the PS

particles would be a body-centered cubic type, yielding ϕ_m value of 0.60. However, after the point of 12.9% surface carboxyl group coverage, the presence of the carboxyl groups on the surface of the PS particles at a high concentration makes it possible to form hydrogen bonds between the carboxyl groups on different PS particles (i.e., interparticle hydrogen bonding). The interparticle hydrogen bonding brings about a driving force among the PS latex particles, and allows them to pack more tightly. This would allow PS particles to pack in a hexagonal-close packed array. Thus, it would be a good approximation to choose ϕ_m as 0.74 in equation 11 to model the modulus of the PS/P(BMA/BA) latex blend films when the carboxyl group coverage on the PS particle is higher than 12.9%. Theoretical curve 2 in Figure 6 is calculated using equation 11 and setting $\phi_m = 0.74$. It is noted that the accuracy of the prediction by theoretical curve 2 is acceptable for most of the experimental points. It may be concluded that the Young's moduli of the PS/P(BMA/BA) latex blend films could be modeled using equation 11 at different carboxyl group coverage on the PS latex particles by choosing $\phi_m = 0.60$ when the carboxyl group coverage is not more than 12.9% and $\phi_m = 0.74$ when the carboxyl group coverage is higher than 12.9%.
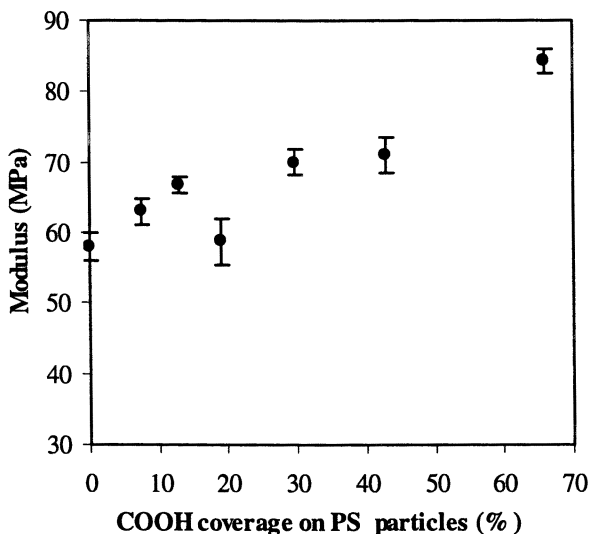
Figure 5. Young's modulus vs. the carboxyl group coverage on the PS latex particles in PS/P(BMA/BA) latex blend films: volume fraction of PS, $\phi_2 = 0.35$; no carboxyl groups on the P(BMA/BA) latex particles (see Table V for raw data).

Table V. Raw Data of Young's Modulus vs. Carboxyl Group Coverage on the PS Latex Particles in PS/P(BMA/BA) Latex Blend Films

σ_{COOH} (%)	Young's modulus (MPa)	Standard deviation (MPa)
0.0	58.00	2.09
7.6	63.03	1.80
12.9	66.84	1.57
19.1	58.82	3.30
29.7	70.01	1.85
43.0	71.03	2.60
65.8	84.44	1.66

volume fraction of PS, $\phi_2 = 0.35$; no carboxyl groups on the P(BMA/BA) latex particles
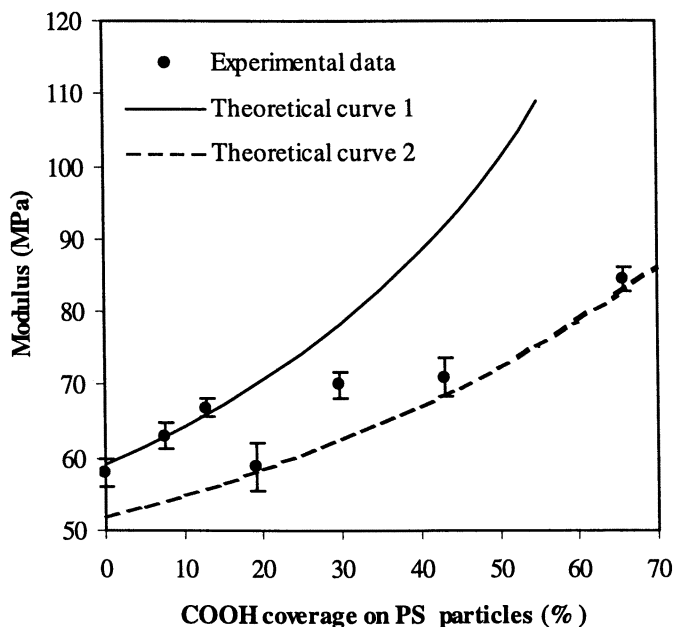
Figure 6. Young's modulus vs. the carboxyl group coverage on the PS latex particles in PS/P(BMA/BA) latex blend films: volume fraction of PS, $\phi_2 = 0.35$; no carboxyl groups on the P(BMA/BA) latex particles; the theoretical curves were calculated using equation 11 using the values listed in Table II except for ϕ_m, which is 0.60 for curve 1 and 0.74 for curve 2; T = 0.13.

Modification of the Takayanagi Equation using the T Constant

The model that predicts Young's modulus of the PS/P(BMA/BA) latex blend films considering the carboxyl group coverage on the PS particles can also be derived by modifying the Takayanagi model. The schematic diagram shown in Figure 7 illustrates the Takayanagi model used for composite materials in which the dispersed phase is the high T_g (plastic) component and the continuous phase is the copolymer matrix (rubber) (28,29). The Young's modulus of the composite materials (E) is given by equation 12.

$$E = \lambda \left(\frac{\varphi}{E_2} + \frac{1-\varphi}{E_1} \right)^{-1} + (1-\lambda)E_1 \qquad (12)$$

where E_1 and E_2 are the Young's moduli of the copolymer matrix and the dispersed high T_g phase, respectively; the multiplication of φ and λ represents the volume fraction of the high T_g plastic phase, ϕ_2, which can be expressed by equation 13.

$$\varphi\lambda = \phi_2 \qquad (13)$$

For each ϕ_2, φ, and λ, specific numerical values are needed to solve equation 12. Instead of arbitrarily assuming the ratio of φ to λ, it is better to define $\varphi = a\lambda$ (assume a is a constant) and to determine the constant a using the experimental data presented in Figure 1 (non-carboxylated latex blend films). The constant a was statistically fitted as 1.52 for the PS/P(BMA/BA) latex blend films. At this ratio of φ to λ ($\varphi = 1.52\lambda$), the Takayanagi model fits the experimental data well (Figure 8).

This model allows one to evaluate the mechanism by which the carboxyl groups present on the PS particles enhance the Young's modulus by increasing the equivalent volume fraction of the high T_g phase. If this mechanism is correct, ϕ_2 in equation 13 should be replaced by ϕ'_2, which is expressed by equation 10 for the latex blend films with carboxyl groups present on the PS particles, leading to equation 14.

$$\lambda = \sqrt{\phi'_2/1.52} \quad \varphi = \sqrt{1.52\phi'_2} \qquad (14)$$

Substituting φ and λ in equation 12 with equations 10 and 14 yields a modified Takayanagi equation (equation 15) which considers both the volume fraction and the carboxyl group coverage on the PS particles.
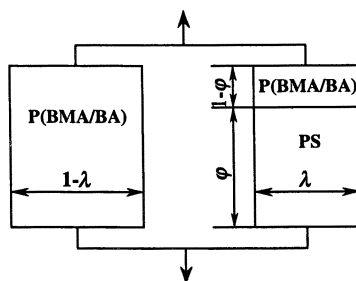
Figure 7. Schematic diagram of the Takayanagi model used for composite materials in which the dispersed phase is the high T_g (plastic) component and continuous phase is the low T_g copolymer matrix (rubber): the quantities λ and φ are used to calculate volume fractions: $\varphi\lambda = \phi_2$; ϕ_2 is the volume fraction of the high T_g phase.
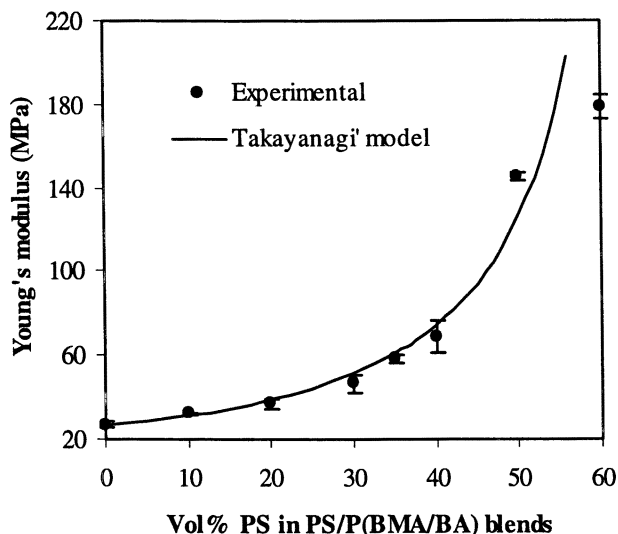
Figure 8. Young's modulus vs. the volume concentration of high T_g PS particles in the PS/P(BMA/BA) latex blend films: neither the PS, nor P(BMA/MA) latex particles were carboxylated; The Takayanagi curve was calculated using equations 12 and 13 and choosing $\varphi = 1.52\lambda$.

$$E = \cfrac{\sqrt{\cfrac{\phi_2}{1.52}\left(1+\cfrac{6T\sigma_{COOH}}{D_v}\right)}}{\cfrac{\sqrt{1.52\phi_2\left(1+\cfrac{6T\sigma_{COOH}}{D_v}\right)}}{E_2} + \cfrac{1-\sqrt{1.52\phi_2\left(1+\cfrac{6T\sigma_{COOH}}{D_v}\right)}}{E_1}} + \left[1-\sqrt{\cfrac{\phi_2}{1.52}\left(1+\cfrac{6T\sigma_{COOH}}{D_v}\right)}\right]E_1 \quad (15)$$

If the T value obtained from the modified Nielsen equation (equation 11) can also be applied to the modified Takayanagi equation to fit the experimental data of the latex blend films with carboxyl groups present on the PS particles, it would offer strong evidence to support the proposed mechanism. Figure 9 confirms this postulation. By using the same T constant (0.13) obtained from the modified Nielsen equation, the theoretical values calculated from the modified Takayanagi equation match the experimental data very well.

Conclusions

The presence of carboxyl groups on the PS latex particles in the PS/P(BMA/BA) latex blend films significantly enhances the Young's modulus of the latex blend films. The carboxyl groups present on the PS latex particles could form hydrogen bonds with the carbonyl groups present in the P(BMA/BA) copolymer matrix or with the carboxyl groups on adjacent PS particles
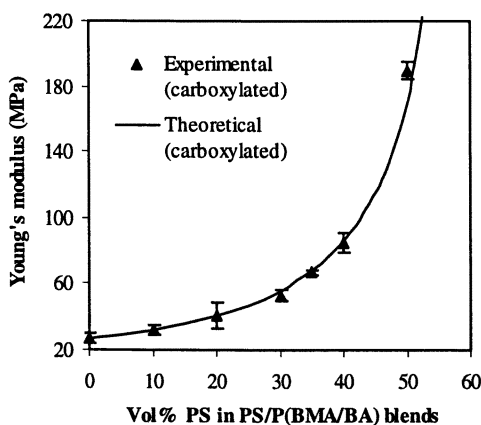
Figure 9. Young's modulus vs. volume concentration of the PS latex particles in PS/P(BMA/BA) latex blend films: carboxyl group coverage on the PS particles = 12.9%; no carboxyl groups present on the low T_g P(BMA/BA) latex particles; the theoretical curve was plotted using equation 15 by choosing $T = 0.13$ (D_v = 125 nm; E_1 = 27 MPa; E_2 =3200 MPa).

(interparticle hydrogen bonding). The formation of hydrogen bonds between the carboxyl groups on the PS particles and the carbonyl groups in the copolymer matrix increase the equivalent high T_g volume of the interphase between the high T_g and low T_g phases, which is the reason why Young's modulus is improved in the presence of carboxyl groups. It was found that the carboxyl groups present on the PS latex particles at a low concentration ($\leq$ 13% coverage) primarily form hydrogen bonds with the carbonyl groups present in the P(BMA/BA) copolymer matrix. This kind of hydrogen bonding results in a random- or body-centered cubic packing of the PS particles in their maximum packing state. When the carboxyl groups were present on the PS latex particles at a high concentration (> 13% coverage), hydrogen bonds between the carboxyl groups on adjacent PS particles may form. The formation of the interparticle hydrogen bonds induces an attractive force among the PS particles, resulting in tighter packing (hexagonal) of the PS particles at their maximum packing state. A model was proposed based on Nielsen's equation by considering the surface characteristics of the latex particles in predicting the modulus of the PS/P(BMA/BA) latex blend films for different carboxyl group coverages on the PS particles. The predicted moduli match the experimental data closely. The mechanism of an equivalent volume of the high T_g interphase can also be used to modify the Takayanagi equation, yielding another equation which predicts the Young's modulus of the PS/P(BMA/BA) latex blend films as a function of the carboxyl group concentration on the PS particle surface. The predicted moduli by the modified Takayanagi equation also match the experimental data very well, indicating that the proposed mechanism of the equivalent volume of the high T_g interphase is reasonable.

Acknowledgment

References

1. Kerner, E. H. *Proc. Phys. Soc. London*, **1956**, *69B*, 808.
2. Takayanagi, M. *Mem. Fac. Eng. Kyushu Univ.*, **1963**, *23*, 11.
3. Hashin, Z.; Shtrikman, S. *J. Mech. Phys. Solids*, **1963**, *11*, 127.
4. Takayanagi, M. *J. Appl. Polym. Sci.*, **1966**, *10*, 113.
5. Hashin, Z.; Shtrikman, S. *J. Appl. Phys.*, **1962**, *33*, 3125.
6. Gordon, M.; Taylor, J. S. *J. Appl. Chem. (London)*, **1952**, *2*, 493.
7. Hoftyzer, P. J.; van Krevelen, D. W. *Angew. Makromol. Chem.*, **1976**, *56*, 1.

8. Takeshita, Y.; Ichino, T.; Nishi, S. *J. Polym. Sci.: Part A: Polym. Chem.*, **1998**, *36*, 2493.

9. Charmeau, J. Y.; Berthet, R.; Gringreau, C.; Holl, Y.; Kientz, E. *Int. J. Adhes. and Adhes.*, **1997**, *17(2)*, 169.

10. Lepizzera, S.; Pith, T.; Fond, C.; Lambla, M. *Macromolecules*, **1997**, *30*, 7945.

11. Eckersley, S. T.;. Helmer, B. J., *J. Coat. Tech.*, **1997**, *69(864)*, 97.

12. Kolarik, J. *Polymer*, **1996**, *37(6)*, 887.

13. Xu, J.; Dimonie, V. L.; Sudol, E. D.; Shaffer, O. L.; El-Aasser, M.S. *J. Appl. Polym. Sci.*, **1998**, *69*, 977.

14. Park, Y.–J.; Kim, J.–H. *Colloids and Surfaces A: Physiochemical and Eng. Aspects*, **1999**, *153*, 583.

15. Tang, J.; Dimonie, V. L.; Daniels, E. S.; Klein, A.; El-Aasser, M. S. *J. Appl. Polym. Sci.*, **2000**, *77*, 644.

16. Huheey, J. E. *Inorganic Chemistry;* Harper and Row: New York, 1978; p. 846.

17. Nielsen, L. E., *Mechanical Properties of Polymers*; Van Nostrand Reinhold: New York, 1962.

18. Harris, W. D. in *Testing of Polymers*; Vol. 4, W. E. Brown, Ed., Interscience: New York, 1969; p. 399.

19. Tang, J.; Daniels, E. S.; Dimonie, V. L.; Vratsanos, M. S.; Klein, A.; El-Aasser, M. S. *in preparation*.

20. Hashin, Z. *Appl. Mech. Rev.*, **1964**, *17*, 1.

21. Van der Poel, C. *Rheol. Acta*, **1958**, *1*, 198.

22. Budiansky, B. *J. Mech. Phys. Solids*, **1965**, *13*, 223.

23. Smith, J. C. *J. Res. Nat. Bureau Stand.*, **1975**, *79A*, 419.

24. Nielsen, L. E. *J. Appl. Phys.*, **1970**, *41*, 4626.

25. Nielsen, L. E.; Landel, R. F. *Mechanical Properties of Polymers and Composites*, 2nd edition, Marcel Dekker, Inc.: New York, 1994.

26. Rudd, F. *J. Appl. Phys.*, **1957**, *28*, 1096.

27. Tang, J.; Daniels, E. S.; Dimonie, V. L.; Klein, A.; El-Aasser, M. S. in *Film Formation in Coatings*, Provder, T.; Urban, M. W. Eds., *ACS Symposium, Series 790*, **2001**, Chapter 12, *in press*.

28. Takayanagi, M. *Mem. Fac. Eng. Kyushu Univ.*, **1963**, *23*, 11.

29. Sperling, L. H. *Polymeric Multicomponent Materials*, Wiley & Sons, Inc.: New York, p. 37, 1997.

Chapter 17

Morphology and Adhesive Force of Natural Rubber Latex Films by Atomic Force Microscopy

C. C. Ho[1,2] and M. C. Khew[1]

[1]Department of Chemistry, University of Malaya, 50603 Kuala Lumpur, Malaysia
[2]Current address: Omnigrace (Thailand) Ltd., Tambon Banpru, Hatyai, Songkhla 90250, Thailand

Commercial natural rubber latex concentrate is used almost exclusively in the production of rubber-dipped goods, the bulk of which is in the form of gloves. When a 'former' is dipped into the latex, a latex film is formed after the water evaporates and the particles come into contact and fuse together. Any factors that hinder good film formation of the latex would adversely affect the film morphology and hence its application as a barrier material. In view of its low glass transition temperature, natural rubber (NR) latex film is soft and tacky and cannot be used as a glove in its native form. Vulcanization and chemical modification by chlorination of the film surface are additional process steps in glove manufacturing that enable NR latex film to become finally donnable. Basically these processes reduce the surface friction and improve the lubricity of the film surface. A clear understanding of the nature of the surface of the latex film in relation to its performance is pivotal in ensuring product quality. The adhesive force of various NR latex films such as powdered, vulcanized, chlorinated, and polymer-coated was determined from the force-distance curves using atomic force microscopy (AFM)

© 2002 American Chemical Society

239

and compared with those of synthetic polymers and commercial glove samples. Distinctive adhesive forces between the AFM probe tip and these materials allow them to be distinguished from one another. Results indicate that the magnitude of the pull-off force is strongly influenced by surface inhomogeneity and topography of the film. The behavior of the pull-off forces agrees with interpretation based on current understanding of this phenomenon. The technique is well-suited for assessing the structure-performance relation of gloves.

Natural rubber (NR) latex, like its counterpart synthetic latex, is a stable colloidal dispersion containing dispersed latex particles in an aqueous phase. Fresh NR latex from the *Hevea brasilensis* tree contains about 4-5% of non-rubber, made up by proteins (1.0%), carbohydrates (1.0%) and lipids (1.6%) (*1*). The fresh latex, containing only 30 – 35 % rubber, putrefies within hours after leaving the tree and auto-coagulates. Technically-specified commercial latex concentrate, at a solids content of ca. 60% rubber, is produced from the fresh latex by preservation and centrifugation. The latex particles in commercial NR latex concentrate are stabilized by an adsorbed layer of mainly long-chain fatty acid soaps (the hydrolysis products of phospholipids), polypeptides, and proteins (*2*). Commercial ammoniated NR latex concentrate finds extensive use in the production of rubber-dipped goods, mainly in the manufacture of medical examination gloves. The necessary condition of such application is the formation of a continuous film with the appropriate mechanical strength.

An inherent difference between the synthetic and NR latexes is that NR latex contains a host of non-rubbers that originate from the tree as mentioned above. The bulk of these non-rubber materials are removed by centrifugation during the concentration process in the production of commercial latex concentrates. Some residue plant proteins and lipid materials are, however, tenaciously bound to the rubber particles and become incorporated into the film when the latex dries. Thus, in the manufacturing of NR rubber gloves, it is necessary to extract the latex film by leaching it with water at an elevated temperature to remove the remaining residue proteins and processing chemicals (*3*). The actual amount of residual non-rubbers remaining after leaching really depends on the vigor of the leaching process employed. The evaporation of water during drying of the film has aided the migration of these non-rubbers to the latex film surface. Our recent work (*4*) on the visualization of the latex film surface by atomic force microscopy (AFM) has shown very clearly the exudation and accumulation of these materials at the film surface during the film formation

process. Some of the lipids are known to be natural accelerators and natural antioxidants. They are beneficial to the final products. However, rubber proteins may cause an allergic reaction in certain sensitized users. The actual amount of residual proteins on the *surface* after leaching may be minute (non-rubbers in the original commercial latex concentrate are ca 1.0 % (*5*)), and therefore difficult to quantify as such, but their effect on the quality of the final product is significant and cannot be easily ignored. Various leaching steps are thus essential stages in glove manufacturing to ensure that the glove meets the stringent standards set by the regulatory body for medical devices. For example, the lowest acceptable water-extractable residue proteins as determined by the current ASTM D5712 test method is limited to 50 μg/g of glove (*6*). Reports and excellent monographs on the properties of these NR proteins and lipids are available (*7-10*). The effect of these substances on the colloid stability of the NR latex has been reported by us previously (*2*).

Apart from the presence of non-rubbers, one other difference between synthetic and NR latex is that the particle size of the NR latex varies widely whereas, the synthetic latex particles are more monodisperse and the particle size is also smaller. When these water-based latexes are spread on a substrate, a latex film is formed after the water evaporates and the particles come into contact. A mechanically continuous homogeneous film will result via flattening of the latex particles concurrently with inter-particle diffusion of polymer chains if the film is at a temperature above the glass transition temperature (T_g) of the latex particles (*11,12*). In the case of NR, since the T_g (-63.6 °C) is low, a continuous latex film is formed which is soft and tacky. This renders NR latex films useless and unsuitable in its native form as a barrier material in glove manufacturing. In practice, vulcanization of the latex increases the hardness as well as the tensile strength of the latex film. In particular, pre-vulcanization of NR latex in combination with leaching of the film was found to result in an increase in the modulus and tensile strength of the film (*13*). This was attributed to an increase in integration of the film following the removal of the non-rubbers from the original latex particle surface. The AFM results on the morphology of prevulcanized latex film surfaces lend further support to the occurrence of inter-particle diffusion of polymer chains during gradual coalescence of the film-forming process (*14*). In addition, chemical modification by chlorination of the film surface would increase both the surface hardness and roughness. Both of these modifications result in reduced surface tackiness and hence better donning of the glove. Recent results (*15*) on solution chlorination of NR latex films have confirmed that chlorination increased the hydrophilicity and reduced the surface tackiness of the film. Chlorination was accompanied by cracking and hardening of the film surface. Cross-linking reactions brought about by the chlorine on the rubber molecules also contributed to a hardening of the film surface. This results in a lowering of the adhesive force and surface friction of the latex film against

another surface. This clearly demonstrates that chemical modification of the film surface, or more drastically, the modification of the latex itself, to meet performance requirements is usually required of NR latex films.

While natural rubber is well suited for the tire tread and footwear industries in view of its high surface coefficient of friction, this property is a distinct disadvantage for its use as sheeting, liners, and wipers. Similarly, the necessary application requirement of a glove is good donnability where a low surface tack and sliding friction of the glove surface is essential. This is related to the lubricity of the film surface against another surface, in the case of gloves, the human skin. A common method used to reduce surface friction and tack is by the use of solid lubricant such as talc or corn starch. This solution, as employed in powdered gloves, is at best semi-permanent, as the lubricating particles are easily removed from the surface during service. This is deemed unsatisfactory, in particular, for a surgeon's glove which has tight regulatory requirements.

Chemical modification of bulk rubber vulcanizates such as wiper blades and belting to reduce surface tack using aqueous chlorination have been reported by Noakes (16). Results of simple friction tests on halogenated rubber sheets by acidified hypochlorite solution were given by Roberts and Brackley (17-19) and Romberg (20). Basically, chlorination roughens and hardens the rubber surface, and thus reduces the effective areas of contact between the surfaces, leading to a decrease in frictional resistance of the rubber surface. The chlorination process is simple but beset with poor reproducibility and accompanied by possible deterioration in physical properties, in particular, for rubber gloves which are thinner and more flexible compared to other rubber vulcanizates. In addition, major concerns are health and safety hazards associated with the process. Any improvement resulting in a safer and more environmentally-friendly production process would be most beneficial to the glove industry. An entirely different approach in surface friction reduction is by coating the glove surface with a low friction polymeric material. For example, surgeon's gloves coated with a proprietary material known as biogel are available in the market. This new approach depends on the availability of suitable materials that can adhere well to the latex film surface without flaking during service. Various commercial polymeric materials of the polyurethane type are currently being investigated also, with a view to eventually replace chlorination.

Surface chlorination studies (16-19) on bulk rubber vulcanizates in the literature were confined mainly to physical property changes such as the surface coefficient of friction. The surface morphology and extent of surface chlorination had not been fully established. Recently, a systematic study (15) of the effect of aqueous chlorination on surface morphology and compositional changes of thin rubber latex films confirms the simultaneous occurrence of surface hardening and roughening. Chlorinated and oxygenated species were found on the film surface following chemical reactions of the double bonds of

the rubber molecules with chlorine and the hydrophilicity of the chemically-modified surface improved after chlorination. The thickness of the chlorinated layer on the film surface was less than 10 μm. We have now extended the investigation to include the correlation between the extent of chlorination with the adhesive force of the film surface as measured by AFM. It is hoped that such information together with similar measurement on some commercial glove samples could shed some light on the relationship between film morphology and the performance of rubber latex gloves.

Experimental

Thin latex films (about 36 μm thick) of ammoniated latex concentrate were prepared by dipping a newly-cleaved mica surface into the latex and the deposited gel was allowed to dry at room temperature for at least an hour before observation. NR latex films (0.3 mm thick) were surface chlorinated in acidified aqueous hypochlorite solution as described previously (15). These films were prepared in the absence of any vulcanizing agents. Thin films prepared from prevulcanized latex after maturation for 8 days were post-vulcanized according to reported procedures (14). The morphology of the latex films deposited on the mica surface was observed in a Leica S440 scanning electron microscope (SEM) after sputter-coating with a very thin layer of gold. Images were acquired at a probe current of 500 pA and voltage of 10 kV. Commercially-available powdered and chemically-treated NR latex gloves were used as received. A small test piece of the cut glove was held unstretched with the donning side facing upward on the AFM sample holder by double-sided tape. For comparison, latex films of polystyrene (PS) and poly(methyl methacrylate) latexes (PMMA) were also investigated (21).

The spring constant of a 200 μm long and 36 μm wide V-shaped Si_3N_4 cantilever was measured according to method developed by Cleveland et al. (22). Atomized tungsten spheres with a wide size distribution were used as the test masses (23). The sphere was positioned exactly near the end of the cantilever on the same side of the integrated tip. Resonant frequencies were measured from the split-photodiode response on a Nanoscope III AFM (Digital Instruments). The size of the attached sphere was determined using the SEM.

Force-distance measurements were performed in ambient air (~ 28 °C) using a scanning probe microscope (Nanoscope III Multimode AFM, Digital Instruments). A single Si_3N_4 cantilever was used to acquire the force-distance curves of all the samples within a given series to ensure that the spring constant and tip radius are the same between samples. On the average, about 50 force-distance curves acquired at different locations over a 5 μm x 5 μm scan area on

the sample surface were recorded and the average pull-off force for the polymer determined.

Results and Discussion

Since its development in the 1980s (24), AFM has seen tremendous expansion and extension of its operation to cover diverse areas of applications. Perhaps the most notable extension of AFM capabilities so far is the realization that lateral forces between the AFM probe and the sample could be measured too. Thus, in addition to topographical imaging, the scanning force microscope (SFM) can measure the very small force between the probe and the sample surface to provide unique localized chemical and nanomechanical information about the sample surface. Using the force-distance curve, the surface force, adhesion, friction and elasticity could be measured directly which are dependent on the probe, contact surface and the surrounding medium (25). Microscopic adhesion and friction affect a wide variety of surface phenomena and the SFM offers a new tool to study these important parameters. This technique is particularly suited for polymer systems because of its ability to characterize the surface structure, morphology, and surface properties from nano to millimeter scales. For example, the adhesive forces between a series of polymer film surfaces and chemically well-defined SFM probe tips have been investigated and found to depend strongly on the chemical nature of both probe and sample surfaces (26). The link between surface chemical nature, friction, and adhesion at the nanoscale was established using SFM by Frisbie et al. (27) who demonstrated different adhesion between surfaces (probe and substrate) coated with molecules with different end groups. The adhesive forces of these groups are in the same order as the corresponding frictional forces. In another study (28), it was found that the frictional force showed a clear correlation with the surface energy. Both adhesion and friction are larger on high surface energy materials. Overney et al. (29,30) showed that high adhesion is always associated with high friction and a topographically higher and stiffer substrate yields lower friction. These results translate concepts proven valid on macroscopic experiments to the nanoscale. Softer surface components will give rise to a larger area of contact for an equivalent load which in turn leads to a higher frictional force.

Examples of the force-distance curves for NR, chlorinated NR, vulcanized NR, PMMA and PS latex films under ambient air conditions using a Si_3N_4 cantilever are shown in Figure 1 and Figure 2. The pull-off force (F) is calculated using the equation: $F = k\Delta z$ where k is the spring constant and Δz the cantilever displacement. The different shapes of the force-distance curves for the various polymers demonstrate clearly that the tip-sample interaction is strongly

(a) NR

Force Calibration Plot

---- Extending
⟶ Retracting

Tip
Defl
0.13 µm/div

Setpoint

Z position - 0.11 µm/div
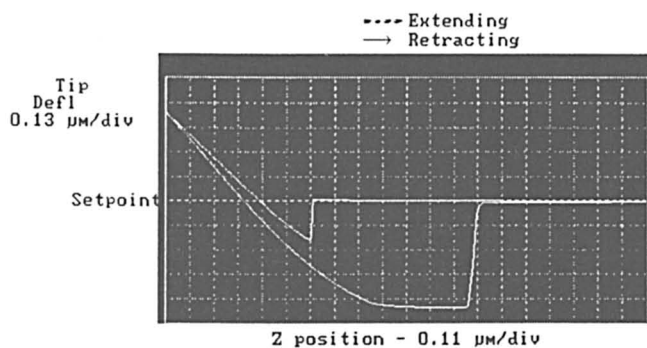
NanoScope	Contact AFM	
Z scan size	2.114	µm
Setpoint	-1.024	V
Z scan rate	2.441	Hz
Z range	1.256	µm

(b) Vulcanized NR

Force Calibration Plot

---- Extending
⟶ Retracting

Tip
Defl
0.11 µm/div

Setpoint

Z position - 0.13 µm/div
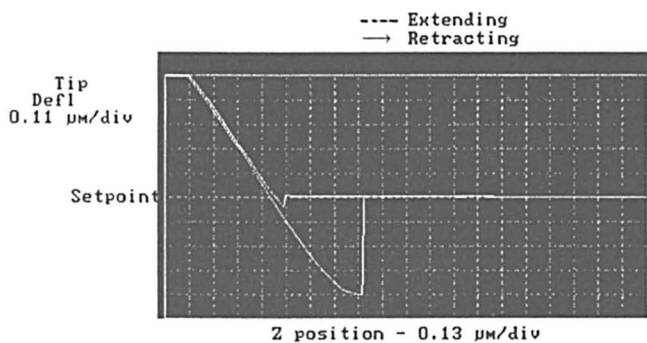
NanoScope	Contact AFM	
Z scan size	2.532	µm
Setpoint	-1.264	V
Z scan rate	2.441	Hz
Z range	1.131	µm

Figure 1. Force-distance curves between the unmodified Si₃N₄ probe-tip and (a)
untreated, (b) vulcanized, and (c) chlorinated NR latex films.
Continued on next page.

(c) Chlorinated NR

Force Calibration Plot
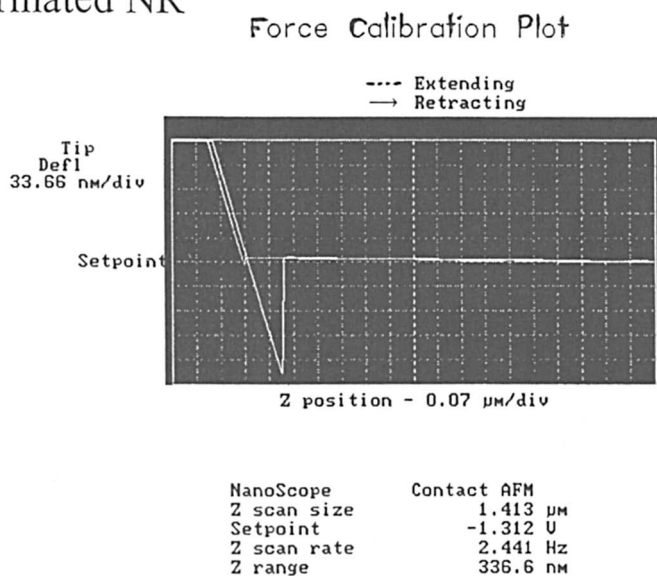
Figure 1. Continued

(a) PMMA
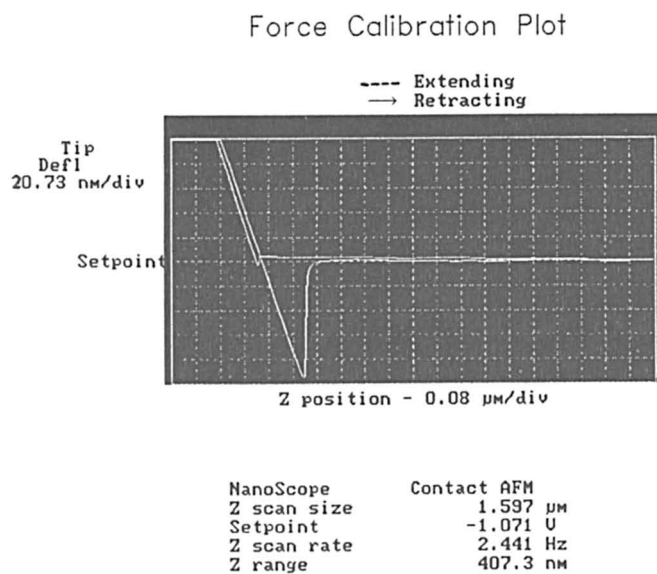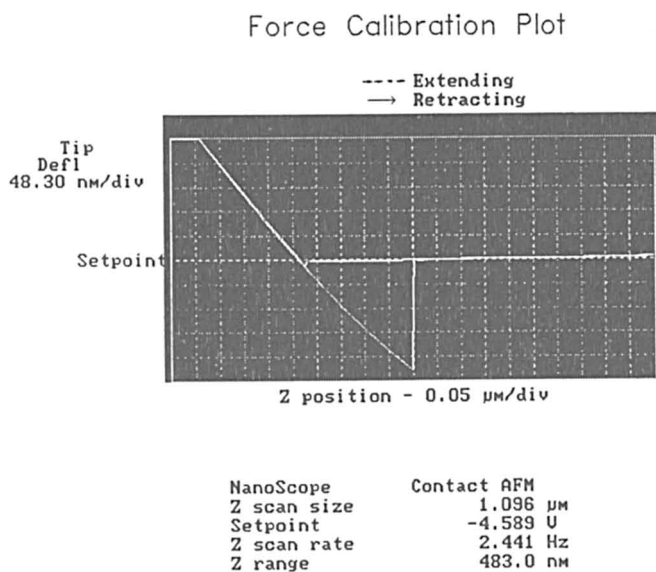
Figure 2. Force-distance curves between the unmodified Si₃N₄ probe-tip and (a) PMMA and (b) PS latex films.

dependent on the nature of the sample polymer material. A high pull-off force is associated with the NR film surface (165 $\pm$ 2 nN), a low T_g, soft and tacky polymer at ambient temperature, in contrast to the rather low pull-off force (27 $\pm$ 5 nN) observed for the hard PMMA latex film with a T_g of 126 °C. The pull-off force for the PS film at 50 $\pm$ 8 nN, is intermediate between those for the NR and PMMA films. The T_g for PS is 105 °C.

The pull-off force for the NR latex film decreased immediately upon chlorination, from 165 $\pm$ 2 nN for the control to $\sim$ 54 $\pm$ 9 nN for the NR latex film chlorinated at a chlorine dosage of 250 ppm (see Figure 3). The pull-off force after the initial drop remained essentially constant when the chlorine dosage was further increased to 2000 ppm. There is a close correlation of the pull-off forces with chlorination as compared with those of the water contact angle on a chlorinated NR latex film surface reported by us previously (15). Both exhibit a steep drop initially followed by a constant value with further chlorination. The hydrophilicity of the film surface increased with the extent of chlorination (15). There is a corresponding increase in the surface mean roughness with an increase in the extent of chlorination (Figure 3). This has given rise to a wide scattering of the pull-off forces of the chlorinated NR films (see histograms in Figure 4), especially at high chlorine dosages (from 750 to 2000 ppm) associated with an increase in surface mean roughness at high chlorine dosage as a result of surface cracking and hence roughening. In comparison, the spread of the pull-off forces for the control sample of unchlorinated NR film was narrow and centred around 160 nN. As pointed out previously, chlorination causes hardening and roughening of the film surface and these have resulted in a lowering of the pull-off force of the chlorinated NR. Roberts and Blackley (18,19) also found that the reduction in the areas of contact of the chlorinated surface with another surface and surface hardening are factors that contribute to a reduction in surface friction.

The above observation is further confirmed by a slight decrease in the pull-off force of vulcanized NR latex film shown in Figure 5b. The pull-off forces of the vulcanized NR film spread over a range, from 110 to 170 nN, compared with those for the unvulcanized NR. Most of these are centered around 160 nN which still bears a strong resemblance to NR characteristics. This value is certainly still much greater than those of the PMMA and PS with a much higher T_g. It is obvious that sulfur vulcanization hardens the rubber but is insufficient to completely eliminate its tackiness. Thus, vulcanized rubber has to be further treated, as in the case of the rubber gloves, by powdering with cornstarch or chemically by chlorination or polymer coating, to become donnable. The vulcanized NR film surface is for the most part essentially smooth and structureless except for some small shallow depressions as shown in Figure 6a.
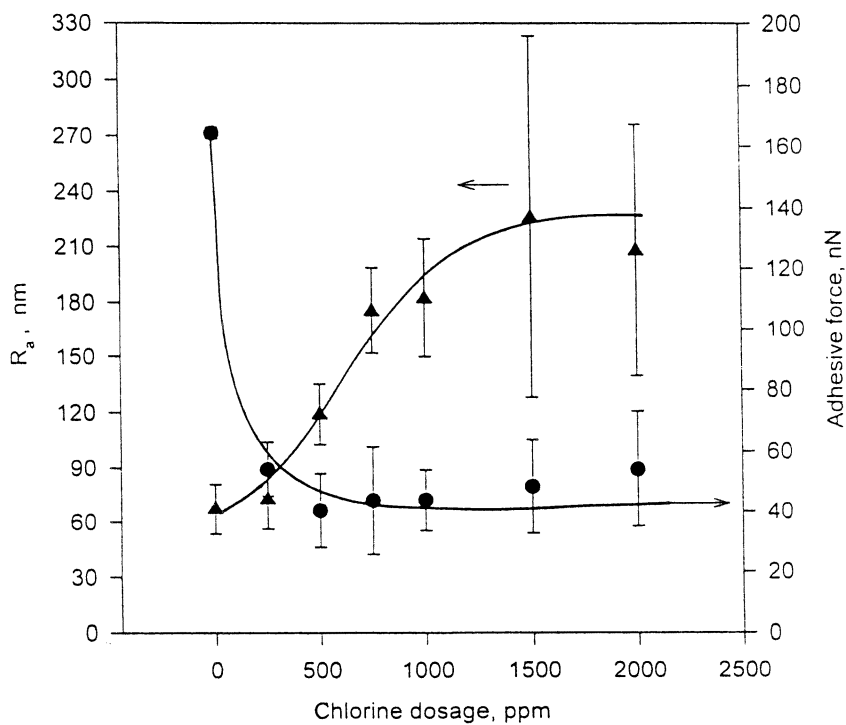
Figure 3. Variation of adhesive forces (pull-off forces) (●) and surface mean roughness (▲), R_a, of NR latex films as a function of chlorine dosage.

Mareanukroh et al. (*31*) showed that the force-distance curves were sensitive to the cross-link density of a styrene-butadiene elastomer. The penetration distance of the surface by the AFM tip decreased with an increase in the cross-link density of the rubber and the maximum force varied from 500 nN to 700 nN over the cross-link density range of 4×10^{-5} mol cm^{-3} to 5×10^{-4} mol cm^{-3}. The experimental values of force per square of distance penetrated vs. cross-link density were in close agreement with those calculated from the cross-link density data and the half-angle of the conical probe tip.

The reduction in the pull-off forces for the powdered NR rubber glove surface as compared to untreated NR latex film is marginal, but the spread of these forces is rather wide (Figure 5c). Two populations of pull-off forces are discernible, one centered around 175 nN corresponding closely to that for NR film and another at slightly lower value. SEM reveals that the film surface was covered by polydisperse corn starch particles (Figure 6b). The substrate surface of the NR film appears smooth and featureless. It would appear that the two populations of pull-off forces are due to NR and the starch particles on the surface, respectively.

In comparison, the reduction in adhesive force for the above surfaces is much smaller than those of the commercial NR glove surfaces as shown in Figure 5d-5f. Commercial glove samples from three different manufacturers were examined: sample A is a powder-free polymer-coated surgeon's glove, sample B a powder-free polymer-coated examination glove, and sample C a powder-free polymer-rinsed examination glove. Different extents of reduction of the pull-off forces compared with NR latex films are evident: a polymer-coated glove (sample A) appeared to be the most effective in reducing the surface adhesive force with a pull-off force of only 49 ± 17 nN. The spread of the pull-off forces for this sample was also the smallest among the three commercial gloves (Figure 5d). The magnitude of the pull-off forces was in the same range as those by chlorination and polystyrene. SEM reveals cracks on the donning surface of glove sample A, resembling the effect of chlorination (Figure 6c). This glove seems to have been completely coated by the polymer. The polymer layer cracks in most areas and appears rather rough. The pull-off forces for the donning surface of sample B (Figure 5e) spread over a very wide range of 45 to 135 nN. In addition, the donning surface (Figure 6d) appears very flaky and a lot more uneven compared to that of sample A. On the other hand, glove sample C gives pull-off forces in the range of 50-150 nN and is bimodal (Figure 5f). The morphology of the surface of glove sample C (Figure 6e) is relatively even with patches of flat and smooth regions, some of which are rather big, which points to a rather poor coating with exposed NR substrate. Again, the non-uniformity in the surface coverage and the uneven topography cause the wide scattering of the pull-off forces of these commercial gloves. It would appear that the magnitude and the spread of the pull-off forces are strongly dependent on the nature of the
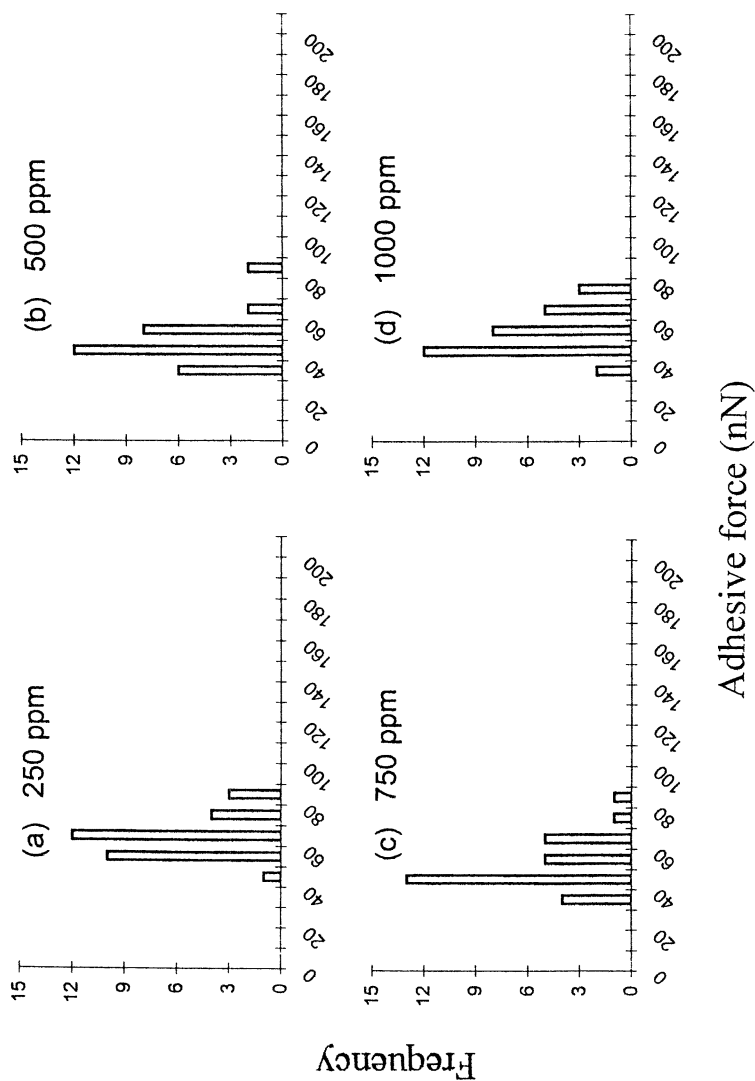
Figure 4. Histograms of pull-off forces measured between unmodified Si_3N_4 probe-tip and chlorinated NR latex films at (a) 250 ppm, (b) 500 ppm, (c) 750 ppm, (d) 1000 ppm, (e) 1500 ppm, and (f) 2000 ppm of chlorine. Continued on next page.
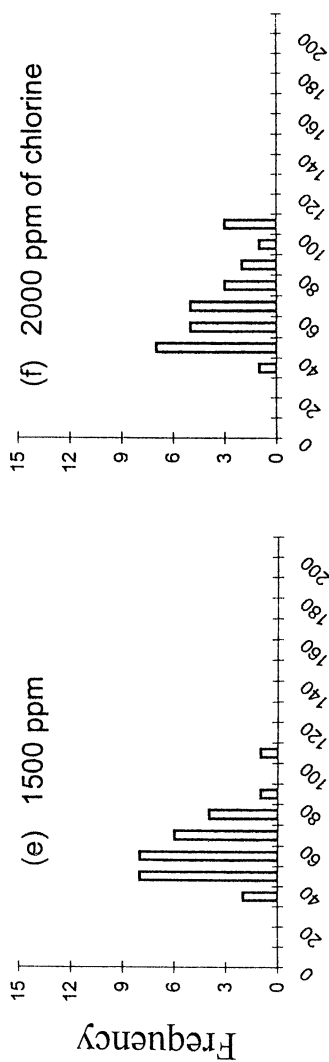
Figure 4. Continued
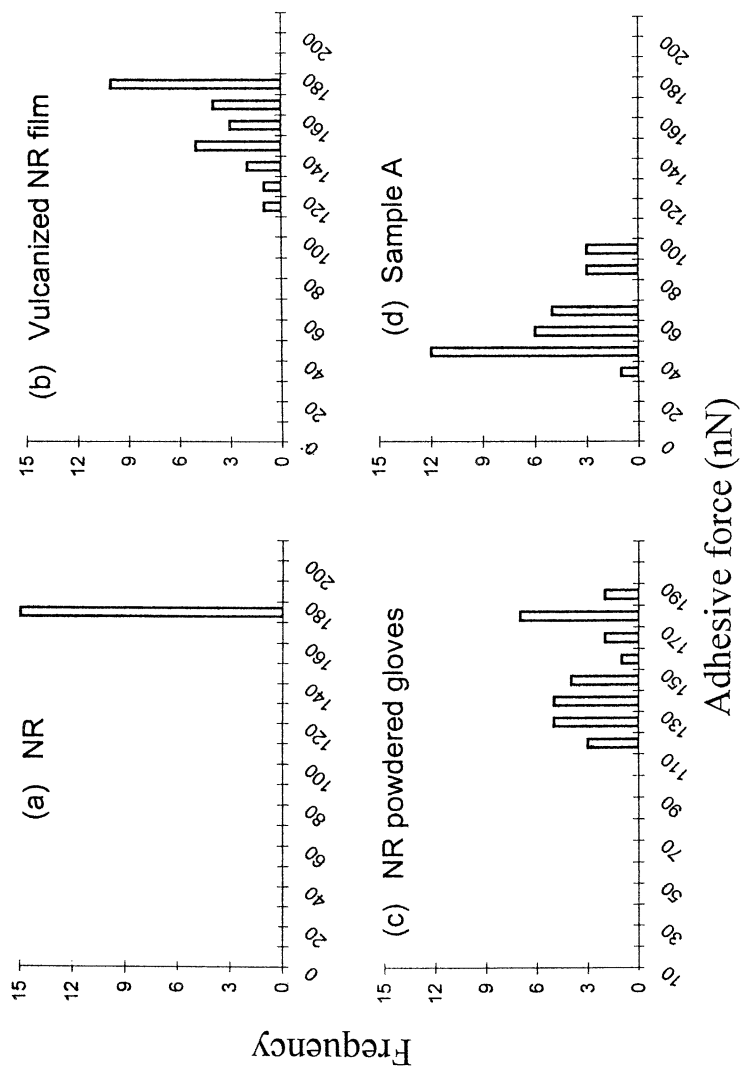
Figure 5. Histograms of pull-off forces measured between unmodified Si_3N_4 probe-tip and (a) untreated, (b) vulcanized, and (c) powdered NR latex gloves, and the donning surfaces of (d) glove sample A, (e) glove sample B, and (f) glove sample C. Continued on next page.
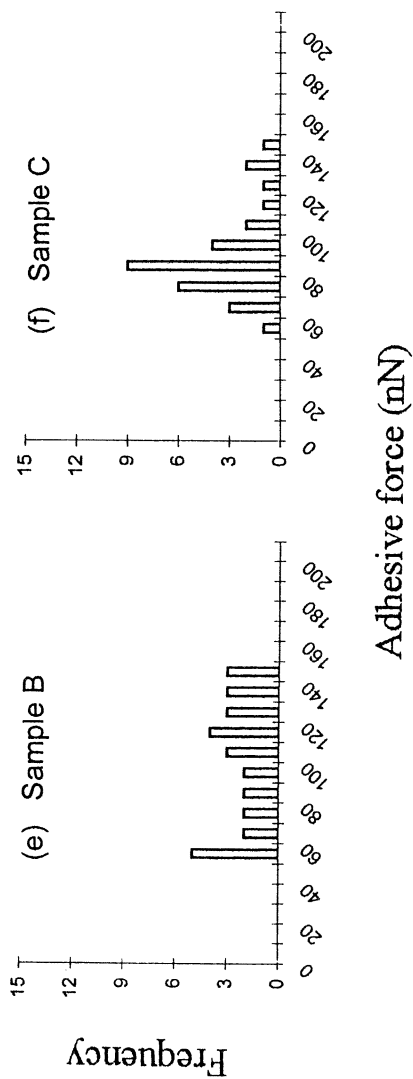
Figure 5. Continued

(a) vulcanized NR

(b) powdered glove

(c) sample A
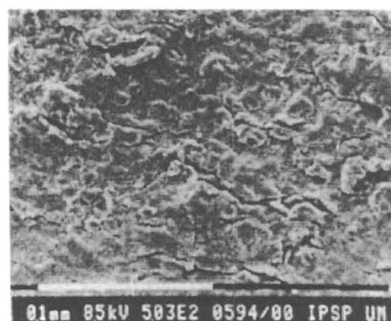
(d) sample B
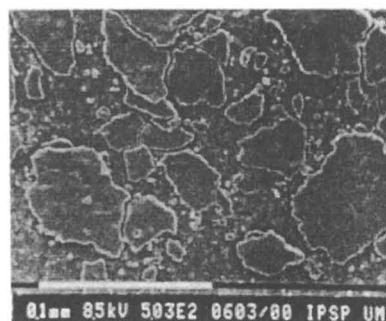
(e) sample C

Figure 6.   SEM micrographs of (a) vulcanized and (b) powdered NR latex glove surfaces, and the donning surfaces of (c) glove sample A, (d) glove sample B, and (e) glove sample C.

coating material used, the efficiency of the coating process and the topography of the coating. Of the five surfaces studied, only the vulcanized and powdered NR gloves show predominately NR characteristics.

Our results are in general agreement with those observed by Feldman et al. (26) that the adhesive force varies with the chemical nature of the polymer surface. Roberts and Blackley (17,19) reported a decrease in the coefficient of friction of halogenated NR surfaces, starch-powdered, and coated glove surfaces against wavy-glass and fingertip skins as compared with the control NR surface. The adhesive pull-off forces of the present study complement the results on coefficients of friction by Roberts and Blackley (17,19) obtained from macroscopic experiments and are summarized in Table I.

Table I. Comparison of Surface Tackiness Assessed by Different Techniques for Various Types of NR and Synthetic Latex Film Surfaces

Surface Type	Adhesive force (nN)[1]	Coeff. Friction[2]
Untreated NR	165 ± 2	1.60
Vulcanized NR	148 ± 7	-
Chlorinated NR	54 ± 9	0.47
Flourinated NR	-	0.41
Brominated NR	-	0.30
Starch-powdered NR	138 ± 23	0.35
Hydrogel-coated NR glove	-	0.13
NR Glove[3] sample A	47 ± 17	-
NR Glove[3] sample B	92 ± 32	-
NR Glove[3] sample C	81 ± 22	-
PMMA	27 ± 5	-
PS	50 ± 8	-

[1] pull-off forces measured between Si_3N_4 probe and sample polymer surface.
[2] coefficient of friction for fingertip skin against rubber sample surface.
[3] value refers to that obtained for the donning side of the glove.

Conclusions

The adhesive forces of various NR latex film types were measured using a SFM for the first time. The results demonstrate clearly that the magnitude of the pull-off forces is strongly dependent on the chemical composition of the surface of the polymeric material and the physical nature of the surface. The spread of the pull-off forces of a particular surface is influenced by the surface roughness

and homogeneity in surface composition. The technique is sensitive to chemical composition as reflected by the very distinctive adhesive force range for soft (NR) and hard (PMMA) polymers that were obtained. The very different magnitudes of the pull-off forces of the different surfaces allow their differentiation by this technique. The topographical changes due to surface roughening and hardening following a chemical reaction such as chlorination of the NR films resulted both in a change in magnitude of the pull-off forces as well as a spread of the force. Such information has afforded a rapid means of assessing the extent and effectiveness of the reaction and hence the morphology-performance relation of the film.

This study reaffirms that powdering a glove surface to reduce tack and surface friction may be the simplest procedure, but is by no means effective. In addition, it is beset with adverse health effects to users such as allergic reactions, foreign body reactions, and irritation. For example, glove powder has been shown to be a carrier of airborne allergens (*32*). As a particulate matter, glove powder can cause foreign body reactions, resulting in inflammation, granulomas, and adhesions of the peritoneal tissues after surgery (*33-36*). Glove powder may serve as an adsorbent or absorbent for unbound chemicals that may be irritants or chemical contact sensitizers. It was also reported that glove powder from a non-sterile examination glove may support microbial growth and act as a carrier for endotoxins (*37*). In view of the above, the usage of powdered gloves for medical purpose in advanced countries is slowly being phased out. The present results also show that chlorination can effectively reduce the tack and adhesion of NR film surfaces. The morphology of commercial glove surfaces resembles the rough and hardened surface of chlorinated gloves, in addition to being flaky, the direct results of polymer coating and chlorination or both. Our findings are in general agreement with the observations of Frisbie (*27*), Green (*28*) and Overney (*29, 30*) on the effect of the chemical nature and topography on adhesion between surfaces. It is possible, at least from a fundamental consideration, that a powder-free non-chlorinated rubber glove with good donnability could be within easy reach given the right chemical composition of the coating material possessing the right surface morphology when introduced on top of the NR substrate.

In addition, in spite of all the issues discussed above, NR gloves are still superior to some synthetic gloves in regards to the barrier properties (*38*). It was found that, in particular, NR surgeon's and patient examination gloves have more effective and durable barrier qualities compared to vinyl gloves (*39-40*).

Acknowledgment

References

1. Archer, B. L.; Barnard, D.; Cockbain, E. G.; Dickenson, P. B.; McMullen, A. I. In *The Chemistry and Physics of Rubber-like Substances*; Bateman, L., Ed.; Wiley: New York, 1963; p. 41.
2. Ho, C. C.; Kondo, T.; Muramatsu, N.; Ohshima, H. *J. Colloid Interface Sci.* **1996**, *178*, 442.
3. *Natural Rubber-containing Medical Devices: User Labelling*; Federal Register, Sept 30, 1997, **62** 51021, Food and Drug Administration.
4. Ho, C. C.; Khew, M. C. *Langmuir* **2000**, *16*, 2436.
5. Gazeley, K. F.; Gorton, A. D. T.; Pendle, T. D. In *Natural Rubber Science and Technology*; Roberts, A. D., Ed.; Oxford University Press: Oxford, U.K.; 1989; p. 63.
6. *Surgeon's and Patient Examination Gloves: Reclassification*; July 30, 1999, **64** 41710, Food and Drug Administration.
7. Kekwick, R. G. O. *Proceedings Latex Protein Allergy: the Present Position*, Amsterdam, The Netherlands, December 1993, Rubber Consultants, p. 21.
8. *The Chemistry and Physics of Rubber-like Substances*; Bateman, L., Ed.; Wiley: New York, 1963.
9. *Natural Rubber Science and Technology*; Roberts, A. D., Ed.; Oxford University Press: Oxford, U.K.; 1989.
10. Ho, C. C.; Subramaniam, A..; Wong, W. S. *Proc. International Rubber Conference* **1976**, *2*, 441.
11. Goh, M. C.; Juhue, D.; Leung, O. M.; Wang, Y.; Winnik, M. A. *Langmuir* **1993**, *9*, 1319.
12. Perez, E.; Lang, J. *Macromolecules* **1999**, *32*, 1626.
13. Porter, M. *Preprint: International Rubber Conference,* Manchester, England, June 1996.
14. Ho, C. C.; Khew, M. C. *Langmuir,* **1999**, *15*, 6208.
15. Ho, C. C.; Khew, M. C. *Int. J. Adhesion & Adhesives* **1999**, *19*, 387.
16. Noakes, T. C. Q. *Proc. Inter. Rub. Tech. Conf.* 1988, p. 288.
17. Roberts, A. D.; Brackley, C. A. *J. Nat. Rubb. Res.* **1989**, *4*, 1.
18. Roberts, A. D.; Brackley C. A. *Rub. Chem. Tech.* **1990**, *63*, 722.
19. Roberts, A. D. *Adhesive Preprint, European Conf.* France, 1994, p. 309.
20. Romberg V. G. *ACS, (Rubber Division) Spring Meeting*, 1986.
21. Khew, M. C. Ph.D. Thesis, University of Malaya, Kuala Lumpur, 1999.
22. Cleveland, J. P.; Manne, S.; Bocek, D.; Hansma, P. K. *Rev. Sci. Instrum.* **1993**, *64*, 403.
23. GTE Sylvania, Towanda, PA, USA..
24. Binnig, G.; Quate, C. F.; Gerber, Ch. *Phys. Rev. Lett.* **1986**, *56*, 930.
25. Florin, E. L.; Moy, V. T.; Gaub, H. E. *Science* **1994**, *264*, 415.
26. Feldman, K.; Tervoort, T.; Smith, P.; Spencer, N. D. *Langmuir* **1998**, *14*, 372.

27. Frisbie, C. D.; Rozsnyai, L. F.; Noy, A.; Wrighton, M. S.; Lieber, C. M. *Science* **1994**, *265*, 2071.
28. Green, J. B. D.; McDermott, M. T.; Porter, M. D. *J. Phys. Chem.* **1995**, *99*, 10960.
29. Overney, R. M.; Meyer, E.; Frommer, J.; Guntherodt, H. J. *Langmuir* **1994**, *10*, 1281.
30. Overney R. M.; Leta, D. P. *Tribol. Lett.* **1995**, *1*, 247.
31. Mareanukroh M.; Hamed, G. R.; Ery, R. K. *Rubb. Chem. Tech.* **1996**, *69*, 801.
32. Heilman D., Jones R., Swanson M., Yunginger J. *J. Allergy Clinical Immunol.* **1996**, *98*, 325.
33. Ellis, H. *Surgery, Gynecology & Obstetrics*, **1990**, *171*, 521-527.
34. Edlich, R. *J. Emergency Medicine* **1994**, *12*, 69-71.
35. Hunt,T.; Slavin, J.; Goodson, W. *Archives Surgery* **1994**, *129*, 825.
36. Luijendijk, R.; deLange, D.; Wauters, C.; Hop, W. *Annals Surgery* **1996**, *223*, 242.
37. Williams, P.; Halsey, J. *Annals Allergy, Asthma and Immunology* **1997**, *79*, 303.
38. Rabussay, D.; Korniewicz, D. *AORN J.* **1997**, *66*, 1043-1063.
39. Korniewicz, D., *Immunology Allergy Clinics N. America* **1995**, *15/1*, 123.
40. Korniewicz, D.; Kirwin M.; Cresci, K. *Heart & Lung* **1992**, *21*, 81-84.

Chapter 18

Microencapsulation of Fine Titanium Dioxide Powders from (S/O)/W Emulsion with Subsequent Solvent Evaporation

Anchali Supsakulchai, Guang-Hui Ma, Masatoshi Nagai, and Shinzo Omi

Graduate School of Bio-Applications and Systems Engineering, Tokyo University of Agriculture and Technology, Koganei, Tokyo 184-8588, Japan

Anatase-type titanium dioxide (TiO_2) was encapsulated using conventional homogenizer and also by applying the glass membrane emulsification technique followed by solvent evaporation process. Fine powders of anatase TiO_2 were dispersed in poly(styrene-co-acrylic acid)–toluene solutions, and the suspension was redispersed in an aqueous phase containing dissolved poly(vinyl alcohol) and sodium dodecyl sulfate. Disperbyk-111 and 180 (BYK Chemie) were good stabilizers for TiO_2 in the polymer/toluene solution. A Shirasu porous glass (SPG) membrane (pore size of 1.42, 5.25, and 9.5 µm) was used for membrane emulsification. The (S/O)/W emulsion was gently stirred in a sealed reactor, and the solvent was evaporated under moderate heating with an increasing vacuum.Microcapsules of several microns diameter containing 10-20 wt% of TiO_2 were prepared. The glass membrane emulsification process failed to yield uniform capsules due to some wetting problems. The photo-oxidation performance of the encapsulated TiO_2 powders was also shown in this work.

260　　　　　　　　　　　© 2002 American Chemical Society

Titanium dioxide, TiO_2, non-toxic as well as biologically and chemically inert, has been applied extensively as white pigments as well as photoactive catalysts. In the past decade, extensive literature indicates applications of anatase TiO_2 for the photo-oxidation of dilute halocarbon contaminants in water to the final products comprising inorganic species such as carbon dioxide and halogen ions (1-3). Encapsulation of inorganic powders in a polymer shell has presently been of interest in many applications, such as cosmetics, pharmaceuticals, agriculture, and paints (4). For example, magnetite microcapsules can be used in drug delivery and diagnosis (5-6), while TiO_2 microcapsules can be used as photo-oxidation catalysts, and pigments for cosmetics and paints.These microcapsules can be prepared from (solid-in-oil) in water, (S/O)/W, emulsions by evaporating the solvent in the oil phase. However, uniform-sized microcapsules will be difficult to obtain by employing conventional mixing devices such as stirred vessels and homogenizers. A particular glass membrane called Shirasu porous glass (SPG) has a narrow pore size distribution and is capable of preparing uniform O/W emulsion droplets by pushing through the organic phase into an aqueous phase (7). A variety of uniform polymer particles have been formed by preparing uniform monomer droplets followed by the suspension polymerization (8-11). A major concern which may be raised for the employment of the glass membrane technique to (S/O)/W emulsification is plugging of the pores by the suspended powders in the oil phase. Another possibility is a wetting of the hydrophilic membrane because the oil phase contains normally hydrophilic inorganic powders and stabilizers to promote stable and fine dispersion of the powders in the oil phase. Once the membrane is wet with the oil phase, the formation of uniform droplets is no longer guaranteed. Despite these obstacles, it is a worthwhile challenge to extend the capability of glass membrane technique to the (S/O)/W emulsion. In this paper, a conventional homogenizer was employed at first for selection of the oil phase stabilizer, investigation of the O/W phase ratio, allowable TiO_2 ratio, and so on. Characteristics of TiO_2 microcapsules prepared by two methods are compared. The photo-oxidation performance of encapsulated TiO_2 under ultraviolet (UV) irradiation is also investigated.

Experimental

Materials

Anatase titanium dioxide powders (TiO_2, average size of the primary particle = 50 nm), generously provided by Fuji Titanium Co. Ltd., were used as core materials. Poly(styrene-co-acrylic acid) (PS-AA) (96/4, M_w = 45,400 g/mol and M_w/M_n = 5.53) was synthesized in our laboratory by thermal bulk

polymerization and used as the shell polymer. An oligomer incorporating acid group, Disperbyk-111 (acid value = 129 mg KOH/g, M_n= 670 g/mol, M_w/M_n = 2.07) and a block oligomer of alkyl ammonium salt incorporating acid group, Disperbyk-180 (amine value and acid value = 95 mg KOH/g, M_n = 650 g/mol, M_w/M_n = 2.68), generously provided by BYK Chemie, Germany, were used as oil phase stabilizers for the TiO_2 powders. Toluene (Kishida Chemical Co., Ltd.), n-hexadecane (Tokyo Chemical Industry), 1-hexanol (Tokyo Chemical Industry), and methyl laurate (Tokyo Chemical Industry) were all reagent grades. The latter three solvents were added to the oil phase to promote the hydrophobicity and also for the modification of surface morphology of the microcapsules. Methanol (Kishida Chemical Co., Ltd.) was a commercial grade. Sodium dodecyl sulfate (SDS) (Merck Co., Ltd.), a biochemical grade, was used as surfactant together with poly(vinyl alcohol) (PVA) (Kuraray, PVA-217, DP=1700, 88.5% hydrolyzed), used as a protective colloid. Methylene blue [3,4-bis(dimethylamino)-phenothiazine-5-thionium chloride] (MB) (Kanto Chemical Co.) was used as a chemical substrate to investigate the photo-oxidation performance of the TiO_2 microcapsules. Aqueous solution of hydroperoxide at 31 wt% (Kanto Chemical Co.) was used as an oxygen source for the photo-oxidation reaction. All chemicals and solvents were used as received without further purification unless mentioned.

Preparation of TiO$_2$ Microcapsules

TiO_2 microcapsules were prepared by a solvent evaporation method of a (S/O)/W emulsion prepared using either a conventional homogenizer (Ace Homogenizer, Nissei Co., Ltd.) or a SPG membrane (Ise Chemical Co.). The oil phase of S/O emulsion was composed of 10 or 20 g toluene dissolving 5 wt% of PS-AA, 0.3-1.7 wt% of Disperbyk-111 or 180 (based on toluene), and 15 wt% of the oil phase additive (based on toluene). TiO_2 powder (weight ratio to PS-AA =1:10 or 1:5) was added in the oil phase, and the suspension was first mixed using the homogenizer at 10000 rpm for 25 min, followed by sonification for another 20 min. For example, the oil phase of Run 530 contains 0.1 g of TiO_2 powder and 0.5 g of PS-AA in 10.0 g of the total weight. Then the oil phase was homogenized or forced through the pores of a glass membrane into the aqueous solution dissolving 3.0 wt% of PVA and 0.3 wt% of SDS to obtain the (S/O)/W emulsion. The homogenizing time was varied (5, 15, or 30 min) depending on each individual run. Different membrane pore sizes of 1.42, 5.25, and 9.5 μm were used. The resulting (S/O)/W emulsion droplets were characterized using an optical microscope (Olympus BHC), then transferred to a reactor, followed by solvent evaporation at a moderate temperature 60 °C and reduced pressure. The agitation rate was 100 rpm for the emulsion prepared by the membrane

emulsification, and 150 rpm for those obtained by the homogenizer. A steam stripping process was further carried out to ensure complete toluene removal from the polymer shell. The microcapsules were separated from the serum by centrifugation at 3000 rpm, then washed repeatedly with methanol, dried under vacuum at room temperature, and stored in a desiccator for further analyses.

Analyses

Droplet and Microcapsule Size Measurements

An optical microscope equipped with a camera (Olympus DP-10) was used to observe the average diameter of the droplets. Similarly, scanning electron microscope (SEM) (JEOL, JSM-5310, acceleration voltage = 15 kV) was used to examine the general features of the microcapsules as well as the average particle size. Diameters of about two hundred droplets and microcapsules were measured from the photographs to calculate the average diameter and size distribution. The size distributions of droplets and microcapsules were expressed in terms of coefficient of variation, CV, which is defined as

$$CV = [\Sigma(d_i - d)^2/N]^{1/2}/d \times 100 \tag{1}$$

where d_i is the diameter of the ith droplet or particle, d is the average diameter, and N is the total number of droplets or particles counted.

Encapsulation Loading

The encapsulation loading was determined by incineration of the polymer using a Bunsen burner and a ceramic crucible. Meanwhile, the percentage of encapsulated TiO_2 was calculated from the weight of TiO_2 remaining after incineration divided by its theoretical loading calculated from the formulation.

Photo-oxidation Performance of TiO₂ Microcapsules

The photo-oxidation performance of the microcapsules was measured by examining the decomposition of MB under ultraviolet (UV) irradiation using an 8 watt UV lamp (UVLMS-38, 365 nm, UVP INC, USA) as a UV light source. In a 100 mL glass flask, a weighed sample of free TiO_2 powder or microcapsules was added into a mixture of 10 mL of 1 mg/mL of standard MB aqueous solution, 35 g of distilled-deionized (DDI) water and 5 g of 31 wt%

hydroperoxide solution. Then the suspension was gently stirred using a magnetic stirrer. The lamp was placed 5 cm above the 100 mL glass flask with a stopper. Two flasks were placed on a 6-center magnetic stirrer and irradiated in parallel. A digital double beam spectrophotometer (UVIDEVC-310,320, Jasco) equipped with tungsten lump as a light source was used for analysis. All experiments and measurements were carried out at room temperature.

Results and Discussion

Emulsion Droplets and Microcapsules Obtained by the Conventional Homogenizer

(S/O)/W emulsion droplets having 2.5-6 μm diameters and 20-36 % coefficients of variation were obtained using the homogenizer at an agitation rate of 2000 rpm for 5, 15, or 30 min, depending on each individual experimental run. Evaporation of toluene yielded solid spherical TiO_2 microcapsules having 1-3 μm diameters and 20-30 % coefficients of variation. The shrinkage in diameter was due to removal of the toluene during the solvent evaporation process. Disperbyk-111 and 180 stabilized the TiO_2 powders well in the oil phase, as well as during the encapsulation process. The average diameter of the emulsion droplets tended to decrease as a function of the homogenizing time and reached the equilibrium diameter after 15 min of homogenization. The same trend was also observed for the microcapsules. Figure 1 shows general features of the microcapsules prepared without any oil phase additives in the oil phase. The TiO_2 particles are well covered by the PS-AA copolymer. No noticeable amount of unencapsulated TiO_2 was observed on the surface.

Effect of the Various Oil Phase Additives on Morphologies of the TiO_2 Microcapsules

Three different types of oil phase additives, n-hexadecane (δ = 7.9 $(cal/cm^3)^{1/2}$) (12), 1-hexanol (δ = 10.7 $(cal/cm^3)^{1/2}$) (12), and methyl laurate (δ = 8.8 $(cal/cm^3)^{1/2}$) (13), were added to the recipe to observe any changes in the surface morphology of the microcapsules. Figure 2 shows the effect of the additives on the microcapsule surface morphologies. The presence of the oil phase additive caused changes on the surface due to various degrees of phase separation mainly depending on the solubility parameter value of each additive corresponding to those of PS-AA (δ = 9.5 $(cal/cm^3)^{1/2}$) (12) and toluene (δ = 8.9 $(cal/cm^3)^{1/2}$) (12). The surface features changed from several indentations to unevenness after the additive was extracted by washing with methanol. Without
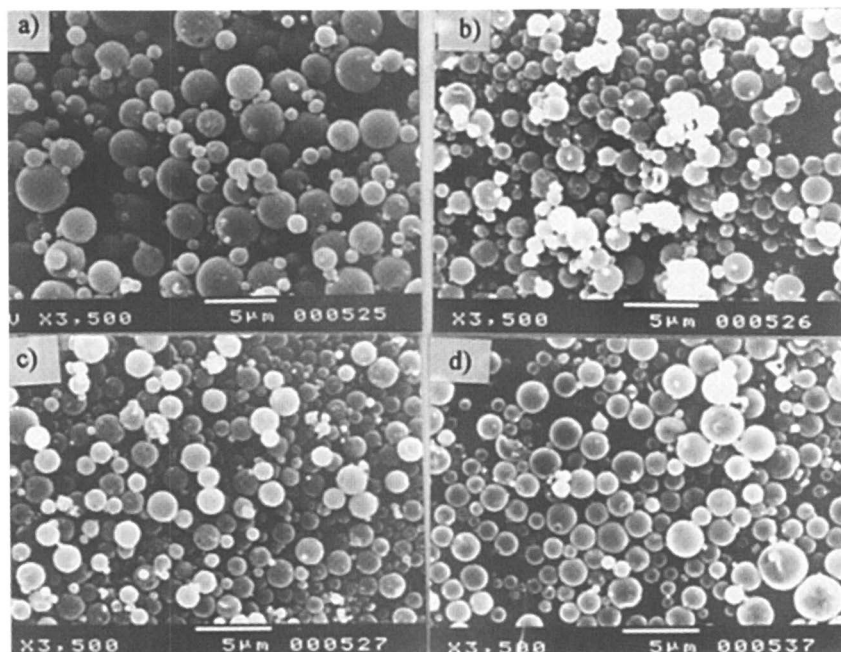
Figure 1. General features of TiO$_2$ microcapsules prepared using the homogenizer: (a) Run 525: 5 min homogenization, $(d_N)_p$ 2.23 μm, CV 36.70 %, TiO$_2$/PS-AA 1:4.6, Disperbyk-111; (b) Run 526: 15 min homogenization, $(d_N)_p$ 1.30μm, CV 32.25 %; TiO$_2$/PS-AA 1:4.6, Disperbyk-111 ; (c) Run 527 : 30 min homogenization, $(d_N)_p$ 1.07 μm, CV 33.24 %, TiO$_2$/PS-AA 1:4.6, Disperbyk-111; (d) Run 537: 5 min homogenization, $(d_N)_p$ 1.34 μm, CV 39.30 %, TiO$_2$/PS-AA 1:9, Disperbyk-180.
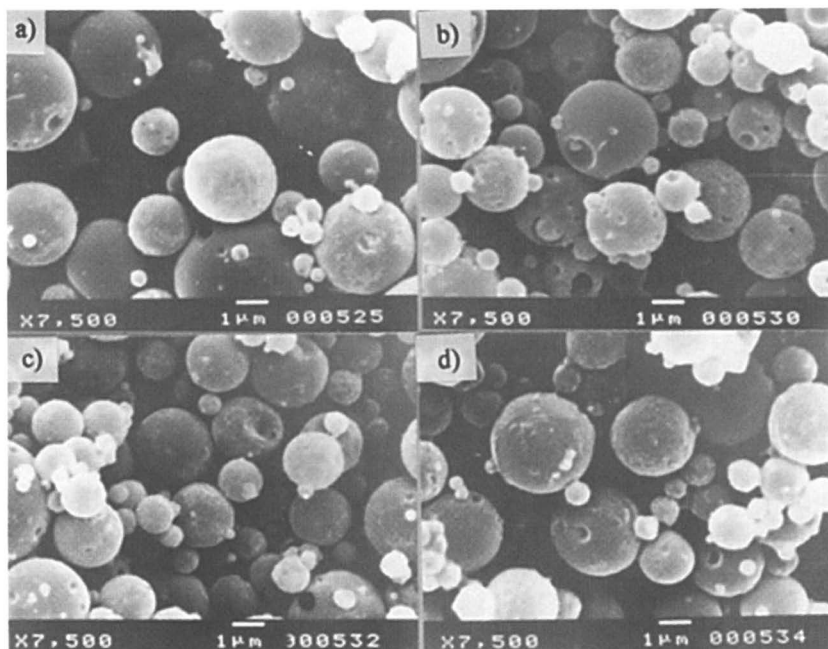
Figure 2. Effect of the oil phase additive on the surface features of TiO$_2$ microcapsules prepared with 5 min homogenization using Disperbyk-111: (a) Run 525 : No additive, $(d_N)_p$ 2.23µm, CV 36.70 %, TiO$_2$:PS-AA 1:4.6 ; (b) Run 530: n-hexadecane, $(d_N)_p$ 1.76µm, CV= 41.0 %, TiO$_2$:PS-AA 1:4.79 ; (c) Run 532: 1-hexanol, $(d_N)_p$ 1.82µm, CV 39.0 %, TiO$_2$:PS-AA 1:4.81 ; (d) Run 534: methyl laurate, $(d_N)_p$ 1.73µm, CV 42.0 %, TiO$_2$:PS-AA 1:4.67.

any additives, the surface feature is normally smooth except occasional crater-like indentations as shown in Figure 2(a), which were caused by an outburst of toluene vapor through the highly viscous skin layer in the later stage of solvent evaporation. With the additions of n-hexadecane (Figure 2(b)) and 1-hexanol (Figure 2(c)), phase separation was induced leaving several indentations with rather a sharp edge. Methyl laurate (Figure 2(d)) revealed a rather uneven surface indicating a mild phase separation. From our previous results in suspension copolymerization of styrene and acrylates (11), more porous features were expected by adding hexanol or methyl laurate. However, no drastic change of the surface feature was observed compared with Figure 2(a). By introducing an adequate modification of the surface, the diffusion of chemical substrates can be promoted to contact the TiO_2 nucleus during the photo-oxidation, while retaining TiO_2 in the capsules.

Emulsion Droplets and Microcapsules Obtained by Glass Membrane Emulsification Process

Three membrane pore sizes, 1.42, 5.25, and 9.5 μm, were used for the encapsulation. The TiO_2/ PS-AA ratio was kept from 1:5 to 1:10 depending on each experimental run. Disperbyk-180 stabilized the TiO_2 powder sufficiently in the oil phase during the whole emulsification process without seriously plugging up the membrane pores. A constant pressure was maintained during the emulsification process. Regardless of the pore size, the SEM results in Figure 3 show large microcapsules and tiny non-uniform ones in contrast to the uniform polymeric spheres reported by Omi et al. (8-11). The latter are called *daughter droplets* being generated from the break up of the wake that was observed in the initial emulsification stage before the system became opaque. The wake probably was formed from Disperbyk-180 in the oil phase, which tended to wet the membrane with the oil phase rapidly especially in the early emulsification stage, and it was stretched to the limit until smaller droplets started to form, leading to the bi-modal size distribution. The phenomenon continued during the whole process. (More discussion will follow in the next section.) The general linear relationship between the average diameter of the droplets and the membrane pore size was not obtained because of the streak formation and uncontrollable flow rate in some experiments. A rather disappointing correlation will be shown later in Figure 4.

Effect of the Oil Phase Stabilizer on the Size Distribution

The amount of the oil phase stabilizer, Disperbyk-180, overwhelmingly affected the size distribution of the droplets and the microcapsules. Uniform PS-
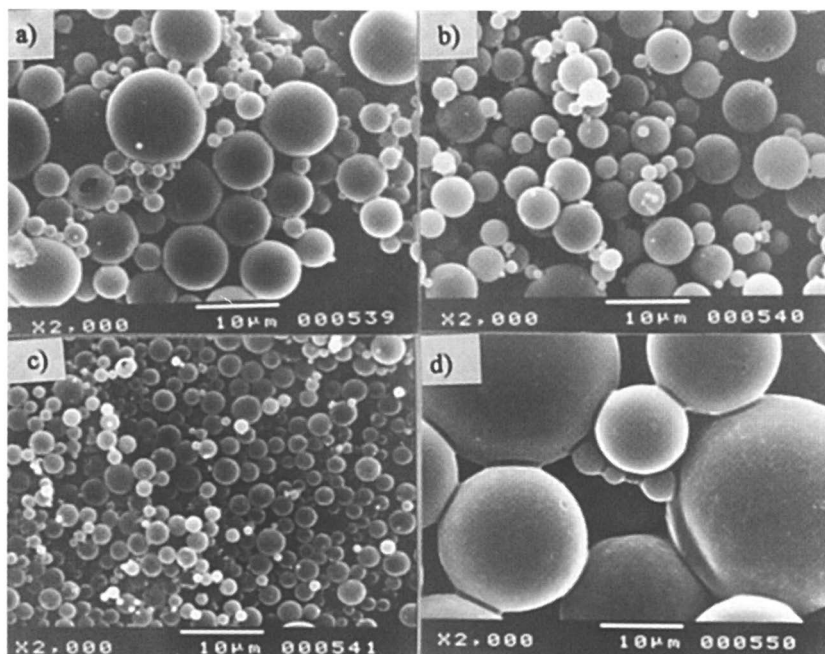
Figure 3. TiO$_2$ microcapsules obtained using different pore sizes of glass membrane: (a) Run 539: pore size 9.5 µm, $(d_N)_p$ 4.45 µm, CV 66.0 %, TiO$_2$/PS-AA 1:9.5; Disperbyk-180 1.5 wt% (based on toluene); (b) Run 540: pore size 5.25µm, $(d_N)_p$ 4.03 µm, CV 39.0 %, TiO$_2$:PS-AA 1:9.5; Disperbyk-180 1.5 wt% (based on toluene); (c) Run541: pore size 1.42 µm, $(d_N)_p$ 2.09 µm, CV 30.0 %, TiO$_2$:PS-AA = 1:9.5; Disperbyk-180 1.5 wt% (based on toluene); (d) Run 550: pore size 5.25 µm, $(d_N)_p$ 19.93 µm, CV 31.0 %, TiO$_2$:PS-AA 1:4.53; Disperbyk-180 0.5 wt% (based on toluene).
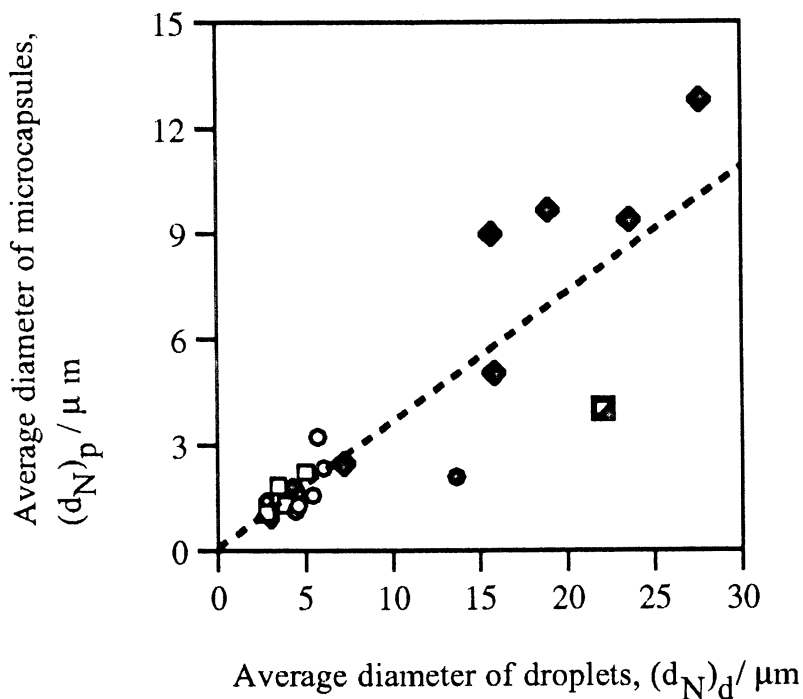
Figure 4. Correlation between the average diameter of TiO₂ microcapsules and their emulsion droplets prepared by the homogenizer and glass membrane emulsification processes: (a) homogenizer: (○) TiO₂/PS-AA 1:9.2; (△) TiO₂/PS-AA 1:4.7; (□) TiO₂/PS-AA 1:4.6; (◇) TiO₂/PS-AA 1:4.8; (b) glass membrane: (■) TiO₂/PS-AA 1:9.51 (9.5μm membrane); (●) TiO₂/PS-AA 1:9:95 (1.42μm membrane); (▲) TiO₂/PS-AA 1:9.97 (5.25 μm membrane); (◆) no TiO₂ ; (c) the broken line (-----) represents the theoretically estimated values for the average diameter of the microcapsules.

AA microspheres ($(d_N)_p$ = 12.8 μm, CV = 14.6 %) were obtained using the glass membrane of 5.25 μm pore size, consistent with the work of Omi et al. (8-11). When 0.3 wt% of Disperbyk-180 was added based on the weight of toluene, PS-AA microspheres having a bi-modal size distribution ($(d_N)_p$ = 5.04 μm, CV = 69.0 %) were obtained. If this distribution was divided into two peaks, one for the main particle, and the other for smaller daughter particles, then the former was 9.37 μm (CV = 12.0 %) and the latter, 2.48 μm (CV = 41.0 %). However, Disperbyk-180 is essential for the stable dispersion of TiO_2 in the oil phase, and cannot be removed from the recipe. Therefore, the oil phase should be modified by either adding an adequate hydrophobic solvent or by tuning the operation conditions more precisely in order to obtain uniform microcapsules. In our recent experiments, it has been revealed that controlling the volumetric emulsification rate along with a strict pressure control is essential to obtain uniform droplets. Inevitably, the emulsification time becomes longer. One last obstacle to be cleared is how to maintain the stability of the oil phase during an over-stretched emulsification process.

Correlation Between the Average Diameters of TiO_2 Microcapsules and their Emulsion Droplets

Figure 4 presents the correlation between the average diameters of TiO_2 microcapsules and their emulsion droplets prepared by the homogenizer and glass membrane emulsification processes. For the microcapsules prepared using the homogenizer, the average diameter of the microcapsules for each individual experimental run is consistent with the theoretically estimated values (broken line in Figure 4) from that of its original droplets. This implied that no serious coagulation or break up of the droplets took place during the solvent evaporation stage. Even an increase of the agitation speed from 150 rpm to 250 rpm still retained this trend. Toluene is removed more rapidly at the higher agitation speed due to an increase in the mass transfer rate. This steady trend ensured the stability of the emulsion droplets during the solvent evaporation process. Since the droplet sizes are reduced as the solvent was evaporated, the total surface area will be also reduced. This will promote a denser coverage of the surface by stabilizer molecules (PVA and SDS), and even excess stabilizer molecules may be released in the bulk phase. This interfacial phenomenon is regarded to have maintained the stability of the droplet during the solvent evaporation process. In contrast, the average diameters of microcapsules prepared by the glass

membrane emulsification process by no means provided a good agreement with the predicted value due to the non-uniformity of the droplets resulting from the wake formation and leading to a possibility of coagulation and/or break up of the droplets during the solvent evaporation process.

Encapsulation Loading of TiO$_2$ Microcapsules

Table I shows the encapsulation loading of TiO$_2$ microcapsules. The encapsulation loadings simply depend on the ratio of core materials, TiO$_2$, to shell polymers, PS-AA. Encapsulation of TiO$_2$ powder was successfully carried out using the homogenizer and about 10-15 wt% TiO$_2$ powder was loaded in the microspheres, at least around 70 wt% of TiO$_2$ powder in the oil phase being encapsulated with PS-AA. From the normally clear surface of the microcapsules observed from SEM photographs, a majority of unencapsulated TiO$_2$ powders were stuck to the agitator blade with PS-AA, and separated from the microcapsules. In contrast, the glass membrane emulsification process, for the present, revealed a somewhat low encapsulation loading because a fraction of TiO$_2$ powders adhered to the membrane surface as well as the SPG module wall. The amount of TiO$_2$ powder adhered to the membrane wall and those remaining in the module can be estimated by weighing dried weights; however, unless they are immediately cleaned up while they are still wet after each experiment, thorough cleaning is technically impossible because of their sophisticated structures. An exact tracing of the unencapsulated TiO$_2$ powders was not pursued for this reason. Besides, the low encapsulation loadings were the result of the streak formation, which occurred during the emulsification, causing the development of non-mature (S/O)/W droplets. As the amount of Disperbyk-180 decreased in Run 550, the streak phenomenon became less noticeable; thus leading to an increase in the encapsulation loading.

Photo-oxidation Performance of TiO$_2$ Microcapsules

Figure 5 illustrates the decomposition profile of MB as a function of UV irradiation time in the presence of the microcapsules as well as free TiO$_2$ powder. TiO$_2$ microcapsules prepared with n-hexadecane (Run 530) were selected to determine their photo-oxidation performance compared to free TiO$_2$ powder. MB conversion using encapsulated TiO$_2$ attained over 90% after 32.3 hours (Figure 5(b)). However, the amount of TiO$_2$ entrapped in the microcapsules is 4.6 times less than that of the free TiO$_2$ employed in the reaction mixture (Figure 5(a)). Encapsulated TiO$_2$ catalysts were easily separated from the reaction mixture by a centrifugal process compared to free TiO$_2$. From the observations
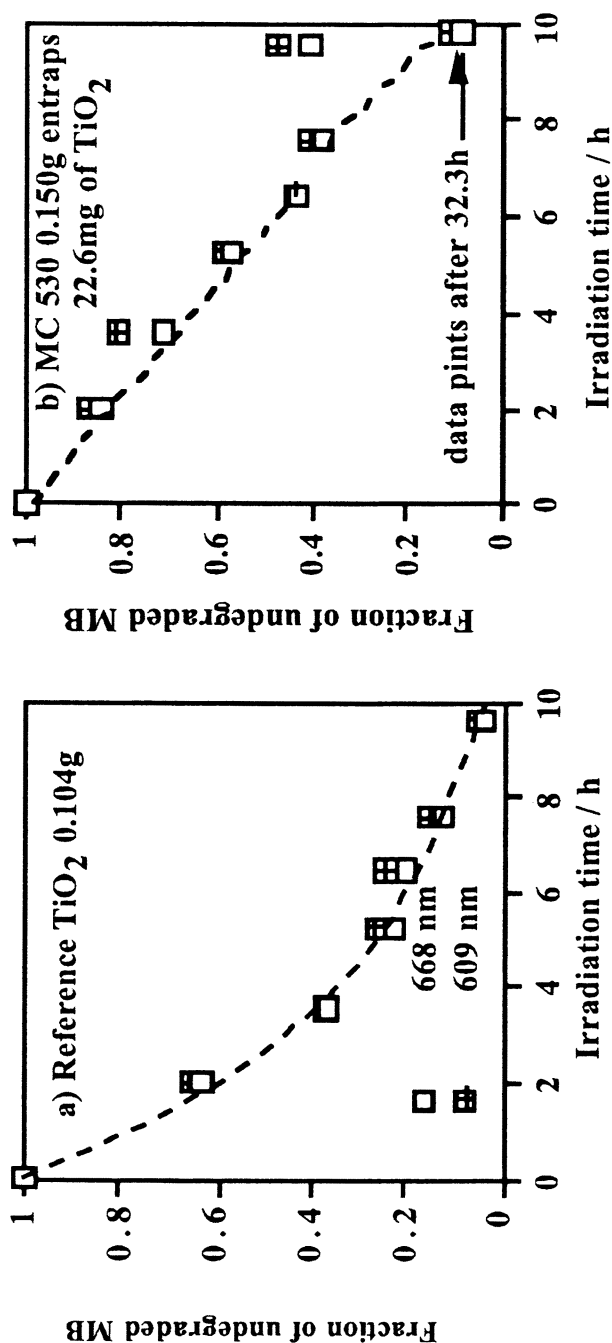
Figure 5. Performance of TiO₂ microcapsules as photo-oxidation catalyst: 10 mg of MB was dissolved in the total 50 g aqueous solution. 1.55 g of hydrogen peroxide was dissolved as an oxygen source. Measured at room temperature. UV source, 8 W and 365 nm, was placed 5 cm above the flask: (a) reference TiO₂ 0.104 g; (b): Microcapsules Run 530 0.150 g entraps 22.6 mg of TiO₂.

of microcapsules by SEM photographs before and after the experiments, the UV irradiated microcapsules remained stable with no serious break-up or leakage of TiO_2 powders and could be used repeatedly. TiO_2 microcapsules were proven to be feasible catalysts for photo-oxidation reactions, and also repeated operations were able to be carried out in the reactor process. Reactors with lower shear field such as packed column or moving-bed type will be recommended for continuous operations and the protection of microcapsules. Uniform size microcapsules are favored for such reactors, and this is a major reason to employ the glass membrane emulsification for its potential to provide uniform particles.

Table I. Encapsulation Loading of TiO_2 Microcapsules

Run No.	Encapsulation Process	TiO_2/ PS-AA	Disperbyk/ TiO_2	$(d_N)_p$ (μm)	Encapsulation %	Encapsulated TiO_2* %
526	H 15 min	1:4.6	0.76:1	1.30	14.20	79.54
525	H 5 min	1:4.6	0.76:1	2.23	14.19	79.45
527	H 30 min	1:4.6	0.76:1	1.07	17.86	100.00
530	H 5 min	1:4.79	0.75:1	1.76	14.97	86.65
532	H 5 min	1:4.81	0.78:1	1.82	13.00	75.53
534	H 5 min	1:4.67	0.88:1	1.73	11.76	66.71
537	H 5 min	1:9	3.0:1	1.34	8.51	85.11
539	M 9.5(μm)	1:9.51	3.24:1	4.45	3.16	33.18
540	M 5.25(μm)	1:9.97	3.30:1	4.03	3.31	36.36
541	M 1.42 (μm)	1:9.95	3.25:1	2.09	4.44	48.67
550	M 5.25(μm)	1:4.53	0.5:1	19.93	10.00	55.30

Note: H = homogenizer; M = glass membrane; Run No. 525, 528, 527, 530, 532, 534: Disperbyk-111; Run No. 537, 539-541, 550: Disperbyk-180; TiO_2/PS-AA and Disperbyk/TiO_2 are presented in weight ratios.

Encapsulation % = (weight TiO_2 (after burning) / sample weight) x 100

* Encapsulated TiO_2 (%) = (weight TiO_2 (after burning) / theoretical weight of TiO_2 in sample) x 100

Theoretical weight of TiO_2 in the sample = (weight of dried sample for burning) x (weight fraction of TiO_2 in the solid)

Theoretical weight fraction of TiO_2 = (weight of TiO_2) / (weight of PS-AA plus TiO_2 in the formulation)

Conclusions

Spherical-shaped TiO_2 microcapsules having diameters of 1-3 µm were successfully prepared with 10-15 wt% of encapsulation loadings depending on the TiO_2/PS-AA ratio. The homogenizer encapsulation method after solvent evaporation provided at least around 70 wt% of TiO_2 powder in the oil phase being encapsulated in the PS-AA copolymer. Meanwhile, the glass membrane emulsification process still remained as a challenge to establish a solid operational control of the TiO_2 encapsulation. The hydrophobicity of the oil phase recipe needs to be modified to reduce the wetting of the membrane during the emulsification process to achieve uniform microcapsules in the future. In our recent experiments, it has become clear that the wake formation can be prevented by controlling the volumetric flow rate of the oil phase pushed through the membrane pores along with a strict control of the pressure. This procedure inevitably prolongs the time of emulsification which leads to the deterioration of the stability of the oil phase. Further experiments are under way to compromise this dilemma. TiO_2 microcapsules were proven to be feasible photo-oxidation catalysts, possibly a reusable catalyst in waste water treatment.

References

1. Pruden, A. L.; Ollis, D. F. *J. Catalyst*, **1983**, *82*, 404-417.
2. Hsiao, C. Y.; Lee, C. L.; Ollis, D. F. *J. Catalyst*, **1983**, *82*, 418-423.
3. Turchi, C. S.; Ollis, D. F. *J. Catalyst*, **1990**, *122*, 178-192.
4. van Herk, A. M. In *Polymeric Dispersions: Principles and Applications*; Asua, J. M., Eds. NATO ASI Series, E535, **1997**; p 435-450.
5. Ugelstad, J.; Mørk, P. C.; Schmid, R.; Ellingsen, T.; Berge, A. *Polymer Int.*, **1993**, *30*, 157.
6. Richard, J. *NATO Advanced Institute on Recent Advances in Polymeric Dispersions* Volume II: June 23-July 5, 1996, Elizondo, Navara, Spain.
7. *Membrane Emulsification, Operation Manual*; Nakashima,T.; Shimizu, M.; Kukizaki, M. Industrial Research Institute of Miyazaki, Miyazaki, Japan, 1991.
8. Omi, S.; Katami, K.; Yamamoto, A.; Iso, M. *J. Appl. Polym. Sci.*, **1994**, *51*, 1-11.
9. Omi, S.; Katami, K.; Taguchi, T.; Kaneko, K,; Iso, M. *J. Appl. Polym. Sci.*, **1995** , 57, 1013-1024.
10. Omi, S. *Colloids and Surfaces, A. Physicochem. & Eng. Asp.*, **1996**, *109*, 97-107.

11. Nuisin, R.; Ma, G. H.; Omi, S.; Kiatkamjornwong, S. *J. Appl. Polym. Sci.,* **2000**, *77*, 1013-1028.
12. *Polymer Handbook*; Brandrup, J.; Immergut, E. H., 3rd Eds.; John Wiley & Sons, NY, 1977; VII/519-557.
13. *Properties of Polymer Correlations with Chemical Structure*; van Krevelen, D. W., American Elsevier Publishing, NY, 1972; p 46, 136-139.

Chapter 19

New Core–Shell Dispersions with Reactive Groups

Hans-Jürgen P. Adler[1], Andrij Pich[1], Axel Henke[1], Carsten Puschke[1], and Stanislav Voronov[2]

[1]Dresden University of Technology, Institute for Macromolecular Chemistry and Textile Chemistry, Mommsenstr. 4, D-01062 Dresden, Germany
[2]State University Lvivska Polytechnika, Bandera Strasse 12, 290646 Lviv, Ukraine

The aim of this work is a new approach to creating polymeric core-shell particles. By means of emulsion polymerization with a reactive peroxidic surfactant ('inisurf') we obtain polymeric nanoparticles with peroxide groups on the particle surface. The polymer chains of shell monomer start growing from the initiator functionality and are finally covalently grafted to the core. The peroxide groups are useful for crosslinking with a matrix polymer. Reactive microgels with good properties for corrosion inhibition and adhesion promotion on aluminum surfaces were obtained via copolymerization with phosphate-containing acrylic monomers.

Polymeric core microspheres and core-shell particles have a large and still growing importance in the past decade for a number of different applications, especially for coatings and adhesives. They are also used in medicine as substrates for biochemical functions.

Core-shell particles are combinations of different, mostly incompatible, polymers. The use of these particles offers the opportunity for introducing

© 2002 American Chemical Society

functional groups on the surfaces of the particles. In this way, useful systems for applications as reactive fillers and impact modifiers are available (*1-3*). Generally these particles are synthesised in a two-stage process by means of the sequential emulsion polymerization of polymers with various natures. However, it was discovered that the morphology of latex particles could vary greatly. A number of morphologies other than core-shell have been reported (*4-6*).

The control of the two-stage latex particle morphology can be considered in terms of two major types of influences in the system which determine the final morphology: the thermodynamic forces and the kinetics of the morphological development.

The core-shell morphology can be built up in a batch or semibatch procedure (by adding two monomers at the same time or one after another) or by seeded polymerization. In this latter case, the shell monomer is mixed with a preformed latex and polymerization of the second monomer is initiated by a free radical initiator (*7*). In the first case, the particle morphology is determined mainly by the copolymerization parameters of the two monomers; in the second case, the polarity and the compatibility of the shell and core polymer, type of monomer addition, type of initiator, and temperature could strongly influence particle morphology (*8*).

We have studied particles with reactive groups located on the particle surface which are able to react with shell-monomers to form a covalently bonded shell layer or to react with a matrix of other polymers as well as with metal surfaces.

According to previous publications of Funke (*9*) concerning functionalized microgels and our own results with self-assembling molecules based on phosphonate- and phosphate groups as reactive groups toward aluminum surfaces (*10*) polymeric nano particles with phosphate groups were synthesized. These particles can be used for corrosion inhibition of aluminum.

Peroxidic "Inisurfs"

In this work we have used a novel method in which the above polymerization process was carried out by using a polymeric "inisurf". Such a polymer combines the initiator and surfactant functions in one molecule. Several studies have been performed in recent years, where initiators have been attached to the surface of solid substrates or polymer particles (*7, 10*). This special system has a number of advantages with respect to the resulting particles and their properties.

The synthesis of the peroxidic monomers was carried out at the Institute of Organic Chemistry State University–Lvivska Polytechnika, Lviv, Ukraine. The polymeric peroxide was synthesised (*11*) by means of the radical

copolymerization of maleic acid anhydride (MAA) and vinyl peroxide (VP) in acetone media at 333 K with benzoyl peroxide as initiator (Figure 1). The resulting copolymer has a molecular weight of 5000 g/mol.

The polymeric peroxide becomes soluble in water after the reaction of maleic anhydride units with sodium hydroxide as is shown in Figure 1.

The presence of groups with strongly differing polarities in the inisurf chains leads to certain surface-active properties. These properties enable the sorption of these polymers on phase boundaries of various colloidal systems.

The inisurf exibits temperature-time dependent decomposition of the peroxide groups and therefore the emulsion polymerization process can be easily controlled. By means of thermogravimetric measurements the peroxide decomposition was studied in the interval from 90 to 110 °C. The results are presented in Figure 2.

According to this result, after the core polymer synthesis by means of emulsion polymerization was complete, a certain amount of peroxide groups remain on the core particle surface and can be used for the next reaction step, i.e., the creation of a polymer shell. Finally, the shell is covalently bonded to the core particle. After polymerization of the shell monomers the inisurf becomes buried between the core and shell polymer phases which leads to destabilization of such a colloidal system. Therefore, the addition of another surfactant is necessary during the shell formation.

Synthesis of Peroxide Dispersions

By using an inisurf in emulsion polymerization, the polymer nanoparticles are formed where the inisurf remains covalently bonded to the particle surface (Figure 3).

Due to the presence of numerous peroxide groups in the inisurf chain, the resulting particles are crosslinked and, therefore, insoluble.

The kinetics of emulsion polymerization of styrene (St) and butyl acrylate (BuA) in the presence of the reactive surfactant was studied at temperature intervals from 65 to 85 °C. The concentration of inisurf was varied from 1.6 to 3.14 mmol/L. Amounts of styrene and BuA were constant in all experiments; i.e. 1.00 mol/L. Conversion of monomer was determined by dilatometric measurements (checked by gravimetry). The conversion-time data are presented in Figure 4.
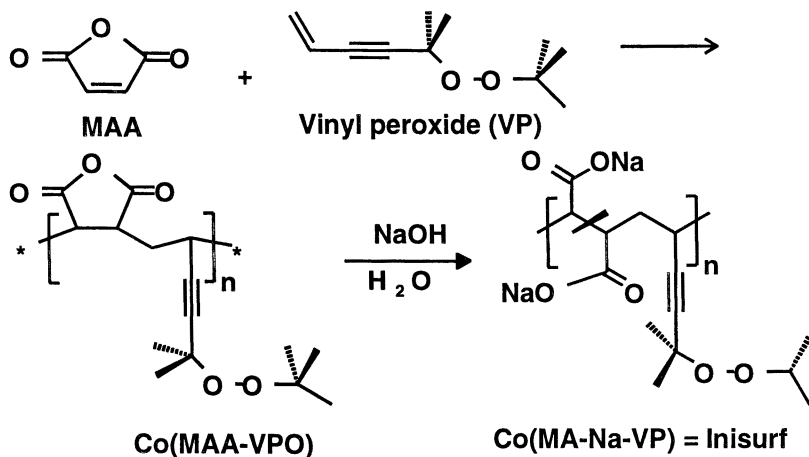
Figure 1. Synthesis of the copolymer of maleic acid anhydride and 5-tert butyl peroxy-5-methyl-1-hexen-3-in with neutralization to peroxidic inisurf.
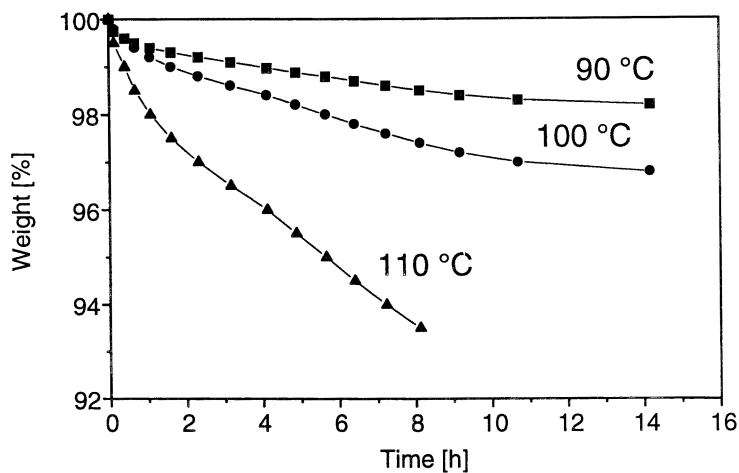
Figure 2. Thermogravimetric decomposition curves of the inisurf at different temperatures.
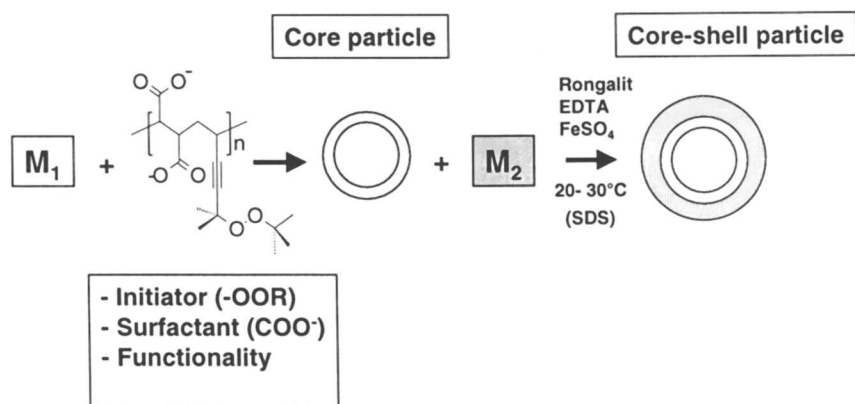
Figure 3. Schematic representation of emulsion polymerization in the presence of the inisurf and the synthesis of the shell (Redox-system: FeSO$_4$, Na-hydrogen sulfoxylate*CH$_2$O (Rongalit), EDTA).
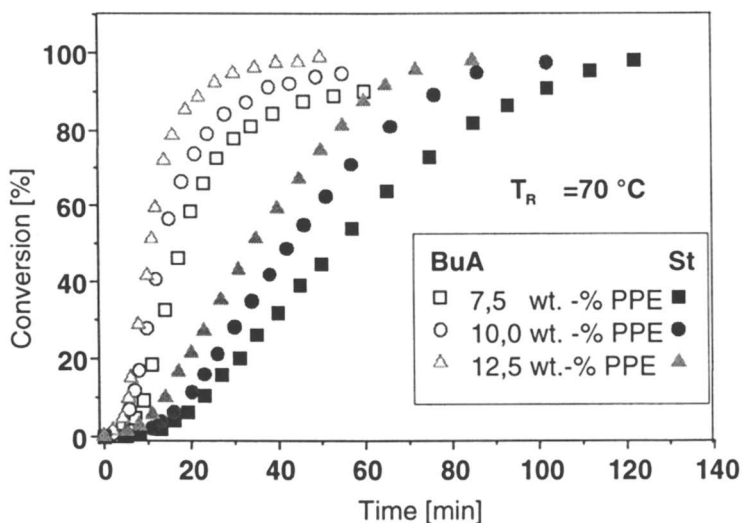
Figure 4. Conversion-time curves of the emulsion polymerization of styrene and butyl acrylate with different inisurf concentrations.

One can see that the polymerization rate for BuA is significantly higher if it is compared with styrene. This effect is probably due to the higher resonance stabilization of styrene radicals. In the case of BuA, the polymerization rate decreased rapidly at ca. 80% monomer conversion and for the samples where low inisurf concentrations were used, limited conversion was detected. On the contrary, polymerization of styrene is nearly quantitative for all inisurf concentrations.

The kinetic data were used to calculate the polymerization rate and the overall activation energy (61 kJ/mol and 40.6 kJ/mol for styrene and butyl acrylate, respectively).

Particle diameters of the obtained polymeric dispersions were investigated with dynamic light scattering (DLS) and Flow-Field-Flow-Fractionation (F-FFF). The size of the particles decreased with increasing inisurf concentration and reaction temperature (Figure 5) and this indicates that the inisurf shows similar behavior to low molecular mass initiators and surfactants in emulsion polymerization.
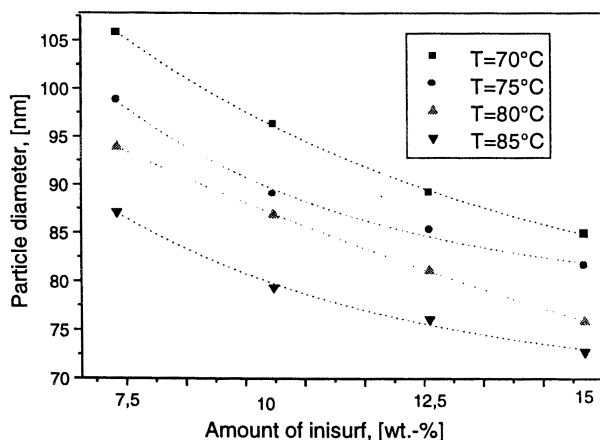
Figure 5. Influence of temperature and inisurf concentration on the final particle diameter in the emulsion polymerization of styrene.

Microscopy investigations indicate that polymeric particles synthesized with the inisurf possess spherical shapes. SEM images of different core particles show that the polymeric particles are small with a relatively narrow particle size distribution (Figure 6).
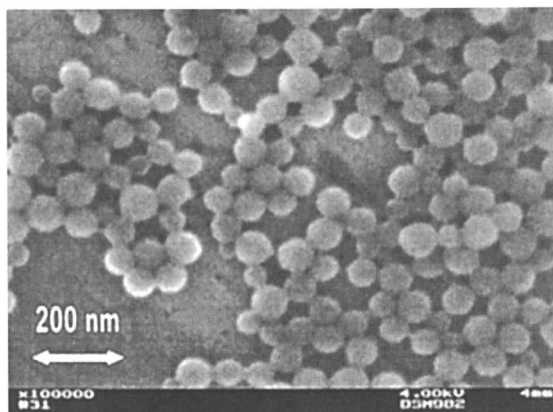
Figure 6. SEM micrograph of PS core particles prepared with the inisurf.
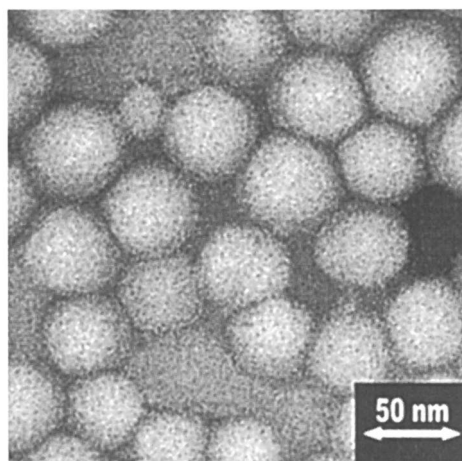
Figure 7. SEM micrograph of PBuA core particles prepared with the inisurf.

In spite of crosslinking, the PBuA particles are soft and film formation is possible (Figure 7).

With differential scanning calorimetry (DSC), the peroxide decomposition during the core synthesis was determined. After different reaction times, samples of core-dispersions with the same starting amount of the inisurf were dried and analyzed using DSC. One can see from Figure 8 that not all peroxide groups are destroyed during thermal initiation and the remaining peroxide functions can be used for the synthesis of the shell. The amount of remaining peroxide can be controlled by varying the reaction time and reaction temperature.
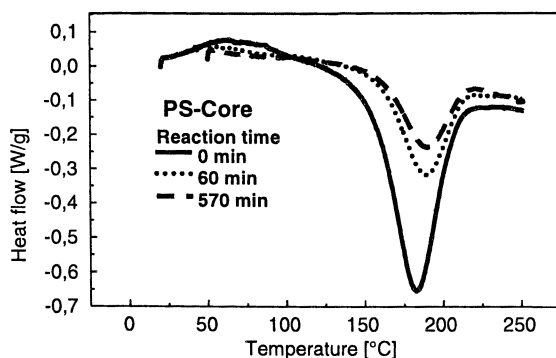
Figure 8. Dependence of peroxide decomposition on reaction time.

Synthesis and Characterization of Core-Shell Particles

The core-shell particles were synthesized at different reaction conditions (variation in the addition of shell monomer, reaction time) by using a redox-system (FeII/Rongalit) to start the polymerization at lower temperatures (40 °C) and to ensure the complete decomposition of the remaining peroxide groups. It was found that the polymerization has to be carried out under starved-feed conditions; i.e., when the shell monomer dosing rate is smaller then the polymerization rate. An additional surfactant, sodium dodecyl sulfate (SDS) was added before the shell-monomer was introduced into the reaction system.

The latexes were characterized by TEM and F-FFF. Figure 9 shows a TEM micrograph of the final particles, which consists of a PS core and a PBuA shell.
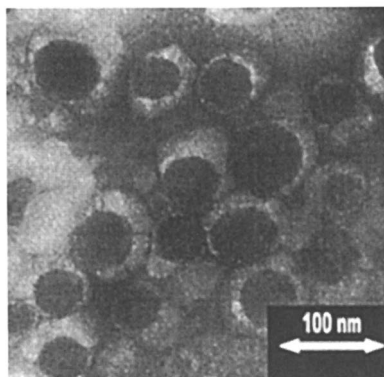
Figure 9. TEM micrograph of PS core/PBuA shell particles.

The polystyrene core was stained with RuO_4 (black regions). The poly(butyl acrylate) shell (light grey regions) is more soft and mobile because of its low T_g and this is the reason for visible non-symmetrical architecture of the composite particles.

The F-FFF in combination with multiangle laser light scattering (MALLS) gives important information about the particle size and the particle size distribution. According to this method, polymer particles are passed through a thin rod-like channel where a sample is directed with a carrier solvent in a laminar parabolic flow profile. A field, perpendicular to the channel flow, forces the sample to different layers of the parabolic flow according to its diffusion coefficient. Therefore particles with different sizes can be separated in the channel and eluate at different times.

In Figure 10 the hydrodynamic particle radii of core and core-shell dispersions are presented. One can see the increase of the particle hydrodynamic radius after shell formation at constant particle size distribution.

Applications of Reactive Particles

The polymer particles that were obtained in this study can be used as crosslinking agents. Due to the presence of peroxide functional groups on the particle surface, these latexes can be incorporated into blends and improve their properties via thermal or catalytic crosslinking.

The PS core dispersion (amount of the inisurf = 12 wt%) was mixed with polystyrene-polybutadiene (PS-PB) latex, and the films that were obtained were kept in the oven at 150 °C. After thermal treatment the hardness of the blends was measured (Figure 11).
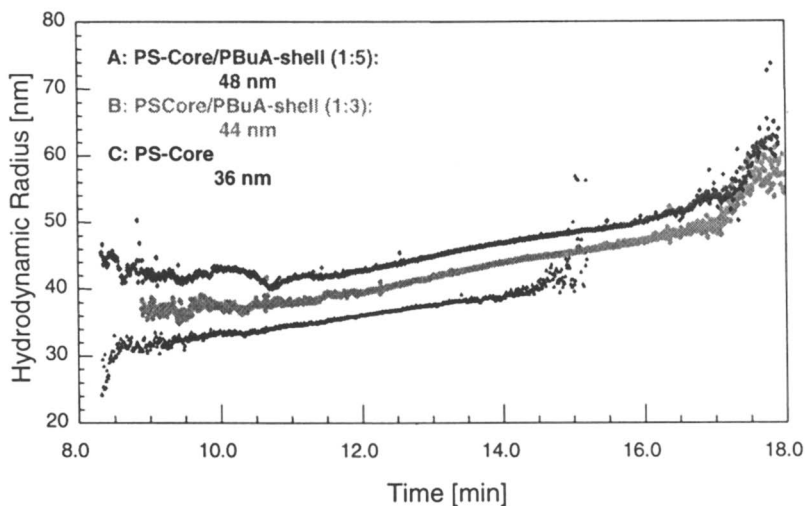
Figure 10. Hydrodynamic radius of various core and core-shell particles.
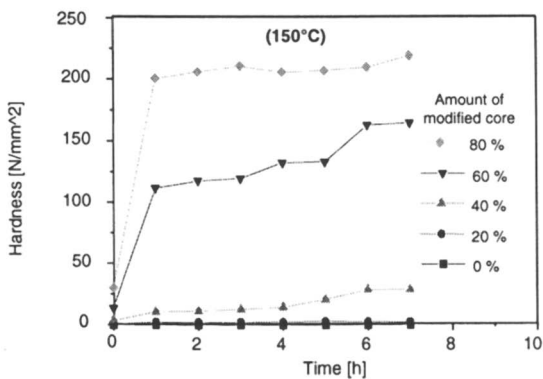
Figure 11. Hardness versus treatment time curves of the blends prepared at different mixing ratios of PS/inisurf and PS/PB latexes.

In Figure 11, it is possible to observe an increase in the blend hardness after the crosslinking process. This effect is greater as the PS/inisurf latex content in the mixture was increased. It was found that crosslinking process is strongly affected by the curing temperature.

Synthesis of Functionalized Dispersions

According to Figure 12, functionalized particles were synthesized in a two-step emulsion polymerization process. In a first step, crosslinked BuA/St particles were formed. In a second step a mixture of functionalized acrylate and BuA/St was added to the system. In this way, composite particles were obtained.
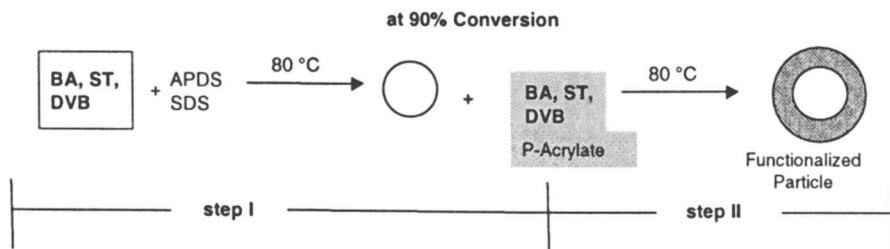
Figure 12. Synthesis of functionalized composite particles.

Different functionalized acrylates (see Figure 13) were used to incorporate various functional groups into the particle surface. Different reaction conditions, such as temperature, feed rate, concentration of emulsifier were varied.

The dispersions were characterized in terms of their particle size distributions (DLS, F-FFF) and glass transition temperatures. The mean diameter of the particles was in a range from 50 to 200 nm. By changing the reaction conditions it was possible to control the particle size and particle size distribution.

For phosphate-functionalized dispersions it was possible to show the distribution of P-species around the particles by an energy dispersive TEM-picture. Figure 14 shows two particles in the range of 160 nm in a P-sensitive TEM picture.

It was found that phosphate-functionalized dispersions are useful for corrosion protection of AlMg1 panels. AlMg1 panels were dipped in phosphate-functionalized dispersions. After a few seconds particles were found on the AlMg1 surface. An untreated surface and surface after 30 sec exposure time to the dispersion are shown in Figure 15.
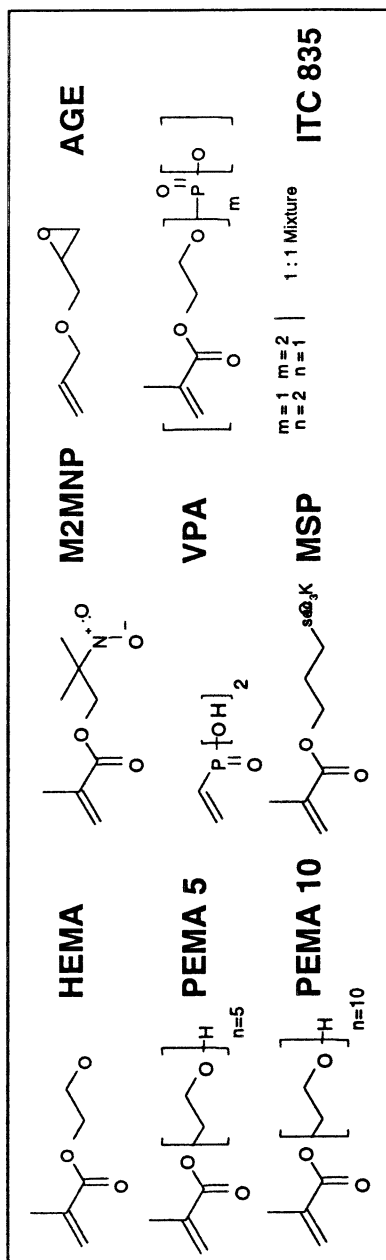
Figure 13. Acrylates used for functionalization of particles.
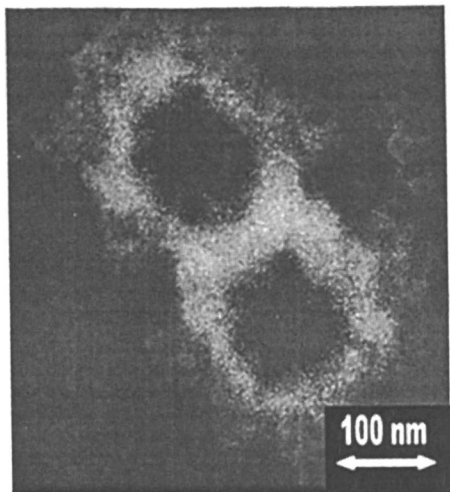
Figure 14. P-sensitive TEM picture of two phosphate-functionalized particles.
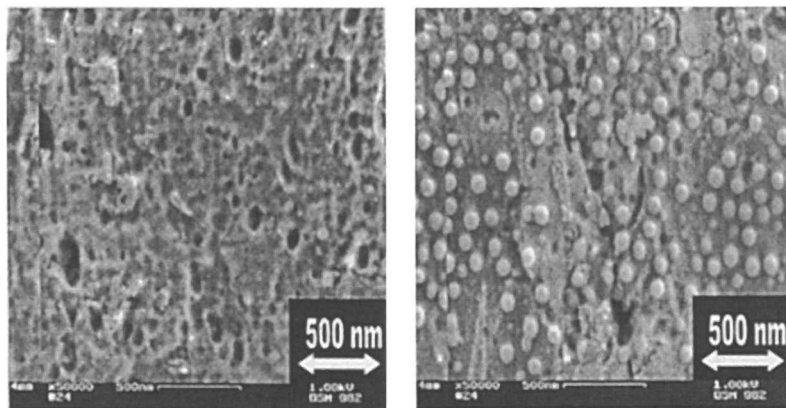
Figure 15. SEM images of blank (left) and a AlMg1 surface after dipping in a phosphate-functionalized dispersion (right).

The adsorption rate depends on the particle size and adsorption time. In Figure 16, time-dependent SEM pictures for 160 nm particles are presented. One can see that the metal surface is not completely covered with polymeric particles after 30 seconds.

Figure 17 shows that the film formation process is completed within 10 sec in the case of smaller particles.

Coated panels were tested in a corrosion test according to DIN 65472. After an adsorption process, panels were coated with a clear coat. After that, scratches were made with a steel needle and panels were activated with hydrochloric acid for 1 hour. The panels were placed into the constant climate test chamber maintained at 40 °C. In Figure 18 the panels after 1200 h exposure time in the test chamber are presented.
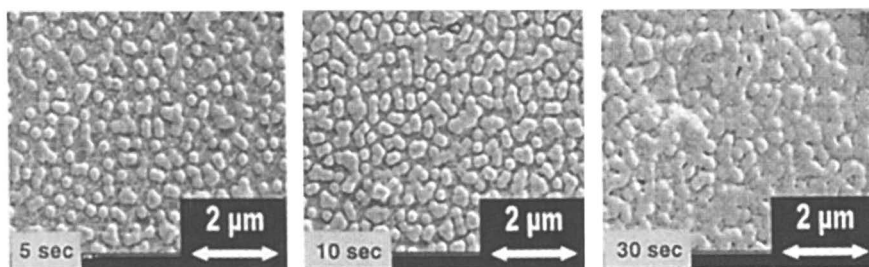
Figure 16. SEM images of time-dependent adsorption of 160 nm particles on an aluminum surface.
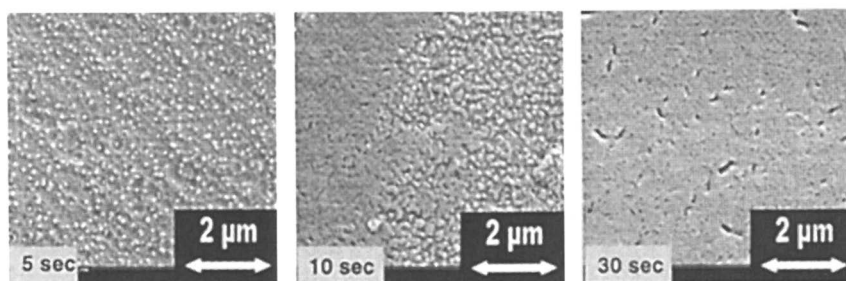
Figure 17. SEM images of time-dependent adsorption of 60 nm particles on aluminum surface.

functionalized   unfunctionalized

100 nm   160 nm   95 nm
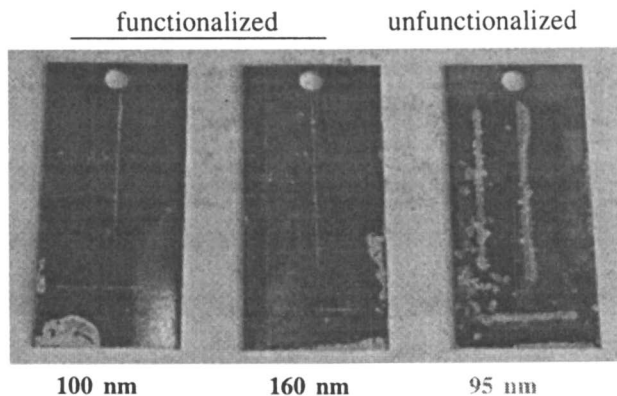
Figure 18. Metal panels covered with phosphate-functionalized and unfunctionalized particles after 1200 h exposure time in test chamber.

Panels coated with phosphate-functionalized particles clearly show better results. Test results also depend on particle size (Figure 19). This in accordance with Figures 16 and 17, which show the film formation dependency on the particle size.

In an application such as corrosion protection smaller particles seem to be more effective due to better film formation properties during the adsorption process.

Conclusions

It has been shown that an amphiphilic copolymer with peroxide groups can be successfully used as an "inisurf" in emulsion polymerization. The remaining peroxide groups on the particle surface were used for the shell formation by direct polymerization of a secondary monomer from the particle surface or also as reactive groups for a filler system which can react with the matrix. In contrast to the other methods, in our system, the polymeric shell is covalently bonded to the core, which minimizes the existing phase separation. This results in a morphology which is retained even during the course of different applications.

By using peroxide monomers in combination with functionalized acrylic monomers it was possible to introduce phosphate groups on the surface of crosslinked microspheres. The phosphate groups play the role of anchoring groups to aluminum surfaces. Adsorbed particles show an excellent corrosion inhibition effect.
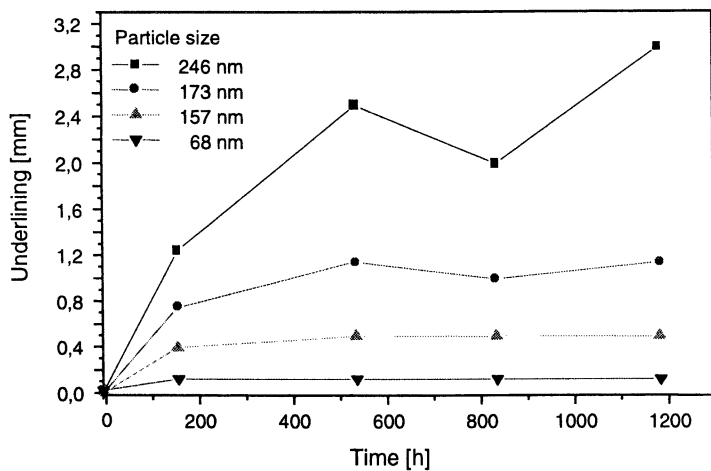
Figure 19. Dependency of underlining on the particle size and exposure time.

Acknowledgment

References

1. Pichot, C. *Makromol. Symp.* **1984**, *88*, 71.
2. Lee, S.; Rudin, A. *J. Am. Chem. Soc.* **1992**, *12*, 234.
3. Rudin, A. *Makromol. Symp.* **1995**, *92*, 53.
4. M. Okubo, *Makromol. Chem. Makromol. Symp.* **1990**, *35/36*, 307.
5. Cho, I.; Lee, K. W. *J. Appl. Polym. Sci.* **1985**, *30*, 1903.
6. Lee, D. I.; Ishikawa, T. *J. Polym. Sci. Chem. Ed.* **1983**, *21*, 147.
7. Landfester, K.; Spiess, H. W. *Acta Polymerica* **1998**, *49*, 451.
8. Dimonie, V. L.; El-Aasser, M. S.; Klein, A.; Vanderhoff, J. W. *J. Polym. Sci.* **1984**, *22*, 2197.
9. Funke, W. *J. Coat. Techn.* **1988**, *60*, 767
10. Maege, I.; Jaehne, E.; Henke, A.; Adler, H.-J. P.; Stratmann, M. *Progr. Org. Coat.* **1998**, *34*, 1.
11. Voronov, S.; Tokarev, V.; Oduola, L.; Yu. Lastukhin *J. Appl. Polym. Sci.* **2000**, *76*, 1217.

Chapter 20

A Novel Surface Functionalization Method for Producing Carboxyl-Functional Poly(methyl styrene) Latexes

Pei Li

Department of Applied Biology and Chemical Technology, The Hong Kong Polytechnic University, Hung Hom, Kowloon, Hong Kong, Peoples Republic of China

A facile synthesis of functionalized poly(methyl styrene) latexes containing aldehyde and carboxylic acid groups using anionic and cationic surfactants or an emulsifier-free system is described. The synthesis involves an emulsion polymerization of methyl styrene, followed by a copper (II)-catalyzed aqueous oxidation with *t*-butyl hydroperoxide under air. Investigation of the effect of metal catalyst, oxidant, surfactant and reaction temperature in these systems are discussed. Properties of the resulting functional latexes including their chemical structure, concentration of functional groups in the surface layer, particle size, size distribution, morphology, and stability are also studied.

Polymer latexes containing reactive surface functionalities have received much interest in the last two decades because of their wide range of applications. For example, they have been extensively used as binders in paints, adhesives, coatings, etc., and as carriers for covalently-immobilized catalyst, antibodies, enzymes, drugs, and other biomolecules (*1,2*). The reactive functionalities include hydroxyl, aldehyde, carboxylic acid, amino, epoxy, sulfhydryl, succinimide, benzotriazole and chloromethyl groups (*3*). The selection of these

293

functional latexes depends on the intended application. For example, aldehyde groups are especially useful for the direct immobilization of amino-containing biomolecules because they can react under mild conditions with primary amino groups, forming the corresponding imine (Schiff base) linkages without prior activation. The imine group can be further reduced to a stable -CH$_2$-NH- linkage with sodium cyanoborohydride. Latexes containing carboxylic acid surface groups are particularly important in water-borne coatings because they are capable of surface crosslinking via hydrogen and covalent bondings. They can also undergo ionic crosslinking with metal cations such as Ca^{2+}, Zn^{2+}. Although various approaches have been reported on the synthesis of functional latexes containing aldehyde or carboxylic acid surface groups, homo- and copolymerization of acrolein or different methacrylate or acrylate acids as the functional monomers have been the dominant approaches. Unfortunately, these reactions have some major drawbacks. For example, significant differences in solubility and reactivity between the functional and matrix monomers in hetergeneous polymerization result in low surface incorporation of functional groups. In addition, a large amount of water-soluble polymers is formed during the polymerization. Thus, an extensive cleaning process is required to purify the latexes.

To bypass the problems associated with the use of functional monomers, we have developed a novel appoach via a direct surface oxidation of poly(methyl styrene) (PMS) latexes to the corresponding aldehyde or carboxylic acid groups (4-8). In this article, the synthesis and characterization of the functionalized poly(methyl styrene) latexes, containing aldehyde and carboxylic acid groups in the presence of anionic and cationic surfactants such as sodium dodecyl sulfonate and cetyltrimethylammonium bromide (CTAB) as well as in an emulsifier-free system will be described. The functionalization process involves an emulsion polymerization of methyl styrene forming highly monodispersed poly(methyl styrene) latexes, followed by an in situ surface oxidation under air with copper (II) chloride and *tert*-butyl hydroperoxide catalysts (Scheme 1).

Results and Discussion

Preparation of Poly(methyl styrene) Latexes

Highly monodispered poly(methyl styrene) latexes were first prepared by the emulsion polymerization of 3(4)-methyl styrene in the presence of either anionic or cationic surfactant, or even in the absence of surfactant. Figure 1 shows an SEM photograph of nearly monodisperse PMS latex (mean diameter = 683 nm) prepared by an emulsifier-free emulsion polymerization using 2,2'-azobis(2-amidinopropane) dihydrochloride (V-50) as the initiator. The particle size could be easily altered by varying the concentration of the surfactant, the

monomer, the initiator, the ionic strength, and the temperature. Thus, monodisperse PMS latexes of a wide size range could be readily prepared.
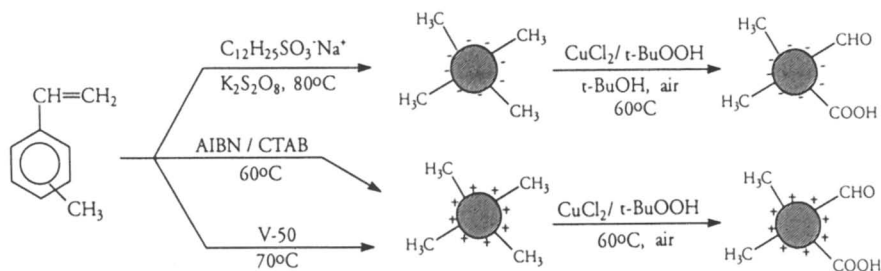
Scheme 1. Synthesis of functionalized poly(methylstyrene) latexes.
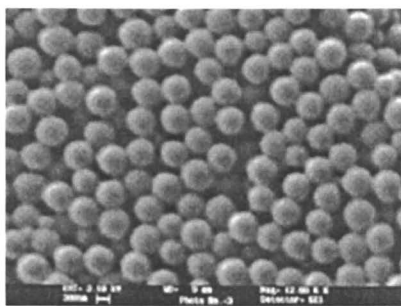
Figure 1. SEM micrograph of PMS latex prepared by an emulsifier-free emulsion polymerization using V-50 as the initiator.

Catalytic Oxidation of the Poly(methylstyrene) Latexes

The stable poly(methyl styrene) latexes prepared in various systems were used directly in the subsequent catalytic oxidation reactions. Scheme 2 shows the reaction mechanism of the catalytic oxidation. The *t*-BuOOH is first decomposed with the metal catalyst to both *t*-BuO˙ and *t*-BuOO˙ radicals. These reactive radical species can readily abstract benzylic hydrogens to generate benzylic radicals, which can be oxidized to the corresponding aldehyde groups under air. Since the aldehyde groups are easily further oxidized to the carboxylic acid groups under the oxidative conditions. Thus, a mixture of aldehyde and carboxylic acid functionalities are generated concurrently. On the other hand,

distribution of the two functional groups can be readily controlled by various reaction parameters including the surfactant, the concentration of metal catalyst and oxidant, the reaction temperature and time.

$$t\text{-BuOOH} + \text{Cu}^{2+} \longrightarrow t\text{-BuOO}\cdot + \text{Cu}^+ + \text{H}^+$$

$$t\text{-BuOOH} + \text{Cu}^+ \longrightarrow t\text{-BuO}\cdot + \text{Cu}^{2+} + \text{OH}^-$$

$$2\ t\text{-BuOOH} \xrightarrow[\text{Cu}^+/\text{Cu}^{2+}]{} t\text{-BuOO}\cdot + t\text{-BuO}\cdot + \text{H}_2\text{O}$$
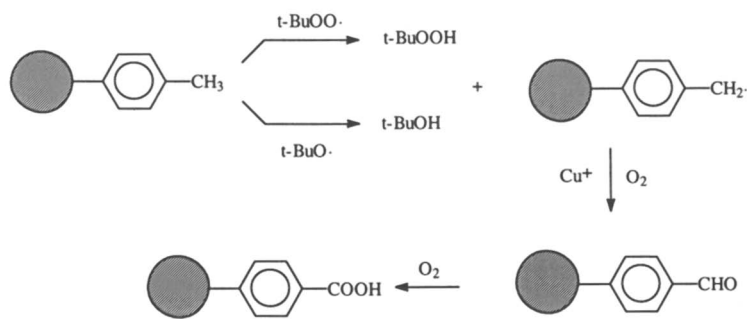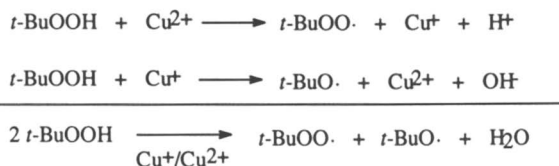
Scheme 2. Catalytic oxidation of poly(methyl styrene) latexes to the corresponding aldehyde and carboxylic acid groups.

Effect of Metal Catalyst

A variety of metal catalysts including cobalt(II) acetate, cobalt(II) chloride, manganese(II) chloride, copper(II) chloride and iron(II) chloride were investigated in both anionic and cationic systems. The copper(II) chloride was found to have the highest reactivity among these catalysts. Although Co^{II}/Co^{III} redox system is known to be one of the most effective autoxidation catalysts for the decomposition of alkyl hydroperoxide because of its comparable stability of the two valence states, it was found to be less effective than Cu^{2+} ions in our systems. This may be due to the deactivation of cobalt ions as a result of the presence of coordinating ligands such as carboxylic acid groups generated during the reaction. In comparison, the transformation between copper(II) and copper(I) can not only occur by the redox reaction as shown in Scheme 2, but also by other mechanistic pathways that are insensitive to redox potential. The

alternative pathways leading to the regeneration of copper (I) include electron transfer oxidation of alkyl radicals and ligand transfer.

The effect of catalyst concentration on the degree of oxidation was also examined. In the anionic system, the concentration of metal catalyst significantly affected the rate of oxidation and the stability of the emulsion. Decreasing the concentration of catalyst resulted in a reduction in the oxidation rate. No oxidation was detected when the concentration of $Co(OAc)_2$ was lower than 3 mM. However, when the concentration exceeded 0.016 M, the emulsion became unstable. Such an effect may be attributed to the decrease of the effective catalyst concentration as a result of complexation between the metal ion and anionic surfactant. On the contrary, in the cationic systems, the concentration of metal catalyst was found to have little effect on the overall rate of oxidation. This can be explained by the fact that the metal cations in the cationic system are unable to form a complex with the cationic surfactant or latex surface, thus their catalytic activity can be retained. For example, oxidation of cationic PMS latexes in CTAB could achieve 18 to 24% after 4 hours at 60 °C with $CuCl_2$ concentrations ranging from 0.004 M to 0.02 M. Similar results were also obtained for the emulsifier-free cationic PMS latexes prepared with V-50. Although the concentration of the metal catalyst had very little effect on the rate of oxidation in the cationic systems, it was found to alter the aldehyde and carboxylic acid concentrations. Higher $CuCl_2$ concentrations facilitated the conversion of aldehyde to the corresponding carboxylic acid groups.

Effect of Oxidant

The oxidant played a key role in the metal-catalyzed oxidation reaction. No oxidation was observed when oxygen was bubbled through the anionic or cationic PMS latex in the presence of metal catalyst. When hydrogen peroxide was employed as the oxidant, the reaction proceeded violently and was difficult to control. In contrast, little oxidation was observed with di-*t*-butyl peroxide. In comparison to all these oxidants, *t*-BuOOH appeared to be an excellent one for all the systems.

The degree of oxidation in both anionic and cationic systems could be controlled readily by varying the amount of *t*-BuOOH. An example of this effect is demonstrated in Figure 2. The degree of oxidation was found to increase linearly as the concentration of *t*-BuOOH increased. However, when the concentration of *t*-BuOOH exceeded 0.5 M, the latex became unstable.
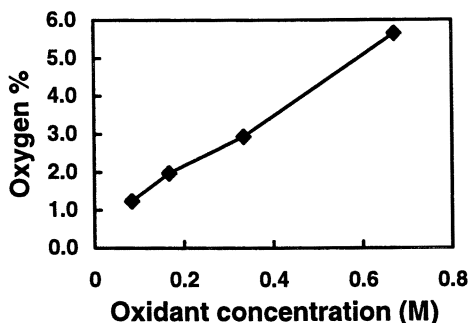
Figure 2. Effect of oxidant concentration on the degree of oxidation for cationic PMS latex in the emulsifier-free system. (Reproduced from reference 8. Copyright 2000 American Chemical Society.)

Effect of Surfactant

Three kinds of anionic surfactant were examined including sodium dodecylbenzene sulfonate, sodium dodecyl sulfonate, and sodium dodecyl sulfate. They were all good for the emulsion polymerization of 3(4)-methyl styrene, giving stable latexes. However, the use of sodium dodecylbenzene sulfonate gave an unstable emulsion during the oxidation, while sodium dodecyl sulfate underwent hydrolysis to give the alcohol. In comparison, use of sodium dodecyl sulfonate (SDS) gave a stable emulsion, even under oxidation conditions. When the anionic PMS latexes containing SDS surfactant were subquently oxidized with t-BuOOH and cobalt catalyst, little reaction took place after 24 hours under air. The lack of catalytic reactivity of the metal ions in SDS might be caused by the metal ions complexing to the sulfonate ions of the surfactant. Thus, attempts to reduce such complexation were made by adding a small amount of t-BuOH. It was found that the rate of oxidation was increased dramatically. The profound effect of the t-BuOH might be attributed to its ability to solvate the metal ions through weak coordination, thus, preventing the interaction between metal ion and sodium dodecyl sulfonate, while still maintaining the reactivity of the metal ion. The rate of oxidation and the stability of the latex were also found to be affected by the quantity of t-BuOH added. When the concentration of t-BuOH was higher than 25% by volume, the latexes became unstable. However, little oxidation (<1%) was observed when the concentration was less than 10% by volume.

When a cationic surfactant such as cetyltrimethylammonium bromide (CTAB) was used, the oxidation proceeded much faster than in the anionic system under similar reaction conditions (Figure 3). This is likely due to the

electrostatic repulsion between the cationic PMS latex and the metal cations of the catalyst. Thus, the catalyst can effectively decompose the t-BuOOH, and initiate the oxidation. A nonionic surfactant, Triton X-100, was also examined, and found to be a poor surfactant for the emulsion polymerization, giving relatively large particles with broad size distribution. Furthermore, the latex was very unstable during the oxidation.
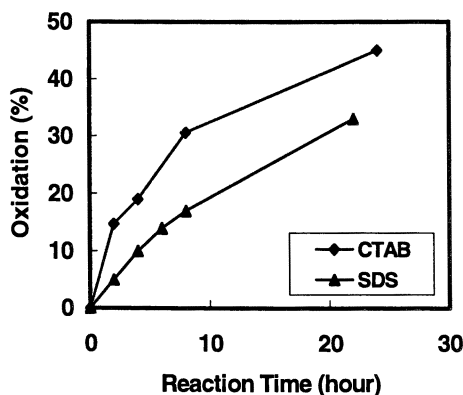
Figure 3. Degree of oxidation of poly(methylstyrene) latexes in (▲) SDS with t-BuOH or in (◆) CTAB at 60 °C under air. The percentage of oxidation was determined by elemental analysis and calculated based on the structure of poly(vinyl benzoic acid).

The types of surfactant used not only affect strongly the rate of oxidation and the stability of PMS latexes, but also the product distribution of the aldehyde and the carboxylic acid functionalities. For PMS latexes prepared with $K_2S_2O_8$ and anionic surfactant or with V-50 in the absence of surfactant, carboxylic acids were found to be the major functional groups during the oxidation. However, for PMS latexes prepared with AIBN in cationic surfactant, aldehdye was identified to be the major functional group in the first 6 hours of the reaction. Generally, copper-catalyzed oxidation with t-BuOOH undergoes a free radical autoxidation, and the aldehyde groups are readily oxidized to the corresponding carboxylic acid group. The high selectivity for the aldehyde functionality in the presence of cationic surfactant is very unusual. This effect may be due to the high OH⁻ concentration surrounding the cationic particle surface as a result of the electrostatic double layer, thus protecting the aldehyde groups from being further oxidized to the corresponding acid.

Effect of Reaction Temperature

Since the catalytic oxidation involves a typical free-radical autoxidation, the degree of oxidation of anionic or cationic PMS latexes generally increases with the increase of reaction temperature. For example, oxidation of emulsifier-free cationic PMS latexes at 60 °C, 70 °C, and 80 °C for 4 hours under air gave oxygen contents of 1.49%, 2.88%, and 3.98%, respectively. It was found that higher reaction temperatures led to more rapid conversion of aldehyde to the corresponding carboxylic acid groups, thus reducing the amount of aldehyde groups. Therefore, if an aldehyde group is the desired functionality on the particle surface, a lower reaction temperature is preferred.

Characterization of the Functionalized PMS

The functionalized poly(methyl styrene) was isolated by precipitation of the latex into methanol. The white precipitate was then dissolved in THF, followed by reprecipitation in a large quantity of hot water. The structure of the functionalized PMS was identified by FTIR. Two strong peaks were observed at 1720 and 1700 cm^{-1}, indicating the formation of aldehyde and carboxylic acid groups. The presence of these two functional groups were further confirmed by ^{1}H-NMR. The aldehyde proton was observed at 9.9 ppm as a broad peak, while the aromatic hydrogens ortho to the aldehyde and carboxylic acid groups appeared at 7.8 ppm. On the basis of ^{1}H-NMR integration of these two peaks, the amount of aldehyde and carboxylic groups of the oxidized PMS could be estimated.

After extracting the functionalized PMS powder with various solvents in a Soxhlet extractor, an insoluble PMS gel was often obtained, indicating that the PMS latexes were partially crosslinked after the oxidation. The crosslinking may have occurred via the coupling of methylene or alkoxy radicals of the PMS generated during the reaction. To examine the thermal properties of the PMS and its oxidized derivatives, the glass transition temperature (T_g) was measured by differential scanning calorimetry (DSC). For the cationic functionalized PMS, it was found that the T_g increased from 93 °C to 118 °C for the insoluble PMS gel due to the crosslinking. The low oxidized PMS (<5%) had little change in its T_g value, while the highly oxidized PMS (>30%) was found to have a lower T_g than its pure PMS. This lowered T_g value may be caused by the decrease of the average molecular weight of the PMS during the oxidation as a result of backbone cleavage. Such cleavage could take place by radicals attacking the tertiary hydrogens of the backbone chain rather than the primary hydrogens of the methyl groups (9).

Control of Surface Functional Groups and Concentration

Controlling the surface functionalization is one of the most important and challenging processes for the synthesis of functional latexes. An ideal functional particle should contain functional groups located on the particle surface. For example, for PMS particles with a mean diameter of 753 nm and a density $\rho = 1.05$ g/cm^3, if a cross-sectional area of 24 Å^2 is taken for the aldehyde group (the value for alcohol) (10), theoretically speaking, the number of moles of aldehyde needed to cover the surface of 1 g of latex particles is 5.26×10^{-5} mol/g, which corresponds to an oxygen content of 0.084%. If all the functional groups located on the latex surface are assumed to be carboxylic acid groups, the oxygen content required should be 0.168%. In other words, if only the surface oxidation occurs, the maximum oxygen content should be lower than 0.168%. When comparing these theoretical values with our elemental analysis results of the oxidized PMS, it was found that the oxidation reaction occurred not only on the particle surface, but also into the inner layer of the particles, especially when a higher oxidant concentration was utilized.

In order to quantitatively determine the concentration of aldehyde groups on the particle surface during the oxidation, a 2.5 pH titration method has been employed (7), and the basic reaction is shown in equation 1.

$$RCHO + HO\!-\!NH_2\cdot HCl \underset{k_2}{\overset{k_1}{\rightleftharpoons}} R\!-\!CH\!=\!N\!-\!OH + H_2O + HCl \quad (1)$$
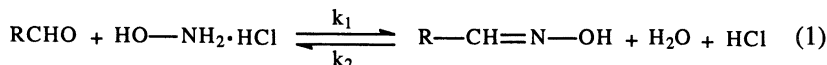
The 2.5 pH method is based on the fact that aldehyde groups can easily react with hydroxylamine hydrochloride at room temperature to form oxime and hydrochloride acid (HCl). The concentration of HCl released from this reaction can be simply determined by the titration with NaOH solution. Thus, the amount of aldehyde groups on the latex can be estimated. Although hydroxyamine hydrochloride used for the determination of surface aldehyde groups has been found to penetrate inside of particles, Yan et al.[11] noticed that concentration of aldehyde groups on polyacrolein-co-polystyrene microspheres, determined with hydroxylamine hydrochloride, was time dependent. Their studies indicated that the hydroxylamine hydrochloride method was appropriate for the determination of surface aldehyde groups if aldehyde functionalized particles reacted with hydroxylamine hydrochloride for only 20 to 60 minutes. Thus, we adopted this method, and allowed the aldehyde functionalized latexes to react with hydroxylamine hydrochloride for 1 hour at room temperature, followed by titration with 0.005N NaOH solution.

Figure 4 shows that the volume of NaOH solution used for the titration of the oxidized PMS latexes obtained in the initial reaction increased to a

maximum, then decreased gradually. These results suggested that the amount of surface aldehyde increased very rapidly in the initial stage of the oxidation for all oxidant concentrations, then slowly reduced due to their further oxidation to the corresponding carboxylic acid groups. Figure 5 exhibits an almost linear relationship between the oxidant concentration and the surface concentration of aldehyde after 60 minutes of reaction. In other words, the desired amounts of aldehyde groups on the particle surface could be easily obtained by applying different oxidant concentrations.
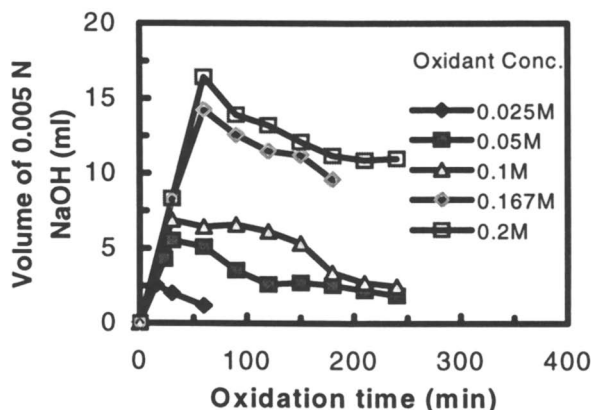
*Figure 4. Concentration of surface aldehyde groups as a function of reaction time.
(Reproduced from reference 8. Copyright 2000 American Chemical Society.)*

Table I shows the concentrations of surface aldehyde groups oxidized with four different t-BuOOH concentrations. The percent surface coverage of aldehyde groups could be estimated by the following calculation. When the PMS particles were oxidized for 15 minutes at 70 °C in the presence of 0.05 M of t-BuOOH, the concentration of aldehyde groups was 4.48×10^{-5} mol/g, which translated to an area per group of about 28.82 Å^2. If a cross-sectional area of 24 Å^2 was taken for the aldehyde group, the implication was that approximately 24/28.82 = 83% of the particle surface was occupied by aldehdyes, if they were uniformly distributed. Based on this calculation, it was noted in the Table I that the percent surface coverage by aldehdye groups exceeded 100% when the t-BuOOH concentration was higher than 0.10 M. These results were similar to the elemental analysis, suggesting that oxidation also occurred in the inner layer of the particles. Thus, a low oxidant concentration (0.05 M t-BuOOH) and short reaction time (<30 minutes) were the most appropriate conditions to achieve high surface aldehyde functionality.
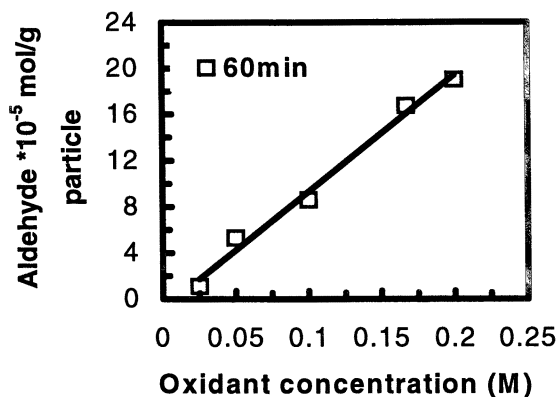
Figure 5. Surface concentration of aldehyde groups of the cationic PMS latex as a function of oxidant concentration. (Reproduced from reference 8. Copyright 2000 American Chemical Society.)

Table I.   Surface Concentrations of Aldehyde using Different *t*-BuOOH Concentrations[a]

Time (min)	$10^5 \times aldehyde^b$ for t-BuOOH concentration of				
	0.025 M	0.05 M	0.10 M	0.167 M	0.20 M
15	2.66	4.48			
30	2.08	5.76	9.05		
45	1.22				
60	1.07	5.31	8.58	16.7	19.0
90		3.69	8.74	15.0	15.4
120		2.71	8.27	14.1	15.4
180		2.66	4.49	11.1	13.5
210		2.29	4.70	3.79	13.2
240		1.93	4.45		13.3

[a] Reaction conditions: PMS:CuCl$_2$ = 50:1, at 70 °C under air. Mean particle size = 753 nm. [b] The number of moles of aldehyde per gram of latex

SOURCE: Reproduced from Reference 8. Copyright 2000 American Chemical Society

The amounts of carboxylic acid groups were also determined by titrating the latex dispersion with NaOH under a nitrogen atmosphere. It was found that both

potentiometric and conductometric titrations of the functionalized cationic PMS latexes, which were oxidized with 0.025 M t-BuOOH after 1 hour, gave two equivalent points, corresponding to a strong acid group (HCl) and a weak acid group (-COOH), respectively. Based on the volume of the NaOH consumed, the surface concentration of carboxylic acid was calculated to be 1.05×10^{-4} mol/g particle. Comparing this value with the amount of aldehyde groups (1.07×10^{-5} mol/g particle) reported in Table I, we could conclude that carboxylic acid groups were the major functionality, which was consistent with FTIR studies for the cationic PMS in the emulsifier-free system.

Control of Particle Size and Size Distribution

The mean diameters of the highly functionalized PMS latexes in both anionic and cationic systems were found to increase due to the swelling caused by: (i) the presence of the carboxylic acid groups on the surface; (ii) the presence of the organic solvent in the anionic system, and (iii) aggregation of latexes due to the particle instability. It was noted that in the anionic system, although the size of the latexes and the polydispersity increased during the oxidation, the latex stability was retained due to the formation of increasing amounts of carboxylic acid groups on the particle surface. Thus, the resulting surface charge could overcome the instability caused by the increase in particle size. However, in the cationic systems, the increased degree of oxidation resulted in the flocculation of the latexes. The carboxylic acid groups formed might interact with the cationic surfactant or surface, thus reducing the total surface charge and the stability of the oxidized PMS latexes. In order to control the size of the functionalized PMS latexes, two approaches were successfully applied: (1) crosslinking of PMS latexes, and (2) lowering the degree of oxidation. For example, Figure 6(b-d) displays SEM micrographs of the cationic PMS latexes in the emulsifier-free system oxidized for 15, 30, and 60 minutes, using t-BuOOH (0.025 M) and $CuCl_2$ (5.0×10^{-4} M) at 70 °C under air. The particle sizes are all comparable to the unfunctionalized PMS latexes (Figure 6a).

Stability of the Functionalized PMS Latexes

The stability of a series of latexes with various degrees of functionalization were examined using a turbidity method. Table II shows the critical coagulation concentration of the functional PMS latexes with different types of salt. It was found that a higher degree of oxidation resulted in a slight decrease in the latex stability.
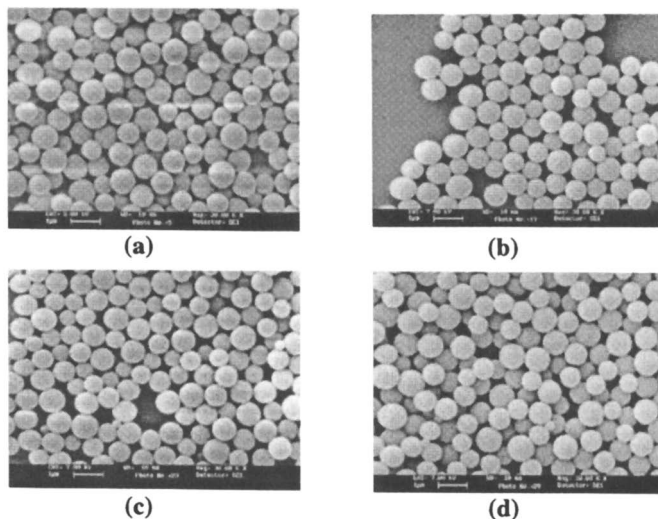
Figure 6. SEM micrographs of cationic PMS latexes in the emulsifier-free system: (a) PMS; (b) 15 min oxidation; (c) 30 min; (d) 60 min. (Reproduced from reference 8. Copyright 2000 American Chemical Society.)

Conclusions

We have demonstrated that poly(methyl styrene) (PMS) latex particles bearing surface aldehyde and carboxylic acid groups can be prepared by the emulsion polymerization of 3(4)-methyl styrene, followed by an *in-situ* oxidation catalyzed by copper(II) chloride and *t*-butyl hydroperoxide in anionic or cationic surfactant, or even in the absence of surfactant under air. This surface functionalization method allows us to control the amount of functional groups on the surface by controlling the degree of oxidation based on the reaction conditions. This method also has an advantage in ease of purification of the functionalized latex particles because the use of water-soluble functional monomer is avoided. Finally, this method provides an alternative synthetic route to the preparation of a potentially large class of functionalized latex particles, which may find many useful applications.

Table II. Critical Coagulation Concentration of Functionalized PMS Latexes[a]

Salt	No oxidn	After 15 min of oxidn	After 30 min of oxidn	After 1 h of oxidn	After 4 h of oxidn
LiCl	200	195	182	166	111
NaCl	158	158	141	126	79
KCl	63	-	-	-	-
NaF	250	-	-	-	-
NaI	35	33	25	16	11
MgCl$_2$	20	18	17	14	7
CaCl$_2$	11	-	-	-	-

[a] Critical coagulation concentration (C_{crit}) was determined by the turbidity method. The concentration unit was mmol·L^{-1}. The latexes were oxidized using t-BuOOH (0.025M) and CuCl$_2$ (5.0 ×10^{-4} M) at 70 °C.

SOURCE: Reproduced from Reference 8. Copyright 2000 American Chemical Society

Acknowledgment

References

1.   Pichot, C. *Polym. Adv. Technol.* **1995**, *6*, 427.
2.   Rembaum, A.; Dreyer, W. J. *Science*, **1980**, *208*, 364.
3.   Slomkowski, S. *Prog. Polym. Sci.* **1998**, *23*, 815, and references therein.
4.   Li, P.; Liu, J. H.; Yiu, H. P.; Chan, K. K. *J. Polym. Sci. Part A: Polym. Chem.* **1997**, *35*, 1863.
5.   Li, P.; Liu, J. H.; Wong, T. K.; Yiu, H. P.; Gau. J. *J. Polym. Sci. A: Polym. Chem.* **1997**, *35*, 3585.
6.   Li, P.; Xu, J.; Wu, C. *J. Polym. Sci., Part A: Polym. Chem.* **1998**, *36*, 2103.
7.   Xu, J.; Li, P.; Wu, C. *J. Polym. Sci., Part A: Polym. Chem.* **1999**, *37*, 2069.
8.   Li, P.; Xu, J.; Wang, Q.; Wu, C. *Langmuir* **2000**, *16*, 4141.
9.   Stöver, H. D. H.; Li, P.; Ferrari, L. P.; Shaver, R. T.; Vlaovic, D.; *U. S. Pat., 5,376,732,* **1994**.
10. LeDissez, C.; Wong, P. C.; Mitchell, K. A.; Brooks, D. E. *Macromolecules* **1996**, *29*, 953.
11. Yan, C.; Zhang, X.; Sun, Z.; Kitano, H.; Ise, N. *J. Appl. Polym. Sci.* **1990**, *40*, 89.

Chapter 21

Temperature-Sensitive Hairy Particles

Haruma Kawaguchi, Yoko Isono, and Reiko Sasabe

Department of Applied Chemistry, Keio University, 3-14-1 Hiyoshi,
Yokohama 223-8522, Japan

Hairy thermosensitive particles containing a small amount of
ionic groups in their hairs exhibited large and sharp responses
to temperature changes through the volume phase transition
temperature. Incorporation of 2-vinyl imidazole into poly(N-
isopropylacrylamide) hairs on anionic core particles was also
effective in sharpening the thermosensitivity in terms of
hydrodynamic size and protein adsorption and desorption
behavior. The significance of ionic group distribution in the
hair was confirmed with designed hairs prepared by living
radical polymerization.

Since Pelton's pioneering work (*1*), much attention has been paid to
thermosensitive particles, primarily those composed of crosslinked poly-(N-
isopropylacrylamide) (PNIPAM) (*2-4*). We also have been involved in the
preparation, characterization, and application of thermosensitive particles. Most
of our particles were core-shell particles whose shell was crosslinked PNIPAM
(*5-7*). They were swollen, hydrophilic and soft below the volume phase
transition temperature (Ttr) of PNIPAM whereas they were shrunken,
hydrophobic and hard above the Ttr. Such particles have been used as a
thermosensitive drug carrier, bioseparator (*8*), (bio)reactor (*9*), cell activator (*10*)

© 2002 American Chemical Society 307

diagnostic reagent, etc. In these applications, the following are believed to be crucial requisites for the particles:

- Monodispersity
- Extensive response
- Sharp response
- Tough and sustainable sensitivity
- Inert against other stimuli / stable response
- Easily mass produced, etc.

Although linear PNIPAM dissolved in water shows a discontinuous transition at the Ttr, crosslinked PNIPAM or PNIPAM gel and their particulate form have never shown such discontinuities. Their properties changed gradually over a wide temperature range through the Ttr.

We were challenged to sharpen the response of particles having crosslinked PNIPAM shells. What we tried first was to decrease the crosslinking density of the shell polymer. With decreasing crosslinking density (until 0.01 methylenebisacrylamide/100 NIPAM on a weight basis), the response of particles to environmental changes became larger but was not sharpened, i.e., the temperature range where the properties changed did not become narrow. Therefore, the crosslinking density of the PNIPAM shell was reduced to the ultimate extent possible, that is, the shell was turned into a hairy structure. Hairy particles are regarded as the type of particles with minimum crosslinks (Figure 1).

Hairy particles can be prepared by several methods such as micelle formation followed by crosslinking (11), binding a polymer chain at the chain end to a particle (12, 13), surface grafting, etc. We adopted surface grafting on core particles. First, particles with incorporated hydroxyl groups were prepared and hairs were grown by graft polymerization using ceric ion which reacts with CH_2OH group on the particle surface to generate radicals on the particles (14, 15). It is worth mentioning that the polymerization was carried out at a temperature lower than the Ttr of PNIPAM where the hairs were grown up an extended form. The hydrodynamic size of the hairy particles thus obtained was measured as a function of temperature and was found to still be insensitive to temperature changes.

There are two possible reasons for this. One is clustering which takes place in an appreciable temperature range below PNIPAM's Ttr. The other is physical crosslinking or, in other words, entanglement of chains which suppress the adequate swelling and shrinking in response to the change in environmental conditions.

The way to overcome these inconveniences is to introduce inter- and intra-chain repulsive forces. Therefore, a small amount of acrylic acid (AAc) was incorporated into the surface grafts. A tremendous effect of the incorporation of

Figure 1. Nature of a hairy particle.

AAc was observed on the sharpness of the thermosensitivity of the particles. In contrast to the insensitive response of the particles having non-ionic PNIPAM hairs, AAc-containing hairy particles exhibited large and sharp transitions at the Ttr. It is worth mentioning that the amount of AAc in the hair necessary to achieve a sharp response was 0.02 %, which was much smaller than that observed in gels studied for their discontinuous volume phase transition (*16*).

Following the successful achievement of high thermosensitivity brought about by the incorporation of AAc into PNIPAM hairs, the influence of ionic species on the thermosensitivity of PNIPAM hairy particles was examined. The incorporated ionic group was changed from AAc to 2-vinyl imidazole (VIm), that is, from an anionic species to a cationic species.

Through these studies, we recognized the significance of the hairy structure. If we carried out a common radical copolymerization, the characteristics of the hair depended only on the monomer concentration ratio and the reactivity ratio. In contrast, the use of living radical polymerization should enable the monomer unit distribution to be controlled, along with control of the monomer charge mode. In the last part of this study we tried a living radical polymerization approach to graft designed hairs from the particle surface and demonstrate the possibility of controlling the monomer unit distribution in the hair. There have been various initiators developed for living radical polymerization such as TEMPO and metal chelates. Ohtsu's iniferters (abbreviation of initiator, transfer reagent, and terminater) were the first active species for living radical polymerization (*17*). Among them we chose an iniferter shown below for our system due to its applicability to surface grafting in an aqueous medium under moderate reaction conditions (*18*). The iniferter (I) was bound to the latex particles in order to grow designed hairs from the particle surfaces outward in which ionic groups are distributed in controlled modes.

Experimental

Materials

Styrene (St), glycidyl methacrylate (GMA), and vinyl benzylchloride (VBC) were purchased from Wako Pure Chemicals Co. Ltd. and distilled under reduced pressures before use. N-Isopropyl acrylamide (NIPAM) was obtained from Kojin Co. Ltd. and purified by recrystallization from a 50:50 toluene/hexane solution. Sodium N,N-diethyl dithiocarbamate (NaDC, Aldrich Co. Ltd.) was used as received. Acrylic acid (AAc) and vinyl imidazole (VIm) were provided by Wako Pure Chemicals Co. Ltd. Azobis-diisobutyronitrile (AIBN, Tokyo Kasei Co. Ltd.) and potassium persulfate (KPS, Tokyo Kasei Co. Ltd.) were used as initiators after recrystallization. Ammonium ceric nitrate (Ce) was of an

extra pure grade by Tokyo Kasei Co. Ltd. and used without further purification. Water was ion-exchanged and distilled.

Particle Preparation

Polystyrene (PSt) core / crosslinked PNIPAM shell particles were prepared by soap-free emulsion copolymerization in which NIPAM monomer was charged into the polymerization system twice. In the second shot of NIPAM, a small amount of crosslinker, methylenebisacrylamide (MB) was added. The typical recipe for the copolymerization is St/NIPAM/MB/AIBN/water = 3.0/(0.3+3.0)/0.1/0.03/100 (g). The polymerization was carried out in a four-necked 200 ml flask at 70 °C under nitrogen for twenty hours.

Hairy PNIPAM particles were prepared by surface grafting polymerization onto PSt/PGMA particles which were prepared by soap-free emulsion polymerization of 1.2 g St and 1.8 g GMA. Surface grafting was carried out using ceric ion which formed a redox couple with the hydrolyzed epoxy group-carrying GMA units on PSt/PGMA particles. 3.75 g NIPAM with a small amount (0.02 – 0.1 % to NIPAM) of ionic comonomers was added to 75 ml of 0.67 % PSt /PGMA particle dispersion buffered to pH 3.0 with phosphate. After purging with nitrogen, 0.75 g Ce dissolved in 5 g water was added. The graft polymerization was continued at 25 °C for 24 hr.

Another type of PSt core / hairy PNIPAM particles were prepared by living radical polymerization using an iniferter to graft the hairy polymer chain on the core particles. To prepare the core particles, 2.85 g St was copolymerized with 0.15 g VBC in 85 ml aqueous medium. The polymerization was initiated by 0.10 g KPS at 70 °C and continued for 24 hrs. The resulting latex was purified by repetitive centrifugation/decantation/redispersion cycles and 2 g of the purified particles were reacted with 0.15 g NaDC at room temperature for 24 hrs. The iniferter-carrying particles thus obtained (0.50 g) were reacted with 2.16 g of NIPAM in 200 g of the dispersion including no or 0.022 g of AAc. Then the system was irradiated with a UV lamp (UVL-400, Riko Co. Ltd.; peak wave length 365 nm) at room temperature. The polymerization was continued for 1.5 hr.

Characterization

The hydrodynamic size of the hairy particles was measured by photon correlation spectroscopy using a PA3000 spectrometer (Ohtsuka Electron Co. Ltd.) The measurement was carried out at every 1 °C around the Ttr and every 5 °C in other temperature ranges (±0.05 °C).

The length of the hair and the density were measured as follows. The molecular weight of the hair polymer on the particles prepared by the ceric ion-CH₂OH redox system was determined by size exclusion chromatography after cutting the hair at the base by immersing the hairy particles in 1 N HCl for three nights. From the molecular weight and total conversion, the density of the hair could be calculated.

Adsorption and Desorption of Protein to and from Thermosensitive Particles

Adsorption of bovine serum albumin (BSA, isoelectric point 4.5~5.0) was measured as a function of temperature. In the adsorption experiment, 3000 ppm BSA solution was mixed with the same amount of 1 % dispersion of hairy particles and the mixture was incubated for 120 min at the appointed temperatures in the range from 20 °C to 45 °C. All of the measurements were carried out at pH 6.5. Then the mixture was centrifuged keeping the temperature unchanged and the supernatant was recovered to determine the amount of BSA in it. The determination was carried out by the BCA method (*19*) in which the absorbance of the BSA-BCA reagent reaction product was measured at 370 nm.

In the desorption experiment, BSA solution, including the particles, was incubated at 45 °C for 30 min and then the temperature was changed to the appointed ones in the range from 20 °C to 40 °C. After incubation for 120 min, the supernatant was separated from the particles by centrifugation and the amount of BSA in the supernatant was measured to calculate the amount of BSA remaining on the particles at each temperature.

Results and Discussion

Preparation and Characterization of VIm-Containing PNIPAM Hairy Particles

Soap-free emulsion polymerization of St and GMA gave particles with 200 – 220 nm diameters. Glycidyl groups were hydrolyzed to glycelol groups during the polymerization initiated by KPS which introduced negative charges to the particles. The particles were used as core particles for the surface graft reaction. Ceric ions effectively initiated graft polymerization of NIPAM on the core particle regardless of the presence or absence of ionic comonomers.

The conversion reached more than 95% but about half of the polymer was found in very fine PNIPAM particles which contained no core particles. The fine particles were supposed to result from chain transfer reaction followed by re-

initiation and propagation reactions in the aqueous phase. The molecular weight of the hairy polymer was in the range of 5,000 to 20,000 g/mol but might not be reliable because the values obtained by GPC depends on the degree of extension of chains in the medium, which is significantly controlled by the presence of ionic groups. Reliable absolute molecular weights of the hairy polymers are going to be measured by static light scattering.

The temperature dependence of the hydrodynamic size of PNIPAM hairy particles was measured for both increasing and decreasing temperature experiments. The temperature dependence of the hydrodynamic size of the particles was significantly affected by the presence or absence of ionic comonomer units in the hair. The hair did not expand even at room temperature if it contained no ionic groups as pointed out in the case of NIPAM-AAc copolymer hairs. Figure 2 shows that sharp and reversible thermosensitivity was attained in the particles whose hairs contained 0.1% VIm in PNIPAM. In the case of AAc-incorporation into PNIPAM hair, 0.02 % of AAc was enough to exhibit very sharp thermosensitivity. The difference in the effects between AAc and VIm in sharpening the transition seems to result from the electrostatic interactions between hair and core particles. Details of the transition were studied by changing the amount of VIm, keeping other conditions the same as those for NIPAM•AAc grafting.

The polymerization using 0.5% or more VIm brought about coagulation. Perhaps a sufficient amount of positive charges in the hair cancelled the negative charges of core particles so that the inter-particle electro-repulsive force was lost. The polymerization using 0.1% or slightly less VIm resulted in the formation of stable hairy particles.

The particles with PNIPAM hairs containing VIm at concentrations less than 0.05% did not exhibit a sharp response although the particles with PNIPAM hairs containing AAc showed a sharp response even though the AAc content was 0.02%. The repulsive force between two cationic species has been reported to be weaker than that between two anionic species (20). This would explain why a larger amount of VIm was necessary to obtain effective inter- and intra-chain repulsive forces and decrease the entanglement of chains. The opposite charges between the core particle surface and a hair might be another reason for the apparent low efficiency of cationic species (21). It is worth mentioning that the net zeta-potential of NIPAM-VIm copolymer hairy particles was negative at pH 6. The fact that the hairs retain a brush structure even under such conditions suggests that inter- and intra-hair cation-cation repulsive forces were evident even when the core particle surface was negatively charged.

Protein Adsorption and Desorption

We observed large and sharp responses in the hydrodynamic size of slightly ionic hairy particles. To find another evidence for the versatility of slightly ionic hairy particles, the temperature dependence of protein adsorption onto the PNIPAM and NIPAM-VIm copolymer hairy particles (SG-N and SG-NI, respectively), as well as the desorption behavior was studied.

Figure 3 shows the amount of BSA adsorption on SG-N and SG-NI particles at different temperatures from 20 °C to 45 °C. The figure indicates that: (1) adsorption on SG-NI was always higher than that on SG-N over the entire temperature range examined, and (2) adsorption increased with increasing temperature through Ttr on both particles. The increase was larger and sharper on SG-NI than on SG-N.

The higher adsorption on SG-NI was attributed to the electrostatic interaction between negatively-charged protein and positively-charged hairs present in SG-NI. The increase in adsorption with increasing temperature through the Ttr was attributed to the temperature-dependent change in the surface properties of the particles and the protein stability. As to the former, the changes in the surface from hydrophilic to hydrophobic and from soft to hard were brought about by an increase in temperature, and these changes were believed to be responsible for the increase in protein adsorption. The larger and sharper change in adsorption on the SG-NI particles compared to the SG-N particles was attributed to larger differences in the surface properties of SG-NI.

A larger contrast was observed in the protein desorption behavior between SG-N and SG-NI particles. The results of the desorption at different temperatures are shown in Figure 4. In both particle systems, proteins were first adsorbed at 45 °C and then the system was cooled to various temperatures. After 120 min incubation, the amount of desorbed protein was measured to calculate the amount of protein remaining adsorbed on the particles. Desorption occurred sharply at 30 °C from the SG-NI particles, whereas desorption continued gradually from the SG-N particles. The difference in the temperatures at which adsorption sharply increased and at which desorption suddenly occurred on the SG-NI particles suggested that once the proteins adsorbed, it became hard to desorb them from the particle surface because the protein increases the points of attachment on the surface with time. The highly hydrated hairy structure of SG-NI seems to be responsible for the reversibility in terms of the amount of adsorption at low temperature (12.5 mg/g particle).
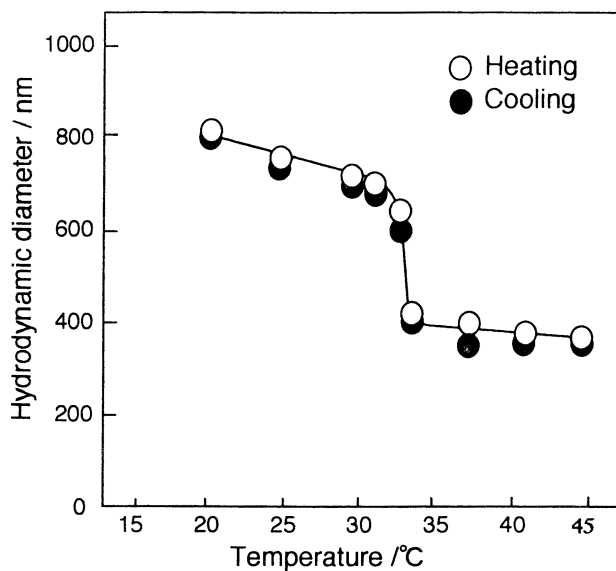
Figure 2. Hydrodynamic diameter of particles having poly(NIPAM-co-VIm) hairs, measured as a function of both heating and cooling process.
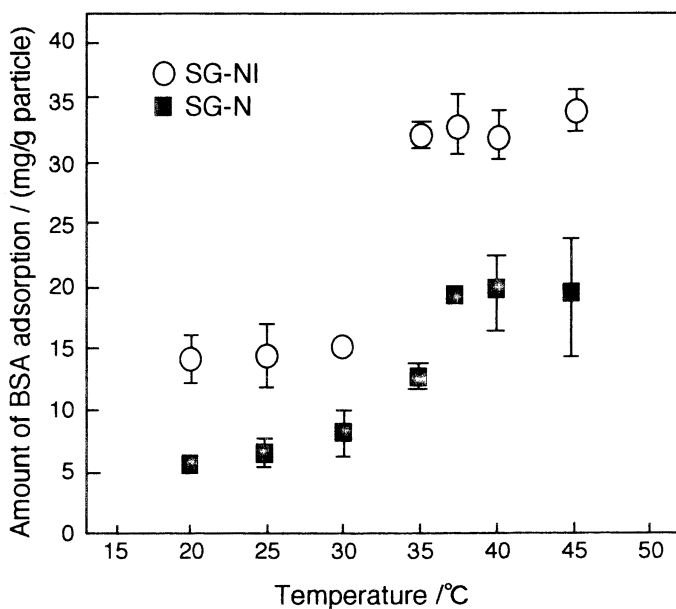
Figure 3. Amount of BSA adsorbed on SG-NI and SG-N particles as a function of temperature.

Living Radical Polymerization for Surface Grafting

The results shown previously suggested that the design of the hairy structures including the density, length, and composition of the hair, and the distribution of components in the hair as well as the conformation and its motion, are crucial for the functionalization of particles. Surface grafting by the ceric ion-CH$_2$OH redox initiation pair was certainly a useful method for the preparation of specifically-designed hairs but could not sufficiently control the chain length and its distribution, or the sequential distribution of components in the hair. The 'living polymerization' process should allow control of these parameters. Quasi-living radical or a controlled radical polymerization was applied for the surface grafting reaction to obtain well-designed hairs.

Among the several controlled radical polymerization processes, using iniferters is an attractive route because the polymerization can be performed under mild conditions, e.g., even at room temperature in water. Among the iniferters developed by Ohtsu, N,N-diethyl dithiocarbamate (NaDC) was selected, which is activated by UV irradiation at room temperature. Core particles were prepared by soap-free emulsion copolymerization of St and VBC instead of homopolymerization of VBC (*22, 23*) because St was effective in preparing monodisperse submicron particles. NaDC was attached to the resulting particles. The possible polymerization scheme on the particle surface is shown in Figure 5.

The availability of NaDC-carrying particles was examined in the surface-grafting polymerization of NIPAM. Samples were removed from the polymerization system at different time intervals during the course of polymerization. The hydrodynamic diameter of the particles in each sample was measured and plotted against the conversion. The gradual increase in the hydrodynamic diameter with increasing conversion shown in Figure 6 is clear evidence for the suitability of the iniferter technique for surface grafting. To show this more quantitatively, the volume of shell in each sample [$\propto (D+2L)^3 - D^3$) where D is the diameter of the core particle and L is the thickness of the shell which was measured at 25 °C] was plotted against conversion. The almost linear relation in Figure 6 suggested that PNIPAM hairs in the swollen layer grow up keeping the density in the shell constant. The details will be discussed after obtaining the precise molecular weight of the hair polymers.

The most important advantage of controlled radical polymerization is the ability to control the sequential distribution of comonomers in the hair. If comonomers are charged with one shot in a controlled radial polymerization, the sequence is decided by the concentration ratio and reactivity ratio of comonomers. Only a special case may give block-like copolymer. In contrast, if two copolymers are changed one by one in a controlled radical polymerization, block copolymer hair can be formed spontaneously.
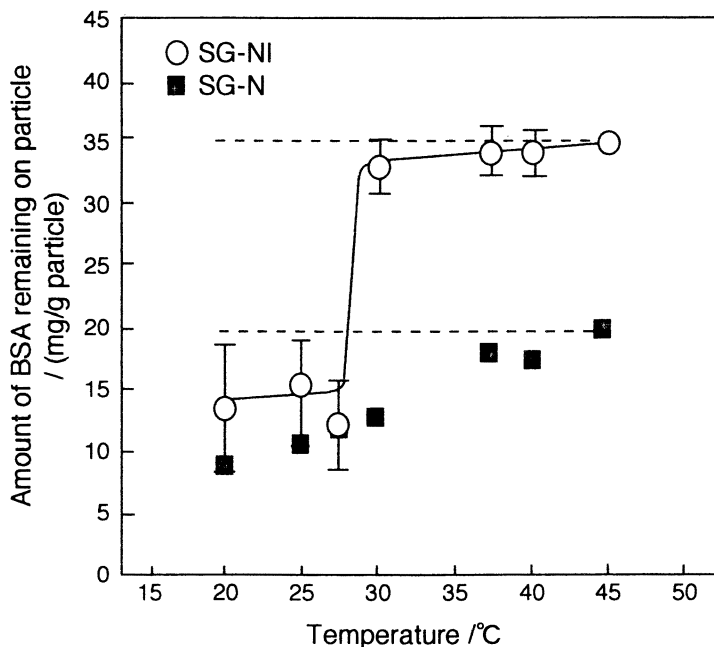
Figure 4. Amount of BSA remaining on SG-NI and SG-N particles when the particles were cooled from 45 °C to the temperatures 20 – 40 °C. The dashed lines indicate the amounts of BSA adsorbed on SG-NI and SG-N particles at 45 °C.
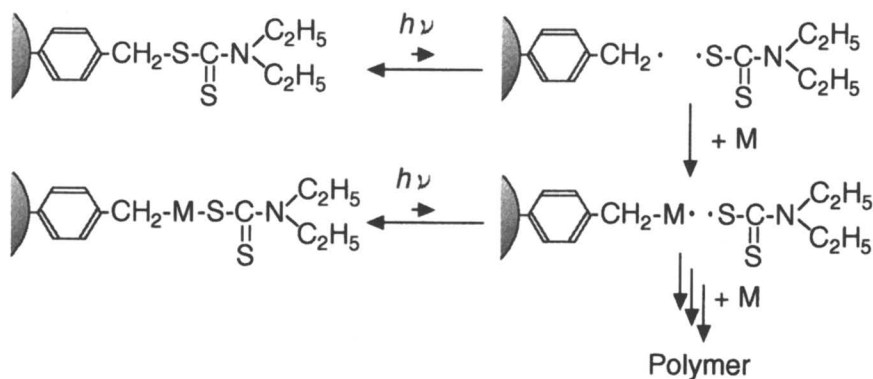
Figure 5. Progress of living radical polymerization using an iniferter to form designed hairs.
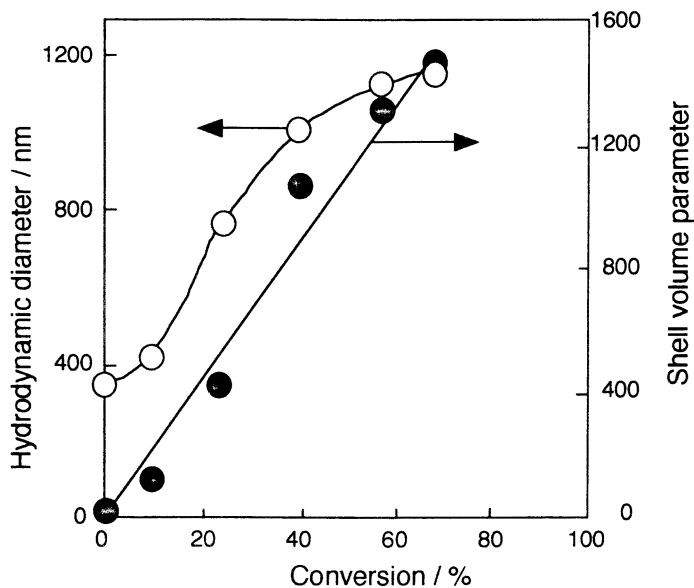
Figure 6. Growth of hairs on core particle surface by living radical polymerization. Shell volume parameter: $[(D+2L)^3 - D^3]$ where D is the diameter of the core particle and L is the thickness of the swollen shell.

One-shot and two-shot polymerizations were carried out using 2.5 g NIPAM and 0.0125 g AAc onto 0.5 g iniferter-carrying particles. Two-shot polymerization was carried out by feeding only 2.5 g NIPAM in the first shot and only 0.0125 g AAc in the second shot.

The hydrodynamic sizes of three kinds of hairy particles, (a) particles obtained by one-shot polymerization, (b) particles obtained only by the first shot of two shots, and (c) particles obtained by two-shot polymerization are shown in Figure 7.

The one-shot polymerization resulted in the formation of hairy particles similar to those obtained by the ceric–C_2H_5 redox system. That is, the hairs of both particles took a brush structure at room temperature but shrunk sharply at the Ttr of PNIPAM. This fact revealed that the living radical polymerization in which all of the monomers were fed before starting the polymerization gave the hairs in which AAc was distributed randomly in the PNIPAM sequence.

In contrast, the use of a two-shot polymerization process formed hairs with a different structure, although the AAc content in the hair was 0.5 %, which was the same to that of the one-shot polymerization system. The second shot, i.e., an AAc feed, resulted in a only slight increase in the thickness of the hairy shell; i.e., the attachment of AAc at the end of the hairs did not impart any inter- and intra-chain electro-repulsive forces and, therefore, could not extend the coiled and entangled hairs.

Conclusions

We showed in our previous papers (*14, 15*) that particles having thermosensitive hairs responded to temperature changes to a greater extent than did particles having crosslinked thermosensitive shells if the hairs contained a small amount of ionic groups which yielded suitable inter- and intra-electrorepulsive forces to give the hairs a brush-like structure. In the present study, we confirmed that this was the case even if the core particles and hairs had different signs of electric charge. A sharp response of ionic group-containing hairy particles was observed by the hydrodynamic size of the particles and protein adsorption and on desorption from the particles.

To achieve a sharp response, the ionic groups have to be evenly distributed in the hairs. This was confirmed by comparing the themosensitivity of particles having hairs with different structures in terms of their ionic group distribution which were prepared by living radical polymerization.
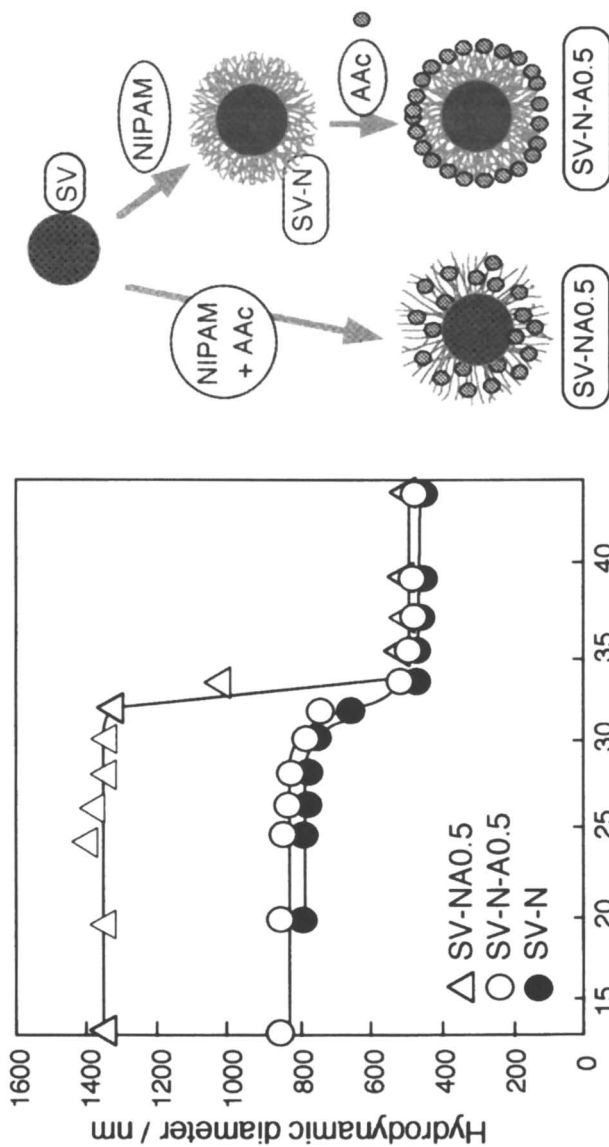
Figure 7. Hydrodynamic diameter of particles having hairs with different structures as a function of temperature.

Acknowledgment

The present work is partially supported by a Grant-in-Aid on Scientific Research on Priority Area (B) on "Laser Chemistry of Single Nanometer Organic Particles" from the Ministry of Education, Science, Supports, and Culture of Japan (10207204).

References

1. Pelton, R. H.; Chibante, P. *Colloids Surf.* **1986**, *20*, 247.
2. Snowden, M. J.; Marston, N. J.; Vincent, B. *Colloid Polym. Sci.* **1994**, *272*, 1273.
3. Oh, K. S.; Oh, J. S.; Choi, H. S.; Bae, Y. C. *Macromolecules* **1998**, *31*, 7328.
4. Duracher, D.; Elaissari, A.; Mallet, F.; Pichot, C. *Macromol. Symp.*, **2000**, *150*, 305.
5. Kawaguchi, H.; Fujimoto, K.; Mizuhara, Y. *Colloid Polym. Sci.*, **1992**, *270*, 53.
6. Ohshima, H.; Makino, K.; Kato, T.; Fujimoto, K.; Kawaguchi, H., *J. Colloid Interface Sci.* **1993**, *159*, 512.
7. Kawaguchi, H. In *Microspheres, Microcapsules & Liposomes*. Arshady, R. Ed., Citus Books; London; **2000**, pp. 237-252.
8. Kawaguchi, H.; Fujimoto, K. *Bioseparation* **1999**, *7*, 253.
9. Kato, T., Fujimoto, K., Kawaguchi, H. *Polym. Gels Networks*, **1994**, *2*, 307.
10. Fujimoto, K.; Takahashi, T.; Miyaki, M.; Kawaguchi, H. *J. Biomater. Sci., Polym. Ed.* **1997**, *8*, 879.
11. Yokoyama, M.; Kataoka, K. *Macromol. Chem., Rapid Commun.* **1987**, *8*, 431.
12. Yasui, M.; Shiroya, T.; Fujimoto, K.; Kawaguchi, H. *Colloids Surfaces*, **1997**, *8*, 311.
13. Zhu, P. W.; Napper, D. H. *J. Colloid Interface Sci.* **1996**, *177*, 343.
14. Matsuoka, H.; Fujimoto, K.; Kawaguchi, H. *Polym. Gels Networks* **1998**, *6*, 319.
15. Matusoka, H.; Fujimoto, K.; Kawaguchi, H. *Polym. J.* **1999**, *31*, 1139.
16. Kawasaki, H.; Sasaki, S.; Maeda, H. *J. Phys. Chem.* **1997**, *101*, 5089.
17. Ohtsu, T.; Yoshioka, M. *Macromol. Chem., Rapid Commun.* **1982**, *3*, 127.
18. Otsu, T.; Yamashita, K.; Tsuda, K. *Macromolecules*, **1986**, *19*, 287.
19. Smith, P. K.; Krohn, R. I.; Hermanson, G. T.; Mallia, A. K.; Gartner, F.H.; Provenzano, M. D.; Fujimoto, E. K.; Goeke, N. M.; Olsen, B. J.; Klenk, D. C. *Anal. Biochem.* **1985**, *150*, 76.

20. Okubo, T.; Suda, M. *Colloid Polym Sci.* **1999**, *277*, 81

21. Shinagawa, T.; Ohshima, H.; Kondo, T. *Biophys. Chem.* **1992**, *43*, 149.

22. Suen, C. H.; Morawetz, H. *Macromolecules* **1984**, *17*, 1800.

23. Verrier-Charleux, B.; Graillat, C.; Pichot, C.; Revillon, A. *Colloid Polym. Sci.* **1991**, *269*, 398.

Chapter 22

Ethylene-Modified Latexes: Preparation, Miscibility Enhancement, and Barrier Properties

Jin-Sup Shin, Doug-Youn Lee, and Jung-Hyun Kim*

Nanosphere Process and Technology Laboratory, Department of Chemical Engineering, Yonsei University, Seoul 120-749, Korea

Ethylene-modified latexes were prepared by the emulsion polymerization of styrene using poly(ethylene-co-acrylic acid) (EAA), [M_n: 18,800 g mol^{-1}, acid number:140], as a polymeric emulsifier. EAA containing 20% portion of acrylic acid could form aggregates like micelles. The rate of polymerization of styrene using EAA is found to increase with increasing EAA concentration. This result is similar to that obtained in emulsion polymerization using conventional surfactant. The polystyrene (PS) latexes prepared using EAA exhibited small particle size and monodisperse particle size distribution in the presence of excess neutralizing agent which reduces the repulsion between charges along the EAA chain. The EAA-grafted-PS formed in situ during emulsion polymerization led to the improvement of miscibility between EAA and PS. The dynamic mechanical properties of the ethylene-modified PS films exhibit single glass transition temperature values, thus conforming to the law of miscibility. The grafted or anchoring of EAA into the particles improved the barrier properties, such as chemical resistance, of ethylene-modified PS films.

It is well known that amphiphilic polymers, which consist of both hydrophobic and hydrophilic groups, can stabilize polymer particles and can form aggregates, like micelles, as a result of intermolecular and/or intramolecular hydrophobic interactions (1,2). Aqueous solutions of such polymers are characterized by unusually low viscosities, and by high solubilization capacities. These properties are attributed to the aggregation of the surfactant side chains providing hydrophobic microdomains in isotropic aqueous solution. Such a behavior resembles the micelle formation of low-molecular-weight surfactants in water. Hence, the micellar polymers were coined (3), and the hydrophobic aggregates formed in polysoaps are referred to as polymeric micelles. Recently, alkali-soluble resin (ASR) containing carboxylated random copolymers were used as a polymeric surfactant in the emulsion polymerization of polystyrene (PS) and poly(methyl methacylate) (PMMA) latex particles (4). Very small latex particles were formed compared with a conventional surfactant system. The ASR was found to become adsorbed as well as grafted on the surface of the latex particles. Thus, this would appear to offer a new route of changing the nature of the polymeric material of the latex particles.

Poly(ethylene-co-acrylic acid) (EAA) containing an ethylene group are flexible thermoplastics having water resistance and barrier properties similar to low-density polyethylene (LDPE). Due to a high degree of inertness to chemicals, polyethylene is an appropriate material for containers and automobile tanks. The role of adsorbed surfactants in the process of film formation has received some interest and has been summarized by Bindschaedler et al. (5), and the barrier properties caused by them have been discussed (6). At high carboxyl levels, there are enough acid groups to be neutralized with alkali in hot water to form a surfactant-free dispersion. This dispersion can be applied as a polymeric surfactant in emulsion polymerization. However, few publications can be found that are concerned with EAA as a polymeric emulsifier in emulsion polymerization (7). The properties of EAA are expected to be similar to those of other polymeric surfactants, but their behavior and contribution in emulsion polymerization would be different from those of conventional polymeric surfactants.

The importance of the interface in multiphase polymer systems has been long recognized. Physical and chemical interactions across the phase boundaries are known to control the overall performance of immiscible polymer blends. Searches have shown that the blending of PET and PA in the melt produces polyester-polyamide block copolymers, which could improve the compatibility of the blends (8). Unfortunately, very few investigations on the improvement of compatibility of the blends without compatibilizer or functional groups present seems to be available in the literature.

The present study was undertaken to investigate the contributions of EAA in the emulsion polymerization of styrene with a water-soluble initiator, potassium

persulfate. The aqueous solution behavior of EAA, such as aggregate formation, and the effects of the concentration of EAA on the latex particle size and size distribution were investigated. Also, the improvement of miscibility between PS and EAA during emulsion polymerization and the barrier properties of ethylene-modified latex films were investigated.

Experimental

Materials

Poly(ethylene-co-acrylic acid) (EAA) [M_n: 18,800 g mol^{-1}, M_w: 111,000 g mol^{-1}, acid number: 140], obtained from Dow Chemical Co. was used as received. Styrene and butyl methacrylate monomers were obtained from Junsei Chemical and were distilled under the reduced pressure of nitrogen. Pyrene was purchased from Fluka. Potassium persulfate, sodium hydroxide, triethylamine, sodium chloride, toluene, and methyl ethyl ketone were all analytical grade materials and were used without further purification. Distilled and deionized water was used throughout.

Emulsion Polymerization Using EAA

Batch polymerizations were carried out in a 1L double-wall round-bottom reactor equipped with a temperature controller, nitrogen inlet, and stirrer. In the reactor, EAA and NaOH were dissolved in distilled-deionized water, and monomer was added. The reactor was maintained for about 30 min for the contents to attain the reaction temperature, 70 °C. During this time, the contents of the reactor were stirred and flushed with nitrogen. The initiator was dissolved in the remaining water and added to the reactor. The addition of the initiator marked the start of the reaction. The polymerization was carried out under a nitrogen atmosphere until the reaction was substantially completed. The basic recipe of the emulsion polymerization in the presence of EAA is given in Table I. The sample I.D. for prepared latex samples is listed in Table II. The conversion of styrene was determined by gravimetry.

Dynamic Mechanical Analysis (DMA)

The simple extension mode was employed for the dynamic mechanical analysis. The dynamic mechanical behavior of the films was investigated using a dynamic mechanical thermal analysis instrument (DMTA) (Polymer

Labotatories, Model MK-III, UK) equipped with an attachment for temperature control. This apparatus enabled us to measure the extension storage modulus (E′), the loss modulus (E″) and the loss tangent (tan δ) over a wide range of temperature (-50 °C ~ 200 °C). The isochronal temperature dependence of moduli and tan δ was obtained for a frequency of 10 Hz at a constant heating rate of 2 °C min⁻¹ under a nitrogen atmosphere.

Table I. Basic Recipe of Emulsion Polymerization Using Poly(ethylene-co-acrylic acid) as a Polymeric Emulsifier

Component	Amount
D.D.I. Water	600
Poly(ethylene-co-acrylic acid) (EAA)[a]	20, 40, 50, 60
Sodium Hydroxide (NaOH)	variable[b]
Styrene or Butyl Methacrylate	100
Potassium Persulfate	0.5

[a] EAA: M_n = 18,800 gmol⁻¹, M_w = 111,000 gmol⁻¹, Acid No. = 140

[b] NaOH or triethylamine was added in all systems in order to change the degree of neutralization of EAA.

Table II. Sample I.D. for Prepared Latex Samples

Composition	Sample I.D.
60 wt% EAA-Ethylene-Modified PS	EMPS-E60
40 wt% EAA-Ethylene-Modified PS	EMPS-E40
20 wt% EAA-Ethylene-Modified PS	EMPS-E20
60 wt% EAA-Blended PS	SBPS-E60
40 wt% EAA-Blended PS	SBPS-E40
20 wt% EAA-Blended PS	SBPS-E20

Chemical Resistance Test

The latexes for the chemical resistance study were dried in a freeze dryer unit at −40 °C. Sheets in the form of disks were obtained by compression molding in a heated press (Carver hot press) at 130 °C and 3000 psi. The preheating time was 10 min and molding time was 60 min. From the prepared sheets, specimens were cut into disks of 50.80 mm in diameter and 3.175 mm in

thickness for the chemical resistance tests. This chemical resistance test was based on ASTM D543. The weight loss of the samples was calculated after their immersion in methyl ethyl ketone for 5 hours to compare the ethylene-modified PS with the simple blends at the same EAA concentration in the film.

Results and Discussion

Aggregate Formation of EAA in Aqueous Solution

Amphiphilic polymers, having both hydrophobic and hydrophilic groups, can form aggregates in aqueous solution. In order to find out whether the random copolymer forms aggregates in aqueous solution, pyrene solubility in EAA solution was studied.

Pyrene is an aromatic hydrocarbon exhibiting a very low solubility in pure water ($[Py]_{s,water} \approx 7 \times 10^{-7}$ M) and is largely used as a probe for the study of micelles and other hydrophobic aggregates in water (2). An increase in pyrene absorbance with EAA concentration was observed (Figure 1). This indicated the formation of polymer aggregates like micelles in aqueous solution. The increase in solubility of pyrene could be attributed to an increase in the number of the aggregates. This trend is similar to that observed for conventional surfactants.
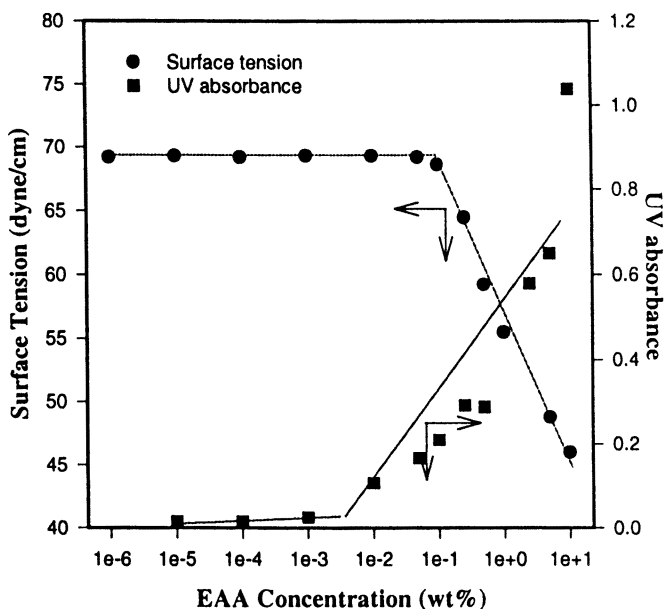
Figure 1. UV absorbance of pyrene at 360 nm and surface tension of EAA solution as a function of EAA concentration (wt% based on total).

In the surface tension versus concentration measurement, an equivalence to the critical micelle concentration (cmc) of low-molecular-weight surfactants is missing. These findings are in general agreement with recent work by Anton and Laschewsky (9) on the aggregation behavior of polymeric emulsifiers. As shown in the pyrene solubility results, however, EAA molecules in the aqueous phase seem to form aggregates at low concentrations before they start to transfer to the air-water interface.

Kinetics of Emulsion Polymerization of Styrene

Investigation of the kinetics of emulsion polymerization typically involve the determination of the polymerization rate and its dependence on polymerization parameters such as the monomer, emulsifier, and initiator concentrations, and the temperature (10). It is suggested that both the solubility of the monomer in water and its polarity affect the mechanism of particle formation (11,12). For the conventional emulsion polymerization of styrene, examined by Harkins (11), the most important sites of particle generation are the monomer-swollen emulsifier micelles; with the increase of monomer solubility in water, the locus of particle nucleation may move to the aqueous phase (12).

In the case of water-insoluble monomer such as styrene, micellar nucleation is the predominant mechanism in the polymerization process. Because of this fact, styrene was used as the monomer for this study on the kinetics of emulsion polymerization. Figure 2 depicts the conversion of monomer versus time for the emulsion polymerization of styrene at different EAA concentrations. Determination of the fractional conversion was accomplished by a gravimetric method. As shown in Figure 2, with increasing concentration of EAA as polymeric emulsifier, the rate of polymerization increased. It is generally expected that the increase of EAA concentration results in an increase in the number of aggregates providing polymerization loci, and thus, the rate of emulsion polymerization increases. This behavior of EAA in emulsion polymerization is similar to that observed with conventional emulsifier (13).

Particle Size and Particle Size Distribution of Latex

Particle formation in emulsion polymerization using EAA would be affected by the properties of the EAA aggregates, which depend on the neutralization of EAA, as well as the content of electrolytes, and the water solubility of the monomer. The PS latexes prepared using excess neutralizing agent, NaOH, exhibits a small particle size (ca. 70 nm) compared to that observed for
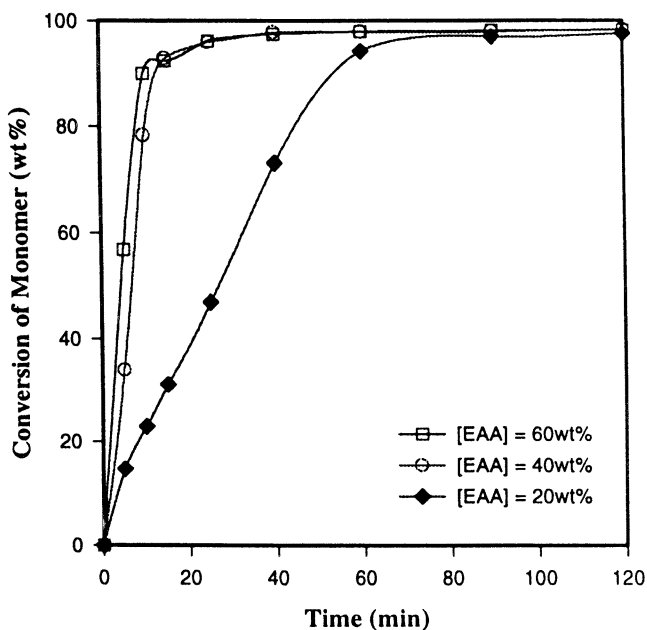
Figure 2. Conversion of monomer versus reaction time for the emulsion polymerization of styrene with different concentrations of EAA (wt% based on monomer).

conventional emulsion polymers. In this system, very stable submicron size latexes are formed with a monodisperse size distribution.

Figure 3 shows the PS latex particle size and size distribution obtained from this system using different ratios of EAA to styrene. The particle sizes of latexes increased from 69.1 to 82.4 nm in diameter with decreasing weight ratio of EAA/styrene and the particle size distribution became monodisperse with increasing weight ratio of EAA/styrene. This result was similar to that obtained in the emulsion polymerization using conventional surfactants, namely, an increase in EAA concentration results in more aggregate formation providing polymerization loci, and therefore, the particle size is smaller.

Grafting

The quantitative separation and characterization of PS homopolymer, alkali water-soluble EAA, and EAA-grafted-PS were carried out by using two consecutive selective solubilization steps. First, the EMPS-E40 powder was stirred in toluene. The toluene-soluble PS homopolymer is then separated from the sample by centrifugation. Second, hot alkaline water was used for selective solubilization of EAA to separate the alkaline water-soluble EAA from EAA-

grafted-PS. PS homopolymer was extracted in the toluene and the amount obtained was less than the amount calculated based on the theoretical PS weights. Thus, it was assumed that the remaining PS, 20.2% based on total PS, was grafted onto the EAA. After the second selective treatment in a hot alkaline water for 48h, 39.9% of the precipitated EAA was dissolved in the alkaline water, while the remaining 60.1% of the total EAA was alkali-water-insoluble (EAA-grafted-PS). Due to grafting of EAA molecules on the latex particles, the hindered desorption of the emulsifier from the latex would improve the latex stability and facilitate a core/shell-like structure. Also, it would prevent the migration and accumulation of EAA molecules (e.g., near the surface) after the film fomation of the latex, which deteriorates the performance of the final polymer products. That is, the EAA-grafted-PS formed in situ will then act as a compatibilizer for the main polymer components. The behavior and contribution of EAA in emulsion polymerization were found to be different from those of conventional polymeric surfactants. The EAA molecules not only act like
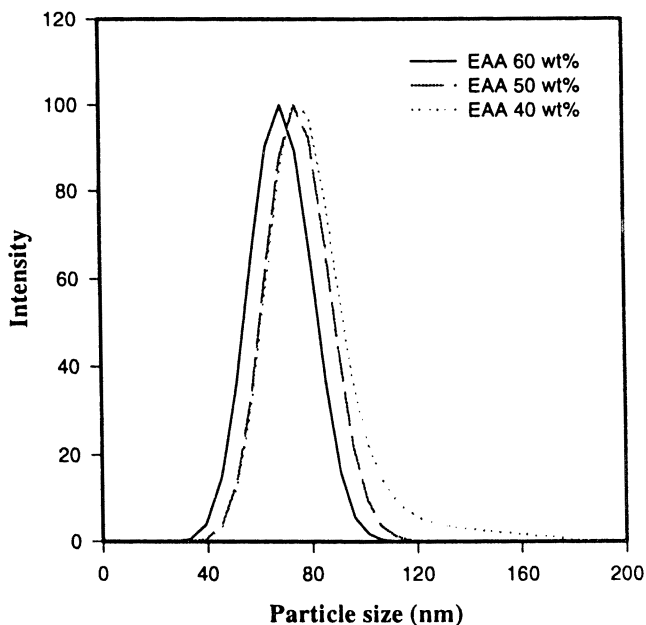
Figure 3. Particle size and size distribution of ethylene-modified PS with different EAA concentrations at 140% degree of neutralization of EAA.

surfactants but also provide their own characteristics to the latex for the EAA-modified emulsion system (4).

Dynamic Mechanical Properties

The miscibility of different polymer blends through various specific interactions can be predicted theoretically using the solubility parameter. The solubility parameter components may be predicted from group contribution theory, using the method of Hoftyzer and Van Krevelen (14). The solubility parameter for a random copolymer can be calculated by using the Hildebrand equation, as follows:

$$\delta = \sum \delta_i \phi_i \qquad (1)$$

where δ_i and ϕ_i are the solubility parameter and volume fraction, respectively, of the homopolymers in the copolymer.

In order to achieve molecular-level mixing of the blend constituents the value of the interaction parameter (χ) should be <0.002, which can be calculated by using the Hildebrand equation, as follows :

$$\chi = V_R / RT (\delta_A - \delta_B)^2 \qquad (2)$$

where V_R is the reference volume, δ_A and δ_B are the solubility parameters of the two blend constituents, T is the temperature, and R is the molar gas constant.

Using the data given in Table III, the miscibility of the binary blend system was predicted. With the solubility parameters, δ_A and δ_B obtained from group contribution theory and a reference volume conveniently taken as 100 cm^3 mol^{-1} at 25 °C, the interaction parameter (χ) was calculated and found to be 0.0425, which is well above the 0.002 value predicted by the Hildebrand approach. This value substantiates the fact that the blends are completely immiscible (15). In the case of the simple blending of EAA solution and PS latexes, phase separation is also confirmed by direct observation after film formation. This immiscibility between PS and EAA is further confirmed by the DMTA test.

Before the DMTA analysis of a simple blend film of PS latex and EAA solution is presented, let us set the stage by defining the relevant features in the tan δ and storage modulus of the individual PS latex film and the EAA film. Both the PS latex film and the EAA film show a single, sharp glass transition temperature (Figure 4).

Table III. Physical Parameters of the Pure Constituents of the Blend

	Molar Volume $(cm^3 mol^{-1})$	Molecular Weight $(g\ mol^{-1})$	Solubility Parameter $(cal^{1/2}\ cm^{-3/2})$
Polystyrene	98.0	104.1	8.90
Polyethylene	33.0	28.1	8.00
Poly(acrylic acid)	38.0	72.1	11.92
EAA			8.395
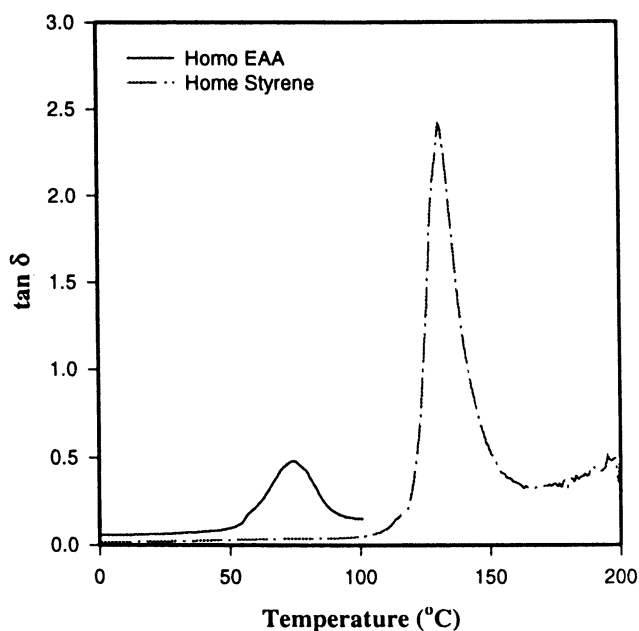
Figure 4. Dynamic mechanical properties of PS homopolymer film and EAA homopolymer film as a function of temperature: damping curves (tan δ).

Figure 5 shows various dynamic mechanical properties, such as damping (tan δ), of a simple blend film of PS latex and EAA solution with respect to variation in the temperature, ranging from –50 °C to 200 °C. The simple blend film of PS and EAA show two glass transition peaks. The peak at 130~135 °C corresponds to the glass transition peak of PS, and the other peak at 60~70 °C corresponds to that of EAA.
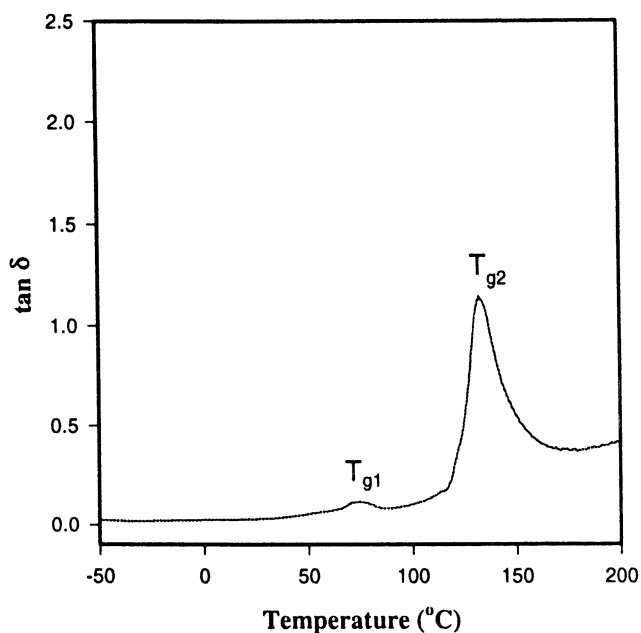
Figure 5. Dynamic mechanical properties of a simple blend film of PS and 40 wt% EAA based on PS as a function of temperature: damping curve (tan δ).

In the case of ethylene-modified PS, however, the damping curve shows a single and sharp glass transition temperature (Figure 6), that is, the miscibility between PS and EAA in ethylene-modified PS was improved during the emulsion polymerization. This result can be also interpreted as the improved miscibility between two phases without adding any compatibilizer. The EAA used as a polymeric emulsifier would be grafted to the main polymer chains or anchored to them during polymerization. This EAA-grafted-PS due to chain transfer would result in the improvement of miscibility and result in no phase separation during film formation.

As most polymer pairs are immiscible except for a few polymer pairs, to improve the miscibility of blends it is well known that a compatibilizer or a functional group to allow a chemical reaction to occur between polymers must be introduced (*16*). For the ethylene-modified system, however, there is no necessity to use a compatibilizer or functional group because the miscibility was improved in situ during polymerization.
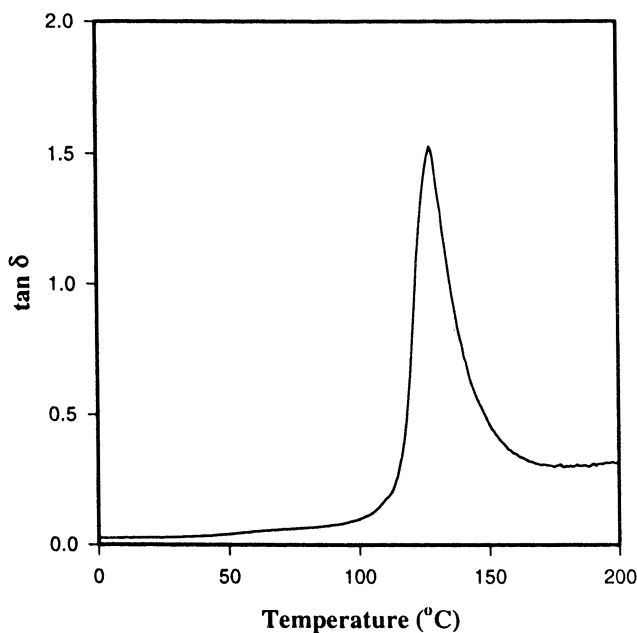
Figure 6. Dynamic mechanical properties of a ethylene-modified PS film containing 40 wt% EAA as a function of temperature: damping curve (tan δ).

Chemical Resistance of Ethylene-Modified Latex Films

Figure 7 shows the percentage weight losses of ethylene-modified latex films and the simple blend films of PS and EAA after their immersion in methyl ethyl ketone for 5 hours. Because of the good compatibility between PS and EAA that originated from PS-grafted-EAA, the chemical resistance of ethylene-modified PS films is dramatically better than that of the simple blends of PS and EAA. For EMPS-E40, the chemical resistance is about 20 times higher than that of SBPS-E40, as shown in Figure 7. These results are in general agreement with recent work by Ju and Chang (*16*). However, they used special functional monomers for compatibilizing those immiscible blends. In the ethylene-modified system, the miscibility between PS and EAA was improved without any compatibilizer added during emulsion polymerization. Also, the chemical resistance of ethylene-modified PS films increased with an increase in EAA concentration. This was attributed to the ethylene group content in these films.
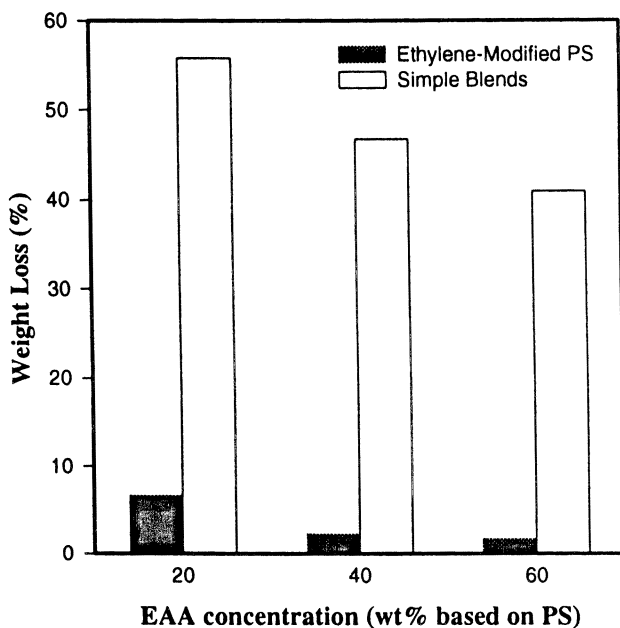
Figure 7. Weight loss of ethylene-modified PS and simple blends of PS/EAA as a function of EAA concentration after their immersion in methyl ethyl ketone for 5 hours.

Conclusions

EAA containing a large number of carboxyl groups formed aggregates like micelles. The kinetics of the emulsion polymerization of styrene using EAA was examined. The rate of polymerization was dependent on the EAA concentration. The study on the rate of polymerization showed that the increased EAA concentration enhanced the rate of polymerization. This result is similar to conventional emulsifier systems. PS latexes prepared using EAA showed a small particle size (ca. 70 nm) compared to that observed for conventional emulsion polymers. The size of ethylene-modified PS latex particles decreased with increasing the concentration of EAA that acted as a polymeric emulsifier.

The quantitative separation and characterization of PS homopolymer, alkali water-soluble EAA, and alkali water-insoluble EAA was carried out by using a two consecutive selective solubilization steps. Quantitative separation showed that 20.2% PS based on total PS and 60.1% EAA based the total EAA

participated in the grafting reaction. EAA-grafted-PS generated in situ influenced both the miscibility and film properties and would act as the compatibilizer for the main polymer component. The interaction parameter (χ) was found to be 4.25×10^{-2}, which is well above the 0.002 predicted by the Hildebrand approach. This value substantiates the fact that the blends are completely immiscible. However, the miscibility of EAA and PS was improved during ethylene-modified emulsion polymerization of styrene. These facts were confirmed by the dynamic mechanical properties. For ethylene-modified PS, the damping curve shows a single, sharp glass transition temperature, that is, the miscibility between PS and EAA was improved by the ethylene-modified emulsion polymerization of styrene.

The chemical resistance of ethylene-modified PS films was dramatically better than that of the simple blends. The EAA-grafted-PS or the anchoring of EAA onto the PS particles influenced both the barrier and mechanical properties.

Acknowledgment

References

1. Kuo, P. L.; Chen, C. J. *J. Polym. Sci., Polym. Chem.* **1993**, *31*, 99.
2. Wang, T. K.; Iliopoulos, I.; Audebert, R. In *Water-Soluble Polymers*; Shalaby, S. W. Ed.; ACS Symp. Series 467; **1991**; p. 218.
3. Strauss, U. P.; Jackson E. G. *J. Polym. Sci.* **1991**, *5*, 649.
4. Lee D. Y.; Kim, J. H. *J. Appl. Polym. Sci.* **1998**, *69,* 543.
5. Bindschaedler, C.; Gurny, R.; Doelker, E. *J. Appl. Polym. Sci.* **1987**, *34*, 2631.
6. Issacs, F. K. *J. Macromol. Chem.*, **1966**, *1*, 163.
7. Shin, J. S.; Lee, D. Y.; Kim, J. H. *Macromolecular Symp.*, **2000**, *151*, 509.
8. Pillon, L. Z.; Utracki, L. A. *Polym. Eng. Sci.* **1984**, *24*, 1300.
9. Anton, P.; Laschewsky, A. *Coll. & Polym. Sci.* **1994**, *272*, 1118.
10. El-Aasser, M. S., Sudol, E. D. In *Emulsion Polymerization and Emulsion Polymers;* Lovell, P. A.; El-Aasser, M. S., Eds.; John Wiley and Sons: Chichester, 1997, pp 38-58.
11. Harkins, W. D. *J. Am. Chem. Soc.*, **1947**, *69*, 1428.

12. Fitch, R. M. In *Emulsion Polymers and Emulsion Polymerization*; Bassett, D. R.; Hamielec, A. E. , Eds.; ACS Symp. Series; 1981; Vol 165, pp 1.

13. Bartholome, E.; Gerrens, H.; Herbeck, R.; Weitz, H. M. *Z. Elektrochem.* **1956**, *60*, 334.

14. *Properties of Polymers;* Van Krevelen, D. W. Ed.; Elsevier: Amsterdam, 1972.

15. Mukberjee A. K.; Gupta, B. D. *J. Appl. Polym. Sci.* **1985**, *30*, 444.

16. Ju, M. Y.; Chang, F. C. *J. Appl. Polym. Sci.* **1999**, *73*, 2029.

Chapter 23

Water-Based Hybrids of Vinyl Acetate–Ethylene Copolymers and Cross-Linkable Epoxy

Lloyd M. Robeson, David Dubowik, and Robert A. Berner

Air Products and Chemicals, Inc., 7201 Hamilton Boulevard, Allentown, PA 18195

Water-based hybrids of vinyl acetate-ethylene (VAE) copolymers and epoxy have been developed offering properties intermediate between the constituents and allowing for a novel method for providing a water-borne toughened epoxy system. Liquid epoxy (specifically the diglycidyl ether of Bisphenol A) can be added (with proper stirring) to a VAE emulsion resulting in a stable, homogeneous emulsion (up to 40 wt% epoxy based on solids). Particle size analysis shows a slight increase in the particle diameter with a narrower particle size distribution, thus indicating that no new emulsion particles are formed and the epoxy is incorporated into the existing VAE particles.

The resultant hybrid can be crosslinked with the addition of water soluble or water dispersed amine curatives. Specific amine curatives have been found that exhibit one part emulsion stability for up to a year while retaining the ability to be film forming even though the included epoxy is crosslinked. A specific example of a one part system involves isophoronediamine (IPDA) as a curative. It was found (based on pH changes) that IPDA slowly diffuses from the water and reacts with the epoxy in the VAE particles. Water-dispersed epoxy-amine adduct curatives (two part systems) gave an

© 2002 American Chemical Society

excellent combination of strength and toughness with mechanical properties intermediate between the highly flexible VAE and the rigid epoxy. The dynamic mechanical results indicate phase separation for this hybrid with a limited shift in the Tg of the VAE phase. The equivalent box model (EBM) has been utilized to predict modulus and strength values for this hybrid. Good agreement between predicted and experimental results for modulus is observed for the two part hybrids, with only fair agreement for strength.

Water-borne polymer systems continue to expand to new applications often at the expense of solvent based polymers. In addition to emulsion polymers, water-borne epoxies, urethanes, and alkyds have been commercially available to meet various coatings and adhesive applications once dominated by solvent based polymers. With the continued emphasis on materials with low/no VOC (volatile organic compounds) levels, water-borne and 100% solids technology are the environmentally acceptable alternatives. Development of new products to meet the property characteristics of solvent based systems continues to be a fertile research area. In order to meet the myriad of cost/performance requirements, hybrid systems offer combinations of properties not achievable with the unblended constituents. This paper will describe an epoxy/VAE (vinyl acetate-ethylene copolymer) water-borne hybrid which can be prepared either as a one component or two component system with amine curatives for the epoxy. One component systems offering room temperature cure are often desired but very difficult to achieve. This paper will demonstrate a system with these characteristics.

Water-borne epoxy systems have been described in various publications and patents. Water-borne epoxy properties have been compared to their solvent-based counterparts by Wegmann (*1*). Waterborne epoxies have been noted for cathodic electrodeposition applications (*2,3*). The grafting of (meth)acrylic acid/styrene copolymers onto epoxy to yield water-borne modified epoxies for can coating applications is discussed in reference *4*. Chutko and Martino discussed a water-borne epoxy grafted onto a styrene/acrylate/(meth)acrylic acid terpolymer which was cured with a phenol-formaldehyde resin to yield a heat curable metal coating composition (*5*). The emulsification of epoxy resins with a styrene/acrylate/(meth)acrylic acid terpolymer (in aqueous ammonia) was noted by Kojima and Watanabe (*6*). An epoxy solution containing volatile solvents to reduce the viscosity was added to the aqueous ammonia solution of the styrene/acrylate terpolymer followed by vacuum stripping of the resultant emulsion.

The combination of epoxy (and curatives) with emulsion polymers (e.g., vinyl acetate or acrylate based) involves three distinctly different methods. The first method involves the addition of emulsion polymer to a water-borne epoxy and a curative (either water-borne or water-soluble). The second method involves the addition of epoxy to vinyl acetate or acrylate monomers (forming a solution) followed by emulsion polymerization and then addition of an amine curative. The third method involves the addition of liquid epoxy to an emulsion polymer followed by curative addition. Examples of each method are noted in the patent literature; however, relatively few examples are noted in the open literature. In reviews of polymer blends (7) and interpenetrating networks (8), water-borne blends of epoxy with vinyl polymers did not appear.

Young (9) noted that epoxy resin/water dispersions could be added to typical emulsion polymers (e.g., VAE (vinyl acetate-co-ethylene), poly(vinyl acetate), polyacrylates, and vinyl chloride-based polymers) to yield improved adhesion to aluminum. The epoxy in these blends was cured by addition of a modified amidoamine. The polymerization of acrylate or vinyl acetate-based emulsions containing dissolved epoxy resin has been described in several patents (10-12). Lee (10) described hybrid polymers of epoxy resin with acrylic polymers prepared by the polymerization of acrylate monomers containing dissolved epoxy resin in a water dispersion. A combination of a water-soluble and an oil-soluble surfactant was employed to provide small particle size and dispersion stability. Shih (11) prepared core-shell emulsion polymers with epoxy dissolved initially in the core monomer. Vinyl acetate and acrylate-based emulsions were proposed for both the core and shell polymers. Crosslinking with amine curatives such as isophoronediamine (IPDA) was noted. The combination of a core VAE polymer/epoxy was found to gel within 5 hours of IPDA addition, whereas, a core-shell variant exhibited a stable emulsion for over one month. Oyamada et al. (12) discussed the emulsion polymerization of VAE copolymers in the presence of epoxy. The resultant emulsion was cured with m-xylylenediamine (MXDA) for adhesive applications. The addition of liquid epoxy to VAE emulsions has been noted (generally at low levels of epoxy addition) for adhesive applications in the patent literature (generally Japanese patent citations). An example (13) noted a blend of a VAE emulsion (100 parts), 50% solid epoxy resin in toluene (15 parts) and m-xylylenediamine (3 parts) applied to concrete to improve adhesion strength. The characterization of epoxy/VAE emulsion hybrids, however, does not appear to be described in the open literature. A solvent-prepared blend of the diglycidyl ether of Bisphenol A (liquid epoxy) and poly(vinyl acetate) was prepared, devolatilized and then cured with diaminodiphenylmethane (DDM) by Zheng et al. (14). It was noted that the liquid epoxy with miscible with poly(vinyl acetate), but phase separated upon curing with DDM addition.

This paper will detail the preparation of one part or two part systems employing amine curatives for the VAE/epoxy hybrids. The addition of liquid epoxy to a VAE emulsion was found to be quite easy to accomplish with minimal mixing, yielding stable emulsions allowing the hybrids to be easily prepared.

Experimental

The emulsions utilized for this study were commercially-available VAE emulsions, the epoxy utilized for most of the studies was liquid epoxy Epon 828 and the amine curatives were primarily commercially-available except for an experimental epoxy-amine adduct. A more detailed description of these components is given in Table I.

The samples were prepared by slow addition of the epoxy liquid to the VAE emulsion with stirring (standard laboratory mixer with a propeller blade). Additional water was added to keep the solids level similar to the original VAE emulsion as well as maintain a low viscosity. Homogeneous mixtures were observed almost as soon as the epoxy was added. No residual epoxy was noted on the sides or the bottom of the plastic beaker employed for mixing, implying incorporation of the epoxy. Samples were cast into 20 to 30 mil thicknesses onto silicone release paper. After one day of drying at 50% RH (23 °C), samples were removed from the silicone release paper (usually turned over and placed back on the silicone release paper) and placed in a desiccator until testing. Note that the solids content of the emulsion and the solids ratio of the constituents refer to non-volatile components even though some of the components are liquid at room temperature (i.e., epoxy).

Particle size and particle size distribution were measured using the disc centrifuge method. This method employs the Brookhaven Model BI-DCP Disc Centrifuge. The emulsion is diluted to ~ 1% solids by weight and is injected onto the surface of the spin fluid (with the disc spinning). The particles sediment radially outward through the fluid, and as the particles pass through a narrow light beam, the scattering is measured. The rate of sedimentation is based on spin fluid viscosity, particle density-spin fluid density difference, rotational speed and particle diameter. From the proper analysis of Stoke's Law, the particle size and particle size distribution can be determined. Accelerated sedimentation testing was conducted to determine emulsion stability. This technique involves dilution of the emulsion with an equal weight of distilled water and pouring 10 ml of the diluted emulsion into a 15 ml centrifuge tube. The centrifuge tube was placed in a IEC clinical centrifuge (Model 05-101-5) and centrifuged at 2800 rpm for 5 minutes. After centrifugation, the supernatant was decanted and the sediment amount was determined on the graduated tube. Samples were also stored at

23 °C and 60 °C and visually observed after extended time to determine stability. Samples were cast on silicone release paper (20-30 mils thick), dried for 16-24 hours at 23 °C and 50% RH, and then released and stored in a desiccator until testing. Dynamic mechanical testing was conducted using a Rheometrics Solids Analyzer (RSA II). Data were obtained every 6 °C over the temperature range employed using a deformation frequency of 6.28 rad/sec in tension. Stress-strain measurements were conducted on die cut tensile specimens subjected to testing on an Instron testing machine at 2 in/min strain rate. pH results were determined on the emulsion hybrids using an Orion Model 520A pH meter.

Table I. Description of Materials Employed for VAE/Epoxy Hybrids

Material	Description	Source
Epon 828	diglycidylether of Bisphenol A	Shell
IPDA	isophoronediamine	BASF
Epilink 700	epoxy-amine adduct (water dispersion)	APCI
Epilink 660	epoxy-amine adduct (water dispersion)	APCI
TETA	triethylenetetraamine	APCI
Ancamine 2049	3,3'-dimethylenedi(cyclohexylamine)	APCI
Ancamine 2168	poly(cycloaliphatic) amine	APCI
Cacamid 350A	polyamide polyamine	APCI
Casamid 360	polyamide polyamine (water dispersion)	APCI
Jeffamine D-230	polyoxypropylenediamine	Texaco
MXDA	m-xylylenediamine	Aldrich
Dytek A	2-methyl-1,5-pentanediamine	Aldrich/du Pont
AEP	Aminoethylpiperazine	APCI
A-405	VAE emulsion, 55wt% solids, non-ionic Surfactant stabilized, DSC mid-point $T_g = 7$ °C	APCI
A-400	VAE emulsion, 55wt% solids, PVOH stabilized, DSC mid-point $T_g = 0$ °C	APCI

APCI = Air Products and Chemicals, Inc.

Results

The addition of liquid epoxy to the VAE emulsions (A-405 and A-400) resulted in rapid incorporation yielding a homogeneous emulsion with no residual epoxy on the sides or the bottom of the mixing container. The incorporation was surprisingly rapid even at high levels of addition (up to 70 wt% epoxy liquid (solids basis)). The addition of liquid epoxy to the emulsions

resulted in an increase in viscosity without additional water addition to counterbalance the solids increase. With water addition, the final solids level was maintained similar to the original emulsion and the resultant viscosity was then observed to be lower than the base emulsion. The stability of the epoxy/VAE hybrid was assessed by accelerated sedimentation as well as long term storage at 23 °C with results given in Table II for samples of epoxy (Epon 828) in A-400 and A-405 emulsions at 40 wt% epoxy (solids basis). The particle diameter analysis is also included. The particle diameter analysis shows that the particle diameter for A-400 and A-405 slightly increases and the particle size distribution narrows as the epoxy is added. This indicates that no new additional particles are being formed and the decrease in the size distribution is hypothesized based on more rapid diffusion into the smaller particles (more surface to volume ratio). Values of accelerated sedimentation of less than 3% are generally considered as stable emulsions. Storage of the A-405/epoxy blend at 40 wt% epoxy (solids basis) for over a year did not show any sedimentation. At higher levels of epoxy, Igepal CO-630 was added at 3 to 5 wt% based on epoxy content. Sedimentation (of an epoxy rich phase) was noted for the 60 and 70 wt% epoxy based epoxy/A-405 blends after six months storage at 23 °C (which could be easily redispersed). In order to determine if the epoxy dissolved in the VAE particles or formed separate particles at the higher levels of epoxy incorporation, particle diameter analysis also employing the disc centrifuge method was conducted with results shown in Table III for A-405/Epon 828 mixtures at 55% total solids and the A-405/Epon 828 ratios (solids basis noted). The results demonstrate that no new particles were formed even at these higher loadings. As the stability of the emulsion/epoxy mixture was best for A-405, most of the experiments involving amine curative addition involved A-405/epoxy blends.

Various amine curatives were added to the A-405/epoxy (60/40 solids basis) blend by slow addition during mixing. The amine curatives were diluted with equal parts of water prior to addition to prevent localized coagulation of particles due to the high pH of the amine. Unless noted, the amine curatives were added at stoichiometric levels based on the epoxy. The resultant hybrid stability was determined by either direct viscosity measurements or visual observations of viscosity increase, coagulation or sedimentation.

The stability of the various hybrids is listed in Table IV. The results show surprising stability for several water soluble amine curatives, specifically, isophoronediamine (IPDA), Jeffamine D-230, TETA, Dytek A, and m-xylylenediamine(MXDA). In some cases, IPDA based hybrids gave 23 °C stability for up to over a year with the ability to cast continuous films with mechanical properties virtually unchanged from samples aged for one month. IPDA was utilized for more in depth studies as Dytek A exhibited poor mechanical properties. M-xylylenediamine gave good observed hybrid stability, however, reddish-brown emulsions and cast films were formed. Several other

amines gave viscosity increases within several hours to several days and thus would only have utility as a two component system.

Table II. VAE/Epoxy Emulsions: Particle Diameter and Sedimentation Results

	$D_n (\mu m)$	$D_s (\mu m)$	$D_w (\mu m)$	D_w/D_n	Accelerated Sedimentation
	Particle Diameter Analysis				*Accelerated*
A-400	0.596	0.729	0.933	1.565	-
60% A-400 40% Epon 828	0.683	0.799	0.974	1.426	8%
A-405 Control 1	0.140	0.172	0.220	1.571	-
60% A-405 40% Epon 828	0.162	0.197	0.238	1.469	3%

Table III. Particle Size Data on A-405/Epon 828 Blends at High Epoxy Loadings

A-405/Epon 828 Epon 828 content (solids basis)	D_n (μm)	D_s (μm)	D_w (μm)	Polydispersity D_w/D_n
50%	0.144	0.183	0.218	1.51
60%	0.157	0.192	0.223	1.42
70%	0.165	0.204	0.235	1.42
A-405 Control 2	0.123	0.154	0.184	1.50

The hybrid emulsion stability was unexpected and could be the result of several factors. One possibility is that the water soluble amine curative remained in the water phase and did not react (completely) with the epoxy until the sample was cast (removal of the water phase). The other possibility is that the amine diffused into the VAE/epoxy particles and reacted without causing coagulation or sedimentation. A method to indirectly determine which hypothesis was most likely involved simply monitoring the pH versus time. Another parameter which needed comparison was the effect of the amine additive on the hydrolysis of the vinyl acetate units in the VAE copolymer. At high pH, hydrolysis of the vinyl acetate units could lead to vinyl alcohol incorporation in the VAE copolymer yielding acetic acid which could neutralize the amine. A comparison of the pH versus time for a blend of A-405/IPDA and a hybrid of A-405/epoxy/IPDA is shown in Figure 1. The hydrolysis rate of VAE is much slower than the apparent diffusion of IPDA into the VAE/epoxy particles and reaction with the epoxy. Thus, the emulsion stability appears to be due to the IPDA diffusion into the particles and reacting and thus changing the oil/water equilibrium solubility

resulting in further IPDA diffusion. A comparison of the pH change of several water soluble amine curatives in the A-405/epoxy hybrid is given in Figure 2. IPDA exhibits the most rapid drop in pH and thus a more rapid reaction with the epoxy and/or higher oil/water equilibrium solubility ratio. Thus, the surprising "one-part" stability of the VAE/epoxy/amine curative systems is due to the diffusion of the amine into the epoxy swollen VAE particle and reacting with the epoxy without causing particle agglomeration or coagulation. The highly-dispersed epoxy phase offers mechanical reinforcement of the VAE particles but allows for film formation when cast at room temperature.

Table IV. Stability Results for VAE (A-405)/Epoxy/Amine Emulsions

Emulsion/ Epoxy Ratio	Amine Curative	Stability Results (Accelerated testing at 60 °C)	Room Temperature Stability
90/10	IPDA	ok at 148 hrs	--
80/20	IPDA	ok at 148 hrs	--
70/30	IPDA	ok at 148 hrs	--
60/40	IPDA	coagulated at 101 hrs	minor sedimentation at 18 mos
50/50	IPDA	coagulated at 52 hrs	~ 6 mos/sedimention
60/40	AEP	coagulated after 3 hrs	--
60/40	Ancamine 2049	coagulated after 2 hrs	--
60/40	Dytek A	sedimentation at 123 hrs	minor sedimentation at 18 mos
60/40	MXDA	ok at 148 hrs; deep brown color	minor sedimentation at 18 mos
60/40	TETA	coagulated at 6 hrs	coagulated at 18 days
60/40	Jeffamine D-230	--	coagulated at 3 mos
60/40	Epilink 700	--	viscosity increase after ~ 2 hrs

Stress-strain measurements were conducted on the various VAE/epoxy/amine curative combinations noted above for the epoxy/VAE ratio held at 40/60 (solids basis). The tensile modulus, tensile strength, and ultimate elongation values are listed in Table V. Samples were measured at room temperature and additionally after 1 hour at 100 °C. The exposure at 100 °C was to qualitatively determine the extent of curing at room temperature. Compared to the base VAE emulsions, a significant increase in modulus and strength is accompanied by a loss in elongation. The resultant hybrid samples are in the

Table V. Mechanical Property Results for VAE (A-405)/Epoxy/Amine Hybrids (VAE/Epoxy Ratio = 3/2 (by wt solids)

Amine Hardener	Room Temp. Conditioning	Room Temp. Conditioning			RT + 1 hour at 100 °C		
		Tensile Modulus (MPa)	Tensile Strength (MPa)	% Elongation	Tensile Modulus (MPa)	Tensile Strength (MPa)	% Elongation
None	7 days	23.2	9.9	576			
Epilink 700	3 days	545	19.3	77	705	33.3	38
Epilink 660	3 days	571	15.8	78	893	21.5	27
Casamid 350A	3 days	437	11.2	33	558	16.3	12
IPDA	3 days	83.4	9.4	252	244	16.7	63
TETA	3 days	22.5	10.8	411	165	18.9	87
AEP	6 days	93.2	6.1	150	482	10.4	56
Casamid 360	6 days	81.4	8.8	257	599	17.9	51
Ancamine 2049	6 days	55.3	7.9	314	1001	18.0	64
Ancamine 2168	6 days	56.2	5.7	261	598	9.4	32
Dytek A	6 days	4.1	2.6	451	850	16.6	36
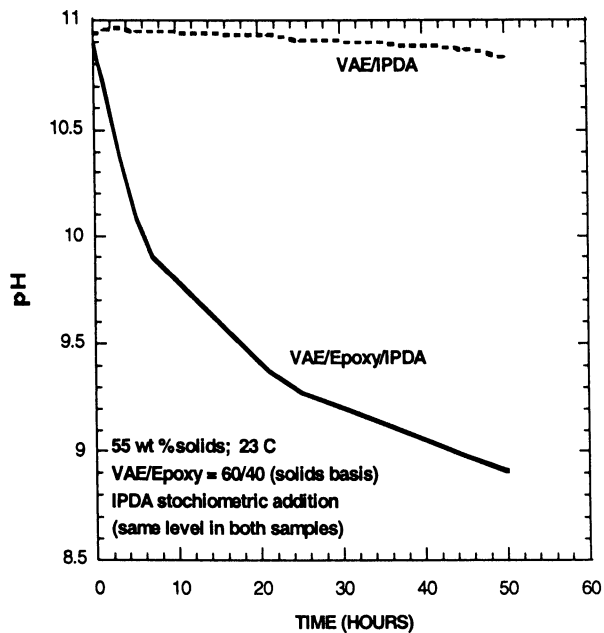
Figure 1. pH versus time for VAE/ epoxy/IPDA samples compared with VAE/IPDA.
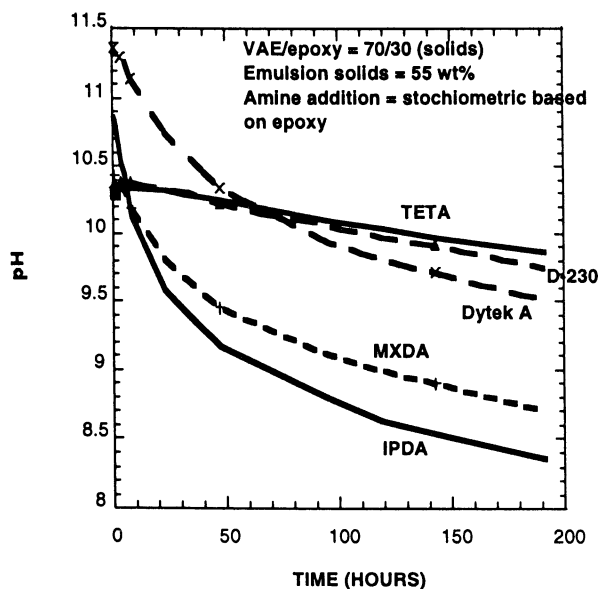
Figure 2. pH versus time for various VAE/epoxy/amine curative hybrids.

range of equal parts of epoxy (plus curative) and VAE thus representing a flexibilized epoxy material.

The stress-strain data on A-405/Epon 828/IPDA hybrids for various A-405/Epon 828 ratios after room temperature cure and an additional hour at 100 °C are illustrated in Figures 3 and 4 respectively. These samples were cast one month after hybrid preparation. The dynamic mechanical results on the same samples (1 hour at 100 °C) are illustrated in Figures 5 and 6 for tensile modulus and mechanical loss (tan δ), respectively. An increase in modulus above the T_g of the VAE phase with epoxy addition is noted indicating a crosslinked modulus plateau due to the epoxy phase. The peak height in tan δ for the VAE phase decreases with epoxy addition with only a minor shift in position, indicating that the VAE-epoxy network is phase separated. The epoxy transition shows up as a broad shoulder between 60 and 140 °C with a small transition emerging at 140 °C at the higher epoxy levels. These transitions are believed to be associated with the epoxy glass transition. The broad transition indicates significant microstructural heterogeneity of the epoxy phase possibly due to compositional variation of the extent of epoxy cure from the particle surface to the center of the particle. The tensile modulus results show the expected modulus increase above the A-405 T_g with increasing epoxy addition. These results clearly show that the epoxy phase is discontinuous within a continuous VAE phase.

The dynamic mechanical results on another amine crosslinker (Epilink 700: epoxy-amine adduct) shows dual phase continuity as noted in Figures 7 and 8. In this case, the sample was cast directly after preparation and diffusion of the epoxy liquid into the amine crosslinker is presumed to give the two phase behavior. The epoxy transition is prominent and has a well-defined peak relating to the glass transition temperature. The VAE transition peak decreases with increasing epoxy content and shifts to slightly lower temperature. A modulus plateau between the VAE and epoxy T_g increases as expected with increasing epoxy content. In this hybrid, the epoxy phase exhibits significant continuous phase behavior. The comparison of IPDA and Epilink 700 with A-405/Epon 828 ratio of 50/50 (compare Figures 5 and 6 with Figures 7 and 8) shows a prominent epoxy transition for the Epilink 700-cured hybrid relative to the IPDA-cured system. The "two-part" Epilink 700-cured hybrid shows significantly more epoxy phase continuity as reflected in the dynamic mechanical results as well as the stress-strain data.

The continuous-discontinuous phase structures for the "one part" IPDA-cured hybrid and the "two part" Epilink 700-cured hybrids will be compared with theoretical predictions based on the equivalent box model (EBM) employing percolation theory predictions (15,16). The equivalent box model employs a parallel element and a series element comprised of the contributions each component to the continuous or discontinuous phase structure. The volume fraction of each component in each phase follows the noted relationships: $\phi_p =$
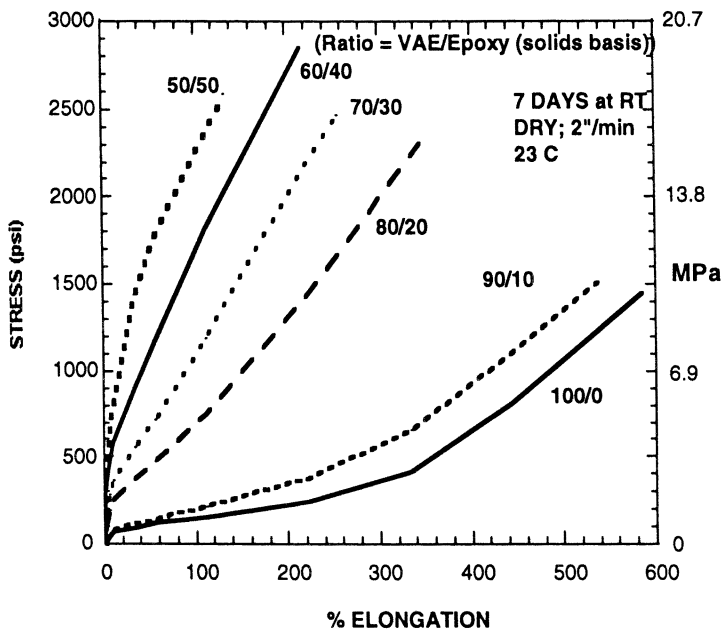
Figure 3. Stress-strain data on VAE/epoxy samples.
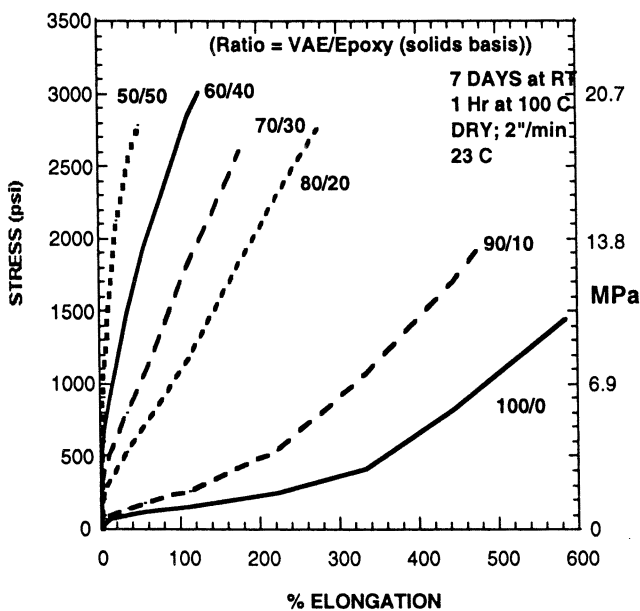
Figure 4. Stress-strain data on VAE/epoxy samples.
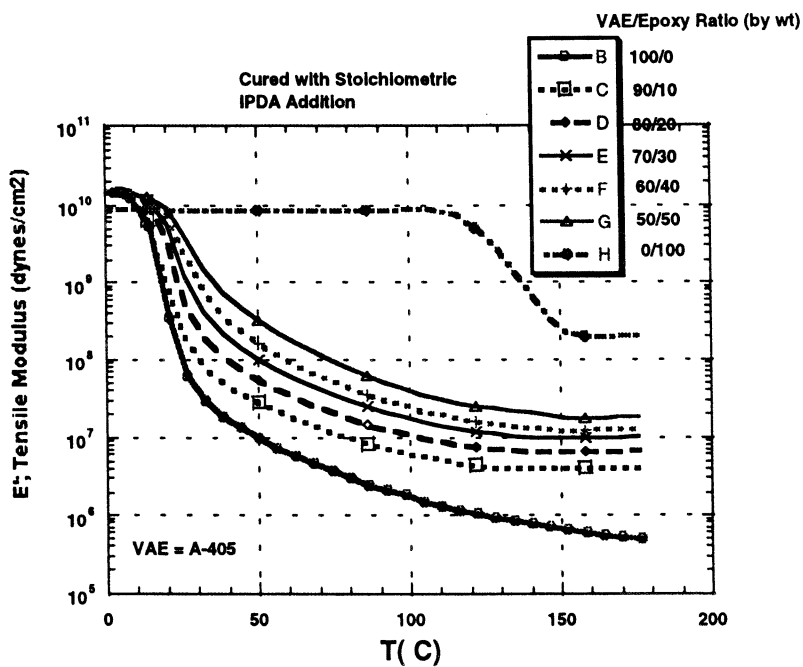
Figure 5. Dynamic mechanical results (tensile modulus, E') on VAE/epoxy/IPDA hybrids; IPDA added at stoichiometric level.
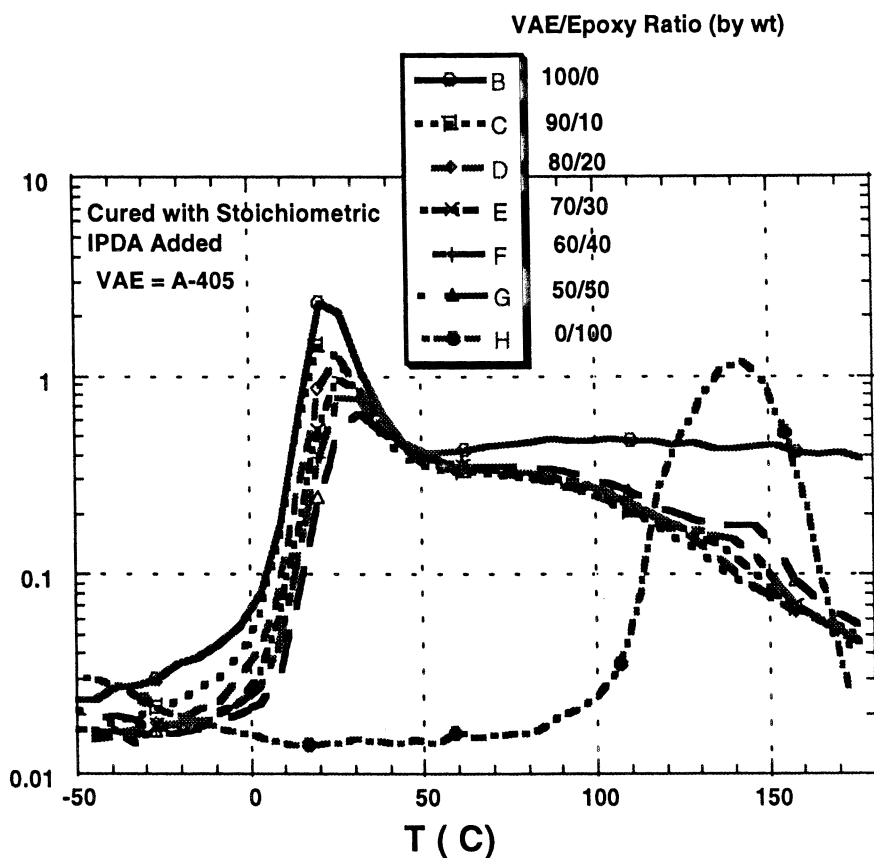
Figure 6. Dynamic mechanical results (tan δ) on VAE/epoxy/IPDA hybrids; IPDA added at stoichiometric level.
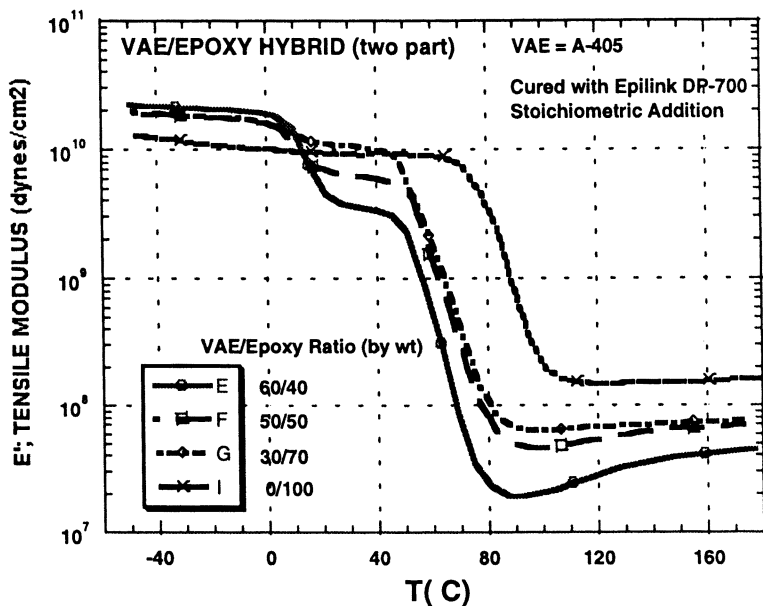
Figure 7. Dynamic mechanical results (tensile modulus,E') on VAE/epoxy/Epilink 700 hybrids; Epilink 700 added at stoichiometric level.
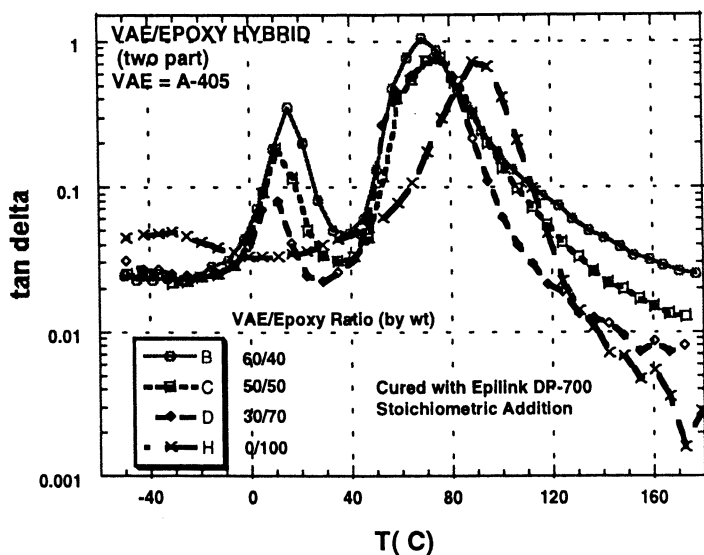
Figure 8. Dynamic mechanical results (tan δ) on VAE/epoxy/Epilink 700 hybrids; Epilink 700 added at stoichiometric level.

$\phi_{1p} + \phi_{2p}$; $\phi_s = \phi_{1s} + \phi_{2s}$; $\phi_1 = \phi_{1p} + \phi_{1s}$; $\phi_2 = \phi_{2p} + \phi_{2s}$; $\phi_1 + \phi_2 = \phi_p + \phi_s = 1$; where ϕ_{1p} and ϕ_{2p} are the parallel contributions and ϕ_{1s} and ϕ_{2s} are the series contributions for polymers 1 and 2, respectively. The volume fractions can be calculated (15) from percolation theory (17).

$$\phi_{1p} = [(\phi_1 - \phi_{1cr})/(1 - \phi_{1cr})]^{T1} ; \; \phi_{1s} = \phi_1 - \phi_{1p} \tag{1}$$

$$\phi_{2p} = [(\phi_2 - \phi_{2cr})/(1 - \phi_{2cr})]^{T2} ; \; \phi_{2s} = \phi_2 - \phi_{2p} \tag{2}$$

The modulus of the blend, E_b, can be calculated from the following expression where E_1 and E_2 are the respective moduli of components 1 and 2:

$$E_b = (E_1\phi_{1p} + E_2\phi_{2p}) + \{ \phi_s/[(\phi_{1s}/E_1) + (\phi_{2s}/E_2)] \} \; \phi_s \tag{3}$$

The tensile strength of the blend, σ_b, can be estimated from the expression as follows where σ_1 and σ_2 are the tensile strengths of components 1 and 2 and A = interfacial adhesion; for excellent adhesion $A = 1$:

$$\sigma_b = (\sigma_1\phi_{1p} + \sigma_2\phi_{2p}) + A\sigma_1\phi_s \quad \text{(where } \sigma_2 > \sigma_1) \tag{4}$$

The values of ϕ_{1cr} and ϕ_{2cr} are the percolation threshold volume fractions and T1 and T2 are the critical universal exponents. The values for discrete spherical domains are $\phi_{1cr} = \phi_{2cr} = 0.156$; and T1 = T2 = 1.833 from the universal parameters of percolation theory (17). The values of ϕ_{1cr} and ϕ_{2cr} and T1 and T2 can be considered adjustable parameters and A was chosen to equal 1. The EBM approach should work well with the percolation threshold and critical universal exponent values noted above for emulsion blends. Good agreement of tensile strength values between prediction and experiment was noted for PVOH stabilized emulsion blends (18). The EBM predictions for the blends using only the unblended modulus and tensile strength values along with the universal parameters are illustrated in Figure 9 for modulus and Figure 10 for tensile strength. The EBM model fits the Epilink DP-700 cured epoxy/VAE hybrid well indicating the transition from a VAE continuous structure to an epoxy phase continuous structure as the epoxy phase is increased, as expected from the dynamic mechanical results shown in Figures 7 and 8. The IPDA cured epoxy/VAE hybrid shows fair agreement up to 0.3 volume fraction epoxy but deviates from the EBM predictions as the epoxy phase remains the discontinuous phase as shown in Figures 5 and 6. The tensile strength data show reasonable
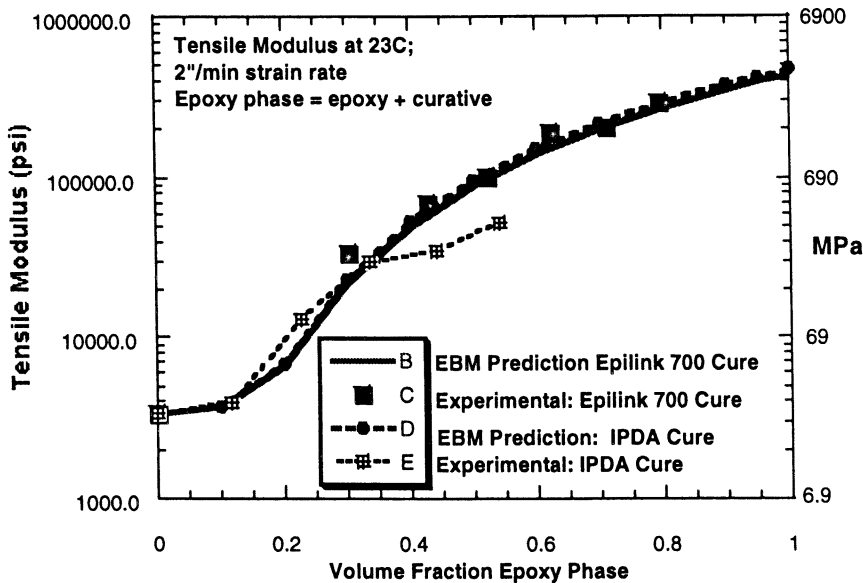
Figure 9. Comparison of tensile modulus prediction (EBM) with experimental results for VAE/epoxy/amine curative hybrids.
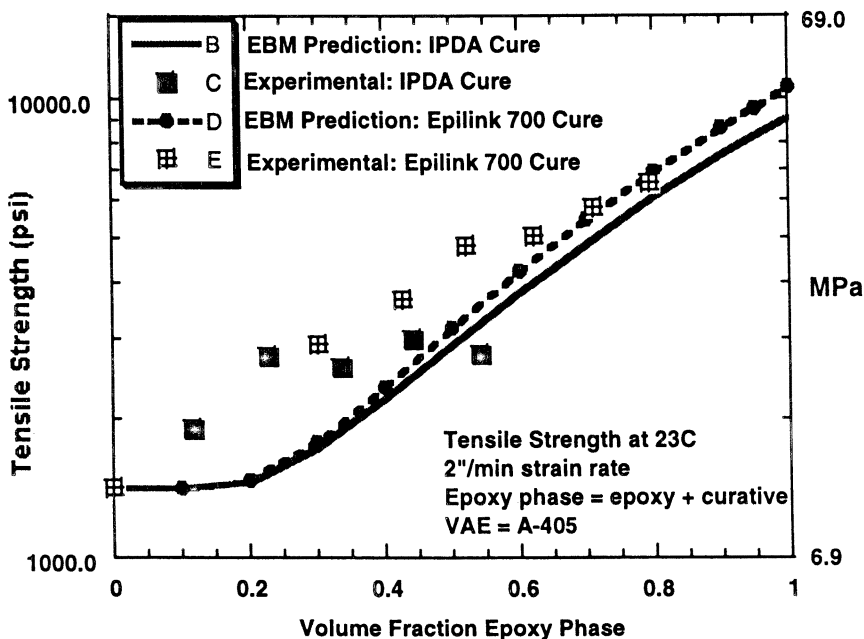
Figure 10. Comparison of tensile strength prediction (EBM) with experimental results for VAE/epoxy/amine curative hybrids.

agreement for the Epilink DP-700 cured hybrid at higher volume fraction with experimental values showing a positive deviation from prediction at lower volume fraction levels. Poor agreement of the EBM predictions with the IPDA cured hybrid is observed. The highly interpenetrating network of this hybrid leads to stiffening of the VAE continuous phase and thus showing positive deviation from expectations.

Conclusions

The addition of liquid epoxy (specifically the diglycidyl ether of Bisphenol A) to VAE emulsions leads to rapid incorporation with an observed slight increase in particle diameter and a reduced particle size distribution. This indicates that no new particles are formed and the epoxy dissolves into the VAE particles with more rapid sorption into the smaller particles (as expected based on surface area arguments). The resultant emulsion is stable to sedimentation/phase separation under room temperature storage conditions up to two years with the epoxy levels of 40 wt% or less (based on solids). Addition of water soluble or dispersible amine curatives can be accomplished yielding a VAE/crosslinked epoxy hybrid upon casting. With several water-soluble amine curatives, long term stability as a one-part system is observed (e.g., with isophoronediamine). In other cases, the viscosity increases rapidly with amine curative addition thus only allowing for a two-part system. Monitoring the pH versus time for the one-part systems shows that the amine curative diffuses out of the water phase as it reacts with the epoxy (thus shifting the oil/water equilibrium for the amine curative) and the epoxy/amine reaction is virtually complete in several weeks. The resultant hybrid, however, is still film forming and the VAE particles contain a reinforcing crosslinked epoxy. The cast film properties are consistent with VAE remaining the continuous phase based on equivalent box model (EBM) predictions. With two part hybrids, the modulus versus composition follows the EBM predictions, thus showing a consistent change from discontinuous to continuous epoxy structure as the epoxy content is increased. The tensile strengths of these hybrids are equal to or higher than the EBM predictions indicating a highly compatible (but not miscible) interconnected structure. These hybrids offer a facile method for reinforcing VAE emulsions or toughening waterborne epoxy systems.

References

1. Wegmann, A. In *Waterborne Coatings and Additives*, Karsa, D. R.; Davies, W. D., Eds., The Royal Society of Chemistry, Cambridge, 1995, pp.33-45.

2. Schimmel, K. F.; Pierce, P. E.; Jones, J. E. U. S. Patent 4,007,154; 1977.
3. Jones, J. E. U. S. Patent 4,009,133; 1977.
4. Evans, J. M.; Ting, V. W. U. S. Patent 4,212,781; 1980.
5. Chutko, M. J.;. Martino, P. C. U. S. Patent 5,976,700; 1999.
6. Kojima, S.; Watanabe, Y. *Polym. Eng. Sci.* **1993**, *33(5)*, 253.
7. Olabisi, O.; Robeson, L. M.; Shaw, M. T. *Polymer-Polymer Miscibility*, Academic Press, New York, 1979.
8. Sperling, L. H. *Interpenetrating Polymer Networks and Related Materials*, Plenum Press, New York, 1981.
9. Young, G. C. *Adhesives Age*, p. 24-27, Sept. 1996.
10. Lee, H. C. U.S. Patent 5,389,703; 1995.
11. Shih, Y.-J. U.S. Patent 5,177,122; 1993.
12. Oyamada, T.; Tsuru, S.; Tomizawa, C.; Taira, Y. U.S. Patent 4,108,819; 1978.
13. Taira, Y.; Sasaya, M.; Kondo, T.; Yano, M. JP 53106733 730918; 1978.
14 Zheng, S.; Hu, Y.; Guo, Q.; Wei, Y. *Colloid Polym. Sci.* **1996**, *274*, 410.
15 Kolarik, J. *Polymer* **1996**, *37(6)*, 887.
16. Kolarik, J. *Polymer* **1994**, *35(17)*, 3631.
17. DeGennes, P. G. *J. Phys. Lett.* **1976**, *37*, L1.
18. Robeson, L. M.; Vratsanos, M. S. *Macromol. Symp.* **2000**, *155*, 117.

Chapter 24

Hybrid Composite Latexes

**Pilmoon Jeong, Victoria L. Dimonie, Eric S. Daniels,
and Mohamed S. El-Aasser**

**Emulsion Polymers Institute and Department of Chemical Engineering,
Lehigh University, Iacocca Hall, 111 Research Drive, Bethlehem, PA 18015**

A direct miniemulsification approach followed by a subsequent polymerization process has been utilized to synthesize a series of hybrid composite latexes. Kraton® D1102 thermoplastic elastomer was dissolved in styrene monomer, emulsified in an aqueous surfactant solution in the presence of a costabilizer using various homogenization devices, and then polymerized to obtain the hybrid composite latexes. It was found that Kraton rubber particles (corresponding to the miniemulsion droplets) obtained using the Manton-Gaulin homogenizer possessed an extremely broad particle size distribution. This resulted in the formation of inhomogeneous hybrid composite particles due to the presence of monomer diffusion during polymerization. The broad size distribution of the Kraton rubber particles could be narrowed by employing a membrane filtration technique. Density gradient centrifugation (DGC) results showed that hybrid composite latexes with relatively homogeneous compositions were obtained from the membrane-filtered miniemulsions, compared to the miniemulsions prepared with a Manton-Gaulin homogenizer. From kinetic studies it was found that an induction period was present that resulted from the presence of radical scavengers such as antioxidant and UV stabilizer within the Kraton rubber when an oil-soluble initiator was employed. This led to the formation of inhomogeneous hybrid composite particles. This induction period was eliminated when a water-soluble initiator was utilized.

357

Rubbery latex polymers have been used as the base polymer in impact modifiers to provide toughness to brittle polymers such as poly(acrylonitrile-*co*-styrene) (SAN), poly(vinyl chloride) (PVC), and polycarbonate (PC). These rubbery latexes are normally prepared by an emulsion polymerization process. Thus, monomer selection for preparing the rubbery latex has been limited to monomers such as butadiene and butyl acrylate in conventional emulsion polymerization. However, this limitation can be overcome by the application of artificial latexes prepared using any existing polymers such as stereoregular polybutadiene, EPDM rubber, etc.

Impact modifiers usually have a core/shell structure where the shell polymer provides compatibility with the matrix polymer. Core/shell latex particles are usually prepared by a two-stage emulsion polymerization process. The core latex is prepared in the first step, which is then used as seed in the second stage polymerization to coat the particles with the second polymer (*1*). A direct miniemulsification process has also been used to prepare core latex particles that could then be used as seed. This approach offers the advantage that one can select any type of polymer to be used as a seed and not be limited to those polymers prepared by emulsion polymerization (*2*). For example, Merkel used toluene as a solvent to prepare an artificial latex comprised of Kraton rubber that was then used as a seed latex, which was then coated by a styrene/acrylonitrile copolymer in a second-stage polymerization step (*3*).

As another approach, if the non-reactive toluene solvent, which Merkel used in the direct miniemulsification of Kraton rubber, is replaced with a monomer such as styrene, the styrene monomer can be subsequently polymerized and a hybrid composite latex will be formed. This hybrid latex would have the potential to be used as an impact modifier without needing any solvent stripping stage that is required in the direct emulsification process approach with a non-reactive solvent.

Experimental

Materials

Kraton® D1102, a SBS (styrene-butadiene-styrene) thermoplastic elastomer (Shell Chemical Co.) was used in these studies. It is composed of a polybutadiene midblock (72 wt%) and two polystyrene endblocks (28 wt%). The Kraton rubber was purified via the extraction of additives using toluene (solvent) and methanol (nonsolvent) and dried under vacuum at room temperature for

three days. The purified Kraton rubber was used only for the kinetic studies. Otherwise, the Kraton rubber was used as received. Styrene monomer (Aldrich) was purified by passing it through a column filled with an inhibitor removal packing material (Aldrich). The purification of styrene was utilized only for the kinetic studies. Otherwise, the styrene monomer was used as received. Sodium lauryl sulfate (SLS; Aldrich) anionic surfactant, cetyl alcohol (CA; Aldrich), and hexadecane (HD; Aldrich) costabilizers were used as received without further purification. Potassium persulfate (KPS; Aldrich), 2,2'-azobis(2-methyl butyronitrile) (AMBN; DuPont), 2,2'-azobis(isobutyronitrile) (AIBN; Aldrich) and benzoyl peroxide (BPO; Aldrich) initiators were also used as received without further purification. Deionized (DI) water was used for all experiments.

Emulsification Procedures

80 mM hexadecane (HD) or 60 mM cetyl alcohol (CA) costabilizer was dissolved in styrene monomer prior to dissolving the Kraton rubber in styrene; the weight ratio of Kraton rubber/styrene was always maintained as 20/80. The Kraton rubber was then added to the styrene/costabilizer solution, left to stand for 12 hrs, and then mixed with a magnetic stirrer for 2 hrs. The styrene/costabilizer/Kraton rubber solution was slowly added to a SLS aqueous solution to form a crude emulsion with stirring. The mixture was further stirred for 2 hrs when a sonifier (Branson Model 450) or a Manton Gaulin homogenizer (model 15 M, APV Gaulin Co.) was employed. Prior to the use of the Manton-Gaulin homogenizer, the crude emulsion was sonified at a power level of 8 and a duty cycle of 70 % for 10 min. The sonified emulsions were then homogenized using the Manton-Gaulin homogenizer at a first stage pressure of 6000 psi and a second stage pressure of 1500 psi with 3 passes through the homogenizer.

Polymerization

Most polymerizations were carried out in a bottle polymerizer unit at 40 rpm and 70 °C. When kinetic studies were carried out, nine or ten one-oz bottles containing 20 mL of the same miniemulsion were placed in the bottle polymerizer unit and each bottle was withdrawn from the polymerizer after a designated time interval to measure the solids content and particle size. Oil-soluble initiators (AIBN, AMBN, and BPO) were dissolved in the oil phase prior to adding the Kraton rubber in the styrene while water-soluble KPS initiator was added to the miniemulsions as a 5 wt% aqueous solution.

Characterization

Latex Particle Size

Latex particle size analysis was carried out using capillary hydrodynamic fractionation (CHDF Model 1100; Matec Applied Sciences) on samples obtained after the polymerization was complete as well as on the samples that were withdrawn for kinetic studies during the polymerization. Residual styrene monomer in the samples withdrawn during polymerization was stripped off using a rotary evaporator at 50 °C under vacuum for particle size analysis.

Density Gradient Centrifugation (DGC)

The density of Kraton rubber is 0.94 g/cm^3. The Kraton rubber particles, and hybrid composite particles containing small amounts of polystyrene, float on water. Thus, it was necessary to prepare a lower density medium to separate these low-density particles. In order to do this, density gradient media were prepared using 10 mM SLS aqueous solution, acetonitrile ($\rho_{20\,°C} = 0.763$ g/cm^3) and sucrose ($\rho_{20\,°C} = 1.5805$ g/cm^3). A desired amount of sucrose was dissolved in the mixture of 10 mM SLS aqueous solution and acetonitrile to prepare density gradients with densities ranging from 0.94 to 1.05 g/cm^3.

The density gradient column (4) was prepared by placing layers of each medium of different density very slowly into the column using a syringe pump. Approximately 0.15 g of latex was then carefully added to the column in order not to disturb the interfaces between the density layers. The tube was then ultracentrifuged at 37,000 rpm at 5 °C for 2 hours using a Beckman high-speed ultracentrifuge (model L8-70M).

Results and Discussion

Influence of the Broad Size Distribution of Miniemulsion Droplets on the Homogeneity of Hybrid Composite Particles

The particle size of Kraton rubber particles, which were obtained from the emulsification of Kraton rubber/styrene solution after stripping off styrene monomer, corresponds to the miniemulsion droplet size assuming that each droplet has the same composition of Kraton rubber/styrene (20/80 by weight). Thus, the Kraton rubber particle size distribution was first characterized to determine the actual droplet size distribution of the Kraton rubber/styrene miniemulsion prepared from SLS/hexadecane (20/80 mM) using the Manton-

Gaulin homogenizer. The emulsion was homogenized at a first stage pressure of 6000 psi and a second stage pressure of 1500 psi with 6 passes through the homogenizer.

The TEM micrograph shown in Figure 1 demonstrates the extremely broad size distribution of the Kraton rubber particles obtained after homogenization, where the particle diameters range from 20 nm to 2 µm. This broad particle size distribution may influence kinetic events such as the radical capture of emulsion droplets (or growing particles) as well as the monomer diffusion process that occurs due to the monomer concentration gradient between various particles/droplets during the course of polymerization. The miniemulsion corresponding to the Kraton rubber particles shown in Figure 1 was polymerized using 5 mM AMBN. TEM micrographs of the hybrid composite particles obtained after polymerization are shown in Figure 2.

Two kinds of particles are present in Figure 2: polystyrene-like small particles and pure Kraton rubber-like large particles. If the polystyrene-like particles are examined closely (Figure 2, right), it can be observed that every particle has a very small black spot that represents the polybutadiene phase present in the Kraton rubber that has been stained with osmium tetroxide. In addition, the amount of polystyrene in the small particles is much larger than the amount of styrene monomer contained in the initial droplets. These observations indicate that the initial small miniemulsion droplets absorbed a large amount of styrene monomer during the course of polymerization and the final particle size became much larger than the initial droplet size. This occurs because small droplets have a much larger total surface area and thus have a higher chance of capturing radicals in the aqueous phase. As the small growing particles absorb styrene monomer from the aqueous phase, a monomer concentration gradient is developed, which cause large droplets (or large growing particles) to supply styrene monomer to the growing small particles through the aqueous phase. Eventually this monomer diffusion process which occurs during the polymerization process results in the formation of inhomogeneous hybrid composite particles, as shown in Figure 2.

Large droplets lose styrene monomer, resulting in the generation of hybrid particles with a smaller amount of polystyrene present. This is the reason why the large particles evident in the TEM micrographs in Figure 2 are very dark; only the polybutadiene phase in the Kraton rubber is stained with osmium tetroxide. This could also result from the mass contrast of the large particles. Polymerization of styrene still took place inside the large droplets, which will be further explained in the kinetics section. Therefore, in order to obtain homogeneous hybrid composite particles, an emulsion with a narrow size distribution is needed, which can minimize the monomer diffusion process during the polymerization.
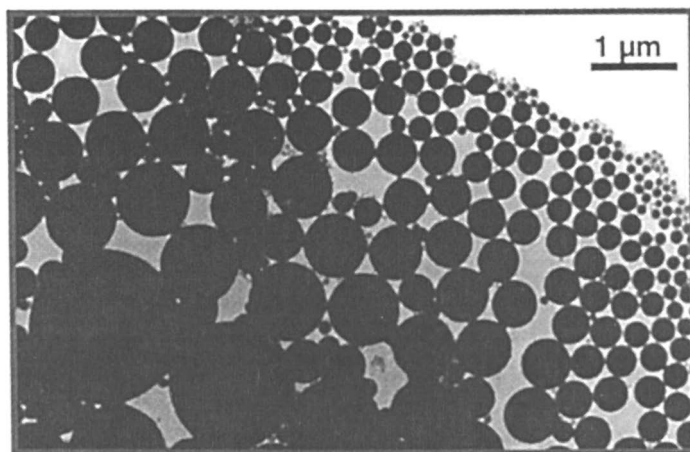
Figure 1. TEM micrograph of Kraton rubber particles prepared with sodium lauryl sulfate (SLS)/hexadecane (HD) = 20/80 mM using the Manton-Gaulin homogenizer.
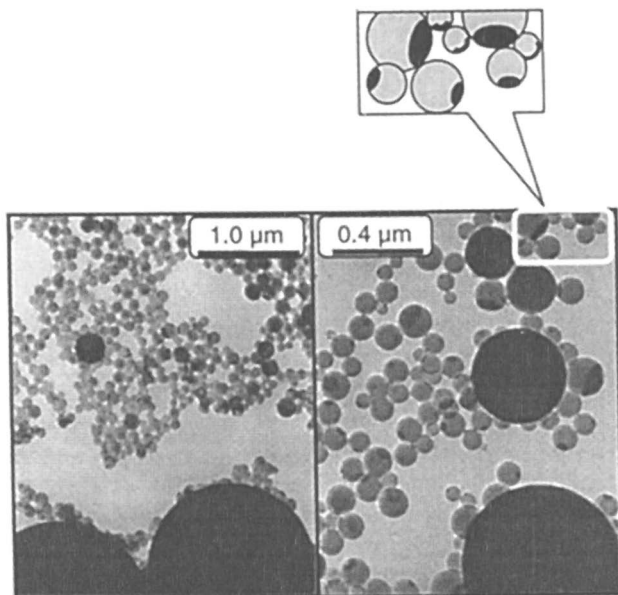
Figure 2. TEM micrographs of Kraton/polystyrene hybrid composite particles prepared with SLS/HD = 20/80 mM and 5 mM AMBN initiator.

Membrane Filtration

In an attempt to remove large emulsion droplets and obtain a relatively narrower size distribution of the Kraton/styrene miniemulsion, a membrane filtration technique was employed. This technique was initially used by Mohammadi et al. (5). They obtained relatively uniform polystyrene submicron particles by a direct miniemulsification process in conjunction with membrane filtration. The oil phase containing 20 wt% Kraton rubber is much more viscous compared to pure monomer and needs to be emulsified properly using a sonifier prior to membrane filtration. In the membrane filtration process, smaller droplets can pass undisturbed through the pores in the membrane. Therefore, only droplets with diameters which are larger than the membrane pore size can be affected by the membrane filtration process. Slightly larger droplets than the membrane pore size can be squeezed through the pores, while much larger droplets are broken down into smaller ones. These processes are depicted schematically in Figure 3. The resulting droplet size is influenced by the number of passes (cycles) through the membrane filtration device and the membrane pore size. In this study, 0.4 μm polyester track-etch membrane filters with a narrow pore size distribution (Osmonics) were used. Emulsions were first prepared by sonification at a power level of 8 and a duty cycle of 70 % for 10 min, and the sonified emulsions were then forced through the membrane filter under a nitrogen pressure of 50 psi.

Comparison of Size Distributions for the Membrane-Filtered Emulsion and the Manton-Gaulin Homogenized Emulsion

An emulsion was first prepared by sonification at a duty cycle of 70 % and a power level of 8 using SLS/HD = 20/40 mM, and then filtered through a 0.4 μm membrane filter for 15 passes. A second emulsion was prepared using the Manton-Gaulin homogenizer with SLS/HD = 20/80 mM. The styrene monomer was removed from these emulsions by vacuum distillation, and the Kraton rubber particle sizes and size distributions were determined by CHDF.

Figure 4 presents the results showing the size distributions of the Kraton rubber particles prepared using the membrane filtration process or the Manton-Gaulin homogenizer. As can be seen from Figure 4, the Kraton rubber particles formed by the Manton-Gaulin homogenizer exhibited a very broad size distribution with a tail extending up to 1.2 μm. If no costabilizer was used in the recipe, the particle size distribution was increased even more, with a tail comprised of larger Kraton particles. However, it can be seen that large particles over 500 nm were eliminated when using the membrane filtration process.

These two emulsions were polymerized immediately after the emulsification processes were complete. Density gradient centrifugation experiments were then carried out to gain a better understanding of the influence of the droplet size
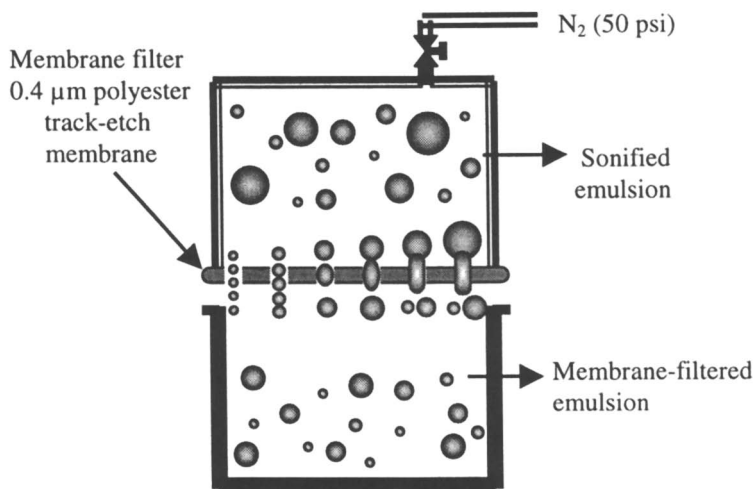
Figure 3. Schematic diagram of the membrane filtration process.

distribution on the particle growth for the two resulting hybrid composite latexes with different Kraton particle size distributions. The density gradient centrifugation results are given in Figure 5. The distribution differences between the membrane-filtered and the homogenized emulsion samples are reflected in the density gradient centrifugation results of the resulting hybrid composite latexes.
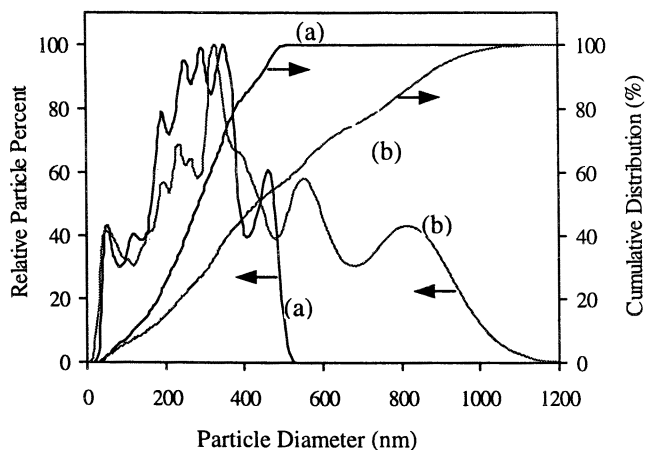
Figure 4. Kraton particle size weight distribution for the two samples prepared from: (a) the membrane-filtered emulsions formed with SLS/HD=20/40 mM and (b) the homogenized emulsion prepared with SLS/HD=20/80 mM.

Assuming that monomer diffusion does not occur during the polymerization process, every particle will have the same composition, with a Kraton rubber/styrene ratio of 20/80 (wt%) and a density of 1.03 g/cm^3. However, large droplets that act as monomer reservoirs lose larger amounts of styrene monomer, and the resulting latex particles obtained after polymerization have a lower density. These low density particles move to a lower density layer in the upper part of the column during centrifugation. Therefore, latex particles formed from the homogenized emulsion with a broad droplet size distribution occupy a broader region up to the 0.94 g/cm^3 density layer as shown in Figure 5. In addition, as can be seen from Figures 4 and 5, the membrane-filtered emulsion which possessed a relatively narrower size distribution resulted in the formation of more homogeneous hybrid particles, and therefore, the region in the column occupied by the particles is relatively small.
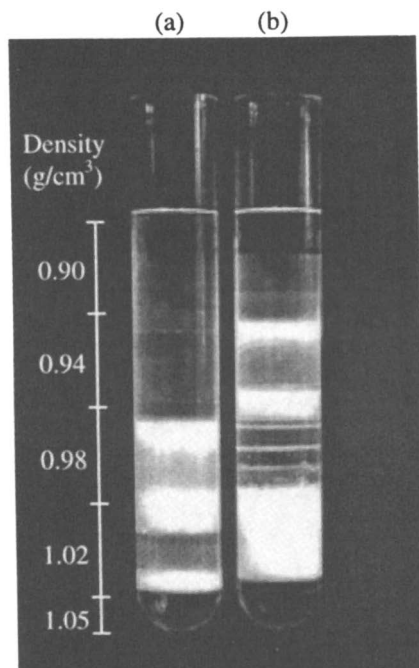
Figure 5. Photograph of the density gradient columns prepared from the two samples with different droplet size distributions: (a) hybrid particles formed from the membrane-filtered emulsion with SLS/HD=20/40 mM; and (b) hybrid particles formed from the Manton Gaulin homogenized emulsion with SLS/HD=20/80 mM.

Morphology of Hybrid Composite Particles

The previous explanation is further confirmed by the TEM micrographs (see Figure 6(a) and (b)) of hybrid composite particles obtained from each density layer shown in Figure 5. The polybutadiene phase present in the Kraton rubber was stained with OsO_4 for the TEM examination. It is seen that the hybrid composite particles in the top layer of the density gradient column shown in Figure 6(a), which were prepared using the Manton-Gaulin homogenizer, are larger in size and darker than those in the top layer shown in Figure 6(b), which were prepared using the membrane filtration process. This indicates that larger emulsion droplets were present in the emulsion formed using the Manton-Gaulin homogenizer compared to the membrane filtration process and they lost a larger amount of styrene monomer during the polymerization process than those

present in the emulsion formed by the membrane filtration. Thus, they look very dark compared to the membrane filtration case.

As can be seen from Figure 6(b), the hybrid composite particles in the middle layer have a smaller diameter than those in the top layer and a relatively larger amount of polystyrene. This implies that styrene monomer was preserved in the emulsion droplets with smaller diameters and that the monomer diffusion process was suppressed. In addition, each particle has a cellular structure, showing that both the polybutadiene and polystyrene phases are co-continuous inside the particles.

Latex particles observed in the bottom layers for both cases (Manton-Gaulin homogenizer and membrane filtration) shown in Figure 6(a) and (b) are almost the same, with pure polystyrene particles present. However, it is still seen that each particle contained a very small black spot (polybutadiene phase), as observed in TEM micrograph shown in Figure 2. The initial droplets for these particles, which absorbed a large amount of styrene monomer during the polymerization process, were formed from the sonification process (10 min) prior to membrane filtration and Manton-Gaulin homogenization. Therefore, it is necessary to employ another device that does not produce very small droplets during the homogenization step.
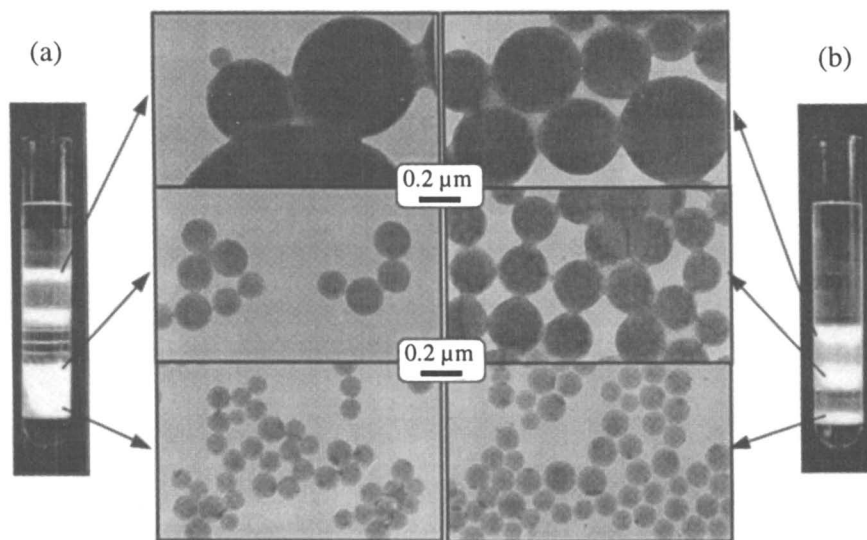
Figure 6. TEM micrographs of hybrid composite latex particles obtained from each density layer after polymerization was complete: (a) via Manton-Gaulin homogenizer or (b) by membrane filtration.

Difference between Water-Soluble and Oil-Soluble Initiators

Kinetic Studies Using Different Types of Initiator

Kinetic studies were performed using water-soluble (KPS) and oil-soluble (AMBN and BPO) initiators to investigate how the locus of radical formation affects the kinetics and the composition of the final latex particles. The evolution of the number of particles during the polymerization was monitored along with conversion. Additives such as antioxidant or UV stabilizer that were present in the Kraton rubber, which can influence polymerization kinetics during polymerization, may not be removed by the one-time purification process using toluene solvent and methanol non-solvent. Therefore, a kinetic study was conducted using Kraton rubber that was purified one or three times for comparison. Emulsions were prepared with 23.1 mM SLS and 46.2 mM hexadecane using 10 min of sonification at a power level of 8 and a duty cycle of 70 % followed by homogenization with 5 passes through the Manton-Gaulin homogenizer at a first stage pressure of 6000 psi and a second stage pressure of 1500 psi.

Results are shown in Figures 7 and 8. It was observed that there was an induction period when oil-soluble initiators (AMBN and BPO) were utilized. After repeating the purification process for the Kraton rubber three times, the induction period was shortened, but it still appeared. This means that additives such as antioxidant and UV stabilizer contained within the Kraton rubber could not be removed by a simple purification process and consumed many radicals generated in the oil phase as a radical scavenger in the early stages of the polymerization. However, in the case of the water-soluble KPS initiator, an induction period was not observed. This is because radicals were generated in the aqueous phase where radical scavengers such as antioxidant and UV stabilizer were not present; however, secondary particles were nucleated in the aqueous phase in this case.

It was observed that the induction time for the BPO initiator is longer than that for the AMBN initiator. In addition, use of the BPO initiator resulted in slower kinetics compared to AMBN. The half-life for BPO is slightly longer than that for AMBN; i.e., 7.3 hrs at 70 °C for BPO (*6*) and 7.0 hrs at 70 °C for AMBN (*7*). However, this small difference in half-life is not enough to explain the kinetic difference between the AMBN and BPO systems. It is possible that the partitioning of the initiator between the two phases would influence the kinetics.

Figure 8 shows the evolution of the number of particles during the course of the three polymerizations where purified (1×) Kraton rubber was used. It is seen that the number of particles in the KPS system is more than two times larger than that observed in the AMBN system. The reason for this is that many secondary

particles were generated in the KPS system via a micellar nucleation mechanism due to the high SLS concentration (23.1 mM, well above its cmc). However, in the AMBN system, the formation of secondary particles in the aqueous phase was limited because the initiator radicals were generated in the oil phase. This result indicates that the use of an oil-soluble initiator is more desirable to obtain a larger percentage of homogeneous hybrid composite particles.

(a)

(b)
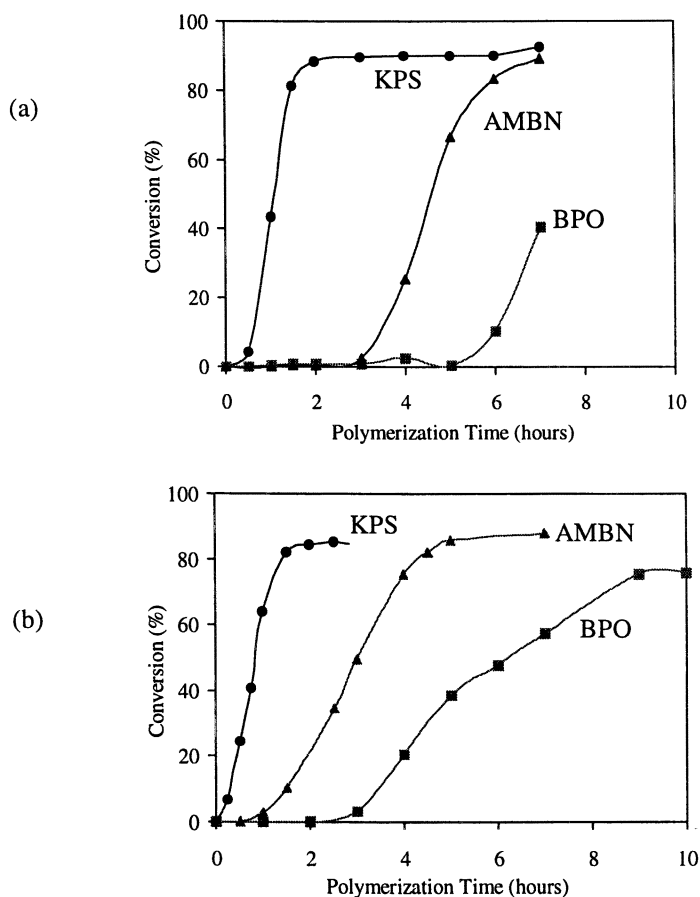
Figure 7. Conversion vs. time curves for three different initiators, KPS, AMBN, and BPO at the same initiator concentration (3 mM) using: (a) 1× purified Kraton, or (b) 3× purified Kraton; $T_r=70$ °C.
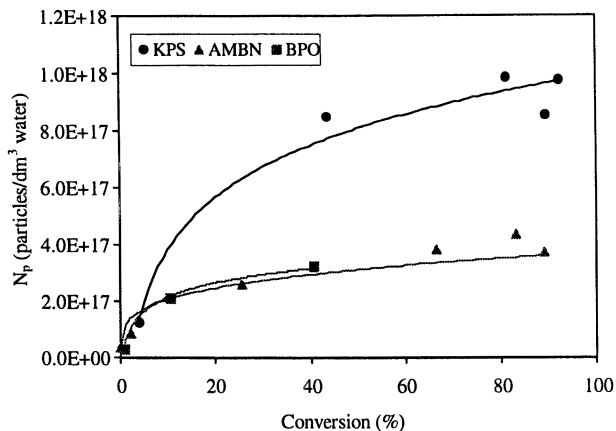
Figure 8. Evolution of the number of particles per dm³ of water as a function of conversion for KPS, BPO, and AMBN (all 3 mM) initiators; 1× purified Kraton used in all experiments.

In addition, it was observed from the density gradient centrifugation results for the AMBN system shown in Figure 9 that no particles were present in the top layer of the column, after 25.6 % conversion, which corresponded to the pure Kraton rubber particles or Kraton rubber particles containing a small amount of polystyrene as shown in the column at 2.3 % conversion. This means that every droplet was nucleated at least prior to 25.6 % conversion. If unnucleated droplets were present in the aqueous phase, the Kraton rubber particles obtained by stripping off the residual styrene in the latex samples withdrawn at each conversion should reside in the top layer of the tube during the centrifugation. However, pure Kraton rubber particles were not observed in the three density gradient columns prepared with latexes sampled at 25.6, 66.4, and 89.3 % conversion. At 2.3 % conversion, it can be seen that most of the particles are located in the top layer of the tube because the density of the pure Kraton rubber is 0.94 g/cm³. It is also seen that the region in the density gradient column occupied by hybrid latex particles decreased with an increase in the conversion due to the increase in the polystyrene content in each hybrid particle. The larger amount of polystyrene present in the hybrid particles results in an increase of the particle density.
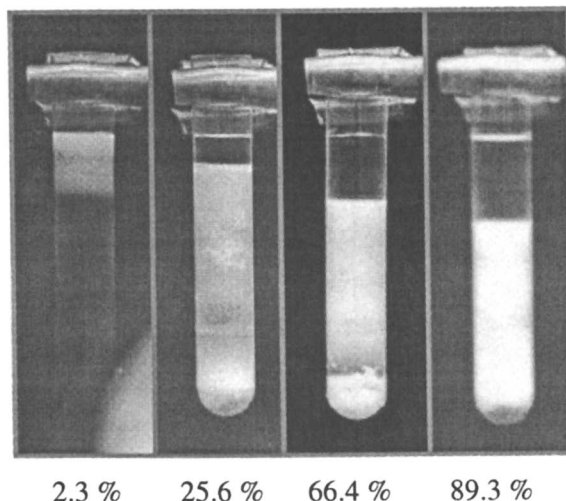
Figure 9. Results of density gradient centrifugation of the AMBN-initiated hybrid Kraton rubber/polystyrene latexes prepared by stripping off the residual styrene in the latexes withdrawn at each specified conversion (2.3, 25.6, 66.4, and 89.3 %).

Proposed Particle Growth Mechanism in the AMBN-initiated Kraton Rubber/Styrene Miniemulsion System

From the results discussed previously concerning the Kraton particle size distribution reflecting the actual droplet size distribution, the kinetic analysis in conjunction with the density gradient centrifugation measurements, and TEM micrographs shown in Figure 2, we can postulate the particle growth mechanism for hybrid composite particles initiated with oil-soluble AMBN initiator in the Kraton rubber/styrene miniemulsion system in the following manner. A schematic model is shown in Figure 10, where the dark phase represents the Kraton rubber, which is completely phase separated during and after polymerization. The droplet size distribution is initially very broad prior to the polymerization: small droplets might be less than 50 nm and large ones might be larger than 1 μm. The small droplets have a much larger total surface area compared to the larger ones and have a greater chance of capturing radicals during the polymerization. Thus, small growing particles absorb styrene monomer from the aqueous phase. This process creates a concentration gradient, causing the large droplets to supply monomer to the small particles as monomer

reservoirs. Finally, the particles become larger than their original droplet size and large droplets become smaller by losing their monomer.
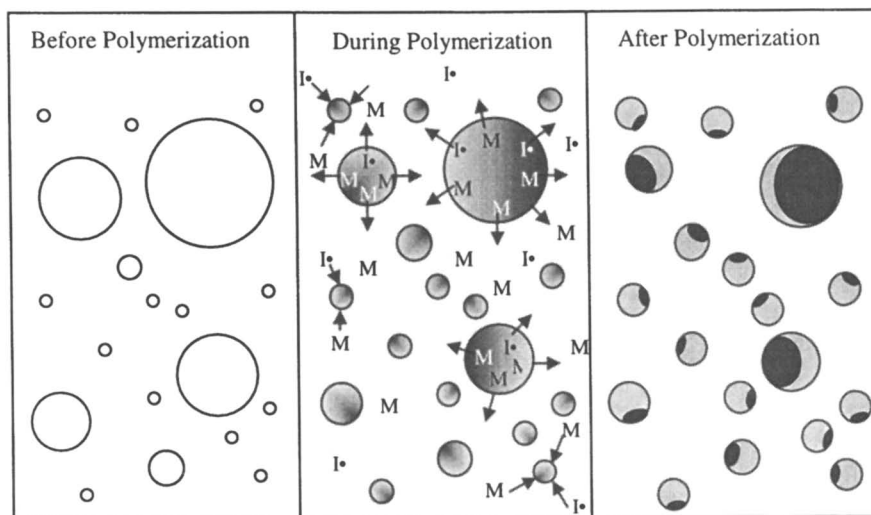
Figure 10. Schematic diagram of the growth mechanism of styrene miniemulsion droplets containing 20 wt% of Kraton rubber; the dark phase is Kraton rubber and the light phase, polystyrene (M= monomer, I• = initiator radical).

However, as discussed from the density gradient centrifugation results, every droplet was nucleated regardless of its size, indicating that styrene monomer is still polymerized in the large droplets that act as monomer reservoirs. This confirms the enhanced droplet nucleation mechanism resulting from the presence of polymer in the miniemulsion droplets as previously observed by El-Aasser and Miller (*1*). Therefore, the resulting polymerized hybrid particles have different compositions depending on how much they absorb or lose monomer. In addition, the small droplets have much greater chances of capturing radicals exiting from small or large droplets due to their larger total surface area. This would be another reason for the small droplets to grow at a faster rate.

Summary and Conclusions

The broad size distribution of miniemulsion droplets (corresponding to the Kraton rubber particles) prepared using the Manton-Gaulin homogenizer resulted in the formation of inhomogeneous hybrid composite particles. Large Kraton rubber/styrene miniemulsion droplets could be eliminated by employing

a membrane filtration method. Polymerization of membrane-filtered miniemulsions resulted in the formation of more homogeneous hybrid composite particles compared to the homogenized emulsions prepared using the Manton-Gaulin homogenizer.

An induction period was observed when oil-soluble initiators (AMBN or BPO) were employed, because radicals were generated inside the miniemulsion droplets that were then consumed by radical scavengers such as antioxidant and UV stabilizer present in the Kraton rubber. However, in the KPS system, the induction time did not appear because radicals were first generated in the aqueous phase and the polymerization reaction began with the formation of secondary particles in the aqueous phase that were not affected by the presence of antioxidant or UV stabilizer.

From the DGC experiment using the hybrid composite latexes prepared with AMBN initiator, it was found that every droplet was nucleated at least prior to 25.6 % conversion, regardless of its size. The hybrid particle density increased due to the formation of polystyrene domains inside the particles as conversion increased. Based on the DGC results and the TEM micrograph of hybrid particles, a particle growth mechanism was proposed for the AMBN-initiated system: small droplets (or small growing particles) absorb initiator radicals and monomer from the aqueous phase due to their larger total surface area, while large droplets (or large growing particles) lose monomer to the aqueous phase and decrease in size. However, styrene monomer is still polymerized inside the large droplets (or growing particles). Eventually, the particle size distribution become narrower, compared to the initial droplet size distribution, and the composition in each particle becomes different depending on the amount of polystyrene formed inside it. Small hybrid composite particles are rich in polystyrene, while large hybrid particles are rich in the Kraton rubber.

References

1. El-Aasser, M. S.; Miller, C. M. In *Polymeric Dispersions: Principles and Application*; Asua, J.M., Ed.; NATO ASI Series E; Kluwer Academic Publishers: Netherlands; 1997; Vol. 335, p. 116.
2. Merkel, M. P.; Dimonie, V. L.; El-Aasser, M. S.; Vanderhoff, J.W. *J. Polym. Sci.: Part A: Polym. Chem.* **1987,** *25*, 1219.
3. Merkel, M. P. *Morphology of Core/Shell Latexes and Their Mechanical Properties*, Ph.D. Dissertation, Lehigh University, 1986.
4. Price, C. A. *Centrifugation in Density Gradients,* Academic Press: 1982; p. 3.
5. Mohammadi, N; Kim, K.D.; Sperling, L. H.; Klein, A. *J. Colloid Interface Sci.* **1993,** *157*, 124.
6. Odian, G. *Principals of Polymerization*, 3rd Ed., John Wiley and Sons, NY, 1991, p. 215.
7. DuPont Technical Bulletin on Vazo Initiators.

Chapter 25

Cross-Linked Acrylate Microspheres for Solvent Absorption by SPG Technique

S. Kiatkamjornwong[1], S. Tawonsree[2], and S. Omi[3]

[1]Department of Imaging and Printing Technology, Faculty of Science,
Chulalongkorn University, Bangkok 10330, Thailand
[2]Multidisciplinary Program of Petrochemistry and Polymer Science,
Faculty of Science, Chulalongkorn University, Bangkok 10330, Thailand
[3]Graduate School of Bio-Application and System Engineering, Tokyo University
of Agriculture and Technology, 2-24-16 Nakamachi, Koganei, Tokyo 184, Japan

Crosslinked polyacrylate beads with a variety of morphologies were synthesized via an SPG technique. The acrylate monomers, 2-ethylhexyl acrylate (2-EHA), cyclohexyl acrylate (CHA), methyl methacrylate (MMA), and lauryl acrylate (LA), were used in this research. The influences of the ratio of monomer to ethylene glycol dimethacrylate (EGDMA) crosslinker, the type and concentration of the solvents, and the monomer type on the polymer particle morphology and the degree of swelling were investigated. We found that an increase in the concentration of EGDMA and heptane resulted in coarser pores. The capacity of these spheres as a solvent absorption material was examined. The highest degrees of swelling in heptane and toluene were obtained when LA was employed as the monomer with 30% by weight of EGDMA based on the monomer concentration and 70% by weight of heptane as an inert solvent. Various microsphere morphologies were observed from deep channels and dented surfaces, to creased surfaces and hollow spheres. The porosity of the polymer microspheres as measured by porosimetry could not be correlated to the pore properties determined by the solvent swelling of the microspheres.

Many varieties of polymer particle morphologies have been prepared by Shirasu porous glass (SPG) membranes depending on the composition of the oil phase (*1-3*). The SPG technique produces a narrow size distribution of emulsion droplets and polymer particles with standard deviations (σ) of about 4, as reported by Omi et al. (*4-7*). Effects of the diluent composition ranging between a good solvent and a poor solvent, and the crosslinking agent amount on the polymer morphology were studied (*8-11*). Different values of the solubility parameters of the good and poor solvents resulted in different porosities of the resulting polymers, which also depend on the crosslinking agent amount. Various applications depend on the polymer morphology; for example, spherical polymers are used as ion-exchange resin, packing materials for column chromatography, and so on, while hollow particles are used as opacifying plastic pigments for various coatings and gloss-enhancing plastic pigments (*12-13*). The present work utilizes the SPG technique in preparing crosslinked acrylate spheres for hydrocarbon solvent absorption.

Experimental

Emulsification and Polymerization

A schematic diagram of the SPG emulsification apparatus was shown in a previous article (*1*). A 20 cm^3 oil vessel comprising a microporous glass membrane (SPG membrane) of pore size 5.25 μm in an annulus cylinder with a diameter of 10 mm, a length of 20 mm, and a thickness of 1 mm, and an emulsion storage vessel of 300 cm^3 were used in the experiment. The glass membrane was installed in a stainless steel cylinder, tightly sealed with two O-rings (2). The dispersion phase, containing a mixture of the acrylate monomers, toluene or heptane, 2,2'-azobis-2,4-dimethylvaleronitrile (ADVN, Wako Pure Chemical, Osaka, Japan), and palimitic methyl ester (Tokyo Chemical, Japan) was stored in the oil storage vessel. The appropriate pressure was applied to the oil storage vessel in the range of 4.6 x 10^{-2} to 8.2 × 10^{-2} kg cm^{-2}. This phase was allowed to penetrate through the microporous membrane. The droplets were stabilized by the adsorption of PVA (poly(vinyl alcohol)) from the continuous phase, which is an aqueous solution of a stabilizer (PVA-127, with a DP of 1700 and 88.5% saponification from Kuraray Chemical, Japan), sodium lauryl sulfate (biochemical grade from Merck, Japan), and an aqueous NaNO$_2$ inhibitor (Kishida Chemical, Japan). A stirring rate of 300 rpm was used to prevent creaming of the dispersion phase. After the emulsification was complete, the emulsion was transferred to a reactor.

A three-necked glass flask was employed as a reactor equipped with an agitator having a semicircular anchor-type blade made of Teflon. A nitrogen

inlet and a condenser were connected to the flask. Nitrogen was purged slowly from the top of the condenser. The nitrogen inlet was then immersed into the emulsion with a stirring rate of 160 rpm for 1 h, and then removed from the emulsion. The suspension polymerization was carried out at 343 K for 24 h in a nitrogen atmosphere. The polymer particles were removed from the serum by centrifugation at 3000 rpm, washed with methanol and dried in a vacuum oven at room temperature.

Characterization of Polymer Microspheres

Particle Morphology

One gram of the dry polymer particles was immersed in toluene or heptane in a closed container for 24 h and the swollen polymer was weighed and the degree of swelling was calculated (14). The weight of the swollen spheres divided by the original weight is the degree of swelling. The morphology of the polymer particles was observed by scanning electron microscopy (SEM, JEOL, JSM 5300, Tokyo, Japan). A SEM sample was prepared by the normal procedure. In the case of a liquid sample, the sample was diluted with distilled water and a drop of the liquid was carefully placed on an aluminum stub and kept in a dessicator until it was dried. Then, it was coated with a thin layer of gold under vacuum before viewing in the SEM.

Porosity of the Particles

A porosimeter (PROSORP VAS-3000) was used to measure the porosity, the pore size distribution, and the specific surface area of the resulting polymer particles.

Results and Discussion

Effect of the Crosslinking Agent on the Morphology and Solvent Swelling of Polymer Microspheres

The resulting poly(2-EHA) synthesized with 20% by weight of EGDMA and 70% by weight of the solvents, heptane and toluene, based on the total weight of the monomer and the crosslinking agent, was coagulated and struck together because a small amount of the crosslinking agent formed networks between the particles. The amount of EGDMA added was not enough to overcome the rubbery nature (low T_g) of 2-EHA, and the particles stuck together, forming a neck-like or dumbbell-like structure. A solid powder was obtained when the concentration of EGDMA was increased to more than 20% by

weight based on the total weight of the monomer and the crosslinking agent, because the higher amount of crosslinking agent formed high-T_g networks successfully and the particles did not coagulate. We found that an increase in the EGDMA concentration resulted in coarser and more porous microspheres. An interesting morphology of these microspheres is the collapse of the polymer walls. Increasing the crosslinking agent concentration resulted in an increase in the elastic-retractile force, which would cause the formation of more crosslinked microspheres and gave a higher degree of phase separation (*15*).

The degree of swelling decreased with increasing the amount of crosslinking agent, except for sample no. 8, because the increased amount of crosslinking agent resulted in a decrease in the polymer chain mobility and free volume (*10*). The more crosslinking agent, the less flexibility of the chains. The highest value of the degree of swelling in toluene was obtained at 30% by weight of EGDMA in 35 and 45% by weight of heptane, and 40% by weight of EGDMA in 70% by weight of heptane. At 40% by weight of EGDMA, the particles ruptured after swelling in toluene because molecules inside of the particles were so densely crosslinked that they were unable to expand freely under the swelling stress and thus ruptured. Kim et al. (*10*) also obtained ruptured particles in the highly crosslinked samples after swelling in a good solvent, because the relaxation rate of the polymer chains was not as fast as the diffusion rate. However, the particles synthesized with 30% by weight of EGDMA did not rupture after swelling with solvent.

Effect of the Diluent on the Morphology and Degree of the Solvent Swelling of Polymer Microspheres

Toluene ($\delta = 18.3$ MPa$^{1/2}$) as a good solvent and heptane ($\delta = 15.1$ MPa$^{1/2}$) as a poor solvent were used to study the morphology of the particles. We found that increasing the concentration of heptane resulted in coarser surfaces of the particles going from finely porous surfaces to creased surfaces. This result has already been confirmed by Cheng et al. (*15*). They found that the presence of non-solvent enhanced the phase separation and structural inhomogeneities. Furthermore, Omi et al. (*6*) found that when a poor solvent was added in the recipe, a porous structure in the polymeric spheres was obtained in the presence of a crosslinking agent, because an *in situ* micro-phase separation took place during the polymerization. The micro-phase separation was indicated by tracks and dented channels on the surfaces of the microspheres. Both transparent beads and opaque beads were obtained when using toluene and heptane as penetrants. The highest value of the solvent swelling of the polymeric microspheres in toluene was obtained when the highest percentage of the poor solvent, heptane, was used at a constant concentration of the crosslinking agent (30% EGDMA) as shown in Figure 1. As for the trend of the swelling in heptane, it was found that, as in the case of toluene, the highest degree of swelling was obtained at 70% by weight of heptane at each constant amount of EGDMA. The polymeric spheres did not rupture after the solvent swelling in either solvent.
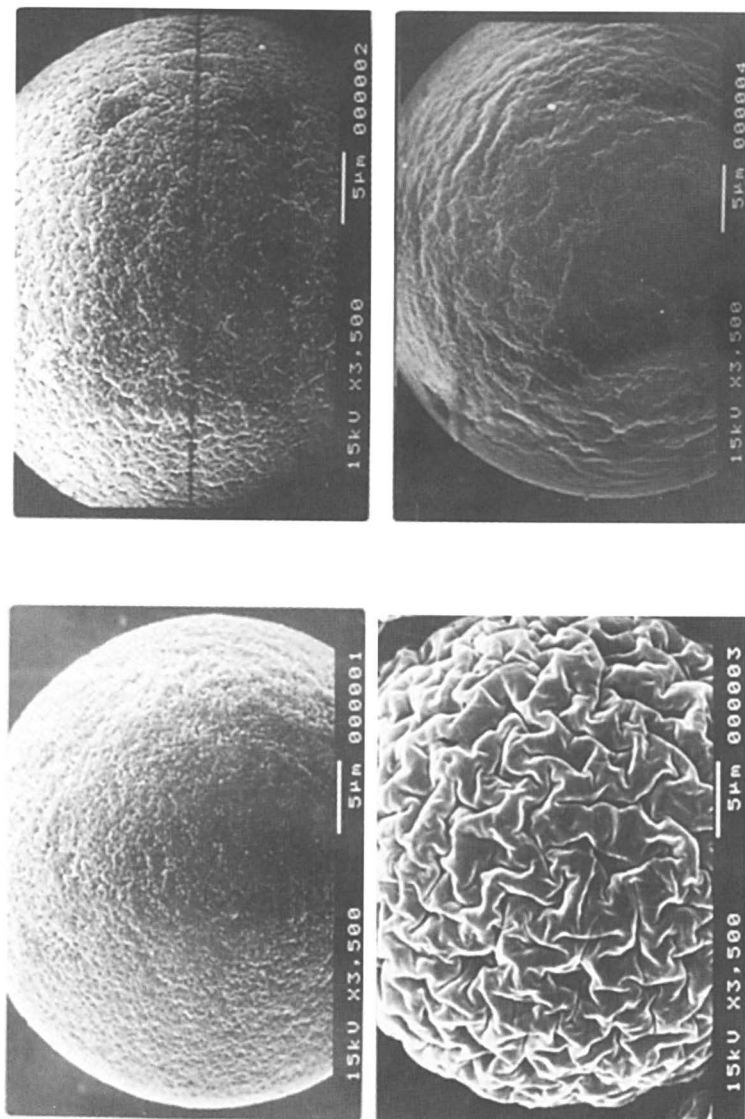
Figure 1. SEM micrographs of the surfaces of poly(2-EHA-co-EGDMA) particles prepared with various ratios of heptane to toluene: sample no. 1, 4.5:2.5 (top left); sample no. 2, 5.5:1 (top right); sample no. 3, 7.0:0 (bottom left), and sample no. 4, 3.5:3.5 (bottom right). (Reproduced from reference 3. Copyright 2000 John Wiley & Sons.)

Effect of the Monomer Type on the Surface Morphology and the Degree of Polymer Swelling of the Microspheres

The monomer type was changed with respect to the chemical structure and the glass transition temperature of the polymer (T_g) from 2-EHA ($T_g = 188$ K) to LA ($T_g = 270$ K), to CHA ($T_g = 292$ K), and MMA ($T_g = 378$ K) (*16*). Polymer particles were synthesized with 30% EGDMA and 70% heptane by weight based on the weight of the monomer and the crosslinking agent. A variety of surface features with each monomer type were obtained as shown in Figure 2. The relationships between T_g, the surface features of polymer particles and the solvent absorption capacity are explained as follows. It was found that the polymer microspheres that had dented surfaces and were hollow inside were obtained with the MMA monomer, while the CHA microspheres had creased surfaces. The MMA polymer moved towards the outer surfaces of the polymer particles adjacent to the aqueous phase and produced free volume within the spheres. Additionally, the solvent absorption capacity of MMA microspheres was lower than that of CHA microspheres because the higher-T_g polymer microspheres resulted in a decrease of the free volume and reduced flexibility of the polymer chains. The solvent absorption capacity of these microspheres in heptane could not be measured because PMMA microspheres floated on the surfaces of the solvent due to the lower density, and thus could not absorb heptane within a short time, because of the incompatibility between PMMA and heptane, since PMMA microspheres are relatively hydrophilic while heptane is hydrophobic. Acrylate monomers such as 2-EHA and LA were used instead. Considering the side-chain groups between LA and 2-EHA, it was found that the longer side chain resulted in the higher degree of the heptane absorption (4.2 times) because of the decreasing polymer polarity with increasing hydrophobicity, and greater free volume in the amorphous region. In addition, the solubility parameter of PLA (16.6 MPa$^{1/2}$) is closer to that of heptane (15.1 MPa$^{1/2}$).

Hollow microspheres of poly(MMA-*co*-EGDMA) with 20%, 30% and 40% EGDMA at 70% heptane could be prepared when using MMA as a monomer. In order to improve the solvent absorption capacity, the composition between MMA and EGDMA was hence varied from 20% to 30% and 40% EGDMA. Regardless of the amount of EGDMA used, an improved hollow morphology was obtained, but the solvent absorption capacity was not significantly improved. Thus, MMA plays an important role in determining the solvent absorption capacity.

Effect of the Third Monomer on the Morphology and Degree of Solvent Swelling of the Microspheres

The effect of MMA as the third monomer at 30% EGDMA and 70% heptane by weight based on the weight of the monomer and crosslinking agent
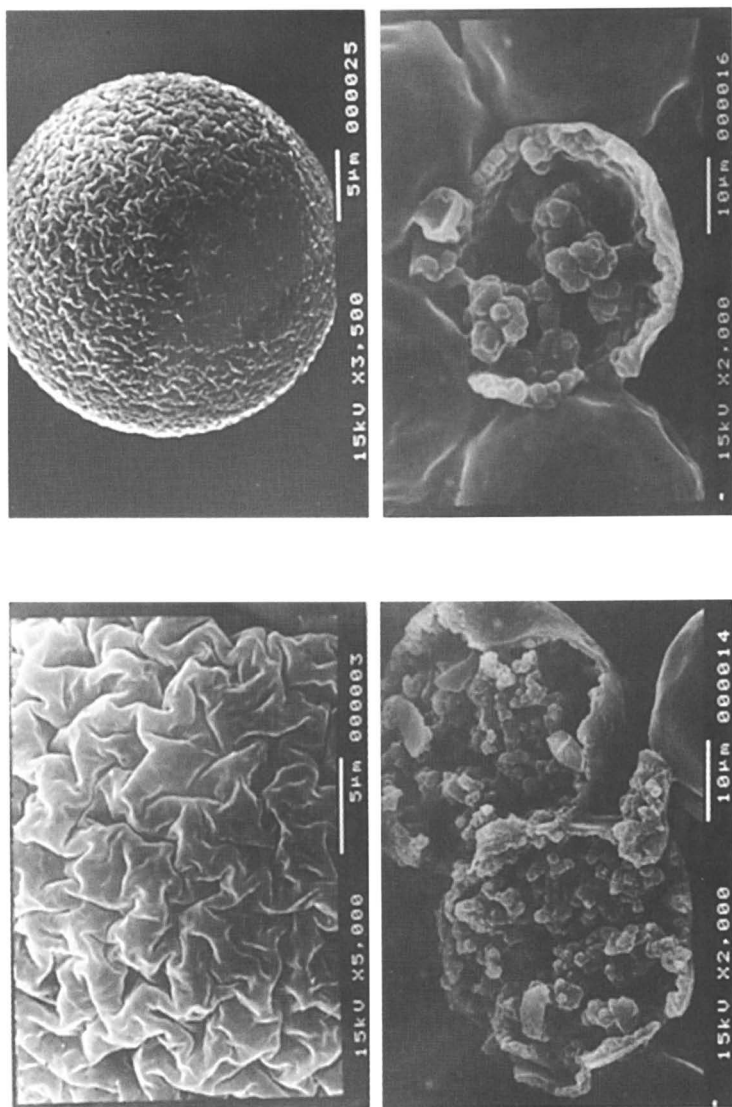
Figure 2. SEM micrographs of polymers prepared with various monomer types at 70% monomer and 70% heptane: 2-EHA in sample no. 3 (top left), lauryl acrylate in sample no. 25 (top right), cyclohexyl acrylate in sample no. 14 (bottom left), and MMA in sample no. 16 (bottom right). (Reproduced from reference 3. Copyright 2000 John Wiley & Sons.)

for various ratios between 2-EHA and MMA was investigated. At 14%, 35%, and 56% by weight of MMA, dented surfaces with hollow morphology were obtained with increasing amount of MMA. The toluene absorption capacity did not depend on the amount of MMA; however, the heptane absorption capacity decreased with increasing MMA due to the decrease of chain flexibility and the polarity. The morphology of polymer microspheres containing increasing amounts of MMA, as shown in Figure 3, had dented surfaces that were hollow inside. The high degrees of swellings of poly(2-EHA-*co*-MMA-*co*-EGDMA) microspheres prepared with respective monomer ratio of 35%:35%:30%, were 3.8 in toluene and 3.4 in heptane (sample no. 17), respectively; but the polymer microspheres were ruptured after the swelling in toluene and heptane. A higher degree of swelling was obtained with decreasing EGDMA and the polymer microspheres were not ruptured after the swelling in toluene and heptane as shown in sample no. 20. This result indicates that the rigid chains resulting from the high crosslinking monomer EGDMA could not stand the stress developed during solvent absorption. For the microspheres with a low degree of crosslinking, the high relaxation of polymer chains could compromise its chain expansion after swelling in the solvents.

Hollow microspheres could not be obtained when only 10% EGDMA was used as the crosslinking monomer, but the highest degree of swelling was achieved. The loosely-crosslinked polymer chains were expanded more easily, increasing their volume upon swelling in the solvents, than were the densely crosslinked polymer chains. The cross-sections of the hollow microspheres are shown in Figure 4. There are two types of wall structure in the hollow microspheres: a spongy hollow microsphere as shown in sample no. 19, and a smooth hollow microsphere as shown by sample no. 17.

Cycles of Solvent Absorption

Poly(lauryl acrylate-*co*-EGDMA) particles were used to test the solvent absorption/desorption cycles with various time intervals and the number of absorption/desorption cycles in heptane. The polymer particles of sample no. 25 (PLA) as shown in Figure 3 were swollen in heptane three times. It was found that the highest degree of swelling was obtained in the third absorption cycle and the lowest degree of swelling was the first absorption. However, such changes in the degree of swelling were insignificant, and the polymer spheres were not deformed or collapsed after the third absorption. The higher solvent absorption in the third cycle could be explained by the material hysteresis. Hysteresis is a viscoelastic nature of copolymer chains; that is, the copolymer chains did not shrunk to the original chain length after swelling in a solvent and drying. It would take quite a long time for the chains to recover their original behavior, i.e., the relaxation time is relatively long. Thus, this polymer is appropriate for repeated uses in absorption/desorption of hydrocarbon solvent.
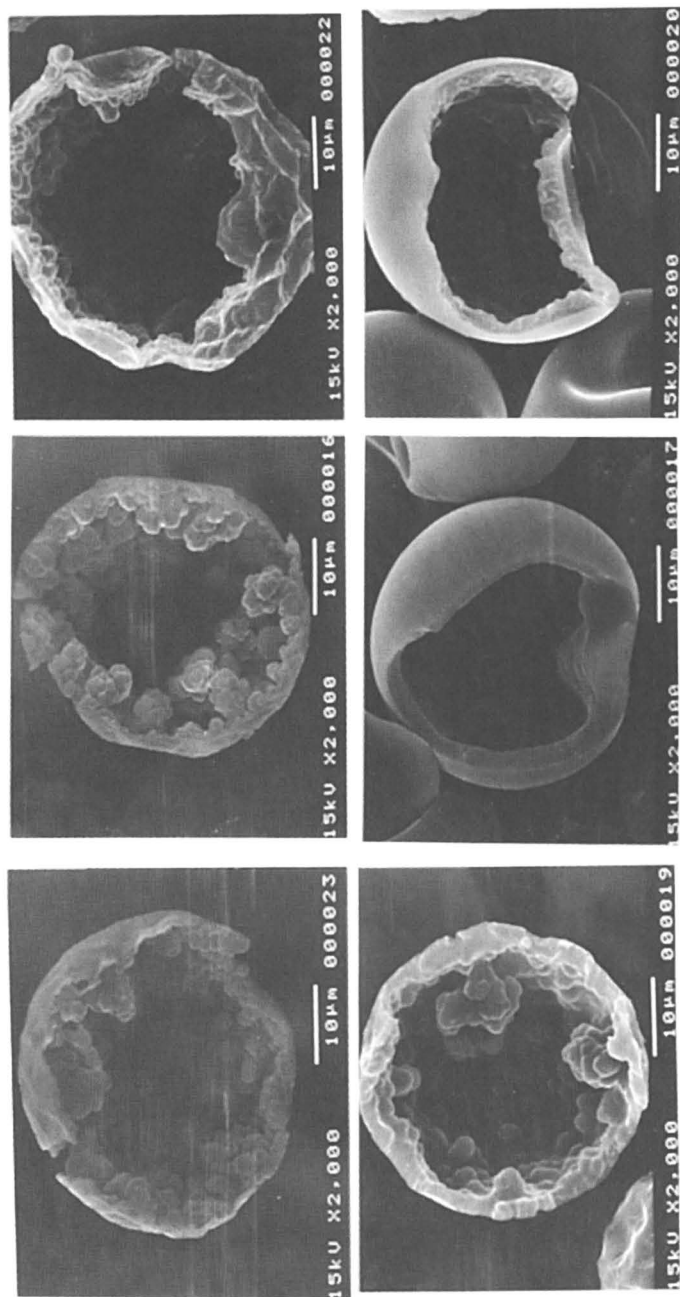
Figure 3. SEM micrographs of hollow polymer particles prepared using various monomer compositions of 2-EHA: MMA: EGDMA at 70% heptane: 0:6.0:4.0 in sample no. 23 (top left), 0:7.0:3. In sample no. 16 (top center), 0:8.0:2.0 in sample no. 22 (top right), 1.4:5.6:3.0 in sample no. 19 (bottom left), 3.5:3.5:3.0 in sample no. 17 (bottom center) and 4.0:4.0:2.0 in sample no. 20 (bottom right). (Reproduced from reference 3. Copyright 2000 John Wiley & Sons.)
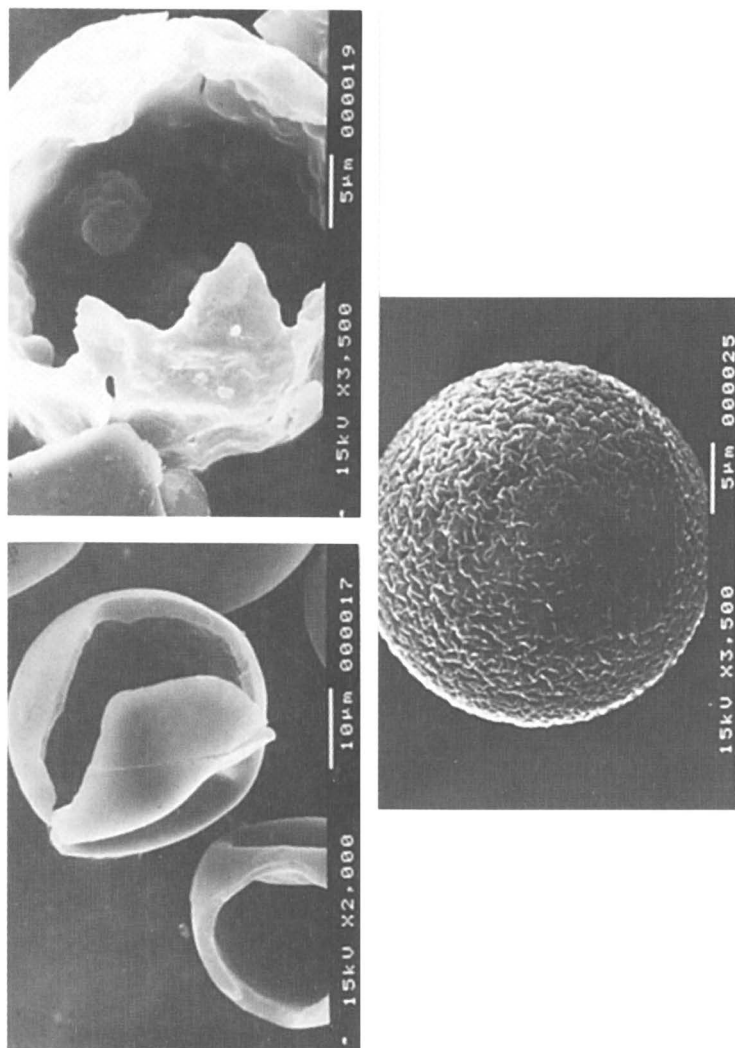
Figure 4. SEM micrographs of the polymer particle microspheres with various surface features and morphologies used in the porosity measurements: smooth hollow morphology in Sample no. 17 (top left), spongy hollow morphology in sample no. 19 (top right), and creased surface in sample no. 25 (bottom).

Porosity of the Beads

A porosimeter (PROSORP VAS-3000) was used to measure the porosity, the pore size distribution, and the specific surface area of the three following polymer particles:

1. The smooth surface hollow particles of poly(2-EHA-*co*-MMA-*co*-EGDMA) prepared using a 2-EHA:MMA:EGDMA ratio of 35:35:30% by weight, respectively, based on the weight of the monomer and crosslinking agent (sample no. 17).
2. The spongy surface hollow particles of poly(2-EHA-*co*-MMA-*co*-EGDMA) prepared using a 2-EHA:MMA:EGDMA ratio of 14:56:30% by weight, respectively, based on the weight of the monomer and crosslinking agent (sample no. 19).
3. The creased surface particles of poly(lauryl acrylate) prepared using LA:EGDMA, 70%:30%, respectively, by weight based on the weight of the monomer and crosslinking agent (sample no. 25).

The surface features and morphologies of these polymer particles were shown earlier in Figure 4. The specific surface areas, the pore volumes, the particle diameters are shown in Table I. Virtually, no sample possessed an appreciable amount of pore volume. All of the samples had mesopores. The lowest specific surface area was obtained for sample no.17, which had a smooth, hollow morphology. However, the highest degree of swelling was observed in sample no. 25, having the creased surface. This did indicate that the creased surface with the lower specific surface area of the pores was able to absorb more solvents, such as toluene and heptane, more than the other porous surfaces with higher specific surface areas of the pores. Thus, in this case, the solvent absorption capacity was only dependent on the type of monomer used and the spongy morphology of the microspheres, which had a solubility parameter close to the solvent being absorbed.

Table I. Characteristics of Polymer Particle Surfaces and Pores

Sample No.	Features of polymer particles	Specific surface area ($m^2 g^{-1}$)	Pore volume ($cm^3 g^{-1}$) 10^4	Pore diameter (Å)
17[a]	Smooth hollow	3.00	1.3	46
19[b]	Spongy hollow	3.67	1.1	41
25[c]	Creased surface	3.37	1.2	44

a: 3.8 and 3.0 times swelling in toluene and heptane, respectively. b: 3.7 times swelling in toluene only. C: 5.3 and 4 times swelling in toluene and heptane, respectively.

Conclusions

A variety of crosslinked acrylate polymer particles with unique morphologies were synthesized employing the SPG with a pore size of 5.25 μm. The appropriate recipe between monomer, crosslinking agent, and heptane is 70:30:70% by weight, respectively, based on the weight of the monomer and crosslinking agent. The amount of EGDMA and solvents, toluene and heptane, had a strong effect on the morphology/surface features. Increasing the amounts of EGDMA and heptane enhanced the high degree of the macro-phase separation resulting in a rougher surface of the polymer particles, which also affected the solvent absorption capacity of the acrylate polymers. Poly(2-EHA-*co*-EGDMA) particles with a high amount of EGDMA (40%) at 45 and 70% of heptane were ruptured after swelling in toluene and heptane, because the densely-crosslinked network was unable to expand freely under the swelling stresses due to the decreasing balance between the diffusion and relaxation rates. Poly(lauryl acrylate) microspheres can absorb and swell the most compared with the other polymer particles. Spongy and smooth, hollow morphologies of the polymer particles were obtained, which depended on the ratios among 2-EHA:MMA:EGDMA monomers at a constant content of 70% heptane. It was found that an increase in the 2-EHA content improved the surface features of the hollow spheres going from a spongy, hollow morphology to a smooth hollow morphology. Decreasing the amount of the hydrophilic MMA segment decreased the hydrophilic moieties, which have decreased affinity for water molecules. Thus, a smooth hollow morphology was obtained. The solvent absorption capacity was not satisfactory because the surface of the particles having a hollow morphology was too hard to absorb the solvents, so the hollow polymer particles were not appropriate for solvent absorption.

The differences in the surface morphologies of the finely porous surface, creased surface, spongy hollow morphology, and smooth hollow morphology exerted various effects on the solvent absorption capacity. It was found that the creased surface of poly(lauryl acrylate-*co*-EGDMA) particles with mesopores of about 44 Å, pore volume of 1.2×10^{-4} cm^3 g^{-1}, and specific surface area of 3.37 m^2 g^{-1}, provided the highest polymer swelling. Poly(lauryl acrylate-*co*-EGDMA) particles were able to absorb the highest amount of heptane and toluene. The particles did not rupture or collapse after swelling in the solvents. Therefore, the polymer particles could be used repeatedly for at least 3 cycles the solvent absorption. Thus, these polymer particles were considered appropriate to apply in solvent absorption, especially in aromatic hydrocarbon solvents.

Acknowledgments

References

1. Nuisin, R.; Ma, G-H.; Omi, S.; Kiatkamjornwong, S. *J. Appl. Polym. Sci.* **2000**, *77*, 1013–1028.
2. Kiatkamjornwong, S.; Nuisin, R.; Omi, S. *Chinese J. Polym. Sci.* **2000**, 309–322.
3. Tawonsree, S.; Omi, S.; Kiatkamjornwong, S. *J. Polym. Sci.: Part A: Polym. Chem.* **2000**, *38*, 4038-4056.
4. Omi, S.; Taguchi, T.; Kaneko, K.; Iso, M. *Macromol. Symp.* **1995**, 92, 309–320.
5. Omi, S.; Katami, K.; Yamamoto, A.; Iso, M. *J. Appl. Polym. Sci.* **1994**, *51*, 1–11.
6. Omi, S. *Colloids and Surfaces, A: Physicochemical and Engineering Aspects,* **1996**, *109*, 97–107.
7. Omi, S.; Taguchi, T.; Nagai, M.; Ma, G-H. *J. Appl. Polym. Sci.* **1997**, *63*, 931–942.
8. Coutinho, F. M. B.; Cid, R. C. A. *Eur. Polym. J.* **1990**, *26*, 1185–1188.
9. Coutinho, F. M. B.; Luz, C. T. Lima. *Eur. Polym. J.* **1993**, *29*, 1119–1123.
10. Kim, D.; Caruthers, J. M.; Peppas, N. A. *Macromolecules.* **1993**, 26, 1841–1847.
11. Rabelo, D.; Coutihno, F. M. B. *Eur. Polym. J.* **1994**, *30*, 675–682.
12. Toda, H.; Takagushi, Y.; Kaino, M. US Patent 5,360,827, **1994**.
13. Lee, D. I.; Mulders, M. R.; Nicholson, D. J.; Leadbetter, A. N. US Patent 5,521,253, **1996.**
14. Mousa, A.; Ishiaku, U. S.; Mohd I. Z. A. *J. Appl. Polym. Sci.* **1998**, 69, 1357–1366.
15. Cheng, C. M.; Micale, F. J.; Vanderhoff, J. W.; and El-Aasser, M. S. *J. Appl. Polym. Sci.* **1992**, *30*, 235–244.
16. "Glass Transition Temperature of Polymers", In *Polymer Handbook*; Brandrup, J.; Immergut, E. H.; Grulke, E. A., Eds. 4th ed., John Wiley & Sons, New York, New York, 1999. pp. 196–97.

Author Index

Adler, Hans-Jürgen P., 276
Alince, B., 52
Aramendia, Esteban, 168
Asua, Jose M., 113, 168
Barandiaran, Maria J., 168
Bednar, F., 52
Berner, Robert A., 338
Blease, Trevor, 168
Cal, Jose C. de la, 168
Carrà, S., 198
Carrà, St., 198
Cheong, I. W., 126
Daniels, Eric S., 1, 221, 357
Dessy, Carlo, 93
Dimonie, Victoria L., 139, 221, 357
Dubowik, David, 338
El-Aasser, Mohamed S., 1, 139, 180, 221, 357
Grade, Jo, 168
Henke, Axel, 276
Ho, C. C., 239
Horský, Jiří, 71
Hough, L. A., 40
Isono, Yoko, 307
Jayasuriya, D. S., 80
Jeong, Pilmoon, 357
Kaška, Martin, 71
Kawaguchi, Haruma, 307
Khew, M. C., 239
Kiatkamjornwong, S., 374
Kim, Jung-Hyun, 126, 152, 323
Kinkal, J., 52
Klein, Andrew, 221
Kostansek, E. C. , 13
Lee, Doug-Youn, 323
Lee, H. J., 152

Lee, J. Y., 152
Lee, K. N., 152
Leiza, J. R., 113
Li, Pei, 293
Ma, Guang-Hui, 260
Malcovati, L., 198
Morbidelli, Massimo, 23
Nagai, Masatoshi, 260
Nomura, M., 126
Omi, Shinzo, 260, 374
Ottewill, R. H., 80
Ou-Yang, H. D., 40
Padtberg, Klaus, 93
Pan, Gaofeng, 139
Pich, Andrij, 276
Puschke, Carsten, 276
Quadrat, Otakar, 71
Robeson, Lloyd M., 338
Sasabe, Reiko, 307
Sefcik, Jan, 23
Shin, Jin-Sup, 323
Sliepcevich, A., 198
Šňupárek, Jaromír, 71
Storti, Giuseppe, 23, 198
Sudol, E. David, 1, 139, 180
Suh, Y. J., 152
Supsakulchai, Anchali, 260
Tang, Jiansheng, 221
Tauer, Klaus, 93
Tawonsree, S., 374
Ven, T. G. M. van de, 52
Verduyn, Marcel, 23
Vicente, M., 113
Voronov, Stanislav, 276
Wang, Xiaoru, 180

Subject Index

389

change during continuous emulsion
polymerization of methyl
methacrylate (MMA), 105*f*
dependence of, of pure water on
temperature, 102*f*
measurements during batch emulsion
polymerization of styrene, methyl
methacrylate, and vinyl acetate,
103, 104*f*
measurements in emulsion
polymerization, 101–106
on-line measurement method, 96
oscillations of, in steady state, 103–
104, 105*f*
sensitivity of BPD apparatus, 104
temperature coefficient of, for
different aqueous solutions, 102*t*
See also On-line monitoring of
emulsion polymerization
Surfactant adsorption isotherm, latex
particles, 29, 32
Surfactant coverage, latex particles,
17, 18*f*
Surfactants
adverse effect during application,
168–169
adverse effects on film properties,
169
functionalized poly(methyl styrene)
latexes, 298–299
role in emulsion polymerization, 2–3,
168, 181
surfmers, 169
See also Reactive surfactants;
Surfmers
Surfmers
AFM (atomic force microscopy) of
methyl methacrylate/butyl acrylate
(MMA/BA) film (Maxemul 5011
surfmer), 174*f*
AFM of MMA/BA film (NP30
surfactant), 173*f*
choice of reactive group, 175–177
comparison (Maxemul 5011,
Uniqema) to conventional

surfactants (NP20, NP30), 169–
175
description, 169
effect of reactivity ratios on
monomer and surfmer conversion,
177*f*
formulation for MMA/BA latexes,
172*t*
formulation for vinyl acetate/butyl
acrylate latexes, 170*t*
improving product quality, 169
mathematical model for emulsion
polymerization using, 175–176
MMA/BA (50/50) latexes, 171–175
parameters of model, 176*t*
permeability of MMA/BA films,
175*t*
vinyl acetate/BA (85/15) latexes,
170–171
water absorption for vinyl
acetate/BA copolymer films, 171*f*
water or vapor transmission rate
(WVTR) equation, 172
Surfmers. *See* Reactive surfactants
Synthetic rubber. *See* Natural rubber
(NR) latex

T

Takayanagi model
equations, 234
predicting Young's modulus, 234
Young's modulus vs. volume
concentration of PS latex particles,
236*f*
See also Young's modulus of latex
blend films
Temperature, monitoring chemical
reaction, 94
Tensile testing. *See* Young's modulus
of latex blend films
Thermosensitive hairy particles
adsorption and desorption of protein
methods, 312